

UNIVERSITÀ  
DEGLI STUDI  
DI PADOVA

UNIVERSITÀ DEGLI STUDI DI PADOVA  
DIPARTIMENTO DI INGEGNERIA INDUSTRIALE

PhD COURSE IN INDUSTRIAL ENGINEERING  
CURRICULA MATERIALS ENGINEERING  
XXXII CYCLE

# LARGE SCALE ADDITIVE MANUFACTURING OF INORGANIC COMPONENTS

Dottorato in apprendistato di alta formazione e ricerca

in collaborazione con DESAMANERA SRL

**Coordinator:** Ch.mo Prof. Paolo Colombo

**Supervisor:** Ch.mo Prof. Paolo Colombo

**Company Tutor:** Antonino Italiano

**PhD Candidate:** Filippo Gobbin



# Abstract

The core of this doctoral thesis is the production of large scale pieces via powder bed Additive Manufacturing (AM) technology. The main advantage of AM is the possibility to easily produce complicated and customized shapes with great benefit in term of materials consumption, production costs and time consumed. Very few companies work in this specific field with inorganics materials. The research project has been carried out in collaboration with Desamanera srl, under a contract of apprenticeship for higher education. The company, founded as innovative startup in Rovigo since December 2014, works in the field of large scale additive manufacturing and special surface finishing, with minerals, ceramics and inorganic materials. Desamanera process allows to consolidate the powder bed composed of aggregate and binder thanks to the selective deposition of simple water. The optimization process has involved different aspects: raw materials analysis and selection (aggregates and binder), printing process improvements and post-printing treatments. All the work was carried out maintaining the proper balance between the basic research and the practical needs that a small company can have.

The study of raw materials has allowed to identify the main characteristics of the various components and to find new products and suppliers, compatible with the company needs of low cost and ease of supply, even in limited quantities.

The printing process optimizations have followed the goal of going to improve fundamental aspects such as the deposition of the water, the laying of the powder mix and the interfaces between the layers. At the same time, the stability and reproducibility of the entire process has been increased.

Starting from printed part analysis, new post-printing treatments are been developed with the aim of increase the strength of the final material or of adding new specific properties.

Finally, a general overview of the already started projects is given and new possible applications are hypothesized and suggested.

Keywords: additive manufacturing; large scale; inorganic materials.

# Sommario

Il cuore di questa tesi di dottorato è la produzione di pezzi di grandi dimensioni attraverso la manifattura additiva a letto di polvere. Il vantaggio principale del AM è la possibilità di produrre con facilità forme complicate e personalizzate con grandi vantaggi in termini di consumo di materiali, costi di produzione e tempo impiegato. Non sono molte le aziende che lavorano in questo specifico campo con materiali inorganici.

Il progetto di ricerca è stato realizzato in collaborazione con Desamanera srl, con un contratto di apprendistato di alta formazione e ricerca. La società, fondata come startup innovativa a Rovigo dal dicembre 2014, opera nel campo della manifattura additiva su larga scala e delle finiture superficiale, con minerali, ceramici e materiali inorganici. Il processo sviluppato da Desamanera consente di consolidare il letto di polvere composto da aggregato e legante grazie alla semplice deposizione selettiva di acqua.

Il processo di ottimizzazione ha riguardato diversi aspetti: l'analisi e la selezione delle materie prime (aggregati e leganti), i miglioramenti del processo di stampa e dei trattamenti post-stampa. Tutto il lavoro è stato svolto mantenendo il giusto equilibrio tra la ricerca di base e le esigenze pratiche che una piccola azienda può avere.

Lo studio delle materie prime ha permesso di identificare le principali caratteristiche dei vari componenti e di trovare nuovi prodotti e fornitori idonei, compatibili con le esigenze aziendali di basso costo e facilità di fornitura, anche in quantità limitate.

Le ottimizzazioni del processo di stampa hanno portato al miglioramento di aspetti fondamentali quali la deposizione dell'acqua, la stenditura della miscela di polveri e la qualità delle interfacce tra gli strati. Allo stesso tempo, la stabilità e la riproducibilità dell'intero processo sono state aumentate.

A partire dall'analisi delle parti stampate, sono stati sviluppati nuovi trattamenti post-stampa con l'obiettivo di aumentare la resistenza del materiale finale o di aggiungere nuove proprietà.

Infine, viene fornita una panoramica generale di ulteriori tematiche il cui studio è già avviato e vengono ipotizzate e suggerite nuove possibili applicazioni.

Parole chiave: manifattura additiva; grandi dimensioni; materiali inorganici.

# Table of Contents

<b>Research Motivation</b> .....	<b>1</b>
<b>Thesis Organization</b> .....	<b>3</b>
<b>1 - General introduction</b> .....	<b>5</b>
1.1 - 3D printing technologies .....	5
1.2 - Additive manufacturing on large scale and construction sector .....	27
1.2.1 - Extrusion-based 3D printing technology .....	33
1.2.2 - Powder-based 3D printing technology.....	45
1.2.3 - The current doctoral thesis .....	56
1.3 - Binders .....	57
1.3.1 – Magnesium phosphate binders.....	62
1.3.2 – Geopolymers .....	67
<b>2 - Desamanera srl</b> .....	<b>72</b>
2.1 – Company overview .....	72
2.2 – Desamanera technology and printing process.....	77
2.3 – Desamanera raw materials.....	84
<b>3 – Process parameters and optimizations</b> .....	<b>92</b>
3.1 – Materials and methods .....	92
3.2 – Tests and improvements .....	94
3.3 – Conclusions .....	111
<b>4 – Raw materials and printed parts</b> .....	<b>114</b>
4.1 – MgO analysis .....	114
4.1.1 – Materials and methods .....	114
4.1.2 – Results and discussion .....	117
4.1.3 – Conclusions .....	120
4.2 – Acid phosphates analysis .....	121
4.2.1 – Materials and methods .....	121
4.2.2 – Results and discussion .....	123
4.2.3 – Conclusions .....	126
4.3 – Evaluation of printing mixes .....	126
4.3.1 – Materials and methods .....	127
4.3.2 – Results and discussion .....	129
4.3.3 – Conclusions .....	133
4.4 – Characterization of printed part .....	134
4.4.1 – Materials and methods .....	134

4.4.2 – Results and discussion .....	136
4.4.3 – Conclusions .....	141
<b>5 – Post-printing treatments .....</b>	<b>144</b>
5.1 – Water addition treatment .....	144
5.1.1 – Materials and methods .....	145
5.1.2 – Results and discussion .....	146
5.2 – Slurry infiltration .....	148
5.2.1 – Materials and methods .....	148
5.2.2 – Results and discussion .....	151
5.3 – Liquid impregnation .....	154
5.3.1 – Materials and methods .....	154
5.3.2 – Results and discussion .....	156
5.4 – Conclusions .....	159
<b>6 – Summary and conclusions .....</b>	<b>161</b>
6.1 – Ongoing works .....	161
6.2 – Conclusions .....	166
6.3 – Future objectives .....	167
<b>Bibliography .....</b>	<b>169</b>

# Research Motivation

In the last decades new manufacturing solutions are strongly researched in all industrial sectors. Additive Manufacturing technologies (AM) have had a considerable development, rapid prototyping is now the first choice in many production sectors, offering great versatility for various application productions.

Additive manufacturing is fundamentally different from traditional formative or subtractive Manufacturing. The latter operates by removing material, obtaining the form desired from a block that is processed and manipulated, as in casting or forming technologies such as forging or machining.

The AM techniques are the closest to the ‘bottom up’ manufacturing where a structure can be built into its designed shape using a ‘layer-by-layer’ approach, obtaining even very complex shapes, impossible to achieve with traditional techniques. AM is versatile, flexible, highly customizable and, as such, can suite most sectors of industrial production. Materials to make these parts/objects can be of a widely varying type. These include metallic, ceramic and polymeric materials along with combinations in the form of composites, hybrid, or functionally graded materials. The fields of application that have developed over the years are many, 3D printers are now used in architecture, restoration, healthcare, paleontology and archeology etc. This PhD project is carried out in collaboration with Desamanera srl, under a contract of apprenticeship for higher education. The company, founded as innovative startup in Rovigo since December 2014, works in the field of large scale additive manufacturing and special surface finishing, with minerals, ceramics and inorganic materials.

While, at the moments, polymers AM is the more diffused one and metal AM has the faster grow up, ceramic AM is less developed among the many commercially available AM systems. This aspect become stronger if we move to large scale AM, with dimension in the range of tens of centimeters or meters. In large scale sector (often “construction” field) the technology used prevalently the direct extrusion of a slurry material, starting from the long experience in making cement paste and mortar, that are substantially now deposited from a moving tube creating the shape layer by layer instead filling the formworks. Or the indirect powder-based technologies, in which particles are consolidated by the selectively deposition of a binder (fluid binder, liquid activator, etc).

Desamanera works with this second type of approach. And with a sensible attention at the ecological and sustainable aspects (sustainable binders, recycled raw materials, reuse of waste), that are also another very important point that is grown up with new manufacturing innovations. The motivation driving this research, following Desamanera already defined important characteristics in term of technology and materials, has been to study and develop this type of large scale technology applied to ceramic and inorganic materials, with a great attention on new sustainable alternative materials. We are moving in a region in which there are not so many certainties, achieved results or milestones. All the potential and the success of this technology approach have to be researched and discovered/revealed.



# Thesis Organization

The state-of-the-art of general AM will be presented in the *General introduction*, with a focus on large scale technologies. Also, the different materials used in large scale will be describe.

A complete overview of the company, with which the project is carried out, will be also provided in *Desamamera srl* order to have the scenario in which some decisions are taken.

*Chapter 3* reports the printing process analysis, the initial parameters setup and the following optimizations that lead to the final configuration. The way for water deposition is been modified and a new device for powder laying is been designed. A great improvement in process stability and repeatability is been completed.

*Chapter 4* describes raw materials and printing mixes characteristics and the final printed part properties. Binders are analyzed to find their fundamental aspects and to research new products and suppliers available to the company necessities. The printed part is studied to control the quality the of the production, to work on possible improvements and to think about new possible applications.

*Chapter 5* is completely dedicated to post-printing process because of the possibility to increase the performance of the product or to add new specific characteristics.

*Summary and conclusions* final chapter presents a part of the new ongoing themes and gives a summary of the principal conclusion and some suggestions for improvement directions and new applications develop.



# General Introduction

In this chapter an introduction of Additive Manufacturing and its characteristics is provide. The traditional ceramic 3D printing technologies are briefly illustrated and then a review about the main large scale technologies (meter size) is given, with the first introductions to the one investigated in this PhD thesis. Later the binders for large scale application are analyzed with a major attention to the ones important for the current work.

## **1.1 3D printing technologies**

The term “Additive Manufacturing” is the most precise to refers to all those innovative technologies that produce parts adding material upon material. According to the American Society for Testing and Materials (ASTM), AM is defined by the “process of joining materials to make objects from 3D model data, usually layer upon layer, opposed to subtractive manufacturing methodologies, such as traditional machining” [1].

Commonly known also as rapid prototyping (RP), solid freeform fabrication (SFF) or three-dimensional (3D) printing, AM provides a cost-effective and time-efficient techniques for producing low volume of complicated and customized pieces, advanced material properties and functionality [2]. Figure 1.1 shows the advantage of Additive manufacturing (AM) in relation with the complexity and/or customization of the pieces and the relative increasing of costs.

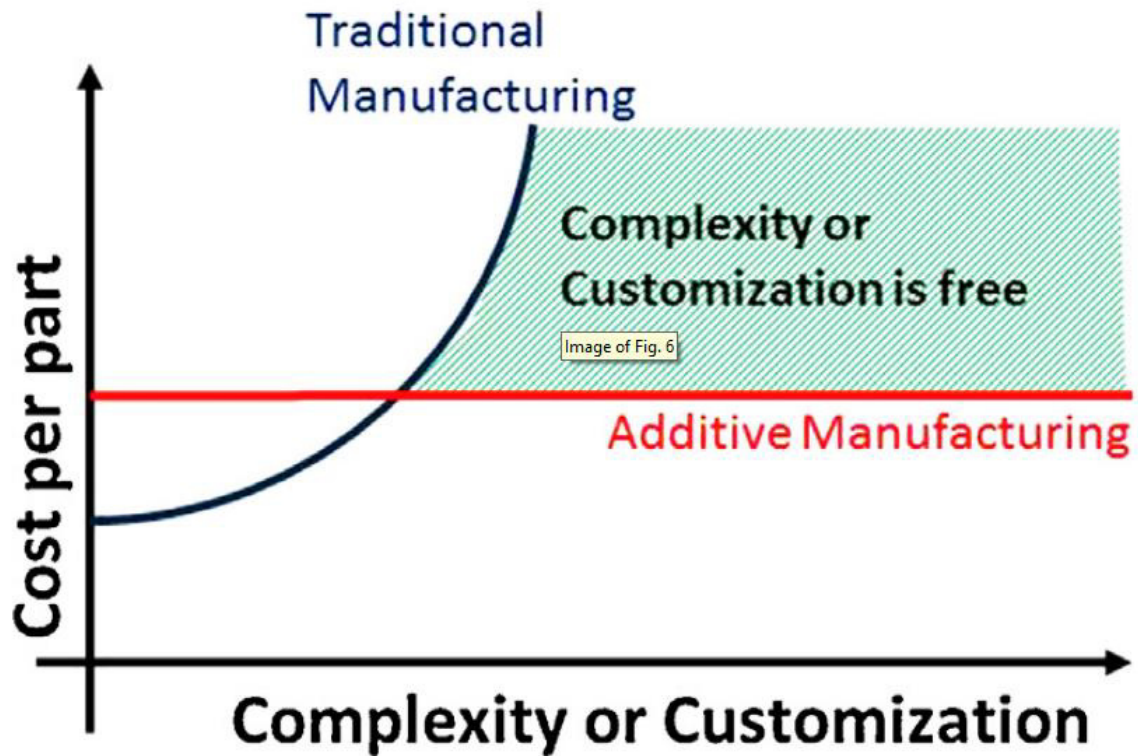


**Figure 1.1.** In conventional manufacturing, increasing complexity and/or customization leads to increased cost. With additive manufacturing, complexity or customization becomes free.[3]

Starting from the first stereolithography (SL) apparatus by C.W. Hull in 1986 [4], a lot of different technologies have been developed and improved; such as fused deposition modeling (FDM), selective laser sintering (SLS), inkjet printing, and many others. Recent innovations in materials and processes are transforming 3D printing from rapid prototyping to rapid manufacturing and production of final objects. This allows manufacturing near the point of use, enabling “on-demand” manufacturing and drastically reducing inventories and wait times.

Additive manufacturing offers some advantages versus conventional subtractive manufacturing that have contributed greatly to the fast growth of the AM market since its early beginning.

Some of the potential benefits [5], [6] of additive manufacturing can be summarized below:

- Direct translation of design to component
- Generation of parts with greater customization with no additional tooling or manufacturing cost
- Functional design allowing manufacturing of complex internal features
- Flexible and lightweight component manufacturing with hollow or lattice structures
- Ability of direct manufacturing of components to their final (net) or near final (near net) shape with minimal to no additional processing
- Potential to approach zero waste manufacturing by maximizing material utilization

- A great reduction in overall product development and manufacturing time leading to quicker transfer to market
- Smaller operational footprint towards manufacturing a large variety of parts
- On-demand manufacturing, moving away from projection-based manufacturing and
- Excellent scalability.

Additive Manufacturing processes have a digital dataflow that generates the instructions for the AM machine followed by a physical workflow that transforms the raw materials into final parts.

[7] As describe in Figure 1.2 various steps can be defined.

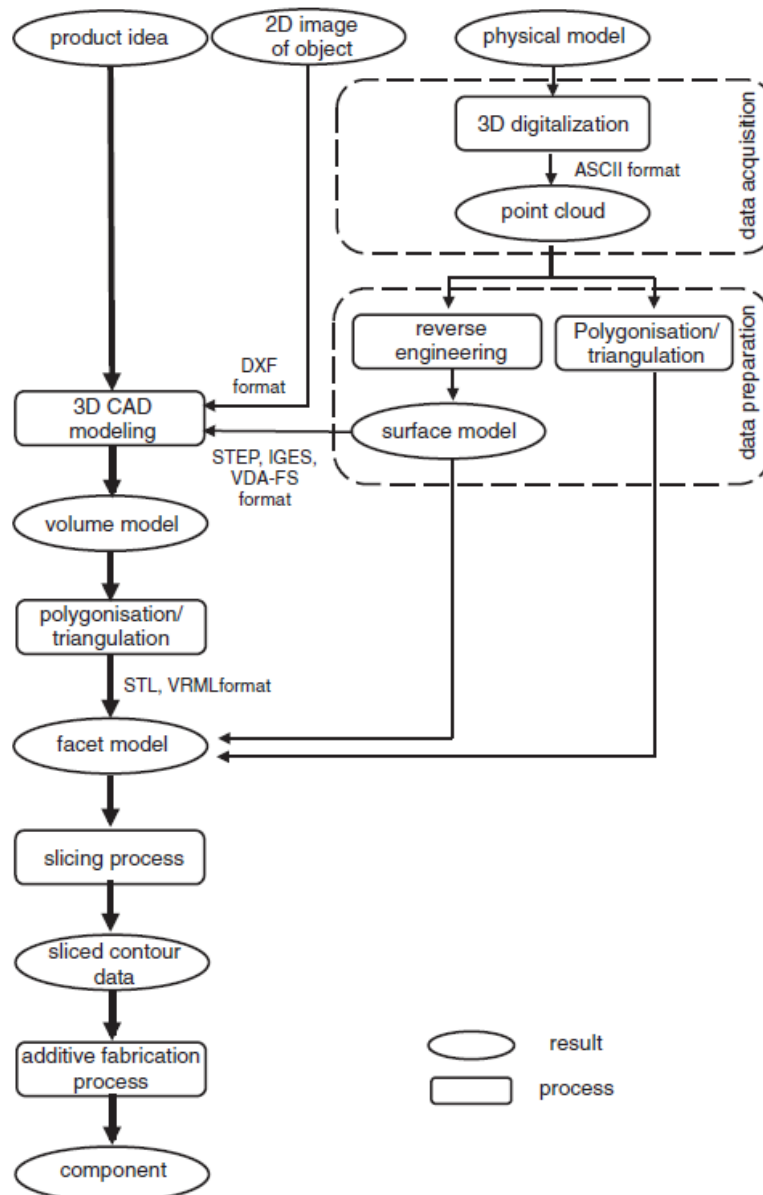


**Figure 1.2.** Digital and physical workflow from product idea to actual component. Redrawn from [7]

Additive manufacturing applications have been growing steadily for many years, as detailed in Wohlers Report 2013 [8] and other studies [3], [9], [10], although the size of this market is limited for the time being (Figure 1.3): 2,2 billion dollars of turnover estimated worldwide in 2012 (+ 28,5% compared to 2011), of which one billion for materials and systems (clear segment in the chart), 1,2 billion for services (dark segment). Obviously, this is still a negligible figure if compared to the value of manufacturing worldwide (about 11,600 billion).

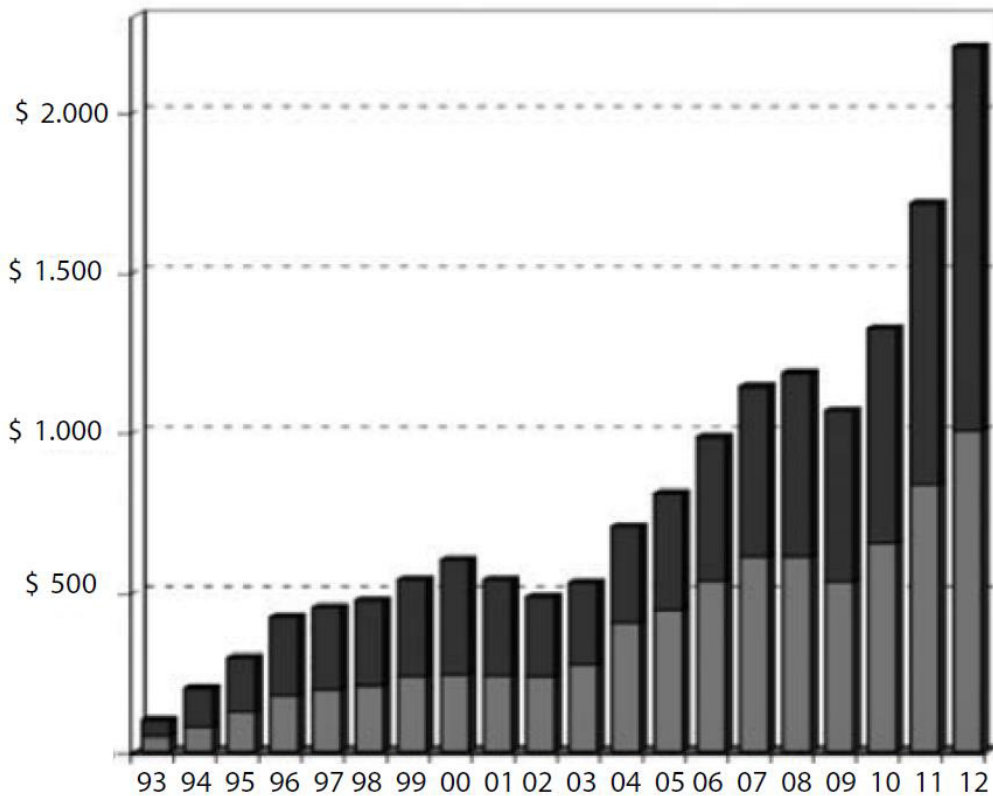


**Figure 1.3.** Annual growth rate of worldwide revenues of AM, billions of dollars. [8]

In any case, the sector trend is well represented by the average annual rate of overall turnover growth at the level worldwide in the last 25 years, estimated of the order of 25,4% (+ 27,4% in the three-year period 2010-2012). Also, the turnover of the raw materials used in manufacturing additive (resins, powders, filaments of plastic, etc.) is obviously in growth (\$ 422,6 million in 2012, + 29,2% compared to 2011, + 495% compared to 2001) (Figure 1.4).

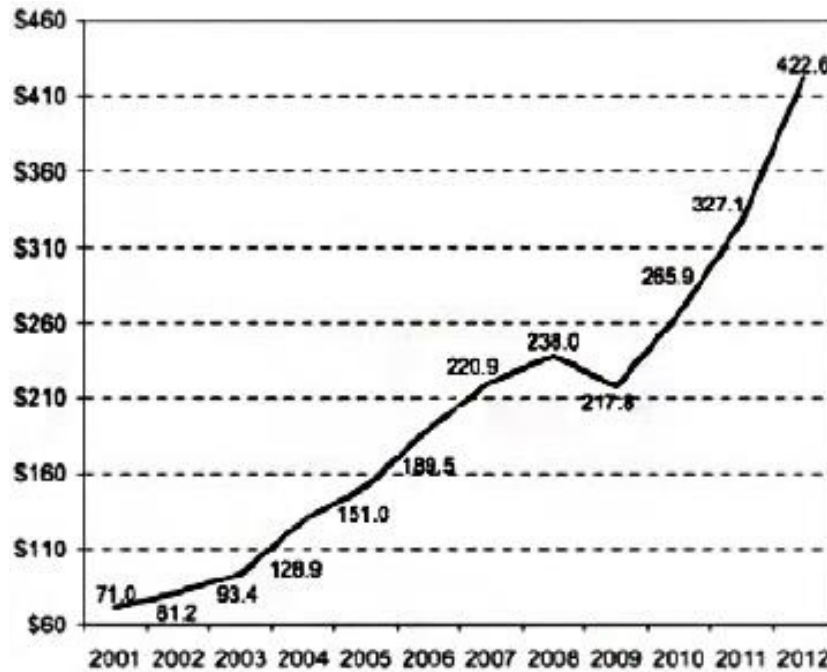


Figure 1.4. Annual growth rate of worldwide revenues of materials, millions of dollars. [8]

The feedstock materials for AM processes can be employed in form of powder, liquid, slurry, filament or sheet. These materials can be selectively deposited only where needed (e.g. by extrusion) or first a complete layer of material is formed and then the material in the layer is selectively joined (e.g. by laser melting) or removed (e.g. cutting of a sheet). [11], [12]

Following similar criteria, ASTM [1] divided AM technologies into seven categories:

1. **Material extrusion (ME):** material is selectively dispersed through a nozzle or orifice (e.g. robocasting, fused deposition modeling (FDM)).
2. **Material jetting (MJ):** droplets of build material are selectively deposited (e.g. direct inkjet printing, DIP).
3. **Binder jetting (BJ):** a liquid bonding agent is selectively deposited to join powder materials (e.g. powder-based 3D printing).
4. **Sheet lamination (SL):** sheets of material are bonded to form an object (e.g. laminated object manufacturing, LOM).
5. **Vat photopolymerization (VP):** liquid photopolymer in a vat is selectively cured by light- activated polymerization (e.g. Stereolithography (SL)).
6. **Powder-bed fusion (PBF):** thermal energy selectively fuses regions of a powder bed (e.g. selective laser sintering/melting (SLS/SLM); selective electron beam melting).
7. **Direct energy deposition (DED):** focused thermal energy fuses a material by melting it as it is deposited.

In figure 1.5 the basic principles and the characteristics of AM technologies are summarized.

ASTM category	Basic principle	Example technology	Advantages	Disadvantages	Materials	Build volume (mm × mm × mm)	Tool manufacturer/country
<b>BJ</b>	Liquid binder/s jet printed onto thin layers of powder. The part is built up layer by layer By glueing the particles together	<ul style="list-style-type: none"> <li>3D inkjet technology</li> </ul>	<ul style="list-style-type: none"> <li>Free of support/substrate</li> <li>Design freedom</li> <li>Large build volume</li> <li>High print speed</li> <li>Relatively low cost</li> </ul>	<ul style="list-style-type: none"> <li>Fragile parts with limited mechanical properties</li> <li>May require post processing</li> </ul>	<ul style="list-style-type: none"> <li>Polymers</li> <li>Ceramics</li> <li>Composites</li> <li>Metals</li> <li>Hybrid</li> </ul>	Versatile (small to large) X = <4000 Y = <2000 Z = <1000	ExOne, USA PolyPico, Ireland
<b>DED</b>	Focused thermal energy melts materials <i>during</i> deposition	<ul style="list-style-type: none"> <li>Laser deposition (LD)</li> <li>Laser Engineered NetShaping (LENS)</li> <li>Electron beam</li> <li>Plasma arc melting</li> </ul>	<ul style="list-style-type: none"> <li>High degree control of grain structure</li> <li>High quality parts</li> <li>Excellent for repair applications</li> </ul>	<ul style="list-style-type: none"> <li>Surface quality and speed requires a balance</li> <li>Limited to metals/metal based hybrids</li> </ul>	<ul style="list-style-type: none"> <li>Metals</li> <li>Hybrid</li> </ul>	Versatile X = 600–3000 Y = 500–3500 Z = 350–5000	Optomec, USA InssTek, USA Sciaky, USA Irepa Laser, France Trumpf, Germany
<b>ME</b>	Material is selectively pushed out through a nozzle or orifice	<ul style="list-style-type: none"> <li>Fused Deposition Modelling (FDM)/Fused Filament Fabrication (FFF), Fused Layer Modelling (FLM)</li> </ul>	<ul style="list-style-type: none"> <li>Widespread use</li> <li>Inexpensive</li> <li>Scalable</li> <li>Can build fully functional parts</li> </ul>	<ul style="list-style-type: none"> <li>Vertical anisotropy</li> <li>Step-structured surface</li> <li>Not amenable to fine details</li> </ul>	<ul style="list-style-type: none"> <li>Polymers</li> <li>Composites</li> </ul>	Small to medium X = <900 Y = <600 Z = <900	Stratays, USA
<b>MJ</b>	Droplets of build materials are deposited	<ul style="list-style-type: none"> <li>3D inkjet technology</li> <li>Direct Ink writing</li> </ul>	<ul style="list-style-type: none"> <li>High accuracy of droplet deposition</li> <li>Low waste</li> <li>Multiple material parts</li> <li>Multicolour</li> </ul>	<ul style="list-style-type: none"> <li>Support material is often required</li> <li>Mainly photopolymers and thermoset resins can be used</li> </ul>	<ul style="list-style-type: none"> <li>Polymers</li> <li>Ceramics</li> <li>Composites</li> <li>Hybrid</li> <li>Biologicals</li> </ul>	Small X = <300 Y = <200 Z = <200	Stratays, USA 3D Systems, USA PolyPico, Ireland 3Dinks, USA WASP, Italy
<b>PBF</b>	Thermal energy fuses a small region of the powder bed of the build material	<ul style="list-style-type: none"> <li>Electron beam melting (EBM)</li> <li>Direct Metal Laser Sintering (DMLS)</li> <li>Selective Laser Sintering/Melting (SLS/SLM)</li> </ul>	<ul style="list-style-type: none"> <li>Relatively inexpensive</li> <li>Small footprint</li> <li>Powder bed acts as an integrated support structure</li> <li>Large range of material options</li> </ul>	<ul style="list-style-type: none"> <li>Relatively slow</li> <li>Lack of structural integrity</li> <li>Size limitations</li> <li>High power required</li> <li>Finish depends on precursor powder size</li> </ul>	<ul style="list-style-type: none"> <li>Metals</li> <li>Ceramics</li> <li>Polymers</li> <li>Composites</li> <li>Hybrid</li> </ul>	Small X = 200–300 Y = 200–300 Z = 200–350	ARCAM, Sweden; EOS, Germany; Concept Laser Cusing, Germany; MTT, Germany; Phoenix System Group, France; Renishaw, UK;Realizer, Germany; Matsuurra, Japan, Voxeljet, 3Dsystems, USA
<b>SL</b>	Sheets/foils of materials are bonded	<ul style="list-style-type: none"> <li>Laminated Object Manufacturing (LOM)</li> <li>Ultrasound consolidation/Ultrasound Additive Manufacturing (UC/UAM)</li> </ul>	<ul style="list-style-type: none"> <li>High speed,</li> <li>Low cost,</li> <li>Ease of material handling</li> </ul>	<ul style="list-style-type: none"> <li>Strength and integrity of parts depend on adhesive used</li> <li>Finishes may require post processing</li> <li>Limited material use</li> </ul>	<ul style="list-style-type: none"> <li>Polymers</li> <li>Metals</li> <li>Ceramics</li> <li>Hybrids</li> </ul>	Small X = 150–250 Y = 200 Z = 100–150	3D systems, USA MCor, Ireland
<b>VP</b>	Liquid polymer in a vat is light-cured	<ul style="list-style-type: none"> <li>Stereo Lithography (SLA)</li> <li>Digital Light Processing (DLP)</li> </ul>	<ul style="list-style-type: none"> <li>Large parts</li> <li>Excellent accuracy</li> <li>Excellent surface finish and details</li> </ul>	<ul style="list-style-type: none"> <li>Limited to photopolymers only</li> <li>Low shelf life, poor mechanical properties of photopolymers</li> <li>Expensive precursors/Slow build process</li> </ul>	<ul style="list-style-type: none"> <li>Polymers</li> <li>Ceramics</li> </ul>	Medium X < 2100 Y < 700 Z < 800	Lithoz, Austria 3D Ceram, France

**Figure 1.5.** Basic principles, materials, advantages, disadvantages, typical build volumes and tool manufacturer of seven ASTM categories of AM: binder jetting (BJ); directed energy deposition (DED); material extrusion (ME); (4) material jetting (MJ); powder bed fusion (PBF); sheet lamination (SL); and vat photopolymerization (VP). Build volumes are rounded to nearest number for convenience. Materials types have been ranked in order of suitability and common use. [5]



Different AM technologies can work with different classes of material, on different volume sizes and with specific advantage/disadvantage.

AM technologies, that are based on the processing of polymeric and metallic materials, have been so far the most successful; ceramic materials are lower developed in industrial sectors. Even multi-material textures and functionally as well as compositionally graded structures can be fabricated during the manufacturing process. [12], [13]

It can also be pointed out that AM technologies can be divided into two categories: direct and indirect. ME, MJ and DED are known as *direct* AM manufacturing technologies, as the material is deposited only where the objects is created. BJ, SL, VP, PBF are classified as *indirect* processes, meaning that they require the deposition of a layer on which the object cross-section is inscribed. Also, *Negative* AM can be classified as the technologies in which a mold is fabricated, to successively used for the production of the real final part.

The excess material in indirect technologies forms a support to the successive layers, enabling the generation of parts with large overhangs, but it has to be removed at the end of the print and in some case this operation can be difficult or impossible. It is the case of powder materials, in closed porosity structures there is no way to remove the excess material trapped inside it; even it may be complicated to remove it completely from small open pores and cells. In the case of powder-bed fusion or binding, partially sintered/bonded particles affect the surface finish of the manufactured object significantly.

The direct deposition of material, instead, does not have such geometrical limitations, but overhangs above a certain dimension can require support structures that present the same problems already described for indirect technologies. In direct technologies a new piece can be printed only after the end of the previous; the material is usually deposited only in a sequence and in specific positions.

Indirect technologies, instead, have the potential to be faster, because the material is deposited in one complete layer and the cross-section can be inscribed over the entire layer. Moreover, simultaneous production of multiple objects is also enabled. [11], [14], [15]

Direct AM appears more promising in the combination with multi-material systems, also including ceramics (functional gradients, ceramic/plastic and ceramic/metal interfaces). Indirect technologies show much more limitations, e.g. the addition of metallic materials acting as conductor in multilayer ceramic systems is possible just for small concentrations. [16]

As it already described in the previous page, AM has great potentiality, but ceramic technologies are not so investigated and optimized until now. Most works in the field have been so far on fabrication of porous structures such as lightweight lattices, scaffolds for tissue

engineering, filters and catalyst carriers. Very few AM technologies have the potential to fabricate fully dense, monolithic ceramics (that generally have superior mechanical properties, thermal resistance and durability). The biggest issue belongs to the post-treatment step, if the product is a green body which needs to be sintered or converted to ceramic with the same limitations involved in conventional manufacturing. Expertise and equipment, such as high temperature furnaces, are needed and restrict the user field. [11], [12], [17]

In large scale AM, as it will be deeply described in the following parts, this problem is generally eliminated by using aggregates and binders with room temperature setting that don't require temperature post-treatments. For this reason, not all the technologies are suitable for large scale. The following sections review the current state-of-the-art of AM of ceramics, giving a general description of the procedures and the potentialities of their use. At the end a detailed focus on large scale, describing the technologies developed so far, will be given.

### **FDM - Fused Deposition Modelling**

Fused Deposition Modeling (FDM), is one of the most commonly used 3D printing techniques. It was developed first for polymers in 1989 and commercialized after 1990 by Stratasys Inc. At present, open sourced consumer FDM machines are believed to have the largest unit shipments among all types of 3D printers owing to their various advantages, such as simplicity in the building process, flexible unit size, ease in use and DIY and, more importantly, the low cost of both machines and feedstock materials.[18]

Its modification to fabricate ceramics (polymer filament with ceramic loaded or preceramic precursor), is often abbreviated Fused Deposition Ceramic (FDC), but variety of synonyms exist (EFF, FBW, ext). [19] A schematic image of the process is presented in Figure 1.6. According to ASTM this technology belongs to ME category.

The process can be schematized as follows:

- The filament passes through the heated liquefier and acts as a piston to extrude a continuous bead of molten material through the nozzle;
- The bead is deposited on a platform that indexes down after each layer is completed.
- Bonding of beads and layers occurs thanks to the adhesiveness of partially molten material, leading to the fabrication of the object.

The main drawback resides in the feedstock preparation: ideally, a continuous filament should be produced, which would be flexible enough to be collected in spools and continuously fed to the printing head.

However, it is very hard to produce such a filament with a high ceramic loading (up to 60vol%), as it immediately becomes too brittle. The high amount of polymer needed can cause issues during subsequent burning and sintering of the parts.

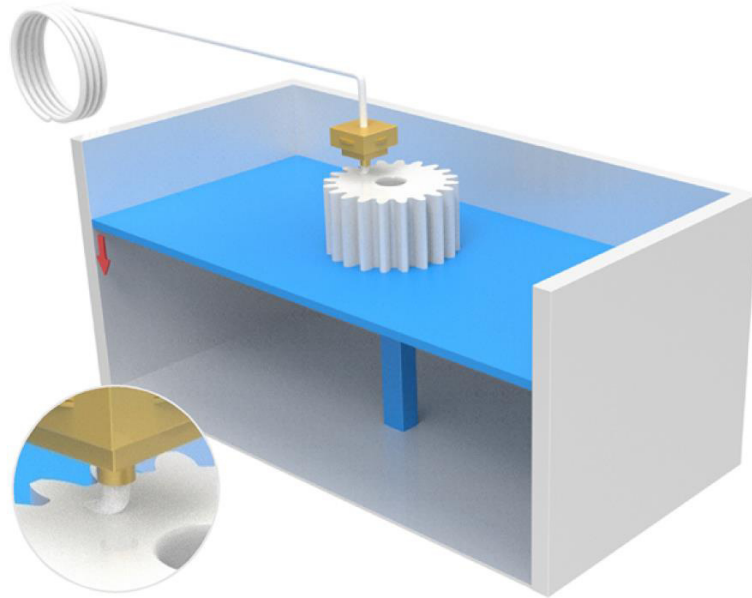


**Figure 1.6.** Schematic diagram of the FDM process.[18]

This technique is been used to produced functional ceramics, such as several ceramic transducers of various shapes fabricated with polymers/piezoelectric ceramics (e.g. lead-zirconate-titanate (PZT) and lead-magnesium niobite (PMN)) composites as feedstocks. Also, fine ceramic (calcium phosphate) periodic woodpile structures with spatial resolutions of  $<100\ \mu\text{m}$  were successfully fabricated using FDM. Current ceramic FDM applications, however, have shifted to the fabrication of bio ceramic scaffolds and lattice photonic bandgap structures. The reason might be that biomedical components require less accuracy and the rod shape (fused ceramic/polymer filament) fits well with the need for 3D woodpile lattice structures. [14], [17]–[19] Examples of FDC samples are presented in Figure 1.7.

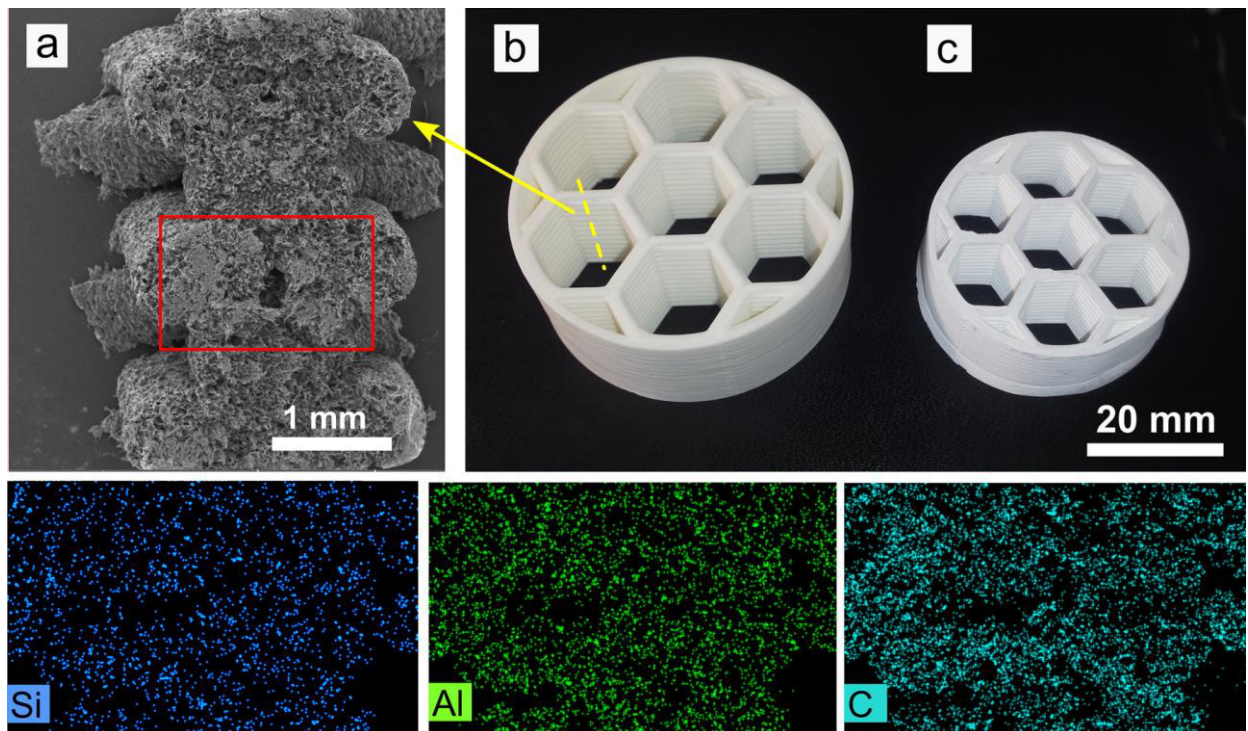


**Figure 1.7.** Honeycomb structures 3D printed using a 40 vol% UF5+Silres MK filament, before firing (b) and after firing (c). Image of the cross-section before firing (a); the investigated region is indicated by a dashed yellow line in (b). Si, Al and C EDS elemental analysis in the region marked with the red rectangle in (a). [20]

Equally to conventional plastic materials FDM in the ceramics FDM, the quality of the printed parts, such as surface roughness, resolution accuracy, homogeneity and mechanical properties, also are closely affected by process parameters, including rod width (fused ceramic/polymer filament), layer thickness, building orientation, etc. A lot of factors, as including ceramic particle load, size, distribution and dispersity, the ceramic/binder/additive ratios, and hence the flexibility of the filaments are affected by ceramic feedstocks. [14], [19]

Surface roughness is the primary concern for FDM processed parts. The main problem is the staircase effect, (it's the major disadvantage of FDM) that can be easily found in printed ceramic parts. This is predetermined by extruded filament size, resulting in limited control in the z direction. Although improvements in surface roughness have rarely been studied for FDM of ceramics. [12], [18]

This technology process could allow to produce large scale pieces (it already happens with polymer materials) but with ceramic material there are big issues with the post-processing to eliminate the organic components and sintering the part.

### **DIW - Direct Ink Writing**

Direct Ink Writing (DIW), also known as Robocasting (RC) was originally filed as a patent by Cesarano and co-workers at Sandia National Laboratories in 1997 [21]. The technique was

originally developed for robotic deposition of concentrated materials such as ceramic slurries and pastes with little organic content. A schematic image of the process is presented in Figure 1.8.

Pieces are constructed by moving nozzles to directly ‘write’ the defined shape layer by layer until the part is completed. Debinding and sintering then follow, so the part is completely ceramics, free of organics. DIW enables a cheaper and faster manufacturing process compared with photocuring 3D printing techniques.

The semi-liquid pastes used allow the shape to be maintained thanks to the high solid load and viscoelastic properties. Therefore, simply freestanding structures with high-aspect-ratio walls or spanning parts can be fabricated without the need for supports (such as powder bed, liquid vat or printed supports), which is very difficult or not possible with other 3D direct printing techniques. [18] Nozzles have a typical size in the range 100 – 1000  $\mu\text{m}$  and, after drying, the material has a high green density (up to 60%), which allows to achieve an almost complete densification upon sintering. The using of fine and dense filaments makes the technology particularly attractive to produce components, based on structural and functional ceramics, suitable for several applications. [11], [12]

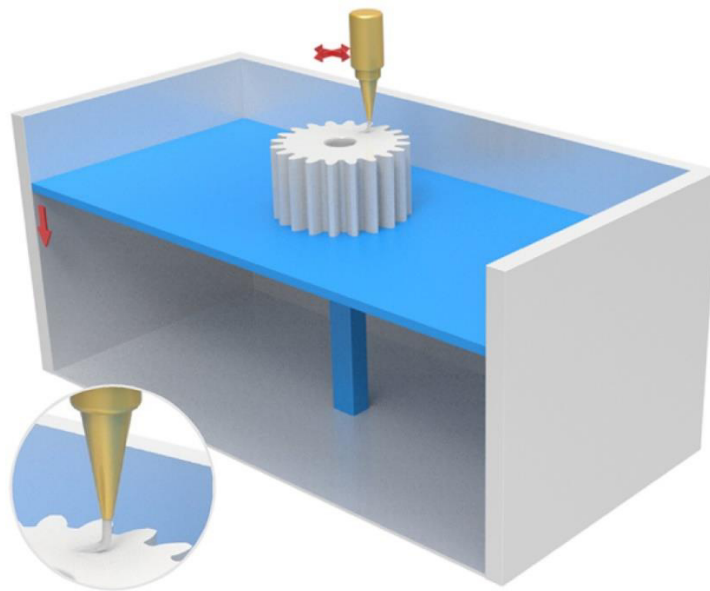


**Figure 1.8.** Schematic diagram of the DIW process, with inset showing the nozzle extruding ceramic feedstock. [18]

DIW is well suited to the fabrication of tailored porous ceramic structures possessing periodic features, with little or no surface quality/resolution needed. Dense engineering ceramics are difficult to process using DIW, thus limiting its applications.

Production of mullite porous meshes and PZT periodic lattices ternary mixtures of BaTiO<sub>3</sub>, BaZrO<sub>3</sub>, and SrTiO<sub>3</sub> are well reported in literature. [11]

Small-sized electronic components as well as woodpile lattice structures have shown considerable prospects in the domains of piezoelectric components such as transducers, bandgap structures such as photonic crystals, catalyst carriers that can be used in energy devices. [18]

Other consistent applications are in electrodes for lithium-ion (Li-ion) batteries, filters for water purification or biofuel catalysis and tissue engineering. Porous structural similarity to bone of calcium phosphate glasses and hydroxyapatite (HA) have considerably boosted research into the fabrication of artificial bone scaffolds. [12], [14]

Different examples of sample are presented in Figure 1.9.

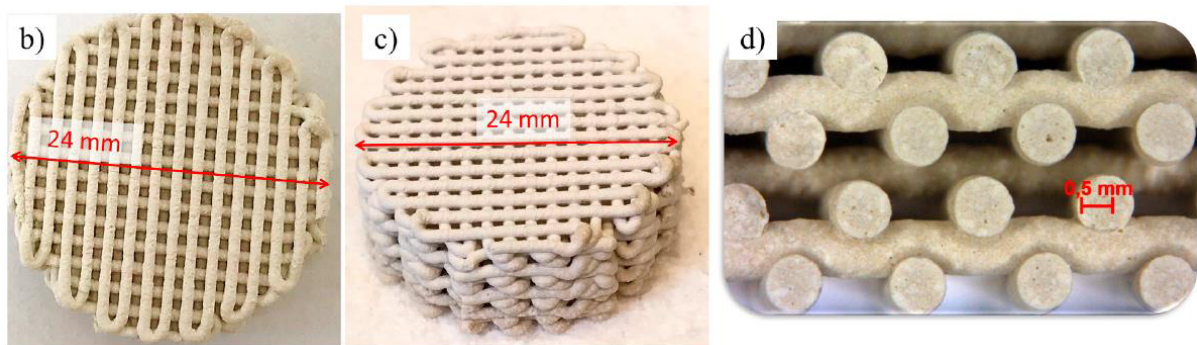


**Figure 1.9.** Graded lattice structure of Na-Geopolymer fabricated using Direct Ink Writing. [22]

As just shown, a great range of different structures can be fabricated using this technique.

A fundamental step is the creation of an ink that can be extruded in from of a continuous filament. It must therefore rapidly solidify to maintain the shape of the printed structures, which is particularly difficult if the filaments pass through the spaces in the underlying layers. The deep study of rheological properties is an essential requirement.

At the beginning, the rapid evaporation of the solvent is exploited to solidify the ceramic suspension with high particle loading. The minimal drying of the slurry, after extrusion in air, converts it from a pseudoplastic to a dilatant behavior. This approach, however, limits the nozzle size to a minimum of 0,5 mm to avoid clogging problems. [11]

A partial solution is the deposition in a non-wetting bath, often constituted by oil, which prevents excessive drying. Other specific ways of achieving the desired rheology can also overcome this issue.

The ideal ink for DIW is a Bingham pseudoplastic fluid, i.e. a fluid that offer an initial yield stress and a decreasing viscosity with the increasing of the shear rate. Such behavior allows an easily extrusion at low pressure and a good shape retention once deposited. This is typical of a reversible gel and can be achieved in several ways. One solution can be the flocculation of a ceramic suspension to form a gel (e.g. by a change in pH, ionic strength of the solvent, addition of polyelectrolytes), or the formulation of a ceramic ink containing addition of polymeric binder and plasticizer. [11], [12]

Extrusion based printing is one of the most used in large scale field, but not all the binding system, developed with DIW, can be used on large scale. Organic additive, debinding and sintering must be avoided on large piece; room temperature inorganic binders (cement-like materials) are the most suitable ones. A brief review regarding the application of DIW printing process in the large scale industry is presented the following pages.

### **SL – Stereolithography**

The SL technique is believed to be the most prominent and popular 3D printing technology and has been extensively used worldwide. It is a process in which a light source of a certain wavelength (usually in the ultraviolet range) is used to selectively photopolymerize a liquid resin in a vat. The resin can be filled with ceramic particles forming a slurry typically including a monomer solution, a photo-initiator, an absorber and dispersing agents; concentrations of 40 – 60 vol% can be achieved. [18] A schematic image of the process is presented in Figure 1.10. According to ASTM this technology belongs to VP category.

Even if SL is an indirect AM process, the material surrounding the part is liquid and therefore it is unable to provide any support. For this reason, depending on the specific geometry of the part, support structures are built together with the part, requiring subsequent removal. The printing process generally proceeds point-to-line, line-to-layer, then layer-by-layer, along with the light scans on the liquid surface. When the first layer is finished, the vat or platform supporting the part being produced is lifted or lowered by the thickness of a layer, depending on whether the building process is being operated in a top-down or bottom-up mode.

Due to the high green densities and the use of fine ceramic particles, stereolithography permits the production of almost dense ceramic parts after a sintering post-treatment; typically pyrolysis to remove organics followed by sintering at high temperatures to reach the packed density, much the same as in conventional ceramic processing routes such as injection moulding. [12], [14]

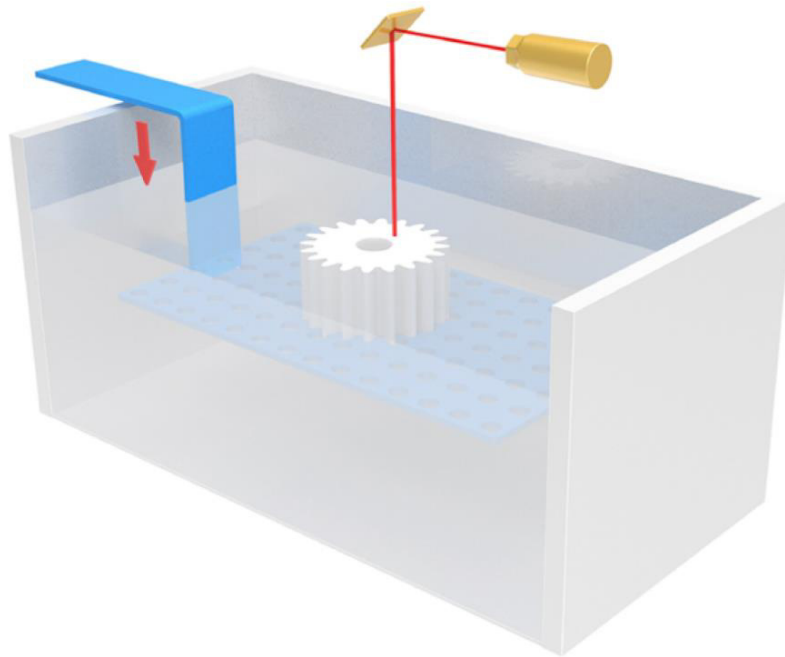


**Figure 1.10.** Schematic diagram of the stereolithography (SL) process. [18]

This technique is been used to produced dense/cellular ceramic parts in a number of fields, ranging from parts with complex structures such as integrally cored casting moulds, microelectronic components such as sensors, photonic crystal (yttria-stabilized zirconia (YSZ) lattices and alumina diamond-like structures). Biomedical implants, such as bone scaffolds and dental components, are other large produced parts by SL wit hydroxyapatite or calcium carbonate solutions. [11], [18], [19]

Different examples of sample are presented in Figure 1.11.

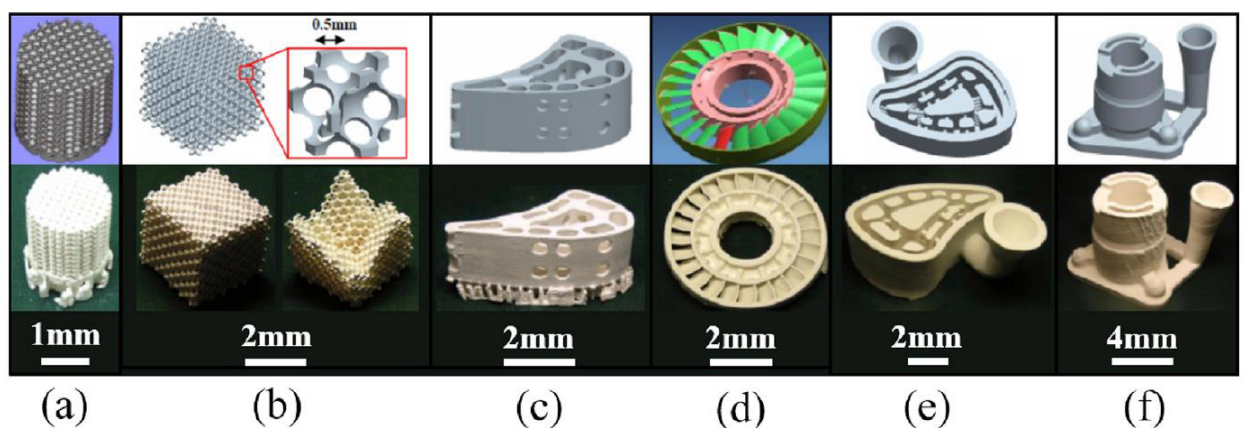


**Figure 1.11.** Advanced ceramic parts fabricated using  $\text{SiO}_2$  via SL: (a) porous bioceramic scaffold; (b) photonic crystals; (c) hollow turbine blade; (d) impeller; (e)–(f): investment casting moulds. [23]



The critical step in achieving full density is de-binding: when it is thermally activated, it transforms the binder and additives into gaseous species which can leave pores and defects behind as they leave the bulk by diffusion. Another fundamental problem that has to be considered is the nontrivial effect of light scattering arising directly from the ceramic particles added into the suspensions, even when the particles themselves are transparent to irradiation. Such scattering is unfavorable to light penetrating into the suspension, but at the same time undesirably broadens the lateral curing area. [14], [18]

This technology is not so suitable for large scale due prevalently to the presence of organic binders and the debinding step, that create problems already in small parts.

### **3DP – 3D printing (powder and slurry)**

3D printing is a powder-based technology, also known as indirect inkjet printing, binder jet printing, selective binder activation, etc. It is similar to the ‘ink on paper’ printing process. The 3DP process consists two repetitive steps: (a) layer formation by spreading dry flowable powder particles, (b) 2D pattern formation by deposition liquid phase selectively (ink/binder).

In the P-3DP process, an inkjet printing head spits a binding liquid onto a powder bed, thus defining the cross section of the object in that layer. Solid layers are formed by the solidification of the permeating liquid binder, which encloses the powder. A new layer of powder is then supplied and spread on the previous layer to repeat the building process until the part is formed. After this, loose powder is removed to reveal the part. [11] A schematic image of the process is presented in Figure 1.12. According to ASTM this technology belongs to BJ category. Different types and formulations of binder can be implemented. Organic binder, that gluing the piece, is removed during sintering, double component binder in which one solid is inside the bed and a liquid activator that is deposited by printing-head, binder derived from preceramic polymer to increment the density, etc. Also, different solutions for the printing -head can be adopted. Multiple nozzles can also be used, allowing to cover a wide printing area. [11] Three-dimensional printing does not require high energy, does not involve lasers or any toxic materials and is relatively cheap and fast. The process can be adapted to suit a variety of powders and to generate the desired pore size and shape. [14]

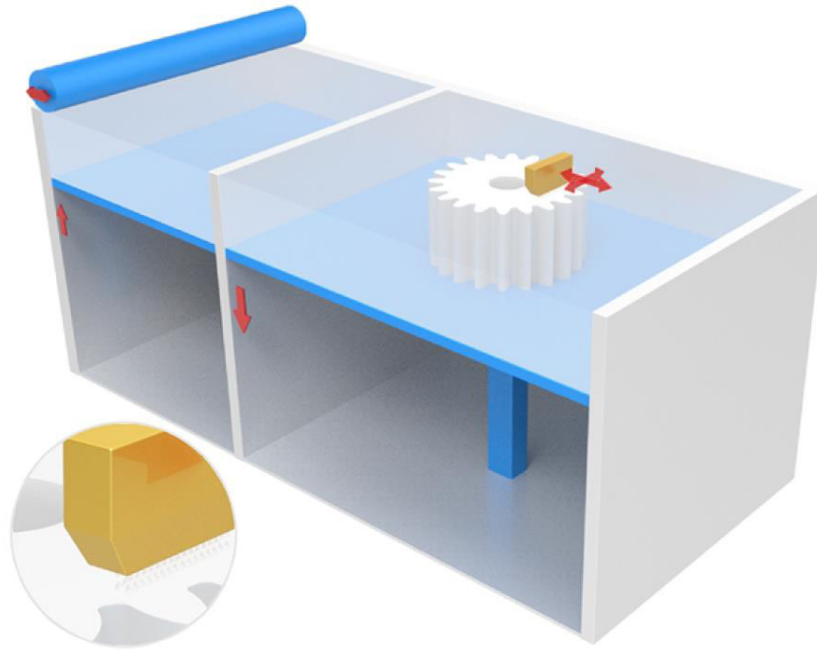


**Figure 1.12.** Schematic diagram of the 3DP process, with inset showing the printhead jetting binder solution on the powder bed. [18]

Due to the high level of residual porosity a lot of biocompatible scaffolds are printed with 3DP. Hydroxy Apatite (HA), calcium phosphate (CP), tricalcium phosphate (TCP), glass ceramic materials are deeply investigated. In the case of dense components are obtained with addition or infiltration of other materials to the primary one: reaction-bonded silicon carbide (RBSiC) ceramics,  $\text{Al}_2\text{O}_3/\text{Cu}/\text{CuO}$  material, TCP with ZnO and  $\text{SiO}_2$  as sintering aids. [14], [18]

An example of sample is presented in Figure 1.13.

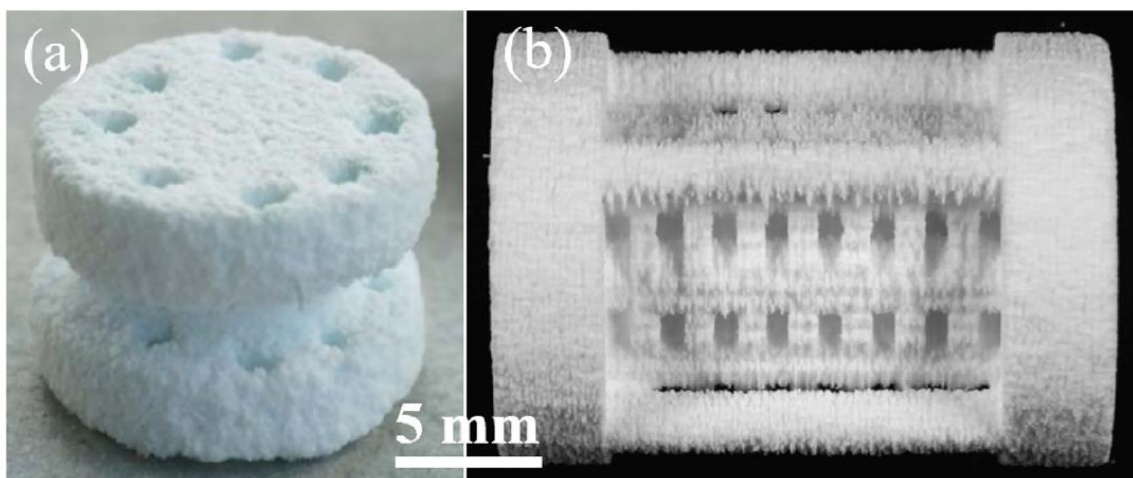


**Figure 1.13.** Scaffolds made by 3DP using biocompatible materials: (a) HA [24]; (b) CP [25].

Summarizing, 3DP advantages consist in the high flexibility of geometrical, no limitation regarding the parts geometry (except for closed porosity) and dimension, design without the addition of supports. Its best application is to the fabrication of porous ceramic parts, without too high mechanical properties. However, limitations of the application of 3DP in the processing of advanced ceramic materials arise as the downsides of this technique, in particular the inferior quality in resolution, surface finishing, density and mechanical performance require extra work, including infiltration and isostatic pressing for further quality improvements. Production of ceramic monolithic parts is only possible for specific material systems, typically involving post-printing infiltration with metals or semimetals. [11], [18], [19]

3DP can be based on slurry bed instead of powder one. A ceramic slurry or slip is used to increase the powder packing density in the powder bed. The release of the part in this case is a little bit complex because the powder compact must be dissolved by a solvent. In case water-based slurries are used for the layer deposition, water can act as a solvent for the powder bed.[11]

This is a second most used technology on large scale field, and in this case not all the binding systems and solutions can be used on large scale. Organic glue, debinding and sintering must be avoided on large piece. Room temperature reactive inks and infiltration pastes (cement-like materials) are the most suitable ones. A brief review regarding the application of DIW printing process in the large scale industry is presented the following pages.

### **SLS – Selective laser sintering (powder and slurry)**

Selective Laser Sintering was invented by Deckard and Beaman at the University of Texas at Austin in 1986 and commercialized in 1992. [26], [27]

A thin layer of powder is spread out and levelled the top surface of the building platform, laser then selectively scans this layer to fuse the forming areas as defined by the geometry of the cross-section of a CAD model and to leave the forming areas as supports for subsequent building. [14] In this way, the process is repeated layer by layer until the designed 3D part is fabricated. No extra support structures have to be intentionally prepared for overhanging regions during an SLS process, as they are surrounded by the loose powder in the bed at all times.[18] The local densification of the powders can be obtained by directly sintering the ceramic powder, or by mixing the powder with a binder phase (inorganic or, more often, polymeric) which is then melted by the laser light.[11] A schematic image of the process is presented in Figure 1.14. According to ASTM this technology belongs to PBF category. Ceramics SLS is complicated by the poor resistance to thermal shock of this class of materials.

Furthermore, poor sintering is favored by the short interaction time between laser and powder that limits material diffusion. Binders within the powder which can be thermally activated, on the other hand, have been successfully used to shape porous ceramic parts. In the context of also this AM technology, preceramic polymers can offer some interesting opportunities. [11]

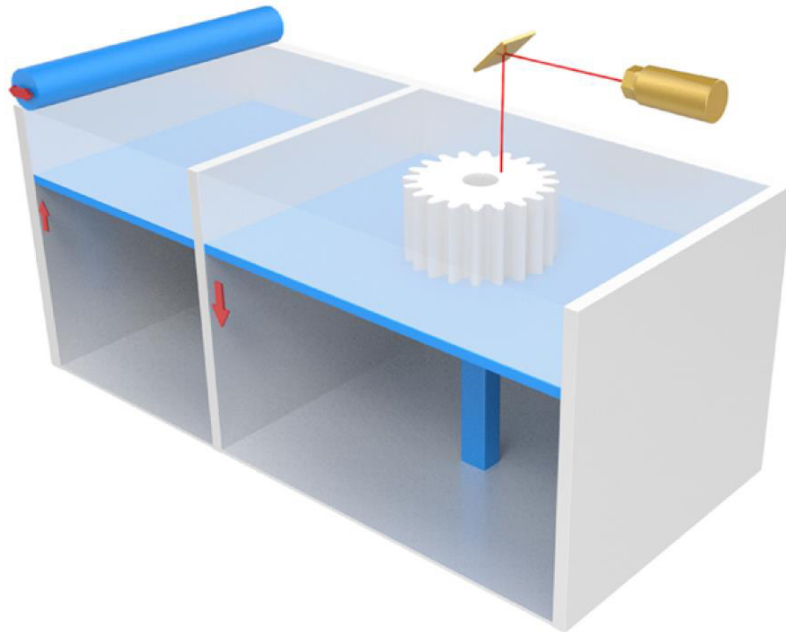


**Figure 1.14.** Schematic diagram of the SLS process.[18]

Materials such as ceramic composites (SiC), biocompatible materials (PEEK/HA, HA/TCP composites) have been adopted to this technique. Laser sintering of zircon sand ( $ZrSiO_4$ ) and silica sand ( $SiO_2$ ) have been employed in industry, while research with ZrSi,  $ZrSiO_2$ , SiC, graphite and other types of ceramic continues. [14], [19]

More recent work concentrates on selective laser melting (SLM), where the formation of a liquid phase ensures rapid densification (use of eutectic mixture). Preheating of the powder bed reduces thermal shock problems. A SLS sample is presented in Figure 1.15.

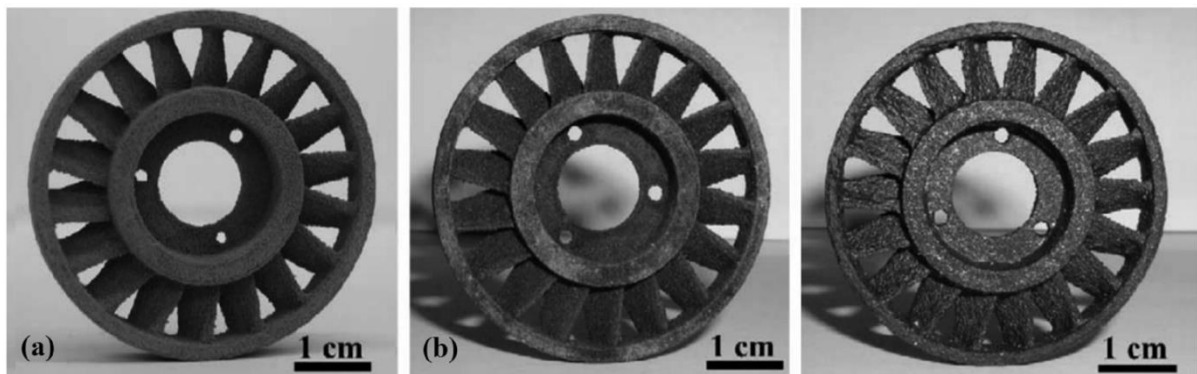


**Figure 1.15.** SiOC/SiC turbine wheel produced: (a) after SLS; (b) after firing; (c) after infiltration with silicon.[28]

Two major concerns in the SLS of ceramics are the high shrinkage of and the high porosity remaining in the final parts.

As for 3DP, also SLS can be based on slurry bed instead of powder one. A ceramic slurry or slip is used to increase the powder packing density in the powder bed. In this case the technology follows a slip casting process, in which the porous body creates the powder compact by capillary force. In Layerwise Slurry Deposition (LSD) process the mold is formed by the previously deposited and dried layers. [11]

SLS process is generally not suitable for large pieces due to frailty of the process, the presence of the laser and the high energy consumption, the shrinkage of the part.

### **DIP – Direct inkjet printing**

Direct inkjet printing (DIP) is a technology which uses a ceramic suspension to build up structures by the successive deposition of individual droplets provided by a moving printing head. Computer-aided high-precision positioning of the droplet jetting allows a point-line-layer-part building process. A proper drying and sintering steps on printing materials are necessary to create the solid ceramic phase. A schematic image of the process is presented in Figure 1.16. According to ASTM this technology belongs to MJ category.

The ceramic suspension, or ink, consists of ceramic particles (typically <30 vol%) dispersed in a liquid carrier containing different additives to stabilize the suspension, adjusts its viscosity and surface tension, and to control the spreading and drying of the deposited droplets. [11], [18]

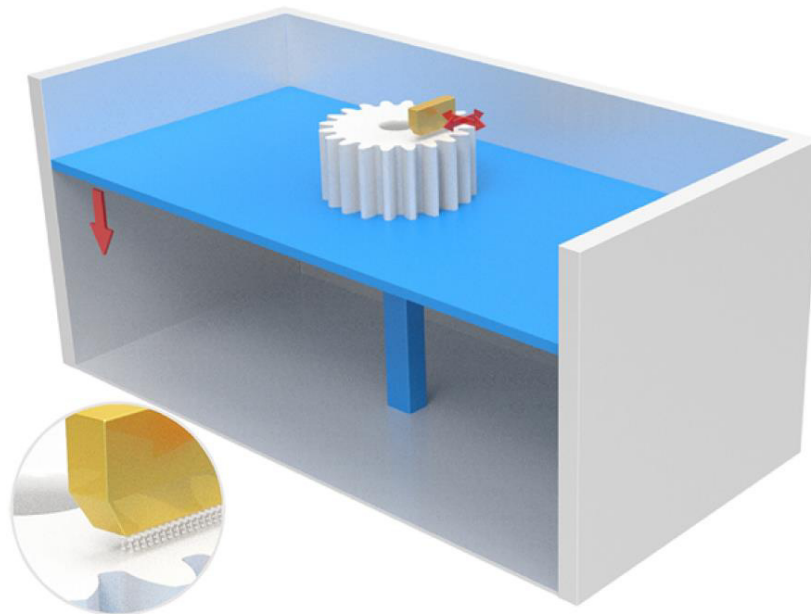


**Figure 1.16.** Schematic diagram of the DIP process, with inset showing the printhead jetting droplets at a higher magnification.[18]

There has been a growing interest in the DIP of ceramic inks for printing parts in various industrial sectors, where the printed components might occur in 2D structures and would not necessarily possess proper 3D features. [11], [19]

Ceramic inks prepared with Zirconia, Titania and Alumina, loading of up to 40 vol%, are used in the fabrication of ceramic parts with a feature size of less than 100  $\mu\text{m}$ . [18]

A DIP sample is presented in Figure 1.17.

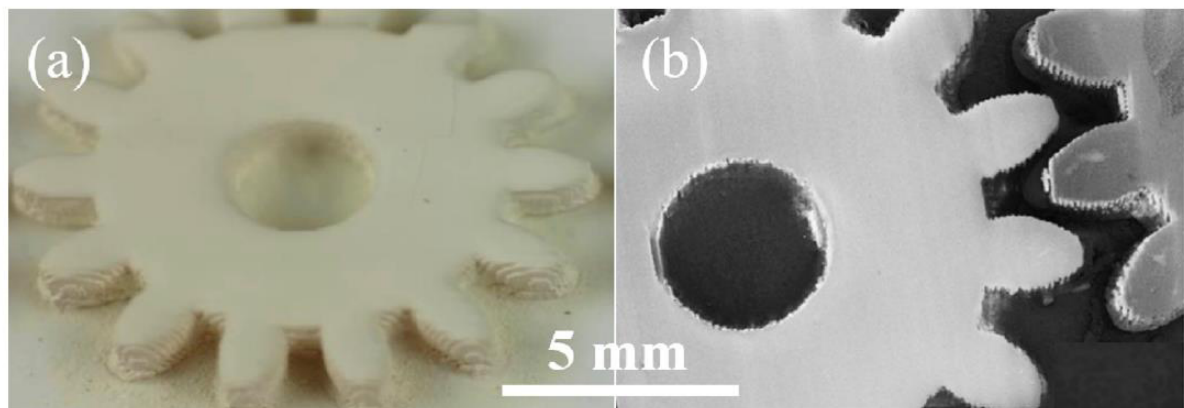


**Figure 1.17.**  $\text{Si}_3\text{N}_4$  gearwheel fabricated by DIP: (a) green part; (b) sintered part. [29]

This process has the potential to produce a wide range of line ceramic contours with high resolution enabling miniature components to be manufactured. It allows functional gradients that are effectively stepless in the direction perpendicular to the printing plane to be produced by ink blending and dilution. Gradients can potentially be made in three dimensions so that both the shape and the composition of an object can be downloaded from the computer. [12], [14]

### **LOM – Laminated object manufacturing**

Laminated object manufacturing (LOM) was developed and commercialized by Helisys Corporation in the USA. Generally, the LOM technique was developed for processing paper, plastic and metal components. In transferring it to ceramic processing, research has focused on using ceramic tapes as building materials. The process generally involves computer-controlled laser cutting of as-prepared thin sheets of materials into cross sections according to sliced digital CAD models and subsequent layer-wise adhesion of one cut sheet on top of another, pre-coated with adhesive agents, to form 3D parts.[11], [18] In one sense, in contrast to most solid free forming processes, LOM is partly a subtractive method because it traces the outlines of the parts

and waste during layer fabrication. [14] According to ASTM this technology belongs to SL category. A schematic image of the process is presented in Figure 1.18.

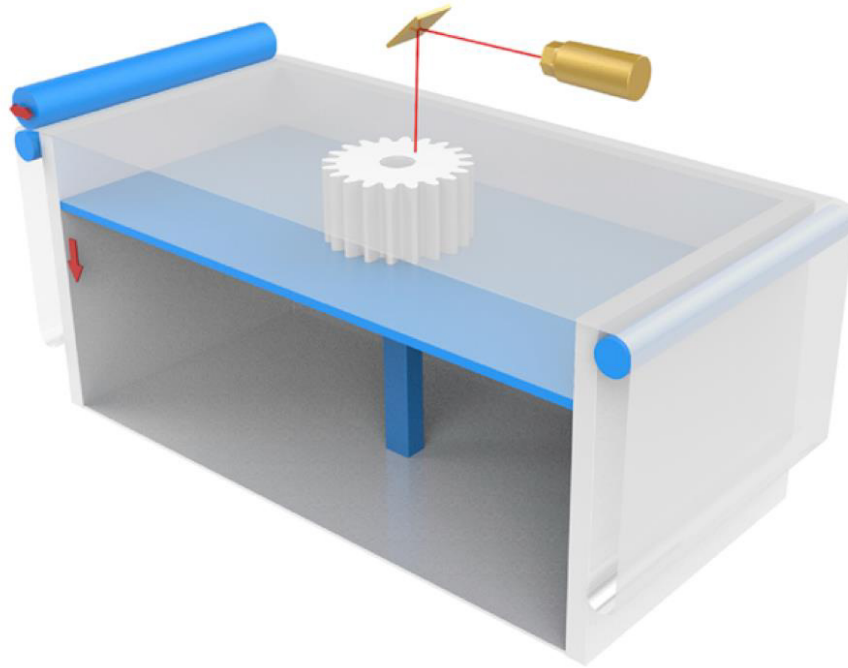


**Figure 1.18.** Schematic diagram of the LOM process. [18]

This technique produces zirconia, alumina and SiC fully dense components, (LZSA) glass-ceramic composite, PZT functional ceramics and HA bone implants. LOM is used to fabricate functionally grade materials or multi-layered composites with alternating composition (e.g.  $\text{Al}_2\text{O}_3$  / Ce-ZrO<sub>2</sub>). [14], [18] The most recent studies use LOM with MAX phase  $\text{Ti}_3\text{SiC}_2$  composite.[19] Different examples of sample are presented in figure 1.19

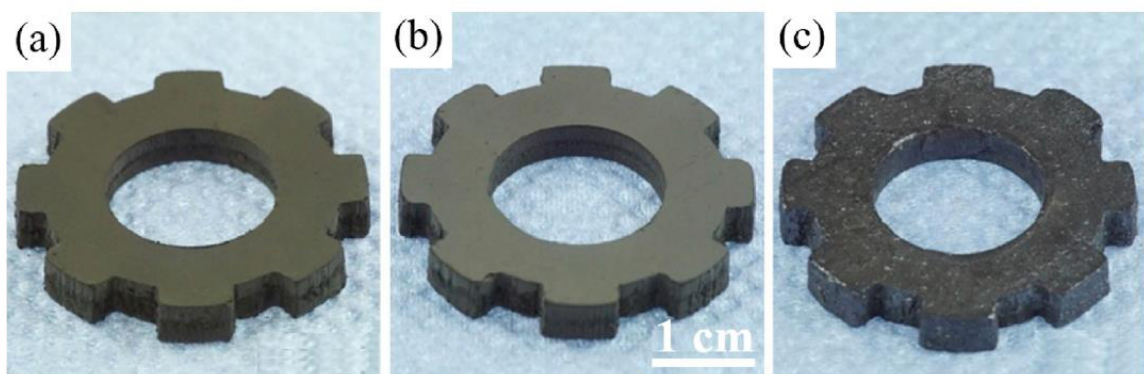


**Figure 1.19.** 3D Gear with MAX phase  $\text{Ti}_3\text{SiC}_2$  fabricated by LOM: (a) green sample; (b) after sintering in Ar; (c) after silicon infiltration. [30]

LOM has the potential of yielding a highly accurate part. The main advantage of this technique is the possibility of using green tapes directly, which in turn are produced by extrusion, tape casting or preceramic paper to produce laminates.

The process does not require higher capillary forces to promote the union between adjacent tapes during thermal treatment and allows the lamination of water-based green tapes, which is not successfully achieved by thermo-compression, for example. [11], [12]

Another advantage of LOM is that two or more types of material with different properties can be added to different regions, creating the conditions to fabricate functionally graded materials or multi-layered composites with alternating compositions. [14]

The applied temperature and pressure are lower, in comparison with low-temperature lamination process, and this prevents delamination caused by an inhomogeneous pressure distribution in complex shapes.

Nevertheless, the main drawbacks of this technology, as in most lamination process, are exactly the quality of the interfaces between tapes, the presence of defects and the limitation in shape, because the surrounding tape material is difficult to remove. Common issues being reported are interfacial porosities, delamination problem and differential shrinkage. [11] For the same reasons this technology is not used on large scale sector.

### **NR - Negative Replica**

Negative replica methods are attractive because they can overcome at least some of the limitations in the physical, functional, and geometrical characteristics of ceramic components produced. A sacrificial polymeric mold or porous structure is printed, impregnated with a ceramic slurry and then the molds are removed. Also, multi-use molds are developed to be filled and give the shape to final objects, similar to the process has long been used for metal castings. After polymer removal (by decomposition, burn-out or dissolution) and sintering, a ceramic component is obtained. However, for complex and lattice structures infiltration is by itself a delicate (this is the reason why AM is a great advantage for such shapes). [11]

Franchin and Colombo (2015) [31] used the negative replica process for manufacturing porous geopolymer scaffolds. The process, as described above, consists in a sacrificial plastic mold fabricated by FDM, and then a geopolymer slurry was infiltrated into the mold. After curing the plastic mold was removed by immersing in strong alkaline solution, and a structure with different pore geometries was obtained. Other studies work on creation of bespoke curved and/or highly complex precast concrete panels and construction elements, that are used to cast



concrete panels. Once the concrete is cured, the hollow molds were melted for recycling. This is the same route followed to use Negative replica in large scale construction materials field.

## **1.2 Additive Manufacturing on large scale and construction sector**

In the very last year Additive Manufacturing is started to be applied also in large scale. While for plastic materials the use is connected to common use piece in various field, in ceramic/inorganic materials field the use of AM in large scale is almost only for construction applications. But in terms of technological development and fulfillment of customer expectation, it can be argued that construction is decades behind other industries such as aerospace, automotive and ship building. [32], [33]

Even if the reach of very high properties is not so easy the use of AM is developed for all the non-structural applications and for artistic and design applications. Nowadays there are also a lot of study that aim to improve the technology in order to be suitable for structural pieces.

The construction industry has become interested and has started exploring proof-of-concept AM applications that could be applied in the sector, looking to mitigate current challenges such as worker safety in harsh environments, decreases in skilled workforce availability, and waste of materials. More broadly, AM is seen as a way of addressing construction productivity challenges. [34]

The AM technology represents a big challenge and opportunity to innovate and evolve the large scale construction sector. The construction 4.0 should become a reality with all its complexity, Figure 1.20. [33], [35]

As already mentioned, large scale AM, dimension in the range of tens of centimeters or meters, is not possible with all the traditional AM technology for ceramics. According to the different binding systems (which means, combinations of ink + material) and also the different process chains, different solution are started to be developed. For example, the BJ can be used with bio-ceramics and cementitious binders. In this case of course the process chain and the materials are different, and consequently the scalability of the process is also different.

For this reason, after the general introduction of large scale field, the specific most developed used technologies will be describe in details (also eve if they are already mentioned in the previous pages).

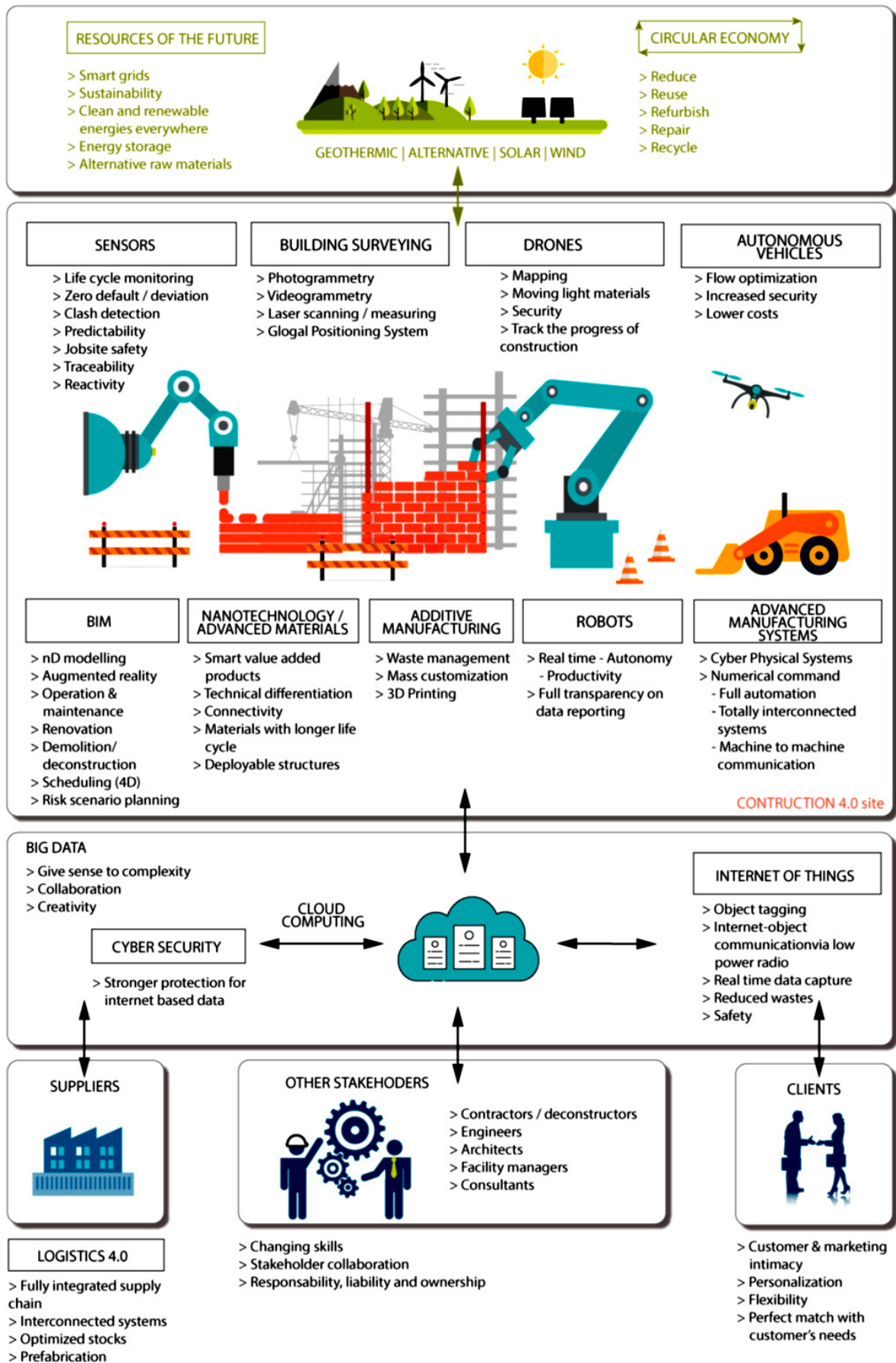


Figure 1.20. The “Construction 4.0” environment enabled by intensive use of digital technologies.[35]

Large scale inorganic pieces are made with one-step room temperature consolidating materials used to aggregate other different powders. Concrete is the most widely used construction material on this planet.

The first challenge for concrete construction industry is the high cost. The significant amount of wastage generated is a second big challenge. Formwork is a significant source of waste since all of it is discarded sooner or later, contributing to a generally growing amount of waste in the construction industry. The problematic role of formwork is even more significant in case of constructing unique objects or complex structures, where the use of formwork is on the one hand challenging (limited geometrical freedom/flexibility) and on the other hand expensive plus time consuming. Significant data, as reported in *Behzad Nematollahia et al. (2017)* showed that the construction industry is responsible for generating approximately 80% of the total waste in the world. [33], [36]

Another challenge is the slow speed of construction (i.e. long and hard to control lead time). The concrete construction often comprises many steps including material production, transportation, and in-situ manufacture of formwork, and each step is time-consuming. And also the safety conditions are another a big issue. [36]

Furthermore, the conventional approach of casting concrete into a formwork limits geometrical freedom for the architects to build in various geometries, unless very high costs are paid for bespoke formworks. Rectilinear forms not only limit the creativity of the architects, but they are also structurally weaker than curvilinear forms owing to stress concentration.

But the biggest challenge, especially nowadays, is the sustainability and eco-friendly approach. In general, the current construction methods and materials are not environmentally friendly. The construction sector is responsible for high environmental impacts worldwide, such as 40% energy consumption, 40% solid waste generation, 38% GHG emissions and 12% water depletion. [33]

The entire construction process, including off-site manufacturing, transportation of materials, installation and assembly, and on-site construction, emits enormous amounts of greenhouse gases and consumes large quantities of energy. [37]

When compared with conventional construction processes, the application of 3D printing techniques in concrete construction may offer excellent advantages including: [33]–[35], [38]–[40]

1. Reduction of construction costs by eliminating formwork.
2. No need for tooling, which significantly reduces production time and costs;

3. Reduction of injury rates by eliminating dangerous jobs (e.g., working at heights), which would result in an increased level of safety in construction.
4. Creation of high-end, technology-based jobs.
5. Reduction of onsite construction time by operating at a constant rate.
6. Minimizing the chance of errors by precise material deposition.
7. Possibility to quickly change designs;
8. Product optimization for function;
9. More economical custom product manufacturing (mass customization and mass personalization);
10. Potential for simpler supply chain, shorter lead times and lower inventories;
11. Increasing sustainability in construction by reducing wastages of formwork;
12. Increasing sustainability in construction by developing easily new sustainable materials;
13. Increasing architectural freedom, which would enable more sophisticated designs for structural and aesthetic purposes;
14. Enabling the potential of multifunctionality for structural/architectural elements by taking advantage of the complex geometry.

AM technologies, not the all, are well suited to bring enormous advantage to large scale and construction industry. Various benefits can be observed in safety, reductions in labor and time, and advances in customization and form. The most interesting industrial advantage is the reduction of the working time and tools necessity, as this can translate to a saving in both cost and time. This reduction in labor should generate both low costs and increased site safety, particularly in difficult or dangerous environments. AM could also minimize costly errors and defects, simplifying the production step and encouraging the off-site modular constructions, reducing the demand of on-site coordination and labor with more benefits design wise as well at no added cost. [32], [35] Different studies evidence in additive construction processes a significant potential to reduce material through topology optimization, produce complex geometries without supporting structures and integrate multi-functionality in building elements, which is not possible with conventional construction techniques. [33] Mass customization and mass personalization are the target. Figure 1.21 shows the advantages of AM in complex shape production.

In addition to these practical aspects, 3D printer also increases the design freedom. For example, the creation of curvilinear shapes in buildings requires special formwork or engineering. This is usually a dramatic increase in expenses and times. AM technologies allow the execution of

new curvilinear and complex designs as easily as the more traditional simple angular structures. This offers a structural as well as an aesthetic advantage. More than that additive manufacturing has been associated with a cost-effective fabrication that lowers energy use, resource demands and CO<sub>2</sub> emissions over the product life cycle.

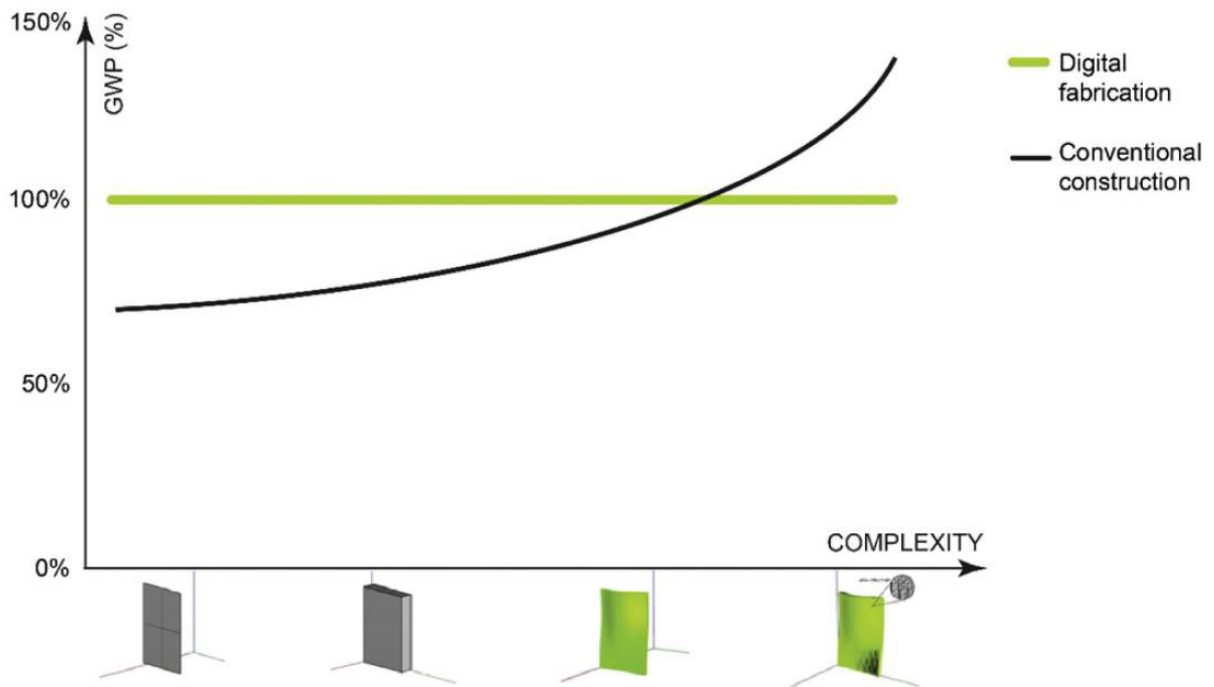


**Figure 1.21.** Complexity-related environmental advantage of digital fabrication vs. conventional construction. The environmental impact is expressed by the percentage of Global Warming Potential (kg CO<sub>2</sub> eq.) per m<sup>2</sup> of concrete wall.[33]

Novel computational approaches integrate structural optimization in form-finding design, offering new possibilities of formal expression and addressing resource efficiency in architecture. Several publications have pointed out the potential of additive construction techniques to reduce the use of material through structural optimization. For instance, high sustainable benefits are related with a more efficient design achieved by placing material only where it is structurally needed, possible only with AM technologies. [33]

However, the evaluation for large scale, with enormous amount of material needs, is not so easy and the recognizably sustainable construction process, life-cycle assessments (LCA) evaluation must be improved to guide the design of 3DP. Nevertheless, the street is surely opened.

It has been noted that there is an exponential rise of technological advancement and attention to 3D Construction Printing (3DCP) since 1997 outlined in a roadmap described by Buswell et al. [38] and Labonnate et al. [39] in Figure 1.22 and Figure 1.23.

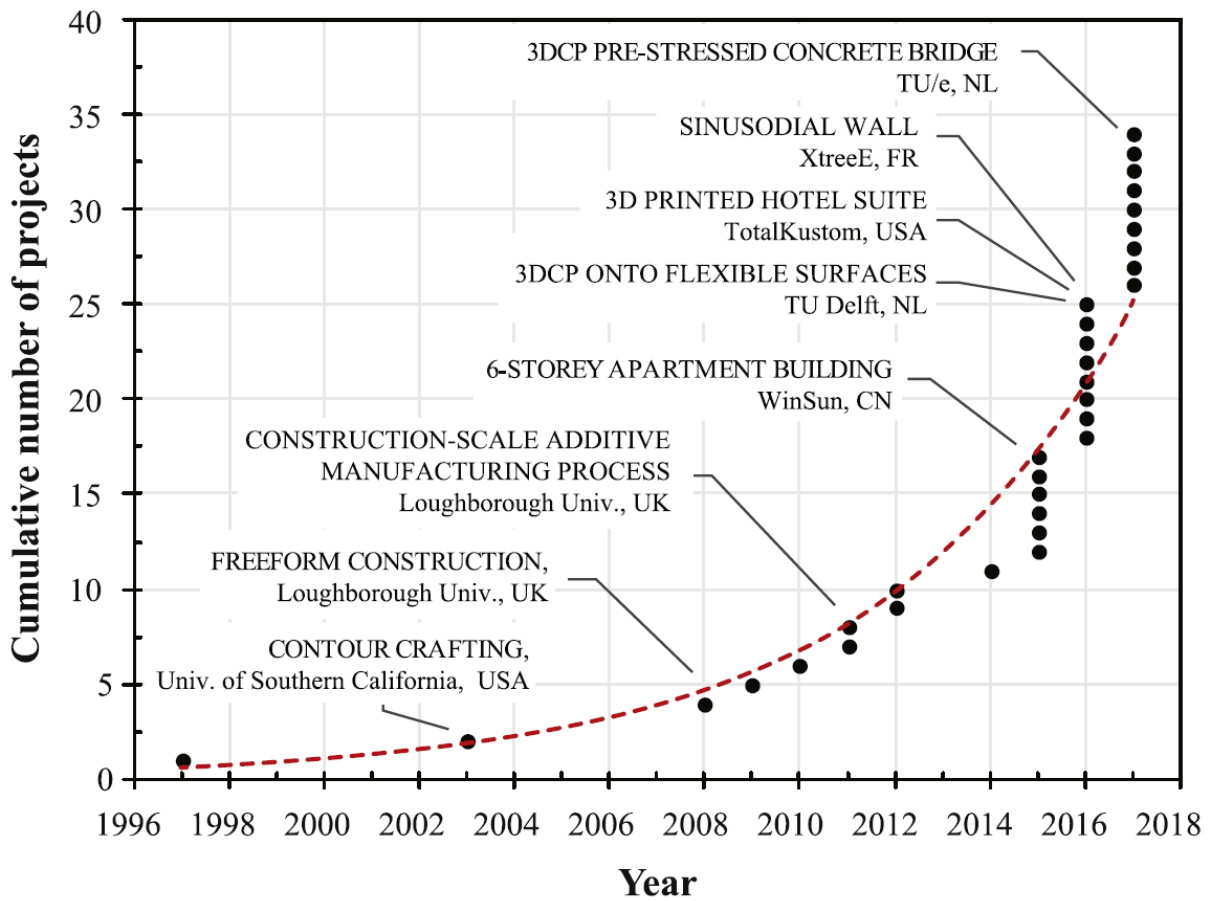


Figure 1.22. The rise in large scale additive manufacturing for construction applications since the concept inception in 1997. [38]

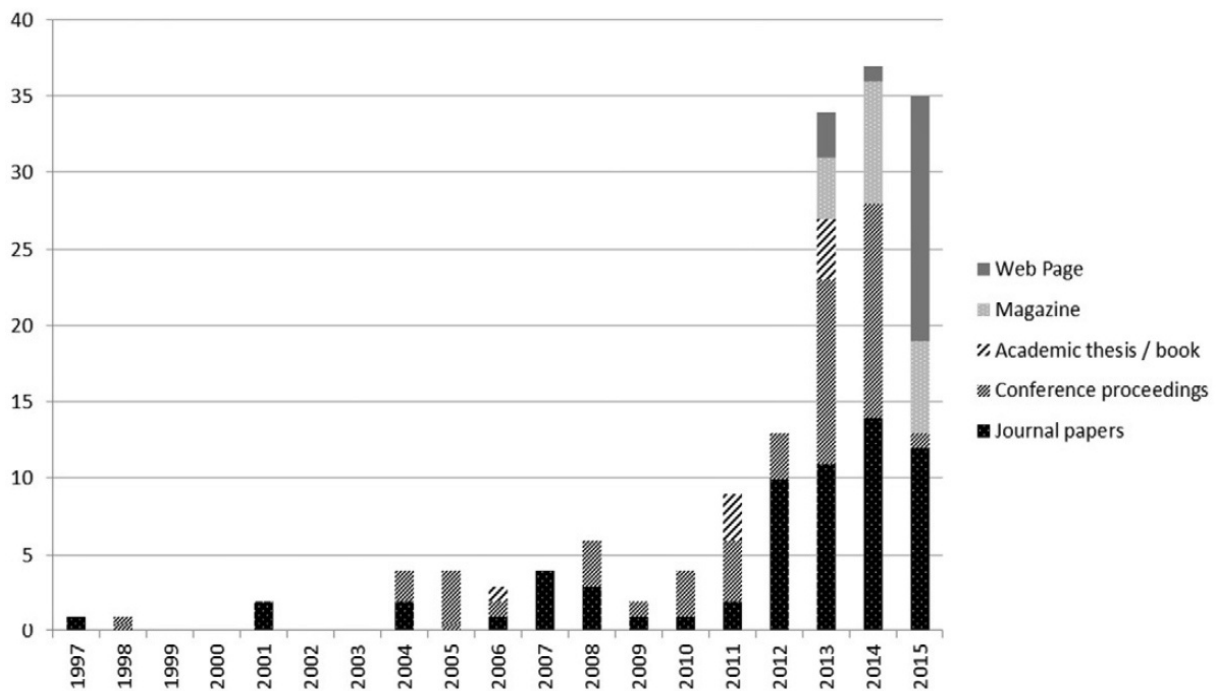
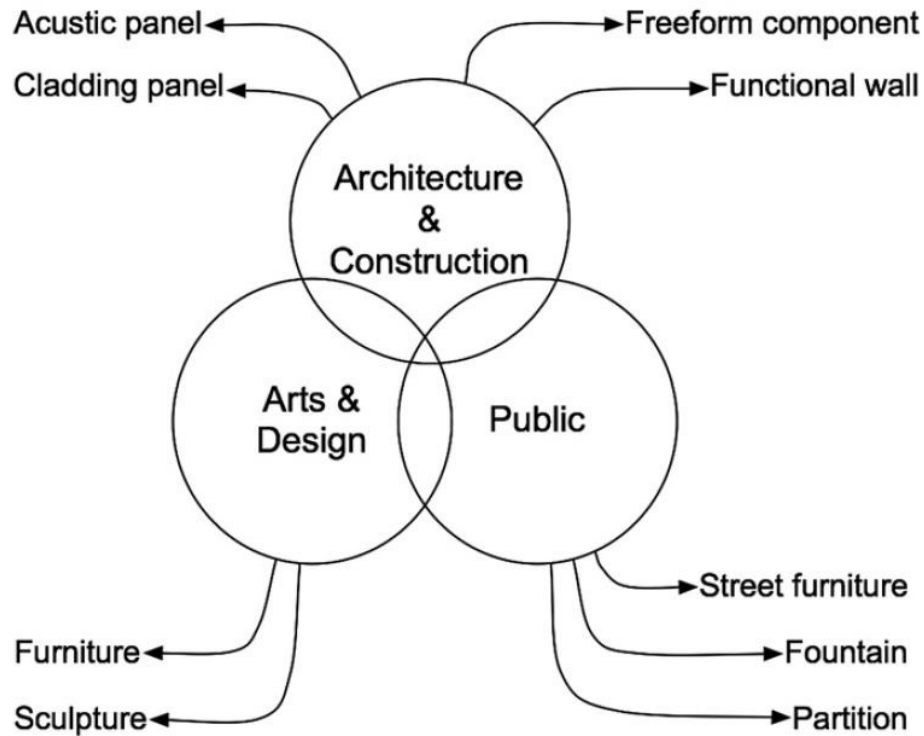


Figure 1.23. Evolution of number and type of publications about large scale AM during the last twenty years. [39]

As well describe above, the large scale technology can be easy used in different fields. Starting from traditional construction and building sectors, moving to more architectural or artistic ones. Figure 1.24 shows a summary of these possibilities.



**Figure 1.24.** Practical applications of large scale AM processes. [41]

All these works are mainly based on two specific technologies, A) extrusion-based (extrusion of paste material placed where required) and B) powder-based 3D printing (dry powder bed onto which the activating agent is sprayed selectively). Negative replica and material jetting are also use in few limited cases.

In the following sections, an overview of the characteristics and application in large scale ceramics/inorganics field is given, also with companies and entrepreneurship developments. The similarities and differences and the pros and the cons of different 3D printing technologies are also highlighted.

### *1.2.1 Extrusion-based 3D printing technology*

The extrusion methodology is probably the main used 3D printing technology for large scale with ceramic and inorganic materials.

The extrusion-based technology is based on the same concept of the direct ink writing (DIW) method which extrudes inorganic paste material from a nozzle mounted on a gantry, crane or a multi-axis robotic arm to print a structure layer by layer.

In this process, the printer core is the extruder fitted with a nozzle of varying size, depending on printing requirements. The nozzle must be continuously charge with a wet mix of cementitious materials. The extruder then moves in a pattern as programmed to deposit out of the head layers of cement

The adopted cement mix must be strongly considered in this approach. There are many requirements that guarantee a good working for this system, including the rate of drying and lap time for each layer, the viscosity of the mixture, strength properties after hardening.

Lim et al. [34] identified four key characteristics of wet-process AM:

- Pumpability: the ease and reliability with which material is moved through the delivery system;
- Printability: the ease and reliability of depositing material through a deposition device;
- Buildability: the resistance of deposited wet material to deformation under load; and
- open time: the period where the above properties are consistent within acceptable tolerances.

Similar issues are highlighted by R.A. Buswell et al. [38]:

- open time, time during which a material may be used in 3DCP, and its influence on pumping and extrusion;
- setting and layer cycle-time, time required to complete one build layer, and its influence on vertical build rate;
- deformation of material as successive layers is added;
- rheology measurements and its importance to quality control (e.g. viscosity which is in turn, a function of the concrete mix composition and water/cement ratio)

Obviously, these parameters are closely interrelated and highly dependent material choice. All the aspects must be studied with parameter sensitivity test programs. [42]

Other considerations include the size of the nozzle and thickness of each layer, the size of the tank that is practicable for the printer, the size of the printer, the transportation of material to the print-head, the precise positioning of the print-head. [33]

The great benefits of extrusion-based 3D printing technique are the ability to upscale and apply on larger applications. This is usually managed with an overhead crane with the printer mounted to it.



Such printers can be used directly outside for on-site construction or even in a factory where components are created and assembled later. A lot of projects and ideas are been developed to show the possibility of an on-site construction.

The first large scale solution is the Contour Crafting (CC) technology, it has been developed by Khoshnevis at the University of Southern California, USA. This technology based on extruding a cement-based paste against a trowel that allows a smooth surface finish created through the buildup of subsequent layers. Generally custom-made reinforcement ties are manually inserted between layers (at every 300 mm horizontally and 130 mm vertically) while the CC machine is constantly extruding the layers. [43], [44]

However, an additional step of troweling the 3D printed layers to produce a smooth finish on the surface is used where this method is focused on large scale fabrication.

The process requires support structures to create overhangs and the surface roughness of printed structures is smoothed out using a trowel. For the fabrication of a door or window, a lintel is placed to bridge the gap between walls, and the upper part of the wall is printed on top of the lintel. The scheme of the process is shown in Figure 1.25.

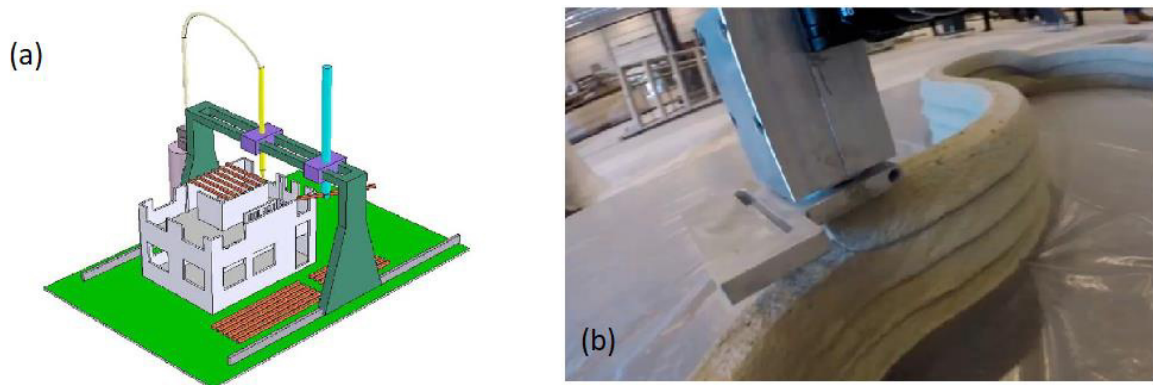


**Figure 1.25.** (a) Schematic idea of CC process; (b) detail of nozzle. [43], [44]

The Contour Crafting technique has been developed to address the issue of high-speed automated construction, and the current deposition head is capable of laying down material to create a full width structural wall with the minimum use of material. It has been validated through the construction of small scale structures and housing scale walls. Materials including clay, plaster and sulfur concrete are used in this process.

The chief advantages of the CC technology are the superior surface finish and the greatly enhanced speed of fabrication. Another key advantage of CC is the possibility of integration

with other robotics methods for installing internal components such as pipes, electrical conductors, and reinforcement modules to enhance mechanical property. [43]–[45]

The main drawbacks for the CC technology are the limiter vertical extrusion, the presence of the initial formwork and of the trowel system, the interrupted sequential casting of concrete within the formwork due to hydrostatic pressure and weak mechanical properties of the extruded concrete may result in weakened interfacial zones between the layers. [46]

Concrete Printing (CP) technology is a gantry-based system developed by a team at Loughborough University in the United Kingdom. This technology also uses the extrusion-based technique, similar to the CC technology. However, the CP technology has been developed to retain 3D freedom and has a smaller resolution of deposition, which allows for greater control of internal and external geometries. [41]

This printer, shown in figure 1.26 (a) creates components by extruding cementitious material through a single nozzle of 9 mm, which is used in conjunction with a softer material to support overhangs and is later removed. Different materials are been tested, such as cement and gypsum mix or high-performance fiber-reinforced fine-aggregate concrete. [41], [47]

Figure 1.26 (b) shows a full-scale piece, *Wonder Bench*, fabricated using Concrete Printing. The footprint is 2,0 m by 0,9 m with a 0,8 m height, and the weight is approximately 1 ton. The bench consists of 128 layers with an average printing time of 20 minutes/layer, and the backside has a dedicated concave-convex surface while the front side has a smoother surface with an integrated seat in order to demonstrate the resolution of the print. The component also demonstrates a reinforcement strategy suitable for large components printed using additive manufacturing. A total of 23 voids were carefully designed to form conduits for the post placement of reinforcement.



**Figure 1.26.** (a) the CP process; (b) detail of reinforced bench. [41]

Concrete Printing requires additional support to create overhangs and other freeform features. The disadvantage of this process is that an additional deposition device is needed for the second material resulting in more maintenance, cleaning, and control instructions and the secondary structure must be cleaned away in a post-processing operation.[41], [47]

The main drawbacks for the CC technology are the trade-off necessary for maintaining its dimensional accuracy makes the process quite slow, the limited vertical extrusion and the necessity of a support material, the use of a gantry system limited the printing area inside the printer. [46]

The 3DCP facility at the Eindhoven University of Technology (TU/e) adopts the Contour Crafting approach. Concrete is mixed with water and pumped into a hose by a mixer pump located on the side of the set-up. The hose is connected to the printer head situated at the end of the vertical arm of a motion-controlled 4 degree-of-freedom (DOF) gantry robot serving a print area of  $9 \times 4,5 \times 2,8 \text{ m}^3$ . [42]

The concrete is forced towards the printer head, an element consisting of several parts allowing the concrete to be printed at the desired location, at the desired speed, and under the desired angle. The end part of the printer head is the nozzle, a hollow steel element with a designated section from which the concrete filament leaves the printer and is deposited on the print surface. [42], [48]



**Figure 1.27.** TU Eindhoven facility and printer. [49]

Several nozzle openings have been tried. Initially, a round  $\text{Ø } 25 \text{ mm}$  ( $491 \text{ mm}^2$ ) opening was used, but resultant round filament, however, was difficult to stack. Then a square  $25 \times 25 \text{ mm}$  ( $625 \text{ mm}^2$ ) section was used. This increases buildability, but also requires the printer head movement to be programmed such that the orientation of the nozzle always remains tangent to the tool path. Currently, a  $40 \times 10 \text{ mm}$  ( $400 \text{ mm}^2$ ) opening is used.[42]

For the research, a custom concrete mix was developed by SG Weber Beamix. The mortar is comprised of: Portland cement (CEM I 52.5 R), siliceous aggregate with an optimized particle size distribution and a maximum particle size of 1 mm, limestone filler and specific additives for ease of pumping, rheology modifiers for obtaining thixotropic behavior of the fresh mortar, and a small amount of polypropylene fibers for reducing crack formation due to early drying. They intensely studied the different parameters, starting from the key assumption that there is a strong interdependency between design, material, print process, and product.[42]

To overcome a part of the limitations of these first approach, a novel one for 3DCP technology for on-site construction, named CONPrint3D, is currently being developed at the TU Dresden, Germany, which intends to bring 3DCP directly into the building sites. [50]

One of the focal points of CONPrint3D is not only to develop a time, labor and resource efficient advanced construction process but also to make the new process economically viable while achieving broader acceptance from the existing industry practitioners.

As a mechanical platform, a modified truck-mounted concrete pump is used. Additional control technology and a newly developed print head ensure the continuous extrusion of the concrete and the geometrical precision on the construction site. Figure 1.28. [50]

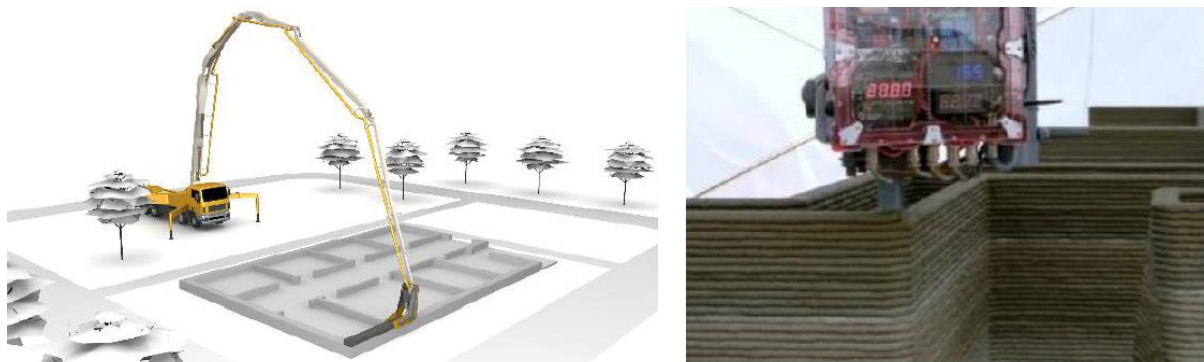


**Figure 1.28.** Scheme of CONPrint3D process on the left; detail of material extrusion on the right. [50]

They test different high-performance printable mortar, with different composition of cement (CEM I 52.5 R), fly ash, micro silica and different particle size sand.

Usage of 52.5 grade rapid setting cement contributed primarily to achieving the high early strengths. In addition, the purposeful choice of proportions of cement, well dispersed micro-silica suspension and fly ash in combination with optimized very fine and fine sands enabled a high packing density of solid constituents, which resulted in both the adequate rheological behavior and the high strength values of the tested material. [51]

Gosselin et al. [46], a research team in France, developed a new technology for large scale 3DCP using ultra-high performance concrete (UHPC), starting from the understanding of the limitations identified in the CC and Concrete Printing technologies mentioned above. The technology uses the extrusion-based technique to deposit UHPC layer by layer through an extrusion print head mounted on a 6-axis robotic arm, Figure 1.29.

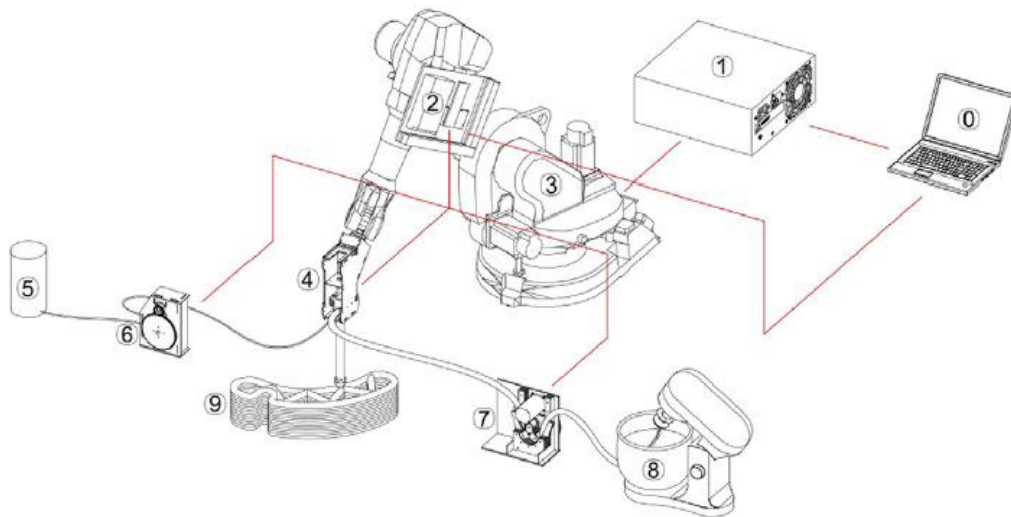


**Figure 1.29.** UHPC schematic process [46]

The proposed technology was used to manufacture a multifunctional wall element and an acoustic damping wall element (Figure 1.30) consisted of an absorptive formwork to be filled either with fiber reinforced UHPC on structural parts or with an insulating material such as foam for thermal insulation.

The premix is composed of original Portland cement CEM I 52.5 N, crystalline silica, silica fume and limestone filler. Once mixed with water in very small proportion the material consists of an ultra-high performance self-placing mortar paste, with an added gripping polymer-based resin for enhancing the quality of interfaces between printed layers, and an accelerating and thresholding agent in order to obtain both the adequate rheology and a setting time compatible with 3D printing contingencies.



**Figure 30.** UHPC printed wall elements. [46]

The main advantages of the proposed technology are: the production of large-scale 3D printed complex geometries without the use of temporary supports, the possibilities of 3D printing by creating layers with varying thickness via the use of the tangential continuity method for slicing, which results in mechanically sounder constructions from a structural viewpoint, the control of geometrical complexity by using on a generic 6-axis robotic arm.

Panda et al. [52] work on developing of 3D printable geopolymers that have never done before for extrusion based large scale printing system. Based on trial-and-error, we obtained a geopolymer mixture that can be extrudable and retain its shape after printing.

From the experimental trails, a printable thixotropic zone was also identified, within which the custom made geopolymer was suitable for extrusion-based 3D printing application.

For printing, a six axis Denso® robot, mounted on a holonomic platform with a rectangular nozzle was used to deposit geopolymer layer by layer, controlled by 3D CAD/CAM program, see Figure 1.31.

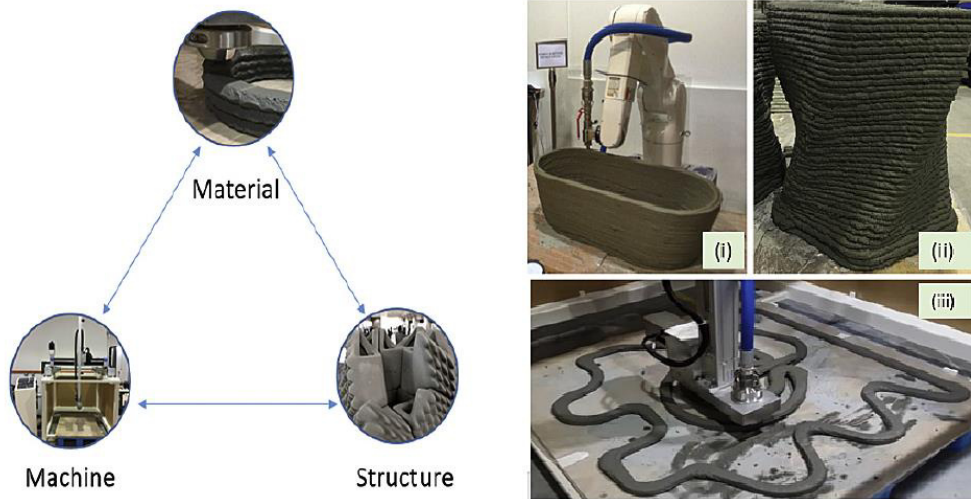


**Figure 1.31.** Geopolymer printing process; (i) bath tub (ii) helix tower and (iii) freeform design by large scale gantry. [52]

They use a geopolymer made by fly ash, GGBS and silica fume blended together, and the addition of thixotropic additives (actigel and cellulose) to achieve no-slump extrudable geopolymer is performed. Then the dry mix was activated by adding alkaline solution (potassium silicate). Soon after, fine river sand was poured and mixed homogenously. At the end, slight addition of water was allowed for getting good workability of the mix.

From the test results, it was found that printed geopolymer samples are stronger in the Y loading direction compare to X and Z directions. To improve this direction strength, addition of reinforcement can be considered in future which may improve the bonding between the layers.

The Institute for Advanced Architecture of Catalonia (IAAC) developed the concept of "minibuilders", using a family of three small robots with a volume of well under 0,05 m<sup>3</sup> for the construction of large scale structures. The robots are shown figure 1.32.

In this case, one or more foundation robots create the footprint of the structure, followed by grip robots clamped onto the footprint to produce the structure, using as support the previously printed layers. The grip robots are capable of printing ceilings and lintels horizontally. Finally, a vacuum robot moves over the printed structure, reinforcing it by applying additional layers. The system is very flexible though not able to print complex shapes and high layer thickness structures. [53]



**Figure 1.32.** Minibuilder robots at work. [53]

The WinSun chinese company has claimed to have printed ten basic houses in a 24-hour timeframe. The size of the 3D extrusion printer used in this project was 150 m (length)  $\times$  10 m (width)  $\times$  6,6 m (height) which enabled it to print large scale buildings within hours using high-grade cement and glass fiber.

In 2015, the company also constructed a five-story apartment block and an 11,840 square-foot (1,100 square-meter), residence (Figure 1.33), which cost \$161,000 to construct. What the company claims are the world's tallest 3D-printed building and the world's first 3D printed large residence are currently on display in China's Suzhou Industrial Park in the eastern Jiangsu province. [54], [55]



**Figure 1.33.** Details of WinSun printed components. [55]



The Apis Cor company, a Russian company, in December 2016 built a whole, functional a 400-square-foot-home house in less than a day. (Figure 1.34) The cost of the building is \$10,000, highlighting just how much potential the 3D printing technology has for the future. The house was built entirely on site using nothing but a mobile 3D printer, which makes all the results impressive. All the walls and foundations of this structure were printed with a concrete mixture and other parts such as windows, fixtures, and furniture being added after construction. The house was finished with a fresh coat of paint. [56], [57]



**Figure 1.34.** (A) Apis Cor printing tools; (b) a printed part. [56], [57]

WASP (World's Advanced Saving Project) company, Massa Lombarda, Italy, developed a series of extrusion based printer, the bigger, BigDelta WASP 12MT (12 meters tall with hexagonal shape), is used in the project Gaia (Figure 1.35). A case study of 3D printed house using the new Crane WASP technology with natural materials from the surrounding area. The Italian company's commitment, since its origins in 2012, has been constantly aimed to the development of equipment for additive manufacturing on an architectural scale.

For the realization of Gaia, RiceHouse supplied the vegetable fibers through which WASP has developed a compound composed of 25% of soil taken from the site (30% clay, 40% silt and 30% sand), 40% from straw chopped rice, 25% rice husk and 10% hydraulic lime. The mixture has been mixed through the use of a wet pan mill, able to make the mixture homogeneous and workable. [58][59]



**Figure 1.35.** WASP Big Delta printer on the left; a detail of printed wall on the right. [58]

In a joint project between Arup, CLS Architetti and CyBe a new 3D printed house, 100 square meter, is printed as part of the Salone del Mobile design festival. Figure 1.36.

The house is made up of 35 modules that have each been printed in 60-90 minutes; the full house has been printed in just 48 hours effective time. The building will be moved from the square to a new location after the festival. A robot from CyBe Construction was used to print the walls, while the roof, windows and doors have been completed afterwards. Italcementi, one of the world's largest cement suppliers, provided advice for the base concrete mix used during the printing operation. [60]



**Figure 1.36.** 3D Housing 05 printed for Salone del Mobile, Milan. [60]

### *1.2.2 Powder-based 3D printing technology*

The powder-based 3D printing technology (P-3DP) was developed in the 1990s at Massachusetts Institute of Technology (MIT), as the other AMs primarily to manufacture small scale ceramic components. P-3DP shows good potentiality also for the development of large scale printing. The powder-based technology creates accurate structures with complex geometries by depositing binder liquid (or 'ink') selectively into to powder bed to bind the powders.

The process consists of several repetitive steps: (1) application and of a layer of dry powders smoothed by the roller or a blade and (2) selective deposition of a fluid phase onto the bed packing by the printhead nozzle(s), causing powder particles to bind to each other. (3) Repeating the described steps, the built part is completed. And (4) finally, the non-bonded particles are removed in a de-powdering process by using vacuum cleaners, air blowers, ecc. (5) When the printing part is extracted and cleaned, the strength and durability of the product can be improved by different post-treatment, such as infiltration, ageing, heat treatment.

This technique is an off-site process designed for manufacturing small-scale building components (compared with an entire house). It is highly suitable for direct printing component (panels, wall parts, interior structures), reusable formworks, permanent formworks which forms a composite with the poured concrete, that can be assembled on site. Figure 1.37. [61]

In comparison with the extrusion-based 3DP process, the powder-based printing does not restrict the design of the form. Due to the possibility of producing components with fine details and intricate shapes, P-3DP is also used to artistic opera or design and architectural pieces. In this process, the unbonded powder can act as supporting structures temporarily. Inclined structures, overhangs, and arches can easily be realized. Another advantage of this process has a much higher resolution than the extrusion-based 3DCP process due to possibility of defining both large and small layer thickness and using fine powder particle size.

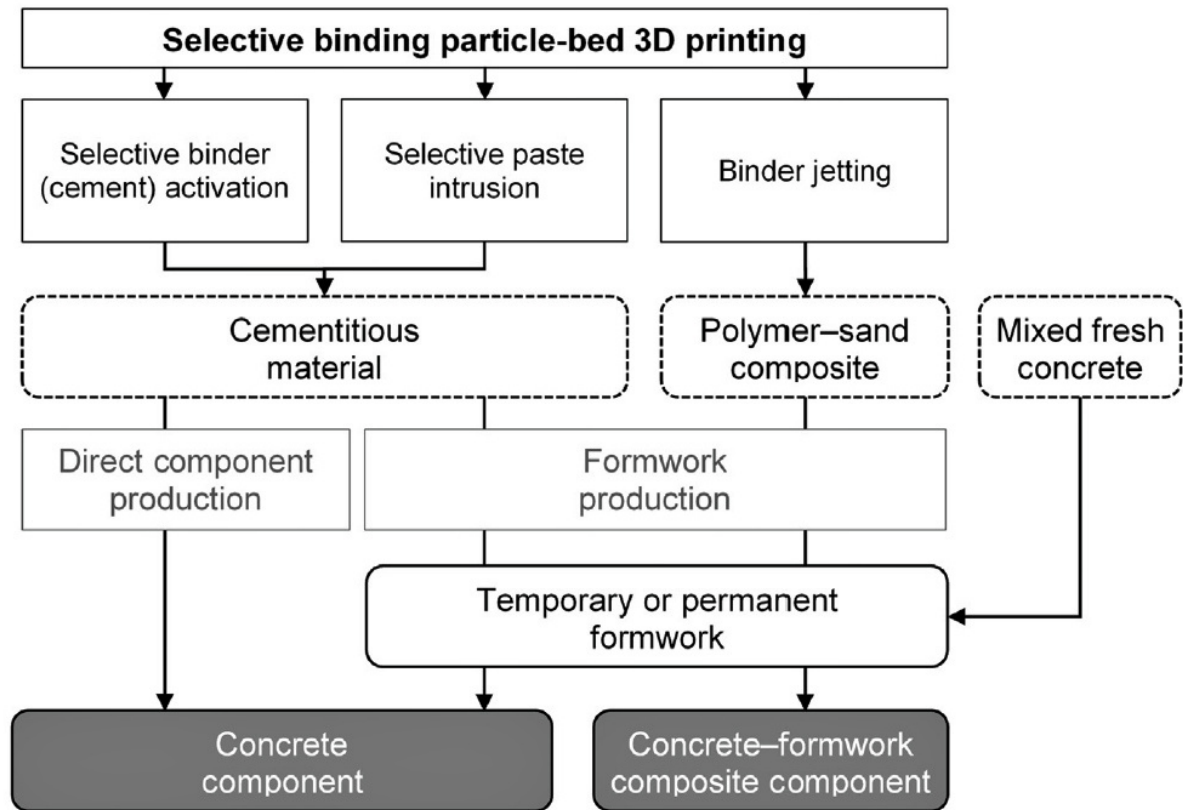
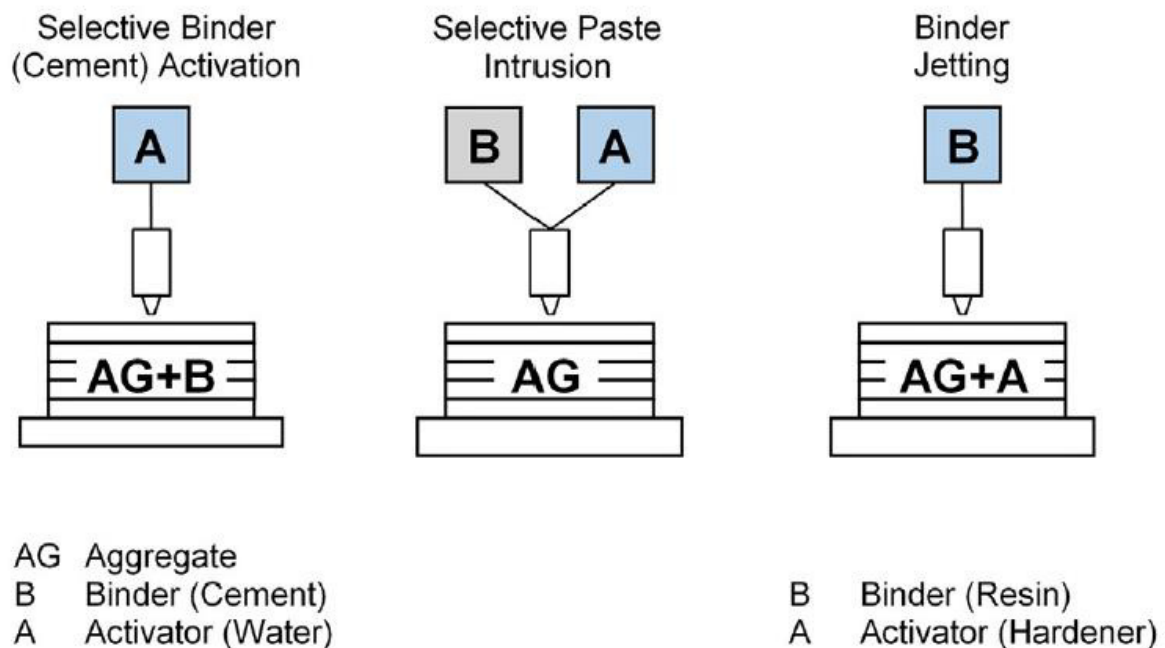


Figure 1.37. Powder-based 3DP and printed components types. [61]

Following the same general process, approaches with little different can be founded, according to the materials used for the printing process, as well described by Lowke et al. [61] and shown in Figure 1.38.

- Selective binder activation (cement): in the selective binder activation technique, the powder bed consists of a dry mixture of very fine aggregate (typically sand <2 mm) and binder. In the case of concrete components, cement is used as binder. The cement is locally activated by spraying or jetting water or a water admixture solution into the packed particles thus forming a cement paste matrix around the aggregate particles.
- Selective paste intrusion: in this case, the particle bed consists of aggregate particles (typically with an average diameter  $\leq 5$  mm) without binder. The binder paste consists of cement, water and admixtures and is applied to the particle bed by means of nozzles. The cement paste must fill the voids between the particles to produce components with a sufficient strength.
- Binder jetting: in the binder jetting technology, a liquid binder is applied to a particle bed. When formworks are printed the binder is typically a resin which reacts with a hardener component in the sand bed.



**Figure 1.38.** Schematic figure of powder-bed 3DP in construction field. [61]

In P-3DP both the aggregate powder, the binder and the liquid must be strongly considered. There are many requirements that guarantee a good working for this system, including powder particle size distribution, binder consolidation reaction and setting time, liquid viscosity and behavior, bed surface quality and final bed density. The other important point is the printer itself, large dimensions printer needs a complex structure, especially for managing, depositing and containing the powders. In the powder-based 3D printing process, incorporating reinforcement into the printed component is quite a challenge due to nature the printing process itself. The last important aspect is the general needs of post-processing treatments.

After de-powdering process, a part ('green part') in which the powder particles are generally bound together by weak binding force, is obtained. The "green part" has usually high porosity and not complete reactions and thus need to be further post-processed to form a densified and reinforced piece. A typical apparent porosity of the green sample before post-processing is in the range of 35% - 55%.

Impregnation and infiltration are the most common post-treatment procedures for cementitious materials. The infiltrating materials should have enough fluidity and viscosity to flow through the open pores with the 'green' sample; a low contact angle with the bulk material makes more effective the operation. On large scale 3D printing the process become obviously even more complicated. [12], [44], [61]

The first large scale solution in powder-bed filed is the D-Shape technology developed by E. Dini starting from 2007 and shown in figure 1.39. The former idea that a conglomerate building block, or even an entire building structure, might be obtained by scaling up the powder-bed 3DP process traditionally used in Z Printer by ZCorp, moving to coarse particles and a volume of liquid in the order of millimeters instead of pico-liters (ink-jet printers), using traditional cementitious materials. [62], [63]



**Figure 1.39.** D-Shape printer. [62]

The printing machine is a sort of gigantic plotter, with a spraying head which moves along two frames in the x–y axis space and selectively sprays on predefined areas of the sand layer a binding liquid a. A set of four stepper motors move the horizontal aluminum frame on the z-axis. The frame contains a print head with 300 nozzles at 20 mm intervals and a blade to spread the sand was placed. To fill the gaps within the array of nozzles and to ensure that the whole cross-section would be uniformly reached by the fluid, each layer was produced in multiple passes with an 5 mm offset of the print head. [63]

D-shape use as binders Magnesium oxychloride cement (also known as Sorel Cement) and additive/admixed ordinary Portland Cements (OPC). The first binder uses magnesium oxide as dry powder in the bed and magnesium chloride hexahydrate dissolved in water as liquid deposited. The second one traditional OPC 32.5 R as dry powder in the bed and water as liquid deposited.

In 2010 the company produced for the Triennale Milano the first one-shot-printed house ever, *UnaCasaTuttaDiUnPezzo*, designed together with the architect Marco Ferrari, Figure 1.40.

The Design was kept very simple to mean the concept of a house: four wall and a roof and it was built in one go with our 3D printer, it's 2,40 m x 4 m.

It contains the bathroom and a kitchen space and bedroom. Printing the house toke three weeks work. It was exposed at Triennale di Milano and now is on the top of a hill in the property of architect Ferreri.[62]



**Figure 1.40.** UnaCasaTuttaDiUnPezzo printed by D-Shape. [62]

Different research projects, by university and research center, have started to investigate the developments of printable cementitious materials for powder-based 3D printing (often in medium scale using a Z-Corp printer), but not so many are already become independent consolidated industrial process (most of them are feasibility studies on the materials).

In 2010 gibbons et al. [64] investigated the feasibility of generating three-dimensional (3D) structures directly in rapid hardening Portland cement (RHPC) instead of plaster of Paris (poP) using piezoelectric printer technology (Z-Corp, model Z402) for the production of specimens with a layer thickness of 0,1 mm, Figure 1.41.

Hydraulic cements would have many advantages: the wide range of cement chemistries, the customization of the properties modifying raw materials and their ratio, the room temperature stable reaction (less post-treatments). Organic modifiers like carboxymethylcellulose, polyvinyl alcohol and glycerol (< 5% by weight) were added to powder and/or liquid reactants to help optimize the resolution and robustness of the green (uncured) printed forms.

The specimens achieved a flexural strength of 2,2 MPa after 26 days immersion under water and 0,8 MPa after 1 day under water. The low strength of the developed RHPC powder limits its use for construction applications.

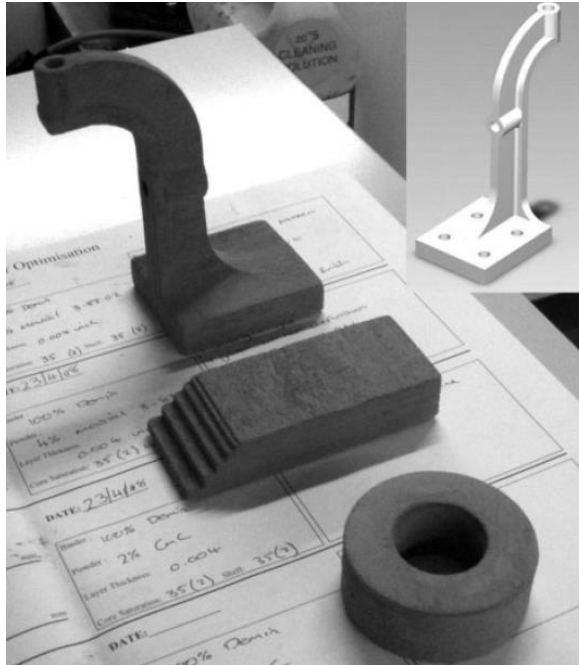


**Figure 1.41.** Demonstration 3D printed parts. Large bracket is 125 mm high. Inset: CAD model of bracket. [64]

In 2011, Vorndran et al. [65] presented a study on MgP based powder–binder systems with regard to their setting time, powder density and spreading property as well as compressive strength and degree of conversion of the setting products. The aim was to study materials that may find application as biodegradable bone substitutes or may be used for the rapid manufacturing of molds for metal casting.

Farringtonite ( $Mg_3(PO_4)_2$ ) powder is the starting point. In a first step, powders were synthesized by sintering and subsequent grinding. Then the ground powder is used in pure state as well as blended with 1 wt-% hydroxypropyl methylcellulose (HPMC) and depending on the applied binder (2M  $K_2HPO_4$ , 0,5M  $(NH_4)_2HPO_4$  or 20%  $H_3PO_4$ ) hydraulic matrix of either struvite-(K), struvite or newberyite were obtained. The best samples are the one with HPMC addition, which swelling prevents the spreading of the liquid and thus allows printing of dimensionally consistent samples. After printing the compressive strength are low due to the small degree of conversion. However, a post-hardening by immersion of the samples in cement liquid for up to 2 h, has increase the compressive strength to 10 MPa for struvite and 35 MPa for newberyite.



Shakor et al. [66] studied a unique mix of cements to be printed with a water-based binder using a Z-Corporation 3D printer. The aims were to firstly, find the proper cementitious powder close to the targeted powder (Z powder); and secondly, evaluate the mechanical properties of this material. The mix consists of calcium aluminate cement (CAC) and ordinary Portland cement (OPC). Moreover, some samples were added lithium carbonate to reduce the setting time for the cement mixture. Cubic specimens with dimensions of  $20 \times 20 \times 20 \text{ mm}^3$  were fabricated and cured with varying saturation levels to measure the compressive strength and determine the pore size distribution of the 3D printed powders, were cast and in various scenarios to enhance the best mechanical properties. The mechanical properties vary from 1 to 4 MPa according to saturation level. Results show that by increasing the saturation level of 3DP specimens, compressive strength values increase gradually while the total porosity decreases. The best conditions bring the strength to 8 MPa after 28 days of curing.

A similar study is been performed by Xia et al. [67], [68] using a geopolymer-bade material as reactive binder for construction applications. Geopolymers are synthesized by activation of an aluminosilicate source (metakaolin, fly ash and slag) with alkaline activators.

Geopolymer mix with different slag to fly ash ratios were investigated in this study. To prepare each mix, the alkaline activator beads were firstly, then fly ash, slag, silica sand and the ground activator powder were thoroughly dry mixed in a Hobart mixer to achieve a homogenous mixture. An aqueous solvent (Zb<sup>®</sup> 63, Z-Corp, USA) was used as the binder during the printing with commercial ZPrinter150 with. A plate structure ( $40.4 \times 40.4 \times 4 \text{ mm}^3$ ) with different pore sizes and shapes was designed to identify the printing resolution. Cubes of 20mm are was printed to be tested. After 6 h of drying within the powder bed, depowering was performed using compressed air to remove the unbounded powder, Figure 1.42.

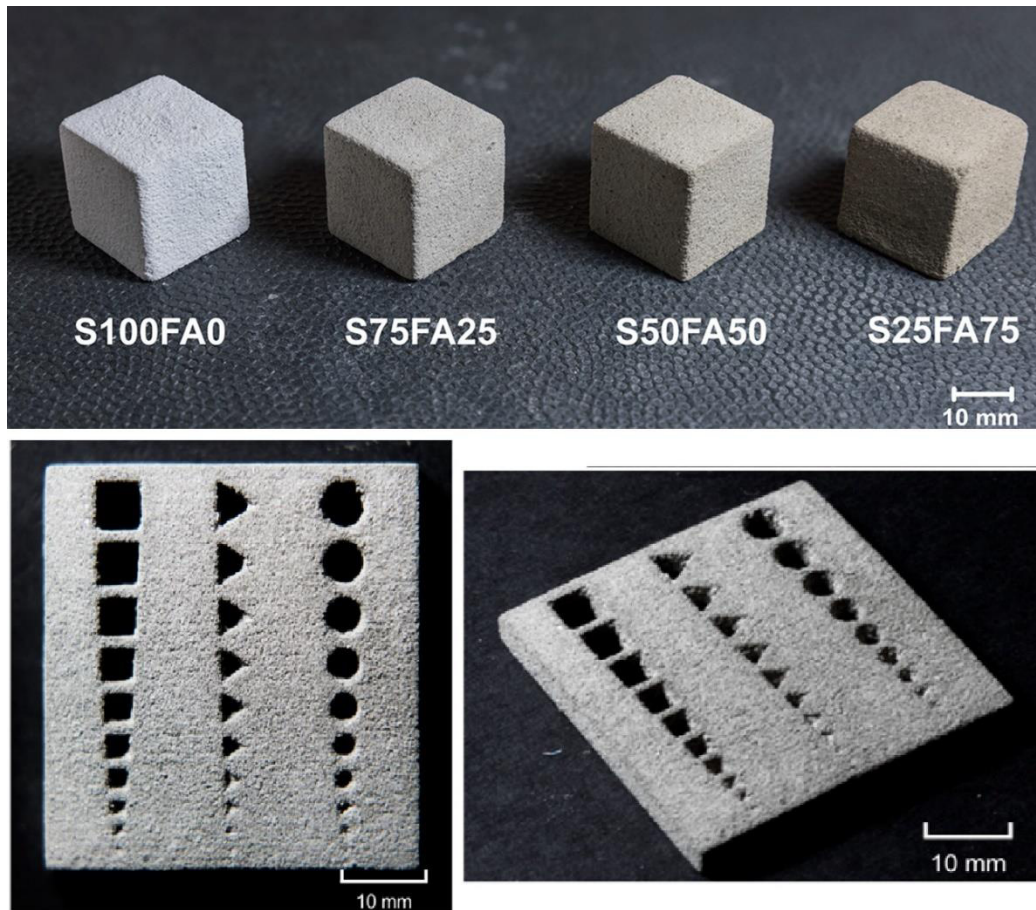


Figure 1.42. Geopolymer printed parts. [67]

The geopolymer-based mixes achieved good results in term of depositability, printability and wettability to be used in a powder-based 3D printer. All printed cubic specimens exhibited an anisotropic phenomenon in dimensional accuracies and mechanical properties. The strength of green part is very poor, around 1 MPa but acceptable to handle the samples with low dimensional expansion of 4%.

So, different combinations of saturated anhydrous sodium metasilicate, N Grade sodium silicate and sodium hydroxide (NaOH) solutions were used for the post-processing of green samples. Post processing by immersion in solution at 60 °C for 7 days gained compressive strength of up to 7 to 26 MPa, depending of the type of post-processing solution and the different compositions considered.

Finally, researchers from the Technical University of Munich has developed a process that use selective paste intrusion (SPI), Figure 1.43. [69]–[71]

This method uses a fluid cement paste to consolidate a layer, with a thickness 3 mm, with relatively coarse aggregate. This method provides the convenience for the recycling of unbound

particle bed because moisture in the air does not significantly affect its property and the incorporation of the relatively large particle, compared with the powder-based 3D printing method, may decrease the material cost in the large-scale construction applications.

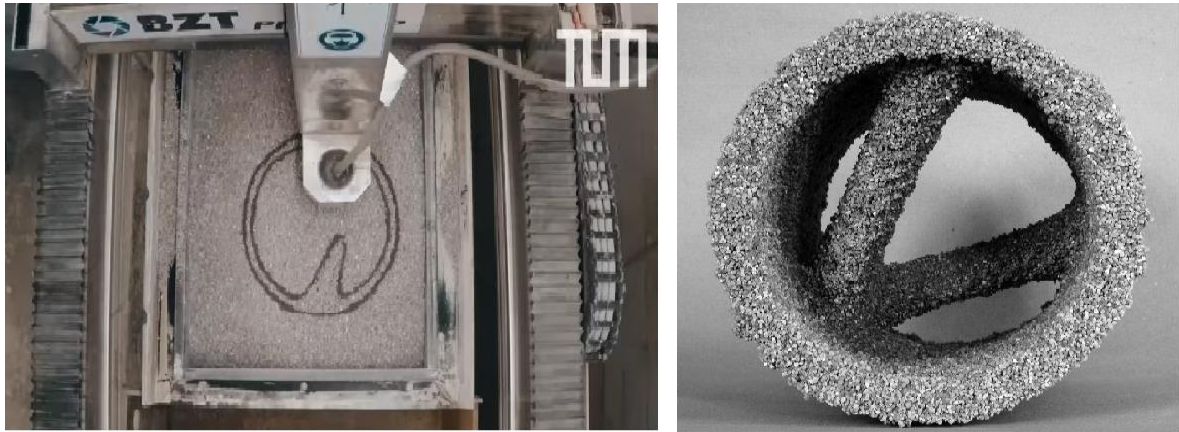


**Figure 1.43.** SPI process and the relative printed object. [<https://www.bgu.tum.de/en/home/>]

The main challenge of the selective paste intrusion technique is the control of the paste intrusion into the particle packing. The degree of paste penetration affects strength as well as the shape accuracy of the 3D printed elements. Both the rheological properties of the cement paste and passing resistance properties of the particle bed need to be carefully controlled.

The compressive strength of cylindrical test specimens with a diameter of 50 mm, a height of 51 mm and a w/c ratio 0,40 was 22,1 MPa. The investigations confirmed a dependence of strength on layer filling which was related to the rheological parameters of the fresh paste. [70] Gradually Weger et al. [71] achieved compressive strengths over 70 MPa after 7 d for 100mm cubes. The layer thickness was 3mm and the w/c ratio of the cement paste was 0,30.

Also, durability property was investigated. The samples had no problem with freeze-thaw cycles and with carbonation after storage at an enhanced CO<sub>2</sub> concentration of 2%.

The Voxeljet Company [72] develops a powder-bed binder jetting technique for the fabrication of small and large size elements, consolidating different powders with polymeric resin. This binder jetting technology can be used to create free-form formworks for concrete or artistic pieces. One of the printers has a build area of 4 x 2 x 1 m<sup>3</sup>, Figure 1.44.

According to the customer necessities two different materials can be used. A quartz sand as powder bed with an average particle size of 0,2 mm in combination with a furan resin binder or a phenol resin binder or PMMA as powder bed with an average particle size of 0,055 mm or 0,085mm in combination with a binder called “PolyPor”.



**Figure 1.44.** Voxeljet printer during production. [72]

Using a furan resin binder, a flexural strength  $> 2,2$  MPa can be achieved. With the phenol resin binder, the flexural strength is between 2,5 and 5,0 MPa. “PolyPor” in combination with PMMA generates tensile strengths up to 4,3 MPa.

Under the main focus on design, Hansmeyer and Dillenburger presented a large room of 3,5 m in height called “Digital Grottesque” produced with a binder jetting technique in 2013 [73], see Figure 1.45.

Digital Grottesque consists of two full-scale grottos that were 3D printed out of sandstone. The aim of the project was to find the limit of digital form finding algorithms and visualize the potential of binder jet printing in architecture. The printed object consists of a highly detailed space with 260 million facets, divided approximately 80 individual components and it takes 9 days for the printing and assembling process.



**Figure 1.45.** Digital Grottesque project [73]

The start-up company CONCR3DE [74] uses an “inorganic polymer powder material” in combination with a large scale inkjet 3D printer to fabricate elements for architectural application, restoration and industry. The properties of the part can reach 20 MPa in compression and 5 MPa in tension. The hardened material has a look like sand stone, Figure 1.46.

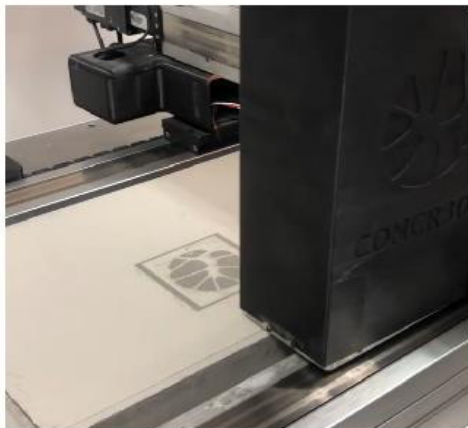


**Figure 1.46.** Concr3de printer during operation and a demonstrative printed part. [74]

### 1.2.3 The current doctoral thesis

As already describe, the large scale AM with construction materials is started to be a reality. This doctoral research focuses on powder-based 3D printing following the technology (materials and process) developed by the company Desamanera srl.

This approach can produce building components with fine details and intricate shapes. It is highly suitable for medium scale (in comparison with an entire building) such as, non-structural architectural components, interior structures, panels but also artistic opera, design structures that then can be moved and assembled on site. The extrusion printing technology is more dedicated to on-site construction applications such as large scale building components with complex geometries.

Table 1.1 makes a comparison, with the more peculiar aspects, between the two approaches.

*Table 1.1.* Comparison between direct extrusion-based and indirect powder-based AM technology.

	<b>Extrusion-based</b>	<b>Powder-based</b>
Printer Components	Robotic, Gantry or Crane system Material delivery system Material deposition system Building platform	Robotic/ Gantry system A dry powder deposition system Binder liquid deposition system Building platform A dry powder recycling system
Object Size	Smaller than the size of the printer with the gantry system Also larger than the 3D printer itself with robotic system	Always smaller than the size of the printer
Printing Resolution	Lower, a layer thickness of few centimeters. (depending of nozzle diameter)	Higher, a layer thickness of a few millimeters (depending on voxel dimension)
Surface Quality	Lower (depending of nozzle diameter)	Higher (depending on voxel dimension)
Build speed	Generally faster (depending of nozzle diameter)	Generally slower (depending on voxel dimension)
Materials	Cementitious and inorganic mortar	Dry cementitious powder and liquid
Self-Support Ability	Lower, possible need of support	Higher, overhangs can easily be realized
Applications	On-site and off-site, small to large scale application	Off-site, components with complex shapes

Desamanera powder-based 3D printing process needs to be developed so that can produce robust and durable components at a reasonable speed to satisfy this industrial demand. Starting already from a good level, especially for the focus on sustainable process and material, the

internal know-how acquired (2 patent application), the collaboration with high level international research center but there is also a big necessity of research on these area (also in technologies general terms). The thesis work has been analyzed the process and printer modification and optimization, the material improvement, both for raw materials selection and used printing mixes, the required post-treatment procedures.

The company profile and technology will be further described in the next Chapter 2.

### 1.3 Binders

In this section an overview of the main inorganic materials used as binder in large scale, construction application is described. After a general introduction of the most used Ordinary Portland Cement and its partial substitutions and additions, passing through the main alternative materials, a specific focus on the materials used in this thesis is been given.

Hydraulic cements are the inorganic binders most widely used in construction and civil engineering with the largest usage in tonnage in the world. Ordinary Portland cement (OPC) is the most common hydraulic cement and its manufacturing rate is rising from 1500 million tonnes in 2000 to over 3 billion tons in 2012.

Ordinary Portland cement (OPC) has established itself a vital and strategic commodity material and such is our dependence on OPC that the annual global cement production has now reached up to 4 billion tonnes due to the rapid infrastructural growth of developing economies. It is estimated that around 50% of world's OPC is consumed to make nearly 11 billion tonnes of concrete per year, while rest is used for mortars, stucco, screeds, coatings, and other applications. [75]–[77]

OPC is made by clinkering the appropriate mixture of limestone, clay or shale, iron oxide and other additives at high temperature (about 1450°C). Normal cement powder has four major components: tricalcium silicate ( $\text{Ca}_3\text{SiO}_5$ ), dicalcium silicate ( $\text{Ca}_2\text{SiO}_4$ ), tricalcium aluminate ( $\text{Ca}_3\text{Al}_2\text{O}_6$ ) and calcium alumino-ferrite solid solution ( $\text{Ca}_2\text{FexAl}_{2-x}\text{O}_5$ ). The resulting substance, called “clinker”, is then ground with a small amount of gypsum ( $\text{CaSO}_4 \cdot 2\text{H}_2\text{O}$ ) into a powder to make ordinary Portland cement. When mixed with water, cement undergoes an exothermic hydration reaction, and then hardens into a amorphous, solid, strong material based on Calcium–Silicate– Hydrate (C–S–H) hydraulic phases.

The chemical reaction in cement saturates the water with calcium (Ca) and hydroxide (OH) ions. The negative hydroxide ions raise the alkalinity of the cement paste to a  $\text{pH} > 12$ , as the water becomes saturated with calcium and hydroxide ions, solid calcium hydroxide and calcium

silica hydrate solids form to precipitate from the solution into the pore spaces. The end products are the same for dicalcium and tricalcium silicates when mixed with water. The rapid reaction of tricalcium silicates in water produces more heat than the slower reaction of the dicalcium silicates in water. However, both reactions produce calcium hydroxide and calcium-silicate-hydrate molecules and heat. [75], [76]

Virtually all the cement produced globally is mixed with sand, aggregates and water, and used to make mortars and concrete. As a construction material, concrete can be cast in almost any shape desired, and once hardened, can become a structural element.

In the last few decades the environmental problems, global warming and ecological changes are become a central issue in all the field of science and engineering (as well as in everyday life). Despite the incremental improvements in process efficiency that have been adopted by the cement industry in recent years, OPC production is still responsible for 5-7% of all man-made global carbon emissions. But not only CO<sub>2</sub> releases from cement processing, but also NO<sub>x</sub> (nitrous oxides), SO<sub>2</sub> (sulfur dioxide), contribute to greenhouse effect and acid rain. More than that cement production contributes to the consumption of natural resources and massive energy large quantities. [75]–[78]

The main sources of emissions in the OPC manufacturing process are in processing filed (calcination) and combustion fuel used to heat the raw materials. Figure 1.47.

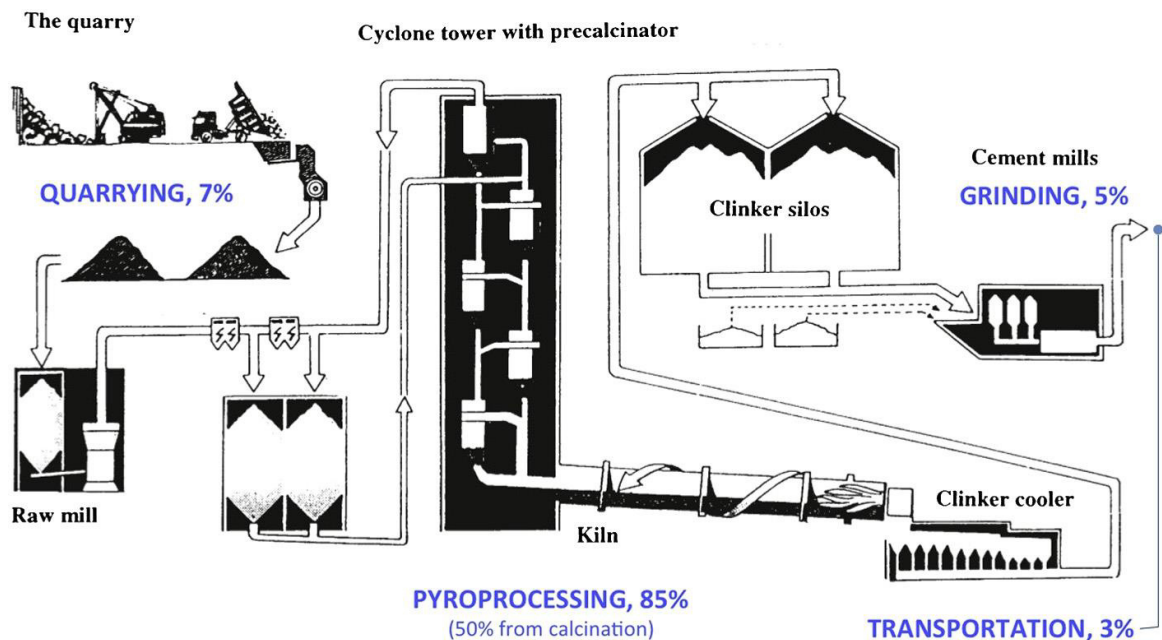


Figure 1.47. Share of total CO<sub>2</sub> emissions across the Portland cement production process [76]



In order to improve energy efficiency and reduce carbon emissions, various approaches have to be adopted: Review and update of manufacturing processes, use and addition of different nature and waste materials, development of novel efficient cements. [79]

Supplementary cementitious materials (SCMs) can be used either as fillers or for their pozzolanic properties. They can either have a natural or industrial origin. SCMs are composed of amorphous aluminosilicates, which react with excessive hydrated lime produced during cement hydration to form calcium aluminosilicate phase C-A-S-H.

The main industrial SCMs are Ground granulated blast furnace slag (GGBS), Fly ash and pulverized fuel ash (FA), ground limestone cement and calcined clay, and silica fume. Figure 1.48 gives a better idea on this products potentiality.

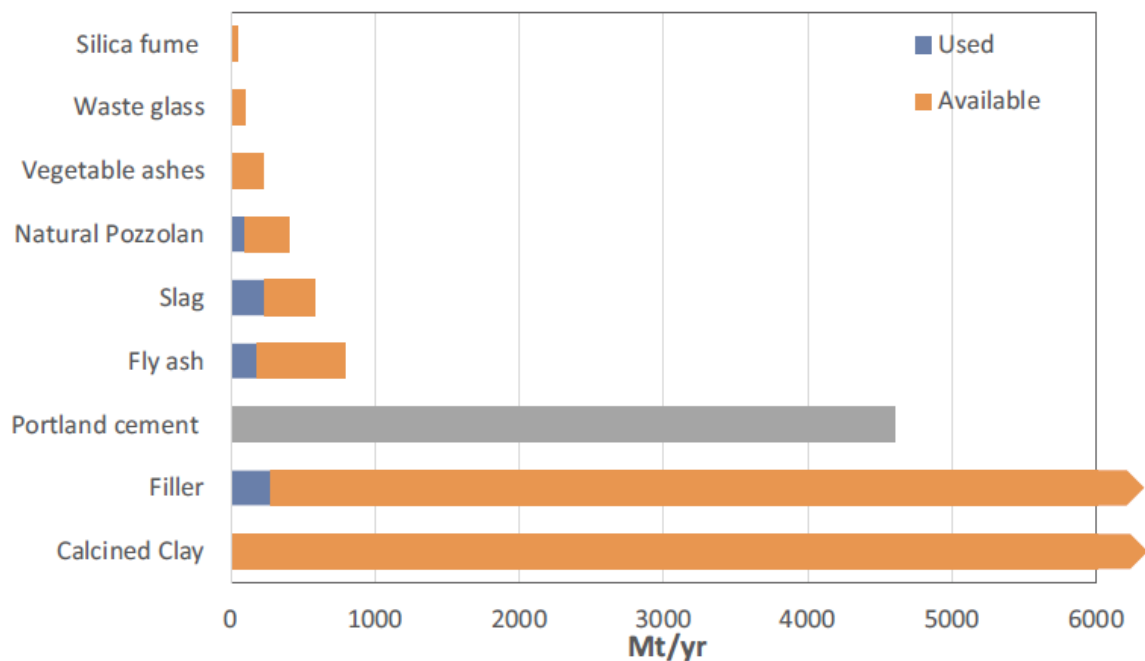


**Figure 1.48.** Use and estimated availability of possible SCMs and fillers. Actual possible use will depend on logistics, exact chemical and mineralogical composition, contamination, local availability of other raw materials, etc. [77]

The alternative binders are studied to introduce different raw materials in clinker and cement manufacturing processes that will emit less CO<sub>2</sub> and utilize less energy without compromising the efficiency and quality of cement. Among the principal alternatives, that are generally in competition each other, we can include green cements and chemically bonded ceramics (geopolymers, oxysalt bonded cements and phosphate bonded ceramics).

- Calcium sulfoaluminate (CSA) cements are types of cements that contain high alumina content and have been used on an industrial scale in China since the late 1970's. The main constituents of the cement powder contain belite phase (C<sub>2</sub>S), ye'elite (C<sub>4</sub>A<sub>3</sub>S), and gypsum (CSH<sub>2</sub>). CSA cement properties can be modulated from rapid hardening

cement to a shrinkage compensated cement when increasing amounts of gypsum are added and it will eventually become expansive and hence self-stressing at sufficiently high sulfate comparison to Portland cement. CSA cement can achieve energy savings as high as 25% and provide environmental benefits by reducing CO<sub>2</sub> emissions by around 20%. But the raw materials cost, high alumina content, increases. [75], [76], [78], [79]

- Calcium silicates cement (CSC) can be hardened by carbonation as well as by hydration. Although using this cement reduces the amount of CO<sub>2</sub> produced during calcination, it is more expensive and less readily available than Portland cement. [76]

Hydration route, materials and production process, is developed by the Karlsruhe Institute of Technology (KIT) and it is based on amorphous hydraulic calcium hydrosilicates (Celitement). But the overall manufacturing process is complex, and this approach is still under laboratory development so no reliable estimates can yet be made for their overall energy- and CO<sub>2</sub>-efficiencies in a real-world industrial context. [78], [79]

The development of special carbonatable calcium silicate clinkers (CCSC) technology has been advanced improving the carbonation process without utilizing excessive energy (Solidia, USA). The need of a specialized curing procedure complicates the process, not allow to protect steel against corrosion in concrete. [78], [79]

- Alkali-activated cements and Geopolymers belong to family of hydraulic cements that are characterized by a high content of aluminosilicates bonding phase. The reaction doesn't start in contact with water but needs an alkaline medium that allow them to hydrolyze and condense forming 3D polymeric structures.

The first alkali activated materials were alkali activated slags, developed and widely used in the Ukraine during the 1970s. [80] The geopolymers are studied and diffused in the 1980s by Davidovits. [81]

They are very competitive with OPC in cost and performance, longer life, better durability, and can use recycled industrial waste. The prime materials used are blast furnace slag, steel slag, metakaolin, fly ash, kaolinitic clays, and red mud. The production emits 95% less CO<sub>2</sub> (if the NaOH and KOH required are assumed to be carbon free). A deeper description of Geopolymer is given in subchapter §1.3.3 because its use in this research work.

- Magnesium-based cements are based on magnesium oxide (MgO) as main reactive ingredient. Using different second reagents different binding system can be developed,

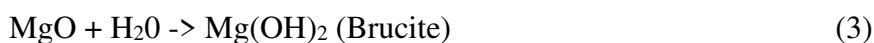
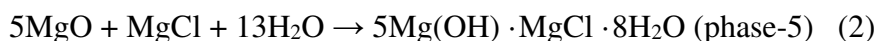
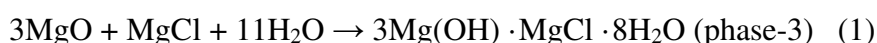
everyone with specific characteristic. In general, MgO-cement requires around 30% less energy to produce and has some significant advantages over OPC, such as permeability and a great strength. Moreover, the setting reaction from magnesia can consume CO<sub>2</sub>, which means this type of cement can act as a CO<sub>2</sub> sink. [78] However, most of the research has been done with MgO produced by calcination of magnesium carbonates, lower temperature than OPC, but for which the emissions are still high. Other MgO source, with much lower CO<sub>2</sub> emission, can be used as basic magnesium silicates or Mg(OH)<sub>2</sub> from saline lake and seawater. Still, the key unresolved issue is to manufacture magnesium oxide from natural magnesium silicates rocks in an energy efficient way feasible to produce on industrial scale.

Different binding system can be developed, everyone with specific characteristic, starting from MgO powder as principal and constant reagent. Magnesium oxychloride cement (MOC), Magnesium oxysulfate cement (MOS), Magnesium silicate hydrate (MSH) and Magnesium phosphate cements (MPCs). [82]

The first, developed by S. Sorel in a 1866 patent [83], is the magnesium oxychloride cements (Sorel cement). The ability of MOC cements to bind and consolidate large quantities of diverse filler materials ranging from granite to sawdust, with good compressive and tensile strengths, has furthered their adoption.

MOC cements are based on the aqueous through the dissolution of MgO in an aqueous solution of MgCl<sub>2</sub>, forming a homogeneous gel from which basic magnesium chloride salts precipitate. The variety of phases, of the ternary system MgO – MgCl<sub>2</sub> – H<sub>2</sub>O, are highly dependent on the precursor molar ratios, temperature and magnesium reactivity.

The most common are:



MOC cements have their principal interest related to the fire resistance of MOC cements, with particular interest in their use as a paintable substrate or internal plasterboard replacement. The ability to incorporate wood filler was exploited to produce “woodstone” panels, which have the appearance of chipboard and the ability to hold screws and nails but are fire-resistant. Their use as flooring and stucco materials present issues with susceptibility to water damage and high costs compared to other traditional products. [82]

Magnesium oxysulfate cements are similar in concept to MOC cements, except that  $\text{MgSO}_4$  is used instead of  $\text{MgCl}_2$ . MOS cements gained interest because of the less hygroscopic nature of magnesium sulfate compared to magnesium chloride. MOS cements are more difficult to form because of the limited solubility of  $\text{MgSO}_4 \cdot 7\text{H}_2\text{O}$  at room temperature and require complex curing process. The development based on sulfates does avoid the use of chlorides, making them significantly less damaging to steel reinforcing, although they still suffer from poor water resistance. These materials are currently use as internal boards or faux-wood panels that can be quickly produced, as well as sprayable fireproof coatings. [82]

Magnesium silicate Hydrate cements are generally formed from a source of magnesium (typically  $\text{MgO}$ ) and a source of highly reactive silica (e.g., silica fume) in situ, rather than forming from the hydration of a magnesium silicate clinker, because magnesium silicates are nonhydraulic. The development MSH binding phase is not so clear yet, but several solid MSH gels with differing compositions can precipitate

The scale up of MSH for commercial cementing applications is very limited. They are partially used as addition of other compounds (extra binding phase for cations in cements blended with blast-furnace slag, which tends to be richer in Mg than is PC).

Recently, MSH cements have been studied for their potential as cements for nuclear waste immobilization, with focus on the less-alkaline pH characteristics of MSH cements compared to PC. [82]

Magnesium phosphate cements are further described in the following specific section.

### *1.3.1 Magnesium phosphate binders*

Magnesium phosphate cements are formed through an acid–base reaction between  $\text{MgO}$  and a soluble acid phosphate (forming a magnesium phosphate salt with cementitious properties. The use of this novel ceramics could be useful for a wide range of applications, such as precursors to sintered ceramics that can be cast into intricate shapes before firing, materials for stabilizing hazardous and radioactive contaminants, structural engineering products, and products for bioengineering applications.

Different species of phosphates can be used to react with  $\text{MgO}$ . Orthophosphoric acid solution,  $\text{H}_3\text{PO}_4$ ; Diammonium hydrogen phosphate,  $(\text{NH}_4)_2\text{HPO}_4$ ; aluminium hydrogen phosphate,  $\text{Al}(\text{H}_2\text{PO}_4)_3$ , ammonium or potassium dihydrogen phosphate,  $(\text{NH}_4)\text{H}_2\text{PO}_4$  and  $\text{KH}_2\text{PO}_4$ .

The last system is the most interesting due to its hydraulic properties and finds application in civil engineering as a material for quick repairs of bridges, roads and other civil engineering

works since it can be worked at room temperature and has a very rapid setting, and recently it is also used in the biomedical field and for the dental prostheses. [82], [84]

The first studies were achieved using mono ammonium phosphate, obtaining a cement to set very fast, widely used between the 1970s and 1980s in the repair of damaged roads and bridges. Despite the initial spread of this type of MPC, the release of ammonia during and after the hardening phase of the cement has caused considerable restrictions for its use, causing it to not take broad foot on the market.

The kinetics of these transformations is very similar to the one in the conventional sol-gel process. The studies of Soudèe and Pèera [85] gave the following explanation for MgO and mono ammonium phosphate (MAP) reaction, Figure 1.49.

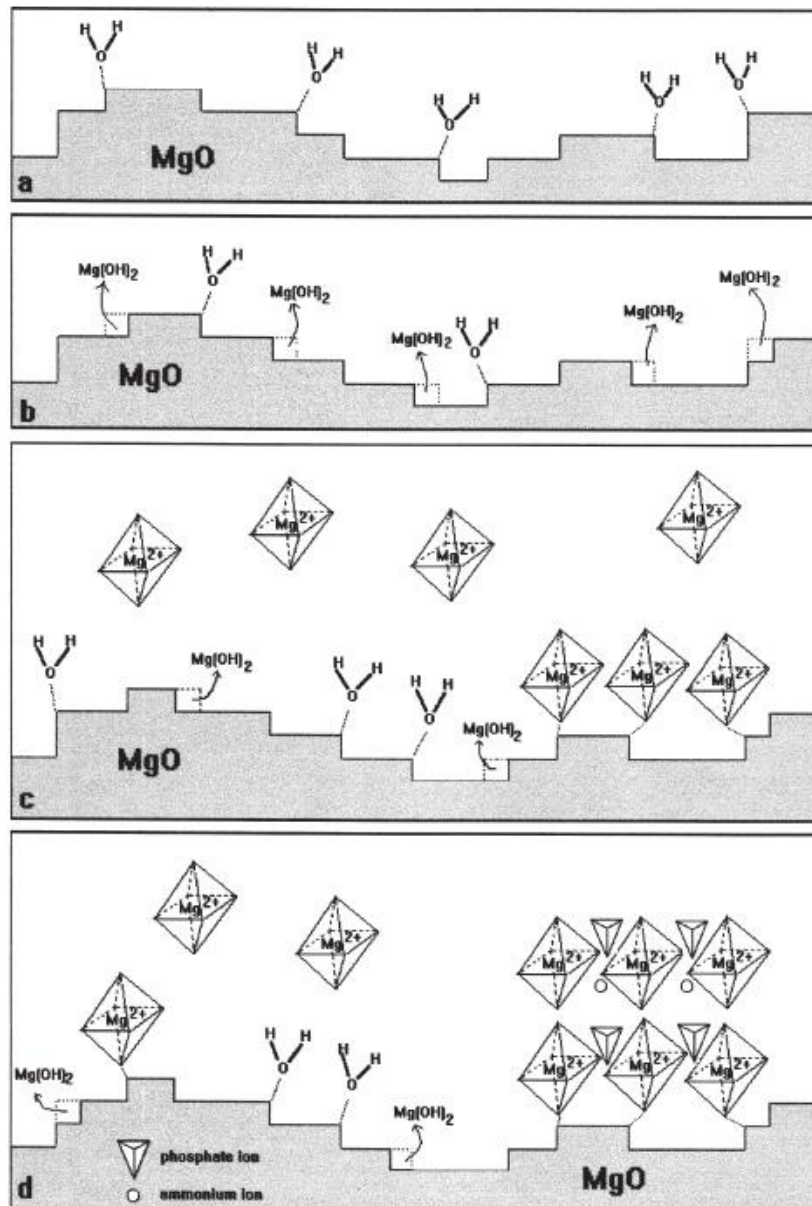


Figure 1.49. Formation of Magnesium phosphate cements. [84]

When water is added to the cement, MAP dissolves in water till saturation and then magnesia is attacked by the acid and started to dissociate. The dissociation depends on magnesia surface state and therefore the kinetics of this reaction mainly depends upon the MgO surface structure. It is believed that  $Mg^{2+}$  ions present in solution are complexed into  $Mg(H_2O)_6^{2+}$  and then substitute water to be absorbed on the MgO surface. Finally the main binding phase, magnesium ammonium phosphate hexahydrate,  $MgNH_4PO_4 \cdot 6H_2O$ , is developed by the  $PO_4^{3-}$ ,  $NH_4^+$  and  $Mg(H_2O)_6^{2+}$  complexes, owing to hydrogen bonds.

The reaction stops when the magnesia grains are entirely covered by hydrates and can no longer dissolve or when one of the reactants is missing.

To obtain a good reaction and crystallization of the binding phase, some aspects are more fundamental than the other: The structure of the oxides for its dissolution, the concentration of acid phosphate solution and the rate of exothermic heat production to allow the crystallization into a well-ordered crystal lattice without interruption and grow into a monolithic ceramic. [84], [86]

The final product, Struvite ( $MgNH_4PO_4 \cdot 6H_2O$ ), also present in nature and belonging to a family of minerals capable of accepting a wide range of different elements that react maintaining the same structure  $M1M2A \cdot 6H_2O$  (Figure 1.50). M1 indicates a monovalent cation such as  $NH_4^+$ ,  $K^+$  or  $Na^+$ ; M2 corresponds to a bivalent cation ( $Mg^{2+}$ ) and A to trivalent oxanion ( $PO_4^{3-}$ ).

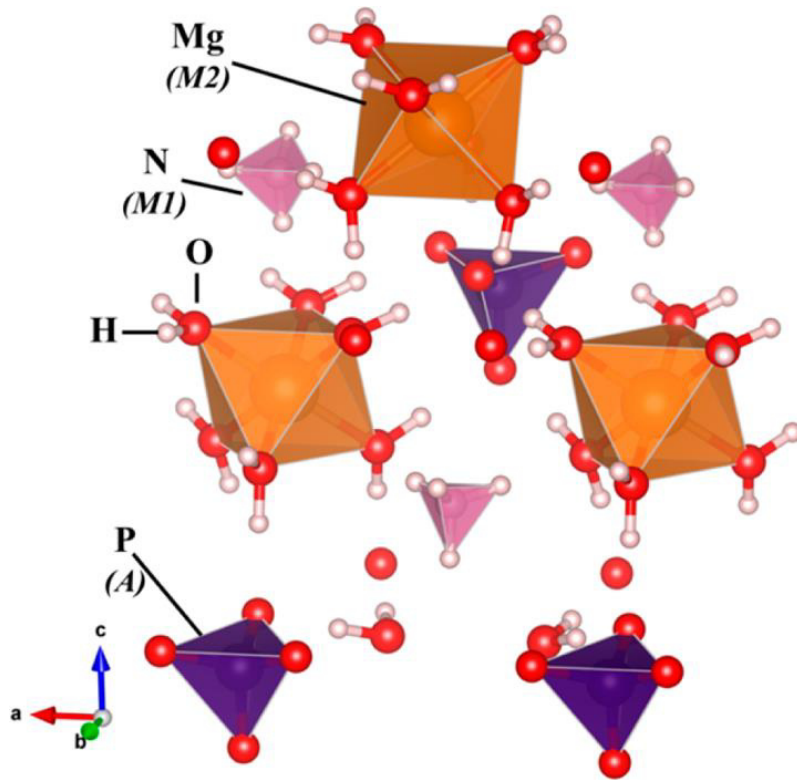


Figure 1.50. Crystal structure of struvite. [82]

Given the problems from an environmental point of view related to the use of ammonium phosphate together with magnesium oxide, instead of the former it was decided to use mono potassium phosphate,  $\text{KH}_2\text{PO}_4$ , (MKP), which reacts with  $\text{MgO}$  and water to form a binder cementitious with hydraulic character, whose main component is still K-Struvite:  $\text{MgO} + \text{KH}_2\text{PO}_4 + 5\text{H}_2\text{O} \rightarrow \text{MgKPO}_4 \cdot 6\text{H}_2\text{O}$

Another advantage in the use of this potassium phosphate-based binder with respect to that with ammonium phosphate is that potassium phosphate has a lower acidity which leads to a slower reaction and consequently a higher setting time. [82], [84]

The  $\text{MgO}$  characteristics strongly affects the behavior of the cement. The calcination of  $\text{MgO}$  controlled its reactivity leading to the formation of particles with fewer defects and better crystallization. reactivity is strictly connected with the specific surface area, SSA, as the reaction occurs on  $\text{MgO}$  particles surface. Also grinding, that destroy the surface structure of  $\text{MgO}$  particles and increased the deformed portion of  $\text{MgO}$  and fineness, smaller the particle size of  $\text{MgO}$ , the faster the hydration and setting, influence the reaction. [87], [88]

The magnesium oxide obtained by decomposition of the carbonate with a process that can take place at different temperature:

- caustic-calcined (also referred as light-burned), 600-1200 °C;
- dead-burned, 1500-2200 °C; and

- fused, >2800 °C.

The reactivity of MgO tends to decrease with increasing processing temperature and the reduction of SSA.

The solubility rate of phosphate is a property that greatly influences the reaction, especially the reaction speed and has effects on the final values of mechanical strength of the product obtained. Also the dimension of the crystal can help to control this aspect.

As shown in Table 1.2, Potassium is in fact one of the least soluble phosphate acids on the market with a solubility of 25,0 g/100g of H<sub>2</sub>O, against a value equal to 40,4 of ammonium phosphate and to 94,9 of sodium phosphate.

**Table 1.2.** Acid Phosphate solubility in water

<b>Type of Phosphate</b>	<b>Solubility at 25 °C, 1 bar [g/100 g of H<sub>2</sub>O]</b>
Potassium, KH <sub>2</sub> PO <sub>4</sub>	25.0
Ammonium, NH <sub>4</sub> H <sub>2</sub> PO <sub>4</sub>	40.4
Sodium, NaH <sub>2</sub> PO <sub>4</sub>	94.9

In addition to ammonium and potassium phosphate it is also possible to use sodium phosphate, which has a higher solubility and potentially could be mixed with press water. Since the Na<sup>+</sup> ion is a monovalent cation (like NH<sub>4</sub><sup>+</sup> and K<sup>+</sup>), the structure of the mineral obtained from the reaction should be of the same type and the reaction product is part of the struvite family. There are very limited studies to the use of this phosphate in MPCs, but from these first approaches seem that the sodium magnesium phosphate phase binding phase is amorphous and offers similar mechanical behavior than ammonium one. [89]

However, other aspects must also be taken into account, if the phosphate is very soluble, the risk is that during the reaction it will dissolve so quickly that it will not be able to come into contact with all the oxide, leaving an unreacted part and not creating a product with characteristics uniform.

Of course, there are also other parameters that influence the reaction that occurs between the MgO, the phosphate and the water, as well as the characteristics of the hardened binder (porosity, mechanical resistance). The main ones are the MgO / Phosphate ratio and the amount of water supplied to the system [87], [90]. Finally, the mechanical resistance of the molded article is also influenced by the ratio between the aggregate and the binder.



### 1.3.2 Geopolymers

Geopolymers are inorganic materials with a variable microstructure (semi-crystallin to amorphous), according to the composition and the synthesis conditions. The chemical composition of geopolymer is quite similar to zeolite. [81]

The term was used for the first time by Davidovits in the late 1970's. [91] Davidovits worked predominantly with clays-based products and calcium-free system, in order to have a stable inorganic structure. It's important to don't confuse the geopolymers with alkali-activated materials and cements which were originally developed by Glukhovsky in the Ukraine during the 1950s. [92]

The reaction involves  $Al_2O_3$  and  $SiO_2$  in a high alkaline medium, and to have a stable structure, the negative charge of  $AlO_4$  tetrahedra has to be balanced from the positive ions (alkali) present in the system. These materials can consolidate at low, even room temperature, leading to amorphous microstructures; heat treatment at temperatures  $> 500\text{ }^\circ\text{C}$  results in semi-crystalline structures. The final structure consists of chains, sheet-like and three-dimensional networks constituted of various Q unit types of connected  $SiO_4$  and  $AlO_4$  tetrahedra. [81], [93]

Davidovits also classified the silicate and aluminosilicate materials depending on the Si:Al atomic ratio, as shown in Table 1.3 and Figure 1.51.

**Table 1.3.** Silicate and aluminosilicate classification based on Si:Al atomic ratio.

<b>Si:Al atomic ratio</b>	<b>Nomenclature</b>	<b>Applications</b>
0	Siloxo	Bricks, ceramics, fire protection.
1	Sialate	Cements and concretes, radioactive waste encapsulation.
2	Sialate-siloxo	Foundry equipments, tools for Ti processing, fire protection fiber glass composites (heat resistance up to 1000 $^\circ\text{C}$ ).
3	Sialate-disiloxo	Sealants for industry (up to 600 $^\circ\text{C}$ ), tools for Al SPF.
$> 3$	Sialate link	Fire and heat resistant fiber composites.

The type of geopolymer, the properties and so the applications are controlled by the atomic ratio Si:Al in the poly(sialate) structure. The higher the Si:Al ratio, the higher the polymeric character provided to the geopolymeric material. A ratio lower than  $Si:Al < 3$  gives a rigid 3D-network.

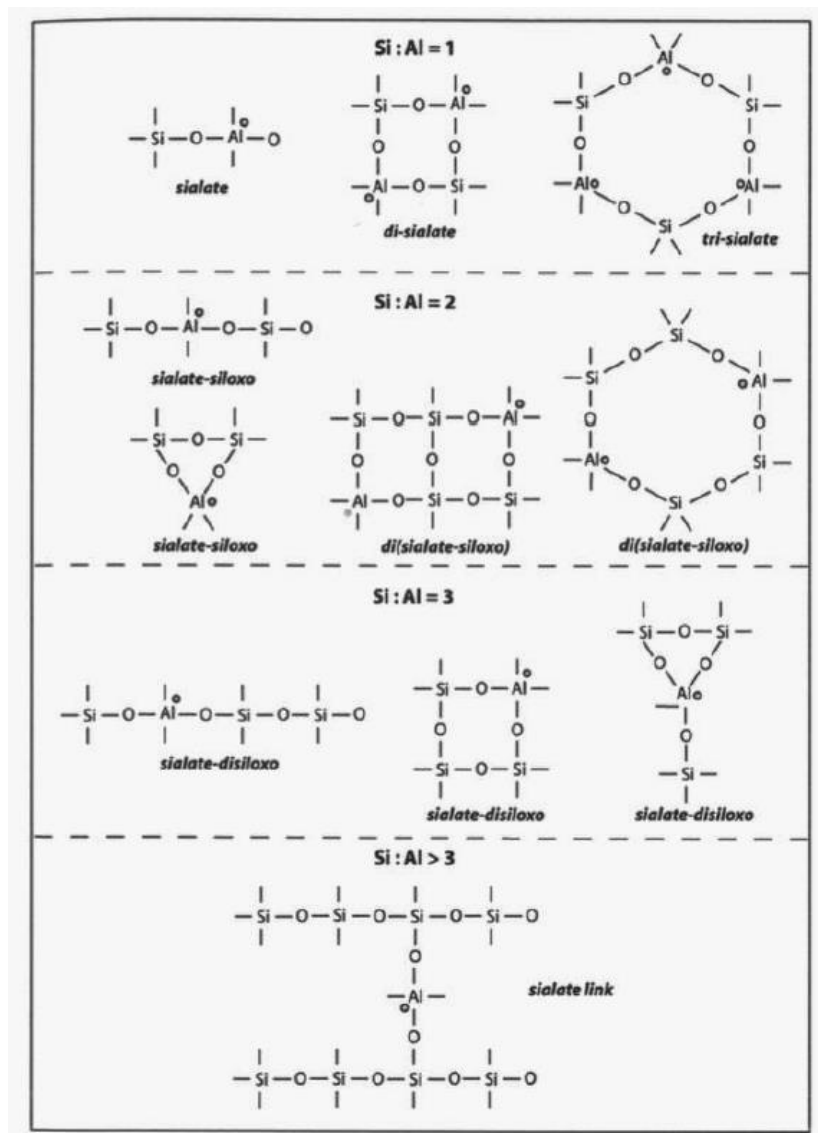


Figure 1.51. Terminology and structure of poly-sialate geopolymers. [81]

As already mentioned, the synthesis happens between an aluminum-silicate source and an activating solution. The most diffused geopolymer are based on alkali system, in particular sodium and potassium based geopolymer. A typical example is the reaction between a dehydroxylated aluminum silicate (metakaolin) within an alkaline comprising hydroxides and alkali-silicates. This is the alkaline route, but also an acid route can be followed. Mainly in acidic medium with phosphoric acid leading to poly(phosphor-siloxo) and poly(alumino-phosphor). [81]

The geopolymerization mechanism depends on the type of cations but can be generalized in the process described in Figure 1.52.

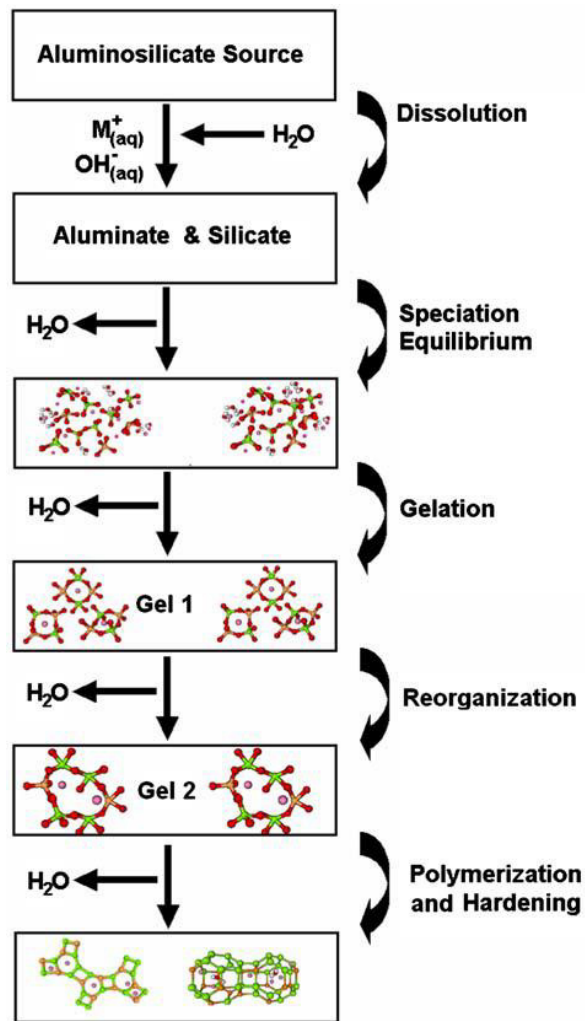


Figure 1.52. Conceptual model for geopolymerization. [92]

The scheme above shows how process transforms the solid aluminosilicate source is converted into a synthetic alkali aluminosilicate.

The dissolution of the solid aluminosilicate by alkaline hydrolysis produces aluminate, silicate and aluminum-silicate species, in general ortho-sialate molecules. Water is consumed during the dissolution (formation of -OH groups). Then the alkaline solution permits the interaction between these molecules leading to the polycondensation into oligomers (gelation) and polymer network (solidification and hardening). The water that was nominally consumed during dissolution is released by this second reaction. Water plays the role of a reaction medium but remains within pores in the gel. A fine grinding of raw materials or a heat treatment can adjust the reactivity of aluminum. [94]

Materials generated by the alkaline activation of metakaolin and/or fly ashes constitute a unique family of materials of a mixed nature, with properties varying from those characteristics of cements, ceramics and zeolites (depending on formulation). [93]

The primary area of application of geopolymers is currently in the development of low-CO<sub>2</sub> construction materials as a greener alternative to Portland-based cements, furthermore with other technological advantages. Other applications include host matrix in waste encapsulation, as a low-cost ceramic (either used directly or as a precursor for calcination), fire protection of structure, bricks, tooling for Al SPF, and heat resistant composites to 1000°C. The cost is limited and generally lower than OPC by a factor of about 10–30%, also in the case of geopolymer concrete derived from fly ash. [81]

In the current work geopolymer solutions are used in post-treatment as infiltration paste (as describe in chapter 5. Xia et al.[67], [68] as describe in the technology description section, use geopolymer materials in powder-bed 3D printing. This strategy should be one of the new future approaches tested for the technology used in this thesis.



# Desamanera srl

This PhD work was carried out in collaboration with Desamanera srl [95], an innovative startup that uses indirect 3D printing in the fields of art and design, interior and exterior architecture, furniture. The company promotes a PhD in apprenticeship for high education and research. The work has been done to analyze and improve the basic aspects of this printing technology and of the materials used.

## 2.1 Company overview

Desamanera is an innovative company, established in December 2014 and has been operational since the early months of 2015, with headquarters in Italy. It is registered in the register of innovative startups of the Chamber of Commerce of Rovigo.

Desamanera operates with the aim of inventing, developing and using innovative 3D production technologies for large scale production, with the use of recycled minerals and the use of sustainable, ecological inorganic binders, without the use of ordinary cements.

Well-established craftsmanship skills also allow to offer customization services to make the opera and objects created and imagined by the customers unique in aesthetics, functionality and performance, the MarbleSkin™ surface finishing. It is a company in which the "know-how", the Italian craftsmanship is enhanced using new production and digital technologies, complementing each other. The world of the Manufacture is heading towards a new global ecosystem, in which the Customer becomes the main protagonist instead of the product, which can no longer be a standard but will always be more personalized and unique.

The company is constantly engaged in research and development both internally and through collaborations with universities, public bodies and private companies. Desamanera is an artisan and beauty but high-tech company.



**Figure 2.1** Desamanera booth during Technology Hub in Milan, 2016. [95]

Desamanera is one of the very few companies in the world specializing in 3D printing technology and systems for large dimensions, 2% of the approximately 800 global producers. The Additive Manufacturing system, in the last year, have confirmed the initial promises and forecasts of growth in an excellent and, indeed, surpassed manner. Now it represents one of the pillars of industrial development, both national and international, on which companies and governments are building competitiveness strategies for the future (Industry 4.0 – Smart Manufacturing). In chapter 1, the potential and growth of AM sector is been already presented and those are the bases in which Desamanera works and develops its business. [96]

The company operates in 3 principal business area: sale of *3-dimensional production technologies and systems*, delivery of *Large 3D printing Service* and *Surface finishing service* (on printed or other objects).

They build custom-made 3D printer according to the needs of customers and / or the specific sector in which they must operate. Printer dimensions (operative printable volume) start from 560 mm and a voxel resolution of 2 mm. Figure 2.2 shows the last printer produced by Desamanera.

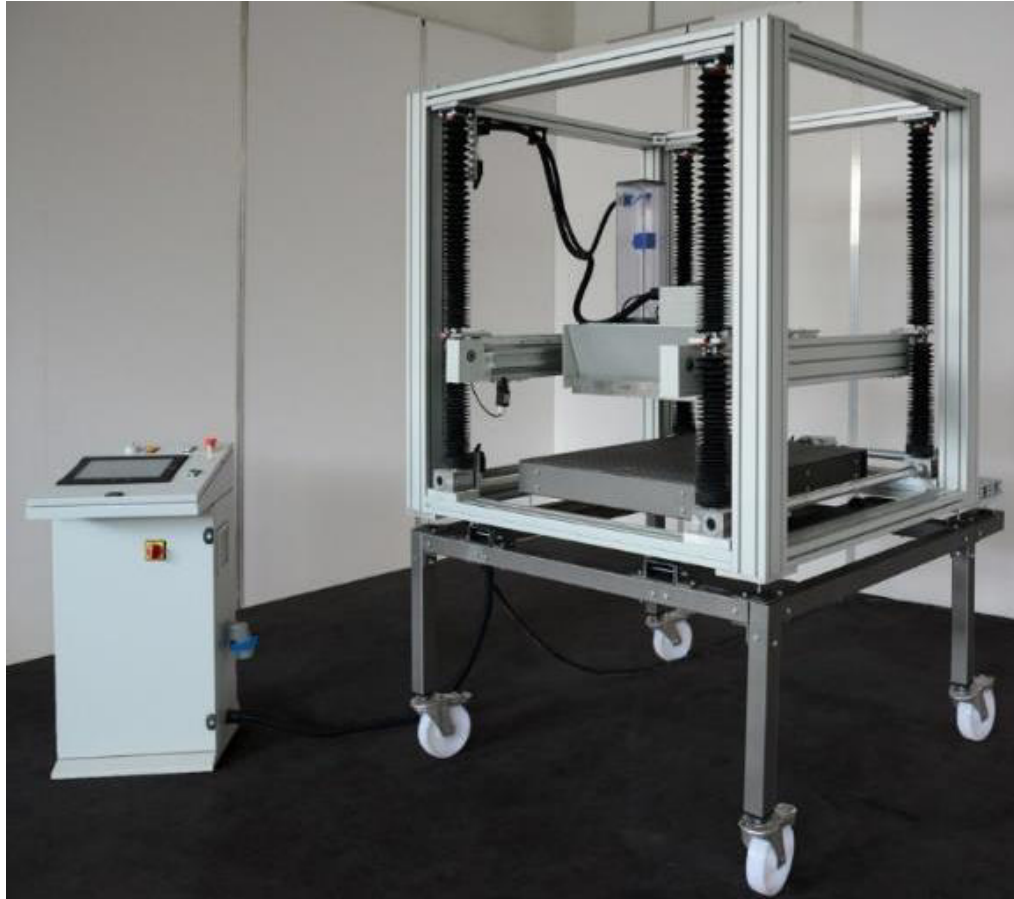


**Figure 2.2.** DESA1 - 60.60 Pa.Sta, 2018. [Images courtesy of Desamanera]

The printing service allow to creatives, artists, designers to produce their creativity, imagination and idea without limits in shape and size. Aesthetic and functional stone-like pieces can be easily printed in a short time. Figure 2.3 shows a piece printed by the company.





**Figure 2.3.** *RYGO: Batsheba Grossman, 2015, Show Room Desamanera. [95]*

The finishing service, produced with the Italian Artisan Culture, enhances the quality of final products. MarbleSkin™ is an original way to (re)use precious mineral powders or granules. Mixing them with specifically developed binders, an amazing coating can be obtained on different materials substrate, also adding innovative functions. Figure 2.4 shows a coated object.



**Figure 2.4.** *Photoluminescent Lavabo: Arch. Santoro Luca, 2016, Show Room Desamanera. [95]*

Desamanera develops inside all the aspects of its technology, with only few high value external collaborations. The team, formed by 8 people, is made up of professionals of great value, whose experience generates an immense synergy in support of the company. Different expertise, from informatic and ICT to mechanical and materials engineering, from communication and marketing to artistic and craftsmanship, coexisting and support each other.

Since 2015, the company has obtained subsidized loans and non-repayable grants for 1,2 Million from different financiers (European Commission, MISE, Veneto del Veneto), in collaboration with Università di Padova, Università Ca Foscari di Venezia, Università di Ferrara, CNR, BAM Berlin, INSA Lyon, EIIT Berlin. The main projects are shown in Figure 2.5.

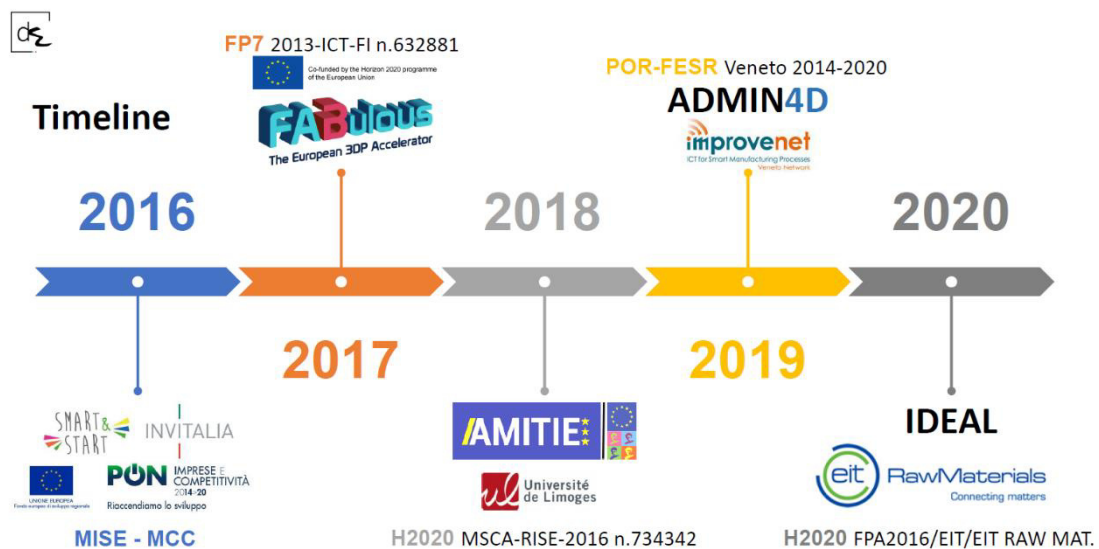


Figure 2.5. Timeline of Desamanera financed projects. [95]

Two projects, H2020 RISIE AMITIE [97] and POR-FESR ADMIN4D [98], are particularly interesting also for this PhD thesis.

AMITIE aspires to reinforce EU capacities in the AM of ceramic-based products and to promote fast technology transfer and training of AM experts with the aim of develop a concept of smart factory based on 3D AM technologies and their hybridization. The project brings together leading academic and industrial players in the field of materials science, processes, materials characterizations, AM technologies and associated numerical simulation.

ADMIN4D project (ADditive Manufacturing & Industry 4.0 as innovation Driver) involves different enabling technologies in the field of smart specialization "Smart Manufacturing". The objective of the project is the development of an innovative system that allows the collection

and processing, through ad hoc developed algorithms, of technical-chemical information coming from the new “materials” used in the products and from production tools (3D printing) patented by the project.

Some studies, analyses and tests, that will be described later in the thesis, are carried out with project partners, during secondment collaboration.

## **2.2 Desamanera Technology and printing process**

Desamanera technology is an indirect powder-based binder jetting technology for large scale production. Different aggregate materials can be consolidated by sustainable inorganic binders during the printing process. According to the production speed necessity the resolution of the system is not so high (in comparison with most common AM technologies), but the artisan post-production allows to obtain a highest level of details.

In the first year of company life, two patents for process and materials are developed in collaboration with the University of Padova. UIBM - N° 1020150000711593 e N° 1020160000200325. [99], [100] These are the starting point for the research and development carried out in this work.

The printer structure is composed of an aluminum supporting frame. Four vertical recirculating ball screw-nut system permit the movement on z axis with great precision. Two linear guides belt-pulley system permit the movement on the x-y plane. Two or more motors can be used to control the two movement directions, according to the size and the necessities. A printing-head with multiple nozzles, moved by the linear guides, deposits selectively the liquid onto the powder bed. A simplified scheme of Desamanera printer is shown in Figure 2.6.

The printing head is the core of the technology. It is composed of modular manifold blocks (it is possible to increase or reduce the length maintaining the same simple scheme). Each block is formed by the structure plastic manifold, the electro valves, the nozzles, that are individually controlled. All parts can be change and maintained one by one. The mechanical electro valves, depending of water pressure, opening time and printing head speed, deposit the desired amount of water per voxel.

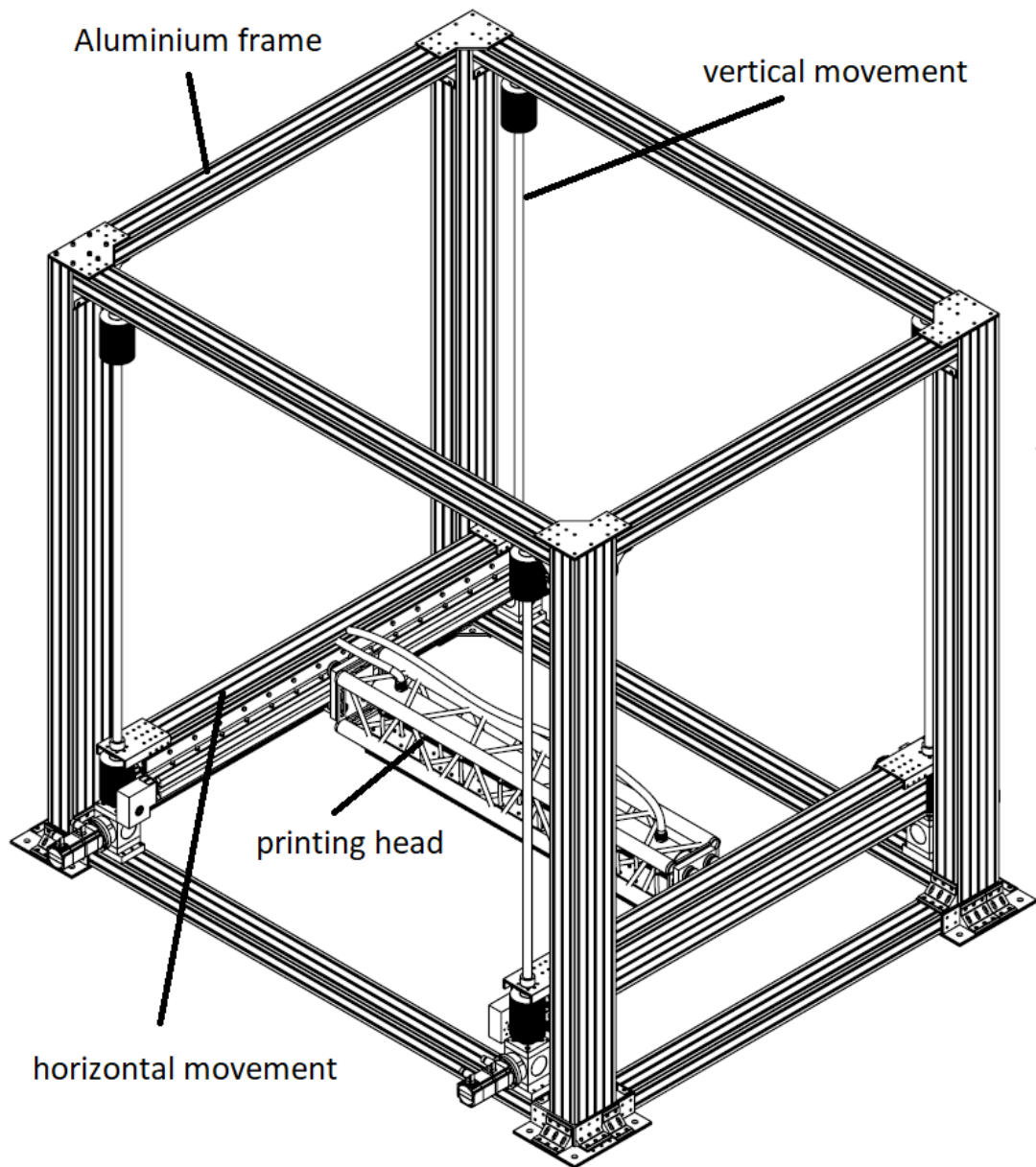


**Figure 2.6.** Schematic figure of the printer and its principal parts. [Images courtesy of Desamanera]

Also software and informatic supports, that control the preparation and the management of printing process, are very important. Desamanera develops internally the slicing software, *D-slicing*, that divides the object in horizontal planes (or sections) with a regular thickness (a lot of other parameters can be set up with D-slicing processing). The slicing software gives a data file, with a dedicated language, that can be read by the PLC and transmits the commands to the printer. The control software of the PLC is specific dedicated and internally developed as well.

The printing time is in the order of 1 meter in 2 hours, variations are correlated to the layer thickness. Dimensions and technical specifications can be adjusted according to customer necessity. Voxel size can be set starting from 2 mm. The printer used at Desamanera, Desal 150.150, has a voxel size of 5,7 mm. A new one developed for Industrial engineering department of University of Padova has an improved resolution at 3 mm.

The phases of the printing process are reported schematically below:

- A. Modeling of the structure with 3D CAD software or evaluation of the received one from customer. Exportation of the file in STL format.

Figure 2.7a shows the 3d file of a lantern designed internally by Desamanera starting from a chess model (1 m high, 30 x 30 cm<sup>2</sup> base).

- B. The 3D model is cut into "slices" (Figure 2.7b) using D-Slicinig (with the general voxel size set to 5,7 mm). The 2D plans obtained are those that the machine will print in ascending order.

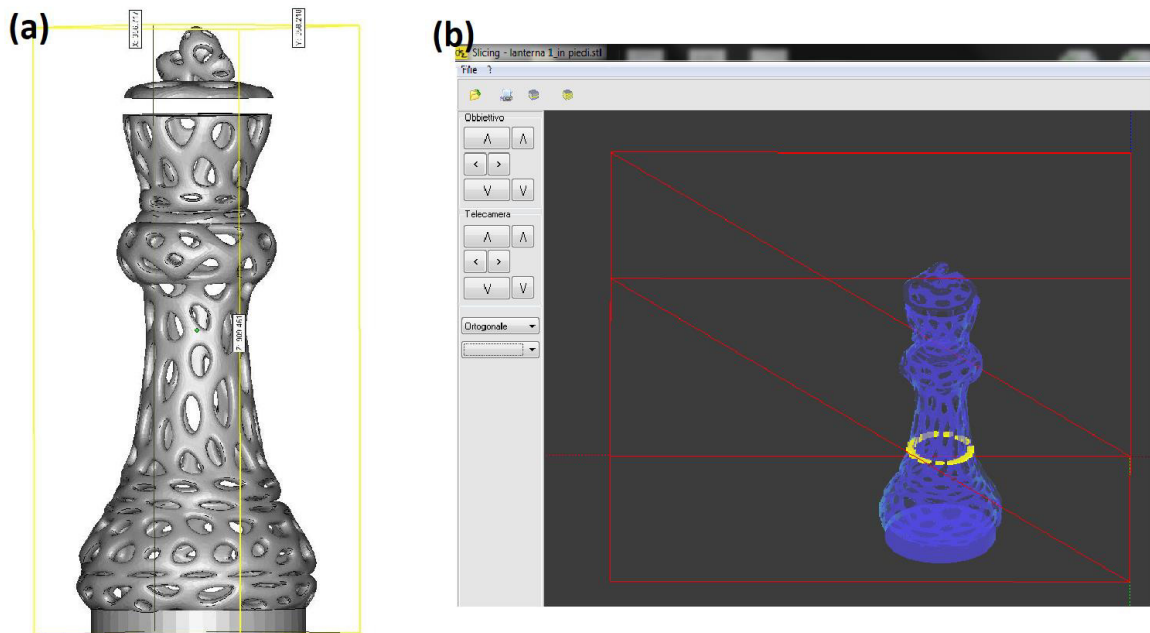


**Figure 2.7.** (a) a 3d file; (b) the same file processed with D-slicing (yellow part is one selected layer). [Images courtesy of Desamanera]

- C. Now object can be printer, following a series of predefined steps:
  - i. The basement of powder-bed is created.
  - ii. A layer of printing mix, with a height equal to the set thickness, is deposited (Figure 2.8a); the printing material already contains the aggregate and powdered dry part of the binder.

- iii. Once the “empty” layer is prepared, the print head rises from the predefined step along z axis. Ready to print
- iv. The printing-head moves horizontally onto the powder depositing, in the areas defined by the 2D slices, the binding liquid that activate the solidification reaction. (Figure 2.8b)

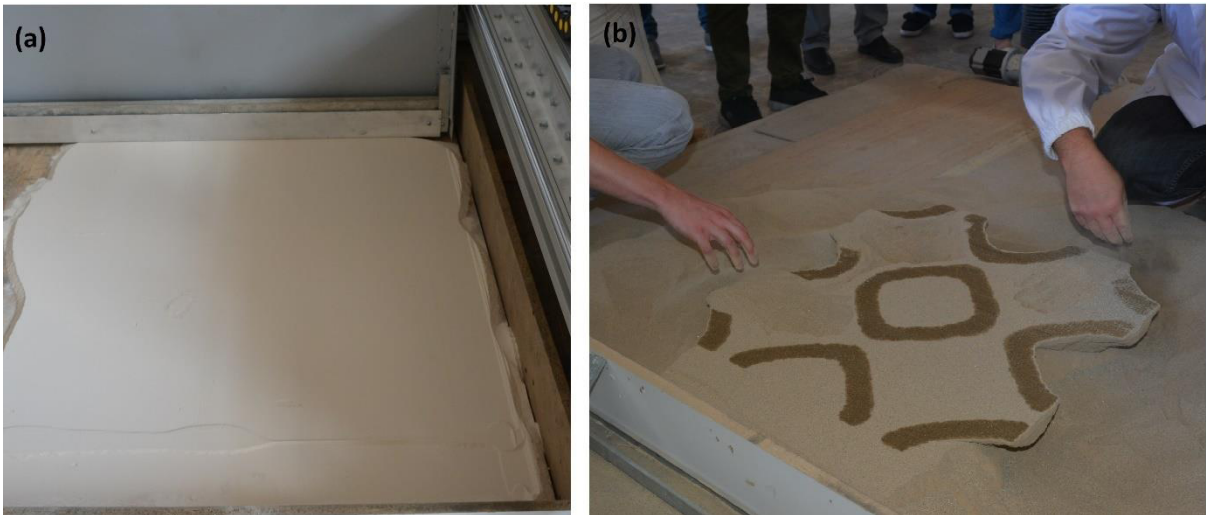


**Figure 2.8.** (a) Empty layer ready to be printed; (b) Selectively printed layer. [Images courtesy of Desamanera]

- v. A new layer, with a height equal to the set thickness, of powder mix is deposited over the first printed one.
  - vi. The print head repeats the operations of point iii, depositing the liquid in the points defined by the new layer.
  - vii. Points iii – v are repeated until the piece is complete. During the building up of the printed part, the powder-bed is contained through the simultaneously growing of the formworks. (Figure 9.A)
- D. When the necessary time for consolidation is reached, the object is extracted from the powder bed and cleaned (Figure 9.B)

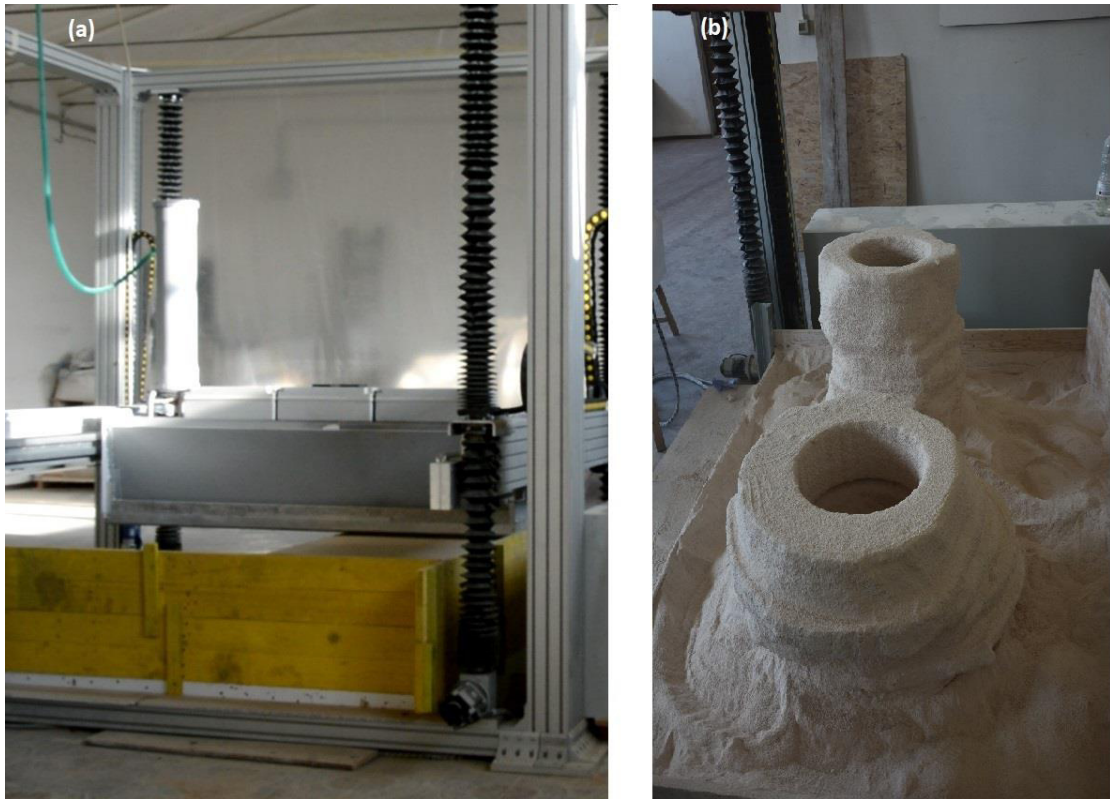


**Figure 2.953.** (a) the formworks structure during printing; (b) pieces partially extracted from the powder bed. [Images courtesy of Desamanera]

E. The object is post-produced according to customer recommendations (Figure 2.10a) and if required the application of Marble Skin™ coating is applied (Figure 2.10b).

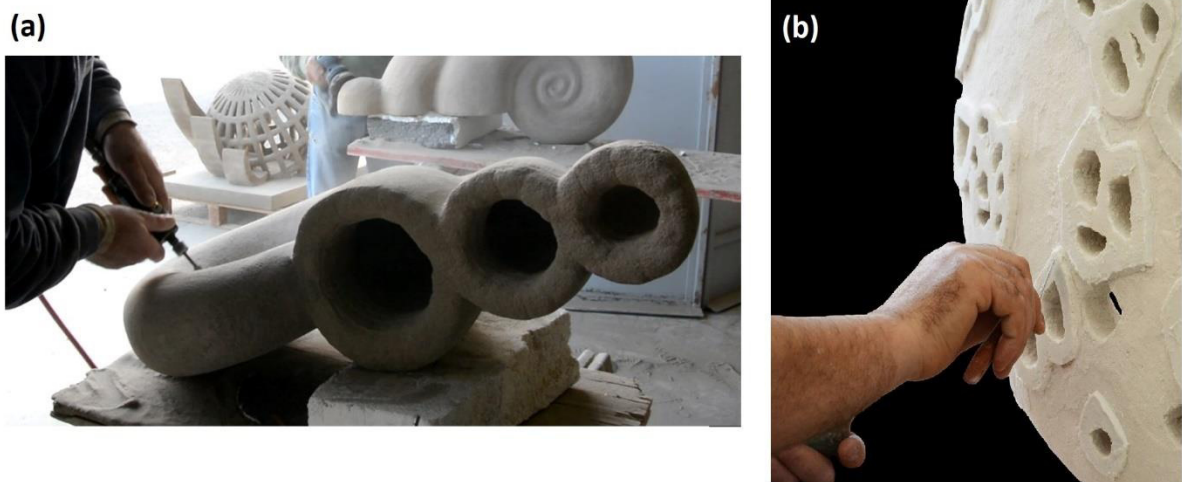


**Figure 2.10.** (A) Postproduction of printed parts; (B) Application of Marble Skin surface finishing. [Images courtesy of Desamanera]

The images used above were selected from the objects actually printed, for different purposes, by Desamanera during the doctoral period. In the next pages a small description of Desamanera printed opera is given. Both only printed and coated are presented to provide a complete overview of company type of products and commodities sectors.

**Digital bio-Form - Stone Pavillion** – Designed by Prof. Arch. Xu Weiguo, Bianco di Zandobbio Dolomite, coated with photoluminescent white marble, 2016



**Figure 2.11.** Digital bio-Form - Stone Pavillion. [Images courtesy of Desamanera]

**Palladio Tables** – Designed by Arch. A. Tognon, Bianco di Zandobbio Dolomite, 2017 – 2019



**Figure 2.12.** Tables Palladio, collaboration with Palladio Scale (VI). [95]



**Schwarz P Surface** – Po Sans, 2018 (printed with BAM during AMITIE secondment)



**Figure 2.13.** Schwarz P Surface. [Images courtesy of Desamanera]

**Triplo shell** – Po Sand, coated with black marble, 2018 (printed with BAM during AMITIE secondment)



**Figure 2.14.** Triplo shell, on the right polished part, on the right coated parted. [Images courtesy of Desamanera]

## Lantern – Bianco di Zandobbio Dolomite, 2018



Figure 2.15. Lantern, on the right a detail of the part. [95]

### 2.3 Desamanera Raw materials

Natural and the Environmental issues are very sensitive nowadays. The increase in temperature, large scale weather anomalies and the chemical, physical and biological consequences caused by environmental pollution, are drastically accelerated in the last few decades. All activities in Desamanera is working on the basis of the most important founding principle: minimizing the environmental impact and protecting the resources of the Planet.

Powder and granular materials are the basic raw materials in Desamanera processes. Aggregates are selected between the local products and the recycled materials or waste from other processes. The binders are chosen from the more sustainable alternatives to Ordinary Portland Cement.

Desamanera, considering the prospect of printing wide components, works commonly with large amount of Aggregates. From the economical point of view these materials, that constitutes most of the printing mix must be of low cost, and consequently of natural origin. And, as far as possible, also be of industrial derivation as waste or reused. Moreover, the aesthetic characteristics of the final product must be good enough to allow direct use, after post-processing, without the application of the coating. Figure 2.16 shows some aggregates currently used in Desamanera.

Consequently, as the main aggregate material the company decide to use the *Bianco di Zandobbio*, a dolomite ( $\text{CaCO}_3\text{-MgCO}_3$ ), which originates from the hilly area of the lower Val Cavallina, in the municipality of Zandobbio (BG), from which it took its name, and in the

neighboring countries. It is mainly used in the sector of plasters and premixed, of prefabricated buildings and floors, of gardening or floriculture and agriculture, of zootechnics and ornithology, of detergents and of wall coverings and restoration. Dolomite powder is available in a lot of different particle sizes, and also used as an inert filler for mixtures with cement or as a raw material for the production of glass and ceramics.

The river sand (silica sand) is a valid alternative to *Bianco di Zandobbio* dolomite (BdZ), in particular from the point of view of cost and availability throughout the national territory. Despite the darker color and the less particle sizes commonly available, also this aggregate, in its finer parts, allows to obtain print beds of the required quality.



**Figure 2.16.** Desamanager aggregates, (a) River Po Sand, (b) Bianco di Zandobbio dolomite, (c) Marble granules.

For special application or necessity, also other aggregate can be use. Potentially every aggregate with a suitable dimension can be used. For more aesthetic components marble granules are used. For components capable of being subjected to high temperatures ( $> 500\text{ }^{\circ}\text{C}$ ), the use of chamotte, which derives from the grinding of baked clay, can be considered. However, these materials are more expensive than the natural materials listed above.

Based on the literature of additive manufacturing that uses a powder bed ("binder jetting" technology), the ideal base printing mix with which creates the powder bed must have the following characteristics:

- Variable particle size from a few microns (better above  $\sim 20\text{ }\mu\text{m}$ ) to a few millimeters (better below  $\sim 2\text{ mm}$ )
- Mix with controlled particle size distribution to guarantee optimal behavior during deposition
- Fraction of aggregate with different average particle size (D50), to have a better packing of the bed, after the automatic distribution

Lower dimension limit is regulated from flowability, upper dimension value from voxel dimension and powder-bed defects. The flowability characteristics can be evaluated for example through the so-called Hausner ratio. [11], [15], [101]–[103]

The analysis on the different printing raw materials and mixes are presented in Chapter 4.

The precious powders and granules, such as marble, onyx, colored quartz, are used for the MarbleSkin™ coating. For this application, larger dimension granules can be used too. In this case, according to the desired results, different texture, roughness, light effect, etc can be achieved without problem of dimension. MarbleSkin™ is a manual handcrafted process.

The binder, that Desamanera decided to use, is an inorganic product with hydraulic characteristics, and not simply an air-hardening one. This distinction, therefore, determines the scope of use and the characteristics of durability (resistance to exposure to outdoor environments), allowing the products service permanently in contact with water.

Ordinary Portland Cement (OPC), that is the most common binder use worldwide, in this case is not used for two important reasons. First of all, the traditional cements are produced to have slow setting times, therefore not compatible with a fast AM process, and they need to be in contact with reaction water for a substantial time to make the hydration reactions proceed correctly. Secondary, as already said, the OPC has sustainability issue.

Among the other possible binder, a magnesium-based cement is been selected. The magnesium potassium phosphate cement (MKPC) is the final choice.

The common ammonium-based phosphate, the first studied in the past, is not considered to avoid the evolution of ammonia gas during setting. While the MOC cement, already use also in 3d printing is refused for their susceptibility to deleterious processes induced by exposure to moisture. In moist conditions, the binding phases dissolve into a solution of  $Mg(OH)_2$  and  $MgCl_2$ , resulting in the loss of the strength of the cement.

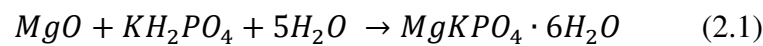
Other important advantage of MKPC cement are the possibility to operate in low temperature condition, when other cements present bigger problem. Obviously, the reaction rate is considerably slowed but the inherently rapid and exothermic reaction and low water content of MPCs are advantageous in this context.[82] The possibility to use different quality of MgO allow a great control in reaction behavior. For the application of additive manufacturing using binder jetting technology, it is better to use a more reactive magnesium oxide (Caustic Calcined Magnesia). The following advantages can be obtained:

- the fast reaction contributes to the capture of all the printing water, leading to a better printing resolution,

- being the quantity of water sprayed by the nozzles in limited quantity, a high reactivity is useful since it limits the diffusion of water inside the print bed with loss of definition of the molded piece,
- the hardening reaction starts immediately and is fast enough to allow the piece to be extracted shortly after the end of printing, with obvious advantages for the speed of production of components.

These are been the preliminary company decisions, the starting point to study and develop the materials and the process. Following these decisions, few preliminary discussions can be made to introduced the investigation on the printing process described in the next chapter.

The consolidation of the binding phase takes place according to the reaction:



where, primarily, the water dissolves the potassium phosphate crystals and then goes to solvate the MgO surface, starting the reaction. The theoretical ratios of the various raw materials deriving from the reaction described above are shown in the table 2.1

**Table 2.1.** Theoretical binder reagent ratio.

Reagent	Molecular weight	Molar ratio	Weight ratio
MgO	40,6 g/mole	1	0,3
KH <sub>2</sub> PO <sub>4</sub>	136 g/mole	1	1
H <sub>2</sub> O	18 g/mole	5	0,66

To form the maximum possible amount of struvite as a binding phase, a stoichiometric 1:1 molar ratio of MgO to KH<sub>2</sub>PO<sub>4</sub> would theoretically be preferred. Actually, in typical usage and literature and patent indication, MgO is used in significant excess. Mg/P molar ratio is around 3-5 to 1, (more or less 1:1 by weight). Numerous studies on this topic have been undertaken, although with wide variations in the use of retarders and the proportions of water used, and high Mg/P molar ratios producing the highest compressive strengths. [87], [104]–[107]

The surplus of unreacted phosphate would be soluble, leaching out of the cement during service, potentially compromising structural integrity but also leading to unappealing efflorescence on the cement surface. The presence of free MgO in hardened cements, in general construction practice, is considered undesirable and a origin of future expansive cracking, due to slowly hydration in Mg(OH)<sub>2</sub>. In these types of cement, however, the excess of MgO is not so

problematic as it has been reported that struvite forms on the surface of MgO grains, effectively enclosing them. A significant MgO fraction could remain inaccessible for reaction with phosphates, and the strict printing conditions do not improve the situation. The results of the first studies in previous thesis confirm the good behavior of this choice. [108]–[110]

The minimum amount of theoretical water required is always the same, the one necessary to react the entire quantity of mono potassium phosphate, which has remained unchanged. But the solubility of potassium phosphate in water (230 g/L at 20 ° C) is not high enough to immediately dissolve all the amount of potassium phosphate present. Due to the short time and absence of mixing between the components the reaction should be not complete. Furthermore, the presence of a considerable amount of dry aggregate which does not take part in the reaction but can inevitably absorb a part of water, creates a further deficit of water and consequent incompleteness of the reaction.

For all these reasons, some very specific of AM application, the amount of water must be surely higher than stoichiometric. Furthermore, in the literature indication about traditional uses (production of cement paste and mortar) where water/cement ratio is generally maintained very low, starting from 0,2-0,3, incompleteness reaction is also found. [87], [104]–[107]

Table 2.2 describes the final ratio hypothesized as good value for the printing process. Probably the reaction could not be completed yet but also resolution have to be maintained in acceptable range.

**Table 2.2.** Final binder reagents ratio.

<b>Reagent</b>	<b>Molecular weight</b>	<b>Molar ratio</b>	<b>Weight ratio</b>
MgO	40,6 g/mole	3,4	1
KH <sub>2</sub> PO <sub>4</sub>	136 g/mole	1	1
H <sub>2</sub> O	18 g/mole	5,7 – 6,4	0,70 – 0,90

The final step involves the evaluation of the water that should be used during printing, according to the composition and the characteristic of the typical printing mix, and the empirical verification of the water deposited materially from the printing head.

The company generally uses printing mixes with an amount of binder variable between 20% to 40%. The standard most used quantity is 25%. For operative convenience, this percentage express the amount of binder reagent calculated from the aggregate amount. For example, 100g

of aggregate with 25g of MgO and 25g of MKP. In the total amount of mix, therefore, there are 66,6% of aggregate, 16,7% of MgO and 16,7% of MKP.

If it is considered to use: the printer located at the company, that has a voxel resolution of 5,7 mm; a printing mix with *Bianco di Zandobbio* and 25% of binder, that has a bulk density of 1,55 g/cm<sup>3</sup> (All the tests on printing mix are described in chapter 4), the precise water amount can be calculated.

Table 2.3 and Table 2.4 summarize the information of materials and quantity of water required using all the value describe above.

**Table 2.3.** Characteristics of 25% binder mix.

<b>Printing mix composition_25% of binder</b>	
Aggregates	66,6 %
Magnesium Oxide	16,7 %
Mono potassium phosphate	16,7 %
Printing mix density	1,55 g/cm <sup>3</sup>

**Table 2.4.** Desire water amount for 5,7 mm voxel

<b>Water in 5,7 mm voxel</b>	
Voxel volume	185,193 mm <sup>3</sup>
Material	0,287 g
MKP	0,048 g
<b>Water</b>	<b>0,038 g</b>

Working with an indirect powder-based technology, another important aspect to consider is the presence and interaction with the porous bed. The free space available (porosity of the bed) has to be enough for water penetration and reaction without saturation and expansion beyond the shape.

As cited above, the printing mix bulk density (BdZ\_25%) is around 1,55 g/cm<sup>3</sup>, instead the real density is 2,80 g/cm<sup>3</sup>, calculated as sum of partial proportion of single components density. The ratio between the two gives 45% as the porosity in the bed.

Getting back the values obtained above the free space in a 5,7 mm voxel is 0,083 mL higher than the 0,038 mL of water deposited on it. The amount of water estimated should guarantee a good resolution too.

An empirical evaluation of the water deposited according to the different optimized parameters and setups is needed. Detailed activities on process configuration, amount of water, resolution, strength, are described in chapter 3.

The application of these material in 3D printing is unusual and new, so there are no products specifically developed for it. Due to the large quantities of material used to print large pieces, the binder price also plays an important role. Raw materials are found among those already commonly used in other common and consolidated industrial fields. MgO can be found among those used for traditional applications in traditional cements (but dead burned quality is more common to achieve a long-time operative time) or in the field of food feeds [111] and agriculture. MKP can be found in the field of irrigation fertilizers [112] or the food industry (much purer and more expensive for obvious needs).

Therefore, there is easily a high variability in raw materials and incompleteness in information and data given from suppliers. The analysis and selection of the raw material could become a very important aspect.

Due to the large amount of materials needed and the small dimension of the company the supply conditions and the costs are very important parameter.

In the following chapters the complete studies, tests and optimizations are described. These activities are been commonly carried out during company everyday activities, using available materials, printer operative setup and environmental conditions.





# Process parameters and optimizations

In this chapter, starting from calculations and evaluations introduced in previous page, the initial printing parameters are studied. The final goal is to achieve a more stable and reproducible printing process at a high-quality level. New configurations are selected with the aim of improve parts quality, controlling primarily the water amount sprayed and the way of deposition. Also, new tools are designed and implemented, and new steps are introduced to simplify process handling. Time after time the improving innovations are consolidated becoming standard parts of the process and leading to the new actual process.

In the next pages, to maintain more continuous and clear the line of discussion a first general introduction of research method and material used is given. Then the studies, the tests, the results and the improvements are been described in detail.

Printed development and optimization are carried out working with the mechanical engineers that work in Desamanager to design the printer. Part of the tests and optimization are outcomes of the intense collaboration with Federal Institute for Materials Research and Testing (BAM), Berlin during AMITIE project secondments. Another part is carried out with the collaboration of mechanical engineering master students, Carlo Tarabotti (2019). [113]

## 3.1 Materials and methods

Since the process optimization is been a continuous work during all the research period, the printing was commonly performed with the raw materials and the printing mixes available at that moment. Both BdZ and Sand could be used as aggregate and the quantity of binder could be modified during time and tests. Standard parameters are always used in reference tests.

A general validation and optimization of the process, identifying and investigating the principal parameters, was completed in the initial phase. Water deposition is the most important aspect that have to be analyzed. Its interaction with the powder consolidates the materials and the amount determines the resolution and strength of the parts.

The water injected from the printing-head was evaluated and compared measuring empirically the amount collected with the different parameters. A tray was fixed above the nozzles, and a shape with regular defined dimensions (30 voxel x 110 voxel), is printed and the water deposited is weighed. At least 2 repetitions of 5 layer was printed to collect the water. The water

quantity of single nozzle is determined divide the total amount for the number voxel that have been printed.

The printing of samples permitted to evaluate the improvement of new printing parameters and implemented tools, in terms of quality, resolution and strength. Pictures and videos of printing were collected. For resolution and strength, bar samples with an average size of 30 x 30 x 130 mm<sup>3</sup>, was produced. The dimensions of the different mixes were collected and compared, after accurate cleaning (no machine post-processing).

The morphology of the parts, especially of water interaction with the powder and layer interface quality, was investigated by an optical stereoscope (STEMI 2000-C, Carl Zeiss AG, Oberkochen, DE) and by SEM microscope (ESEM, Quanta 200, FEI, Hillsboro, OR).

The mechanical strength of the samples was measured with an Instron 1121 UTM (Instron Danvers, MA) with a cross head speed of 1 mm/min. Both the perpendicular and the parallel direction to the layer were tested. Figure 3.1 shows the configuration and sample orientation for the bending and the compression tests.

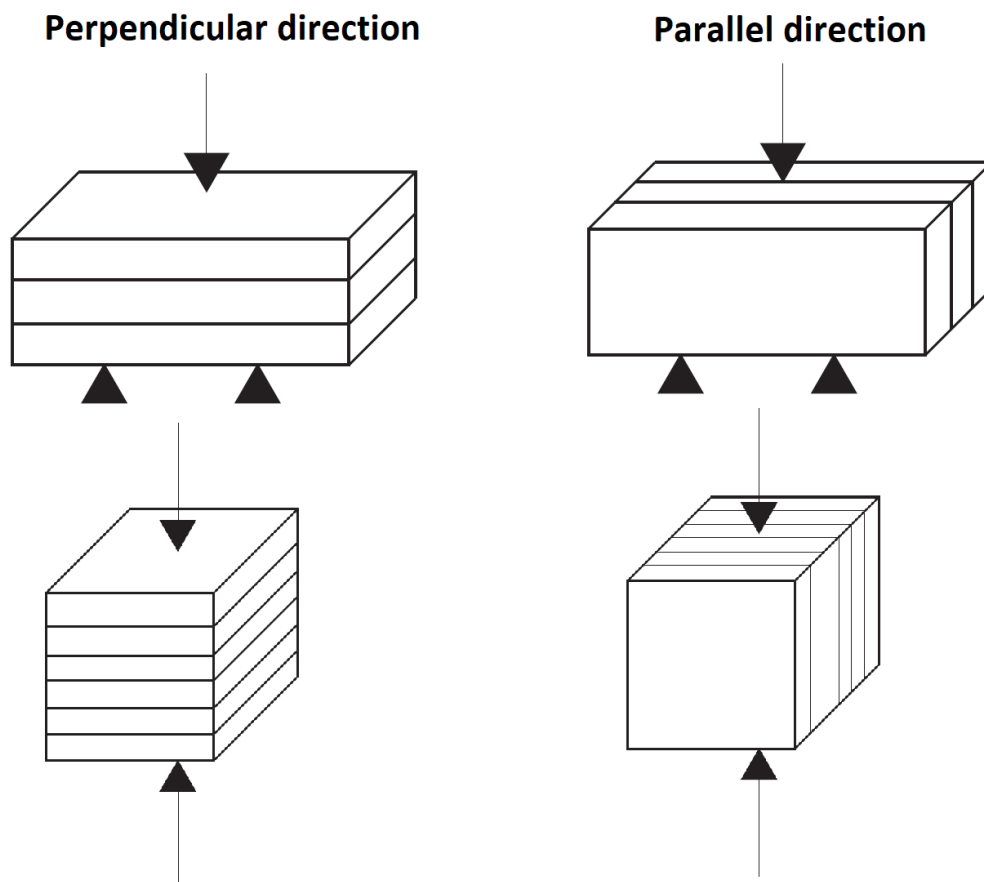


**Figure 54.** Sample position and direction of loading for bending and compression test

The different behavior according to test direction is a particularity of the AM process, various previous works have shown this phenomenon. [52], [114]

At least five samples were tested for each type of loading direction. Samples for compression had an average size of 30 x 30 x 30 mm<sup>3</sup>, while samples for bending had an average size of 30 x 30 x 140 mm<sup>3</sup>. Due to the manual post processing, some samples were not exactly dimensioned, especially in planarity of the plane, and this could determine high standard deviations.

The geometrical bulk density was calculated as mass on volume, sample dimensions collected with a digital caliber. The apparent density of sample was measured by means of a helium pycnometer (Micromeritics AccuPyc 1330, Norcross, GA). The total porosity of the sample was therefore calculated as the ratio between their geometric bulk and apparent density. The porosity value is the average between all the tested sample, both bars and cubes.

### **3.2 Tests and improvements**

Desamanager large dimensions 3D printer, Desamanager 150.150, was assembled during the first month of the PhD period. Therefore, together with the raw material analysis, the printer setup was one of the major activities of the initial period. The printer works, as describe in chapter 2, first creating the powder bed and then activating the same with selectively water deposition. The most important parameters of the process are: (Figure 3.2 e Figure 3.3)

- Speed for powder deposition (laying direction of movement)
- Speed for water deposition (printing direction of movement)
- Layer thickness (generally equal to voxel size)
- Electro valve opening (water deposition control)
- Pressure of the liquid system (water deposition control)

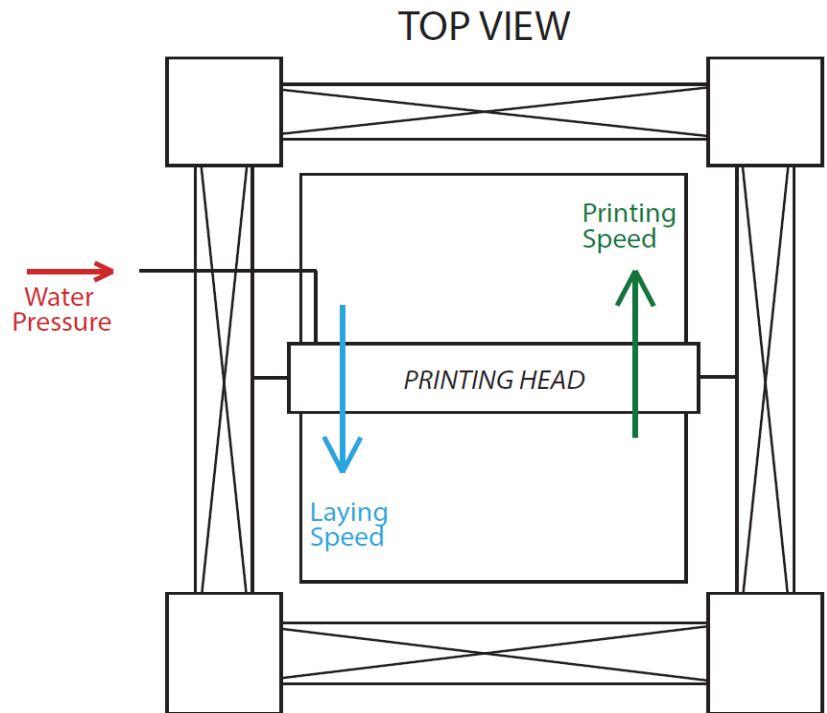


**Figure 3.2.** Printing process scheme and principal parameters from top view.

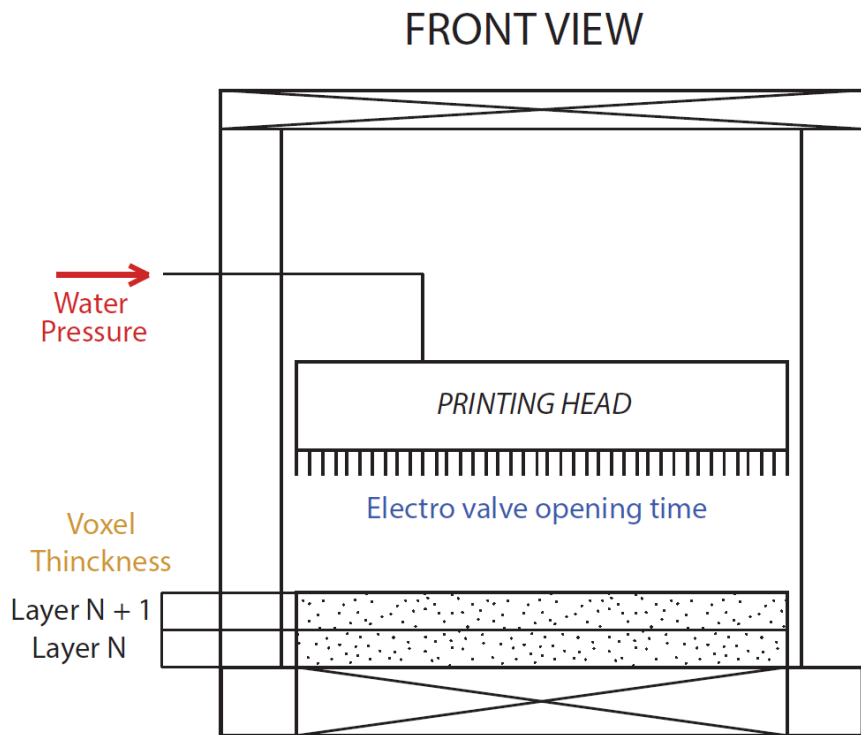


**Figure 3.3.** Printing process scheme and principal parameters from front view.

The preliminary control printings, to verify the correct operation of all the parts, were performed with parameters suggested form Desamanera know-how and experience. Voxel dimension of

5,7 mm (for the printed Desal 150.150, fixed by nozzle center to center distance), a printing speed of 200 mm/s and a laying speed of 100 mm/s were selected, the printing head was directly connected with the municipal supply network, with a pressure adaptor prevent surge of the supplying, generally given at 2 bars, and the electro valves are continuously opened during water deposition.

The management of the printing phases by the software and the powder bed deposition and preparation are correctly performed. However, the liquid pressure is too high and the water deposited amount is enormous. The water jet impact created excessive disruption on the powder and a higher opening pressure was notice, samples are wider in the initial zone.

The first fact discovered is that a good printing requires low pressure (probably tenths of a bar), that cannot be controlled with pressurize liquid system. So, it is decided to work with the hydrostatic pressure of the column of water; a meter of water column ( $m_{H_2O}$ ) is 0,1 bar of pressure ( $1 m_{H_2O} = 0,0980665bar$ ).<sup>[115]</sup> The height of water column is used in rest of the chapter to describe the pressure level, the value is given as is without considering the pressure losses.

For these reasons and to research the correct level, a tank was positioned at a variable height near the printer and a transparent tube on the printing head for checking the level height. Figure 3.4 shows the set up. The final idea, after achieving the correct values, was to put a vessel onto the printing head to guarantee an integral position during head movements.

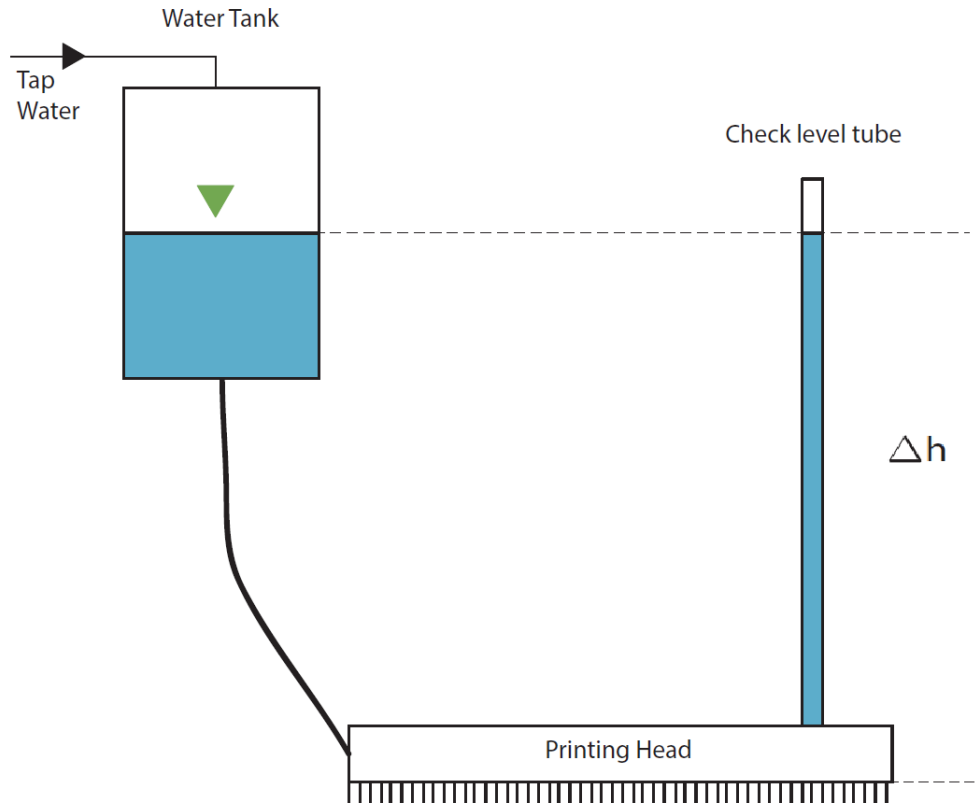


**Figure 3.4.** Water network configuration.

Using the same parameters describe above, different value of water column is tested, analyzing the printing effort in terms of resolution and strength. The results of a water high level ( $\Delta h = 1200$  mm) and a water low quantity optimized level ( $\Delta h = 350$  mm) are now presented. The amount of water deposited with the lower pressure level is 0,033 mL/voxel that is very closed to the value hypothesized in theoretical calculation, in Chapter 2. Table 3.1 shows the values.

**Table 3.1** Amount of theoretical and empirical water per voxel.

<b>Water per voxel</b>	
<b>Theoretical</b>	<b>Empirical</b>
Stoichiometry and resolution compromise	Low pressure level, $\Delta h = 350$ mm
0,038 mL	0,035 mL

Samples printed with BdZ and 25% of binder, showed for high water a lower resolution, with samples deformation and connection each other (Figure 3.5). Also, the dimensional data, collected in Table 3.2, confirm the result suggest from the images.

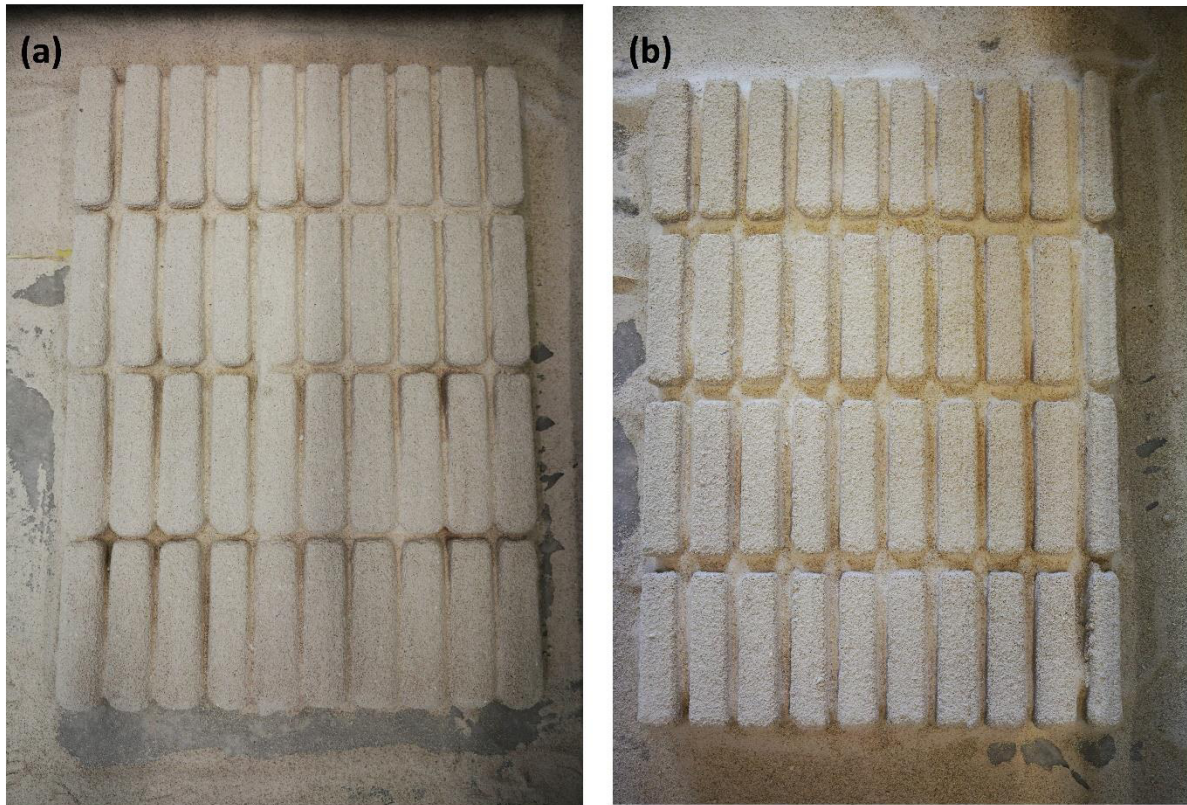


**Figure 3.5.** (a) high level water samples; (b) low level water samples.

**Table 3.2.** Dimensions of bar samples, 3d file value, high water and low water printed samples.

Sample	Bar dimensions			Deviation from 3d file		
	L [mm]	l [mm]	H [mm]	L [%]	l [%]	H [%]
<b>3d file</b>	142,5	28,5	28,5	/	/	/
<b>High level water</b>	154,1	41,2	38,4	8,1	44,5	34,7
<b>Low level water</b>	144,6	34,0	32,5	1,5	19,3	14,0

Low level water amount guaranteed a good resolution, with minimum dimensional errors. It has to be considered that water diffusion smoothes out the contours and a minimal post-production is always required in additive manufacturing for very sharp and defined edges.

The compression and flexion tests were also performed on the same samples.



**Table 3.3.** Mechanical properties of high water and low water samples.

	<b>Mechanical Strength [MPa]</b>		<b>Porosity [%]</b>
	Orto layer	Para layer	
<b>High level water</b>			
Flexural strength	3,02 ± 0,1	2,85 ± 0,14	38,5 ± 0,9
Compressive strength	2,38 ± 0,43	1,91 ± 0,29	
<b>Low level water</b>			
Flexural strength	2,32 ± 0,11	2,32 ± 0,09	39,8 ± 1,4
Compressive strength	1,47 ± 0,54	1,42 ± 0,56	

Compressive strength is similar to the flexural strength (when usually for concrete one would expect a compressive strength up to 10 times higher than in bending). This behavior is generally typical of the cellular/porous ceramics (above 60% of porosity). The fracture of porous ceramics is better described by the quasi-brittle behavior as their ultimate fracture is triggered by many local events (different from essentially brittle behavior of glass ceramics), yet they are not preceded by highly dissipative processes associated with plastic deformation and strain hardening (as observed in ductile metals). Quasi-brittle fracture behavior is also observed in rocks, bones and ceramic composites. [116]–[118]

In this case the porosity alone is not high enough to explain behavior of the printed part; even if first preliminary CT analysis have shown that the porosity at layer interface is higher (up to 50-60%) than in the bulk part of the layer. But the phenomenon is influenced by more than just porosity of the materials: pores amount, distribution, shape, solid material properties, etc. affect the behavior. [116], [117] On these aspects more in-depth studies must be carried out.

In addition, in these tests the value of the first relevant crack (loss of load in the test) is selected for strength calculation, instead the total collapse value. For example, at §4.4, in the value shown in table 4.16, the compressive strength (max collapse load) is double of flexural one.

The compressive values show a higher standard deviation because of, in some cases, the non-precise planarity of facets conditions the test and the exact evaluation of the rupture is complicated.

These explanations are worth also for the other compression test results.

From Table 3.3 it can be also noted that high water samples reached better mechanical properties, but the loose in resolution is too high and the properties could be easily increase optimizing the raw materials and pos-treating the parts. This evidence confirmed the idea that, due to the critical process conditions (e.g. absence of mixing), a completed reaction is difficult

to be achieved. The study of the specific post-printing treatments will be described in detail in Chapter 5.

In conclusion, low water level was selected as standard optimized water column pressure. The printing parameters were layer voxel of 5,7 mm, laying speed of 100 m/s, printing speed of 200 m/s, electro valves continuously opened.

Further investigations on process and materials have highlighted few problems with this configuration. First of all, the continuous jet created evident directional grooves, reported in Figure 3.6 and Figure 3.7, onto the powder bed that create a weak interface between layers. The layer interface is a critical point of AM technologies and the disruption generated from water jet surely affect the strength of the piece.

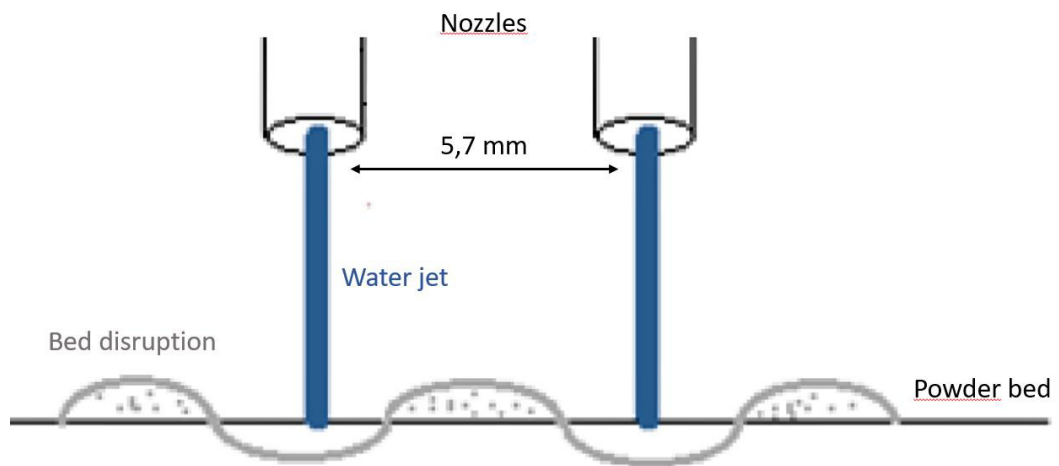
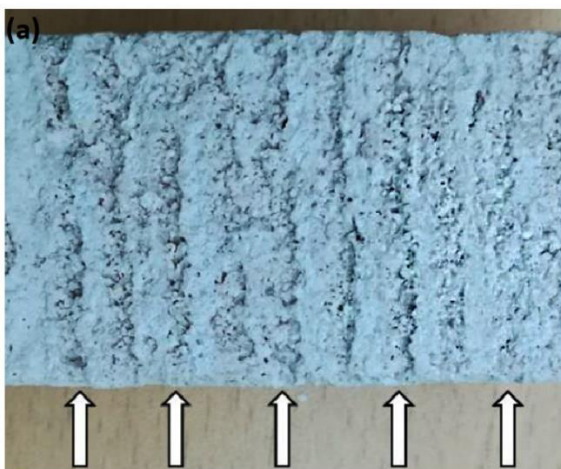


**Figure 3.6.** Deformation effect on powder bed cause by the water jet

**Layer top view**



**Layer section view**



**Figure 3.7.** (a) Interface between layers from the top; (b) the directional grooves created from water jet from the section.

Moreover, with this configuration there was a limited possibility to vary the parameters of the process. The water column height, i.e. the pressure of the system, was limited from the available space and the printing speed cannot be modify too much without vary the amount of water. In continuous deposition the printing speed determined how long the nozzle remains onto a single voxel, and so the amount of water deposited onto a voxel. In table 3.4 the time of passage onto a voxel is calculated for different voxel size and head speed.

The possibility to modify the printing speed, studied in this point, is strictly connected to another improvement idea. The deposition of powder also immediately after the water spraying, laying the powder during movement, at printing speed, of the head in printing direction (recoating system). Generally, the powder bed preparation was made a 100 mm/s (instead the 200 mm/s of the printing) and so printing and powder deposition cannot be carried out at the same time with this configuration.

**Table 3.4.** Summary of time of passage on voxel, according to voxel size and printing speed

<b>Time of passage [ms]</b>		<b>Voxel size [mm]</b>					
		<b>1,0</b>	<b>2,0</b>	<b>3,0</b>	<b>4,0</b>	<b>5,0</b>	<b>5,7</b>
<b>Vel [mm/s]</b>	<b>50</b>	20,0	40,0	60,0	80,0	100,0	114,0
	<b>100</b>	10,0	20,0	30,0	40,0	50,0	57,0
	<b>150</b>	6,7	13,3	20,0	26,7	33,3	38,0
	<b>200</b>	5,0	10,0	15,0	20,0	25,0	28,5
	<b>250</b>	4,0	8,0	12,0	16,0	20,0	22,8
	<b>300</b>	3,3	6,7	10,0	13,3	16,7	19,0

A drop on demand configuration is implemented to increase the configuration possibilities of the operative parameters, to create a more homogeneous patter of water deposited (discontinuous single droplets instead of continuous linear flow), to solve the problem for implementing a recoating system. Water amount in droplets deposition is unlinked to printing speed.

The droplets were created simply setting a short opening time of the electro valves. The opening time and the water column height required to deposit the same optimized water amount of continuous deposition was investigated, verifying that remains lower that the time of passage (otherwise the deposition return continuous).

After various tests the optimum parameters were found with a pressure ( $\Delta h$ ) of 1000 mm and an opening time around 18 ms. Table 3.5 summarizes the values of the different configurations.

**Table 3.5.** Water amount with drop on demand configuration, comparison with previous evaluation.

<b>Water per voxel</b>		
<b>Theoretical calculation</b>	<b>Continuous flow</b>	<b>Drop on demand</b>
Stoichiometry and resolution compromise	$\Delta h = 350 \text{ mm}$	18 ms; $\Delta h = 1000 \text{ mm}$
0,038 mL	0,035 mL	0,036 mL

The definition of the new water column height allowed to design the final water vessel that was mounted onto the printing head, to be integral with the moving up in z axis. The water vessel guarantees always the same pressure level refilling automatically the level with a float valve. The tests, made with different opening times, also highlighted the linearity of the increase of water with the increase of opening time. Figure 3.8 show the behavior of the water per voxel amount.

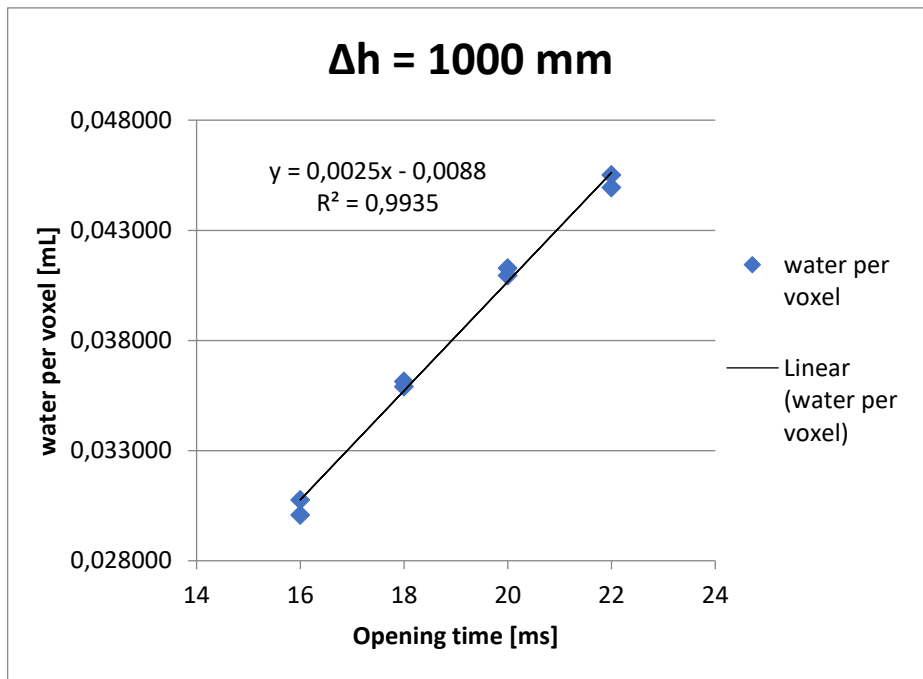


**Figure 3.8.** Behavior of water per voxel amount at fixed pressure and variable opening time.

Following the idea of design different height vessels according to the printer dimension and the free available space, the re-adaptation of parameters (time and  $\Delta h$ ) was studied. Reducing the height of water vessel level, new value fixed at  $\Delta h = 700 \text{ mm}$ , the same water amount (of  $\Delta h = 1000 \text{ mm}$ ) is been achieved with 22 ms as opening time (Table 3.6).

**Table 3.6.** Water per voxel at different pressures and opening times

Pressure	Opening time	Water per voxel
$\Delta h = 1000 \text{ mm}$	18 ms	0,0352 mL
$\Delta h = 700 \text{ mm}$	22 ms	0,0358 mL

Therefore, keeping in mind the limitations exposed in Table 3.4, the height of water vessel can be adjusted to printing size necessities.

As already mentioned, closely related to droplets deposition, the recoating system, shown in Figure 3.10, has also been implemented. The use of recoater allows to immediately coat the wetted zone with new powder, adding the fourth direction for water diffusion, Figure 3.9, and creating an immediate connection of the consecutive layers. Furthermore, the recoating system could contain material for more than one layer, reducing and simplifying the manual operations and above all increasing the repeatability and the accuracy of the process.

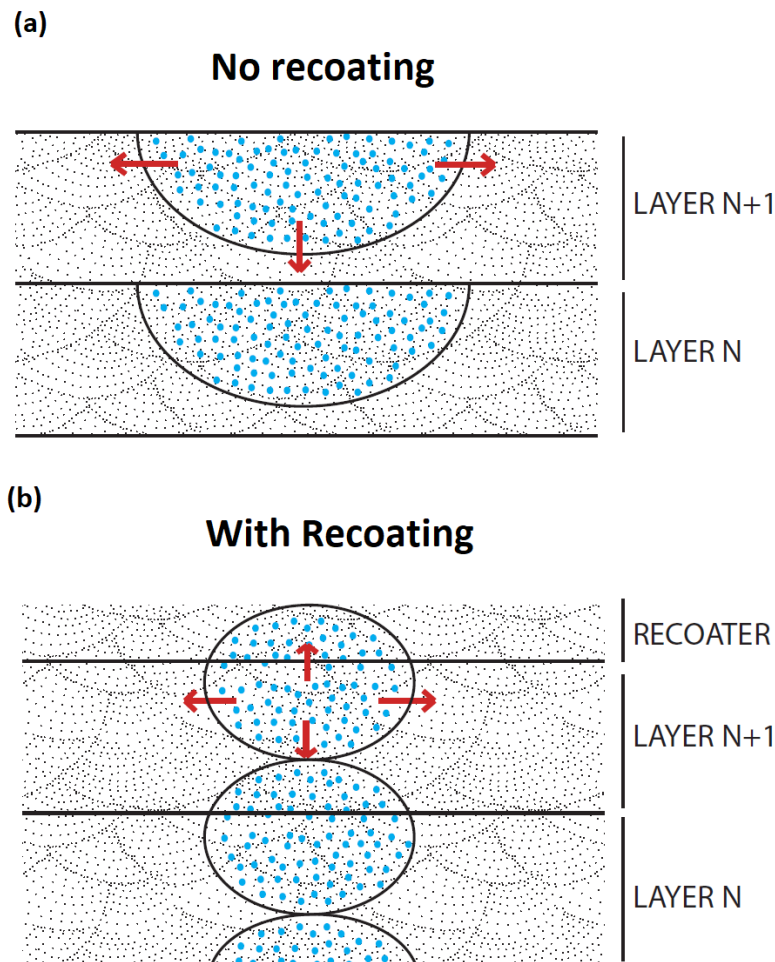


**Figure 3.9.** (a) water diffusion without recoater; (b) water diffusion with recoater.

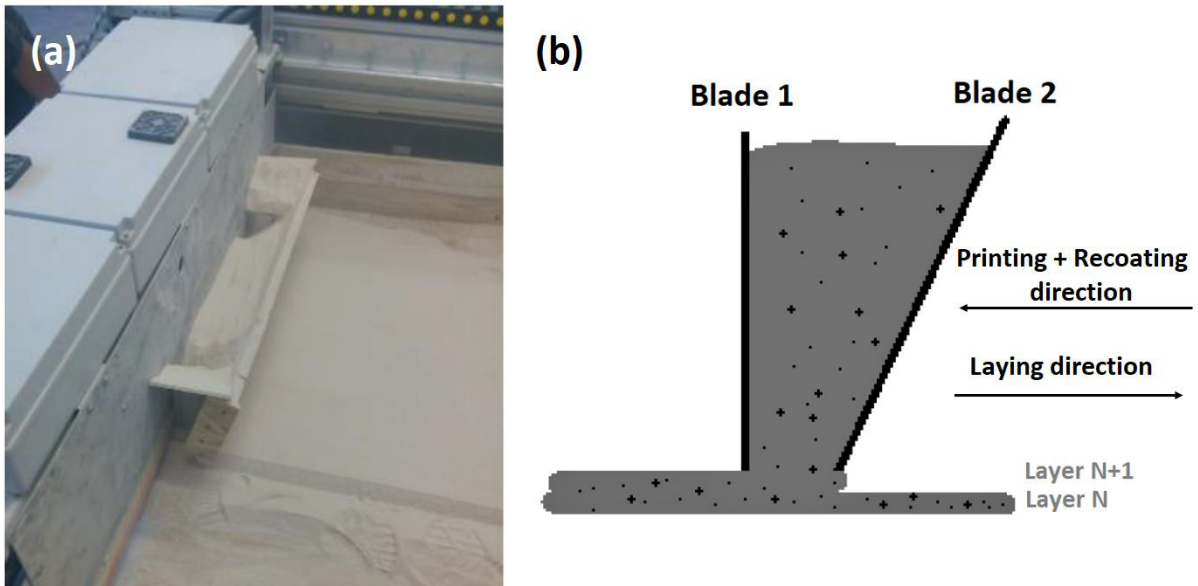


**Figure 3.10.** (a) testing of first recoating system; (b) schematic principle of the recoater.

The first recoater geometry, moving a large amount of powder, gave problems of powder displacements, probably generated from the huge amount of powder that presses and pushes onto the powder bed. An improved recoating system with a smaller opening and sloped walls was implemented, Figure 3.11. And the laying and printing speeds were reduced to 50 mm/s in order to flatten a more precise powder bed.

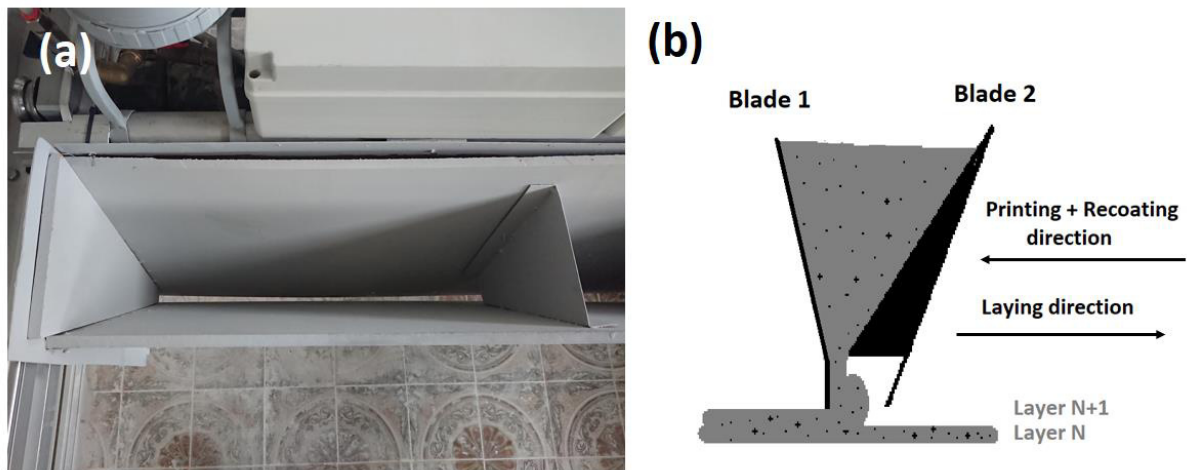


**Figure 3.11.** (a) recoater with reduced opening; (b) schematic principle of the final geometry.

The new tests manufactured samples without defects and the final recoating system was design and mounted in the printer, becoming a new standard tool for printing process. The recoating system, depending of printing area dimensions, contains the materials needed for 3 to 5 layers. Since the recoater was not closed on the bottom, a continuous flow of powder occurred, the

layer distribution was divided 70% after water during printing and the remaining 30% during laying movements.

Samples with BdZ and 25% of binder were printed to compare the new configuration ( $\Delta h = 1000$  mm, opening time = 18 ms, printing speed = 50 mm/s, with recoater) with the old one ( $\Delta h = 350$  mm, opening time = always open, printing speed = 200 mm/s, no recoater). The mechanical properties are shown in Table 3.7.

**Table 3.7.** Mechanical properties comparison between optimized continuous and droplet configuration.

Configuration	Mechanical Strength [MPa]		Porosity [%]
	Orto layer	Para layer	
<b>Continuous flow</b>			
Flexural strength	2,32 ± 0,11	2,32 ± 0,09	39,8 ± 1,4
Compressive strength	1,47 ± 0,54	1,42 ± 0,56	
<b>Drop on demand</b>			
Flexural strength	2,40 ± 0,35	1,86 ± 0,32	41,8 ± 1,0
Compressive strength	2,10 ± 0,17	1,68 ± 0,30	

The resolution of the bars is remained as good as with old configuration. No significant increase in properties is noticed, and even the porosity is a little increased. The reason could be identified in the disruption effect on the powder bed due to the droplet, that remains important and without a sufficient attenuation given the recoating system. The layer interface observation (Figure 3.12) clarified the situation. Even with the droplets the water impact generates a significative alteration in the bed, because of the water surface tension, the acceleration due to falling down and electro valve pushing out.

**Layer top view**



**Layer section view**

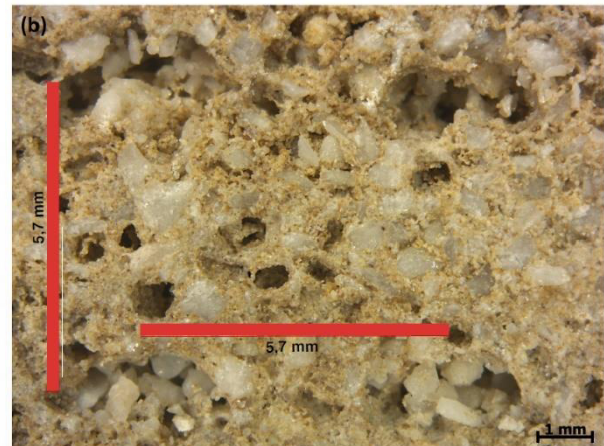


**Figure 3.12.** (a) Interface between layers from the top and (b) the voids created from water droplets from the section.

Although the droplets deposition hasn't increased the mechanical properties, it's become the standard configuration (with recoating system addition) of the printing process. The resolution and the mechanical properties are remained in the same range of before and, surely, the interface is more homogeneous. Moreover, the presence of the recoating system is very useful to increase the repeatability and the stability of the printing process, not to mention the enormous advantage of reducing the manual workload for the powder mix handling. Making improvements in this direction is also important to lay the foundation for process automation (the recoater could be loaded semi-automatically or automatically with the right amount of powder).

In conclusion, the recoating system is been implemented and the printing parameters are been modified to a layer voxel of 5,7 mm, divided in 30% - 70%, a laying speed of 50 m/s, a printing speed of 50 m/s, an electro valves opening time of 18 ms, with a pressure of  $\Delta h = 1000$  mm. A picture of the printer with final implementations is reported in Figure 3.13.





**Figure 3.13.** Actual configuration of the printer with water vessel and recoating system. [95]

Despite the improvements carried out, the interactions between water droplet and powder bed still generated an irregular and altered layer interface. The presence of macro porosity concentrate at the interface is the cause of inhomogeneity microstructure and low resistance. The resolution of this problem is a great but complicated challenge. For this reason, further ideas and tests were carried out.

A first easy solution is to minimize the distance between nozzle and powder bed. In this way the droplet accumulates less kinetic energy and impacts with the powder in a gentle way.

The simple experiment reported in Figure 3.14a, in which a droplet is manually deposited onto a powder bed demonstrated the effectiveness of this action.

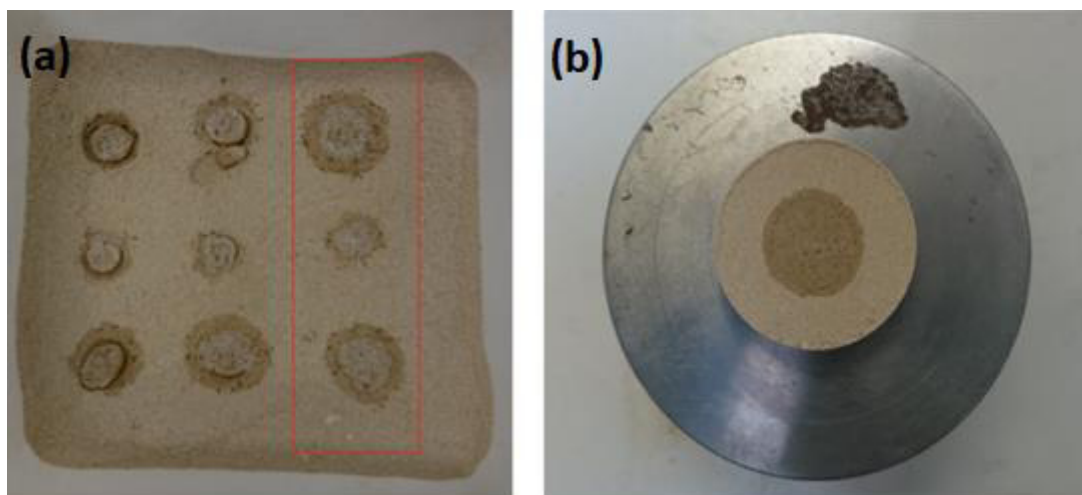


**Figure 3.14.** (a) Droplet impact from decreased distance from the powder; (b) droplet onto a pressed bed.

A compressed (5 kN pressed tablet) bed, Figure 3.14b, showed lower impact zone and flushing away of binders (finest particles). Compression of the bed is a very complex operation during printing process; an easier solution is to prepare very flowable mix that should compact themselves during spreading. More details on mixes behavior will be given in Chapter 4.

The distance between nozzles and powder bed was modified as close as possible, approximately at 5 – 6 mm.

A second idea was to add surfactants in the printing water with the aim of reducing water surface tension and limited the hole generation. Common economic soap was used as surfactant, to keep the concept of using and performing easy operations, as it's possible at the company.

Droplets of water, water + surfactant (common soap), water + ethanol are deposited on the different powder bed. The water with additives seems to give lower impact zone, but the effect needs further investigation. Figure 3.15 reports the results.



**Figure 3.15.** (a) water droplet on BdZ printing mix; (b) water plus soap droplet on BdZ printing mix; (c) water plus ethanol droplet on BdZ printing mix.

The reduction of surface tension could have the secondary advantage of allowing a smaller droplet release. If limited amount of water has to be deposited, the critical condition of minimum pressure or low opening times could be mitigated by the reduced surface tension. After all, the surfactant modification wasn't further investigated because the difficulties of adding soap in printing water. An intermediate step must be introduced to prepare the water and frequently a foaming effect is generated.

A final hypothesis to reduce the impact zone was to modify the nozzle configuration in order to divide the droplet and reduce the compact mass of water that impacts the bed. The division of water flow or droplet is a complex operation, due to the high surface tension that tend to maintain the water attached to small space and the necessity of deposited a specific amount of water in a precise point. Despite the possibility to introduced new issues, the study of nozzle modifications was carried out because the interaction between water and powder-bed is a central point to obtain high quality pieces.

Flow diverters, shown in Figure 3.16, with inclination of 20° or 25° were design, produced and tested on the printer with a Sand printing mix, together with mesh filters of 1 mm and 0,5 mm, Figure 3.17.

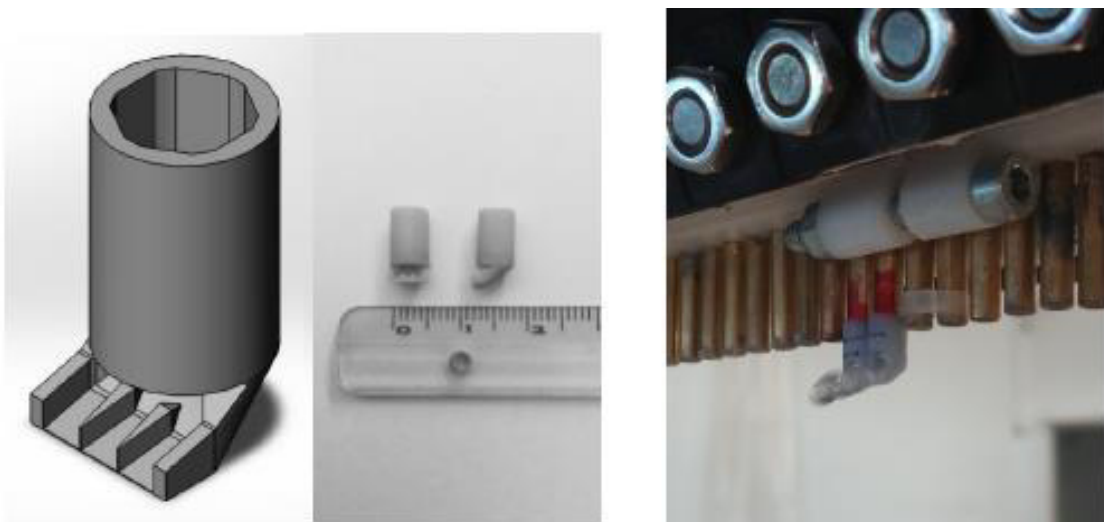


**Figure 3.16.** Flow diverter geometry and test on the printer.

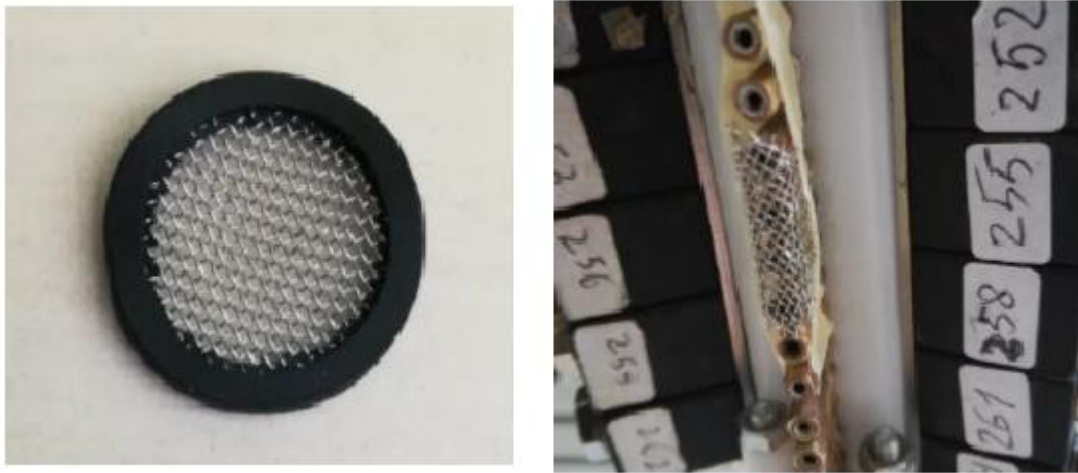


**Figure 3.17.** Filter geometry and test on the printer.

The flow diverter solution shows some problem of stability of the flow. Often surface tension connected two or more nozzle in only one generating an uncorrected deposition and bad resolution of the part. In Figure 3.18 flow union and wrong deposition position are shown.

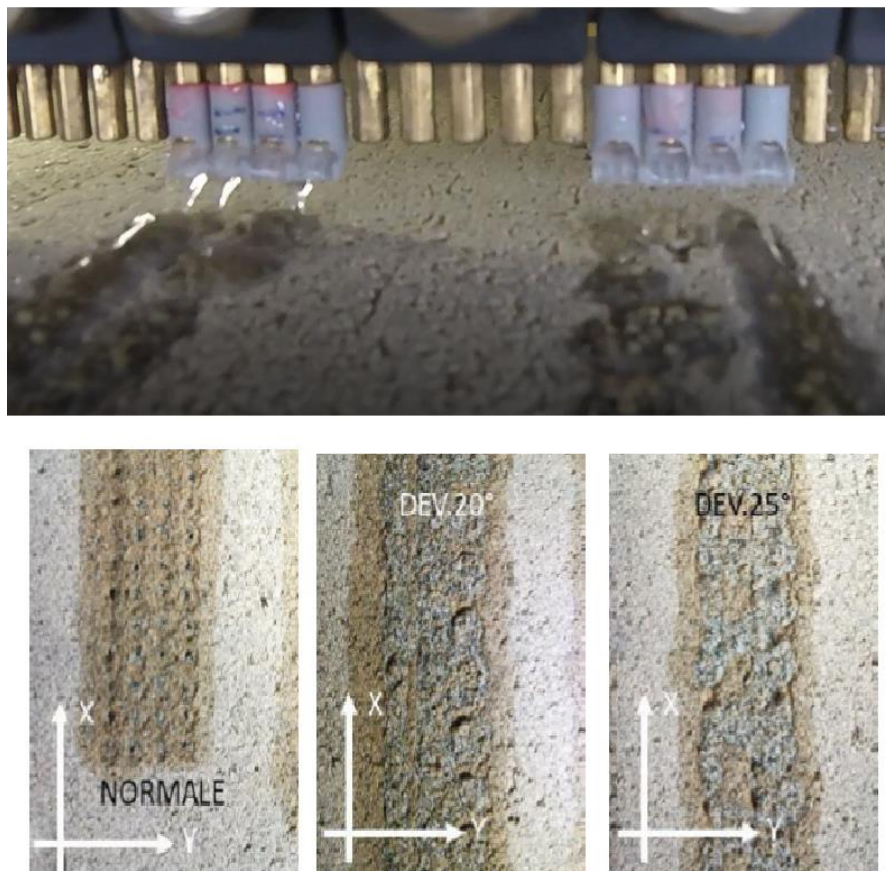


**Figure 3.18.** Flow diverter in action and top view of printed layer.

The filter worked better, without flow connection problems. The resolution was decreased once again. The impact zone and the hole created by the droplet is reduced but the creation of an opened large flow of water adds problem of pushing and flushing out of the finest particle, that are prevalently binder, see Figure 3.19. Although the hole in reduced the connection between layers isn't improved due to the low binder present on the interface.

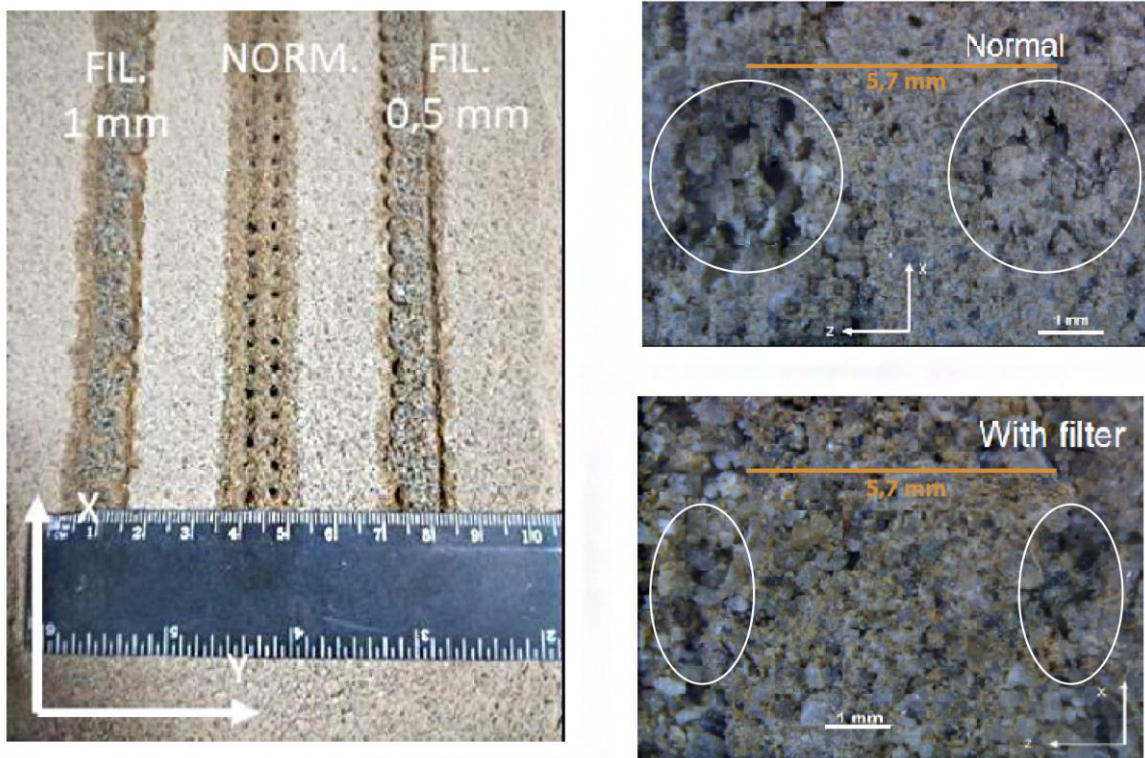


**Figure 3.19.** Top view and microstructure of printed layer with filter.

These preliminary nozzle modifications confirm the lower impact zone/hole of a divided flow, even if showing some new problems in water position and resolution and in homogeneity and presence of binder at the interface.

The interaction between water and powder bed is a critical point. Water deposition system and preparation of powder mixes/bed have to be further investigated and improved.

### 3.3 Conclusions

The optimized configuration for the printer was investigated. The fundamental parameters, speed for powder deposition and water deposition, electro valve opening and pressure of the liquid system, were identified for the initial continuous water flow process. With these

parameters the desired amount of water was deposited, and it was also verified that a good resolution was achieved.

To increase stability and repeatability of the process and to reduce interface defects and inhomogeneity in the microstructure a new process was investigated. A drop on demand water deposition was developed. Meanwhile a water vessel, with automatic refilling, was mounted integral with the printing head and a reacting system, that deposits powder immediately after water, was implemented.

The printing parameters, for a 5,7 mm voxel, were become a laying speed of 50 m/s, a printing speed of 50 m/s, an electro valves opening time of 18 ms, with a pressure of  $\Delta h = 1000$  mm and powder voxel deposition divided in 30% - 70%.

Even if the process was become more stable and the manual operations were reduced, the interface between layer presented an important macro porosity, due to water-powder bed interaction issue.

Several hypotheses were considered to reduce this problem, such as reduced nozzles – powder bed distance, addition of surfactants to reduce surface tension and increase the wettability, modification of nozzle geometry to deposit lower energy droplets.

A final effective configuration wasn't found out, because of complexity of management and other issues generation. Bed disruption and macro porosity at interface remains an open point. Further investigations have to be studied.



# Raw materials and printed parts

In this chapter the characteristics of the raw materials (especially binder components), of the printing mixes and, lastly, of the final product, are evaluated.

As describe in the introduction, the choice of magnesium oxide and acid phosphate quality can strongly influence the binding reaction and the final printed part in terms of setting time, reaction rate, homogeneity, resolution and strength. For this reason, different products are selected and evaluated, not only from the physico-chemical point but also from the economic and availability one.

The analysis of the printing mixes gives useful information about the flowability of the powder and the density and the packing of the deposited powder-bed. In this section also the contribution of the single aggregates is given.

The final product analysis is very important to have the state of art after the various modifications and improvements carried out during the research. New possible applications or improvement hypothesis can be studied starting from the results of specific tests, strong points and weak points.

## **4.1 MgO analysis**

Caustic calcined magnesia (i.d. treated at low temperature, high reactivity) was selected as first binder component to achieve a very fast reaction and set as needed form a printing process on large scale. The most important parameters are the reactivity of the powder, connected to its specific surface area (SSA) and porosity, and the particle size, connected to oxide-phosphate reaction that occurs on particles surface. Using these values and the empirical results from printing tests different magnesium oxides were analyzed and selected from the commercial availability.

### *4.1.1 Materials and methods*

All the MgO considered during this research work are highly reactive light burned magnesia (CCM). The reference MgO is the one that was currently used in the company, MgO OGO 83 Rosso (Eraclit-Venier spa, Venezia, Italy). But following the necessity to find another vendor for a stable supply of product (the first company have had economic issues), different new products were studied. Two were already used in cements field for MOC, and they have same



characteristic a part form activity value, one high value and one low value, MgO 95 HR e MgO 95 LR (Magnesium oxide consulting srl, Bergamo, Italy). The third was prevalently commercialized in animal feed sector, RKM 83 (RHI Magnesita GmbH, Radenthein, Austria). In Table 4.1 the composition and particle size, declared form the supplier, are reported. All the MgO are fine powder, completely below 100  $\mu\text{m}$ , whereas the have different composition and MgO purity. The RKM83 contained larger amount of Iron oxide which give a beige color at the powder, instead of white-reddish.

**Table 4.1.** Different MgO composition and particle size, data given by the producers.

<b>CCM type</b>	<b>MgO (wt%)</b>	<b>CaO (wt%)</b>	<b>Fe<sub>2</sub>O<sub>3</sub> (wt%)</b>	<b>Particle size</b>
Eraclit_OGO 83	83	4	-	82% below 63 $\mu\text{m}$
Carl Spaeter_HR	95,8	1,48	0,37	Below 76 $\mu\text{m}$
Carl Spaeter_LR	95,8	1,48	0,37	Below 76 $\mu\text{m}$
RHI_RKM 83	83	4,5	4	90% below 55 $\mu\text{m}$

The different MgO are analyzed in terms of reactivity and SSA, in relation with the binding phase properties developed by identical conditions printing mixes prepared with them. The tests performed are described below.

All the samples considered in this section were printed with BdZ as aggregate and with the 20% of binder. Large part of these tests was conducted at the beginning of the PhD, and due to the low amount of MgO test dose, the printed samples were produced reproducing the printing process in a manual way. The process consists in a box in which the powder is manually spread with a blade and activated by the water deposited from a syringe. In previous master thesis a comparison between the two procedures was performed, giving result similar enough to validate manual printing as preliminary evaluation test. [110]

All the samples considered in this section were printed with BdZ as aggregate.

MgO activity was evaluated with neutralization time of MgO by a citric acid solution (higher the time, lower the reactivity), following the procedure used form one of the suppliers; a similar method is used also in [90].

A citric acid solution 0,4 N was prepared and brought to the temperature of 30°C, then 2 g of MgO powder was added under stirring. The time required for turning a color indicator (phenolphthalein) was measured. Figure 4.1 shows the procedure and the color change.



**Figure 4.1.** Activity test: on the left the solution before the addition of MgO, on the right the same after the change of the indicator during the neutralization reaction

The evaluation of the indicator color change is visually appreciated. Therefore, it would be advisable to do more tests to have a mediated value, especially for non-white MgOs that "dirty" the solution, making more difficult to observe the color change. The expressed value is the mean of five measurements.

SSA data were collected through N<sub>2</sub> adsorption experiments at liquid nitrogen temperature using a Quantachrome Nova Station A (Quantachrome Instruments, Boynton Beach, FL). All samples were degassed at 250°C prior to the nitrogen adsorption measurements. The Brunauer-Emmett-Teller specific surface area was determined by the multipoint BET method using the adsorption data in the relative pressure ( $P/P_0$ ) range of 0,05 – 0,3.

X-ray diffraction (XRD) pattern of commonly used MgO was collected to have a reference during the analysis of the complete printing mixes, using an X-ray diffractometer (D8 Advance, Bruker Italia Srl, Milano, IT) with Cu K $\alpha$  radiation, step scan 0,02°, 2 s / step. The Match! software package (Crystal Impact GbR, Bonn, Germany) was used for a semi-automatic phase identification, supported by data from PDF-2 database (ICDD-International Centre for Diffraction Data, Newtown Square, PA, USA).

The geometrical bulk density was calculated as mass on volume, sample dimensions collected with a digital caliber. The apparent density of sample was measured by means of a helium pycnometer (Micromeritics AccuPyc 1330, Norcross, GA). The total porosity of the sample

was therefore calculated as the ratio between their geometric bulk and apparent density. The porosity value is the average between all the tested sample, both bars and cubes.

The compressive strength of the samples was measured with an Instron 1121 UTM (Instron Danvers, MA) with a cross head speed of 1 mm/min. Both the perpendicular and the parallel direction to the layer were tested. At least five samples were tested for each type of loading direction. Samples had an average size of 30 x 30 x 30 mm<sup>3</sup>.

Due to the manual post processing, some samples were not exactly dimensioned, especially in planarity of the plane, and this could determine high standard deviations.

The morphology of the parts was investigated by an optical stereoscope (STEMI 2000-C, Carl Zeiss AG, Oberkochen, DE) and by SEM microscope (ESEM, Quanta 200, FEI, Hillsboro, OR).

#### 4.1.2 Results and discussion

First of all is important to note that, due to the high reactivity, the MgO powders must be conserved in closed box and dry place, without humidity an air, to avoid the reactions with water and carbon dioxide.



The reactivity test and SSA analysis give the value reported in Table 4.2. The first three MgO are in similar range, indeed the RKM83 presents significantly lower reactivity and surface area. The very long time, measured for the RKM83 could be partially affected by the presence of iron oxide that made complex the color change evaluation, but the SSA analysis confirmed its lower reactivity

**Table 4.2.** Activity and SSA value of MgO powders.

<b>CCM type</b>	<b>Activity time</b>	<b>SSA [m<sup>2</sup>/g]</b>
Eraclit_OGO 83	50-70 sec	55,0
Carl Spaeter_HR	70-80 sec	41,3
Carl Spaeter_LR	180-190 sec	20,6
RHI_RKM 83	30 min	9,5

A BET surface area of 10 m<sup>2</sup>/g still allow a fast setting as found by E. Soudeè et al. [88]. Moreover, considered the particular conditions in which the reaction takes place, a longer setting time should allow a more homogeneous and continuous binding phase develop. The hydration product crystals contact each other, joining with the core of unhydrated magnesia particles, and form a good net structure. If the hydration reaction rate of magnesia is too fast, the result is numerous tiny hydration products. This can lead to many flaws in the microstructure and thus lower strength. Large internal stresses can form during the growth process of crystals, which can also reduce the compressive strength. [86]

Table 4.3 reports all the data about the mechanical properties and the porosity of the different MgO samples. It is important to highlight again that the manual printing process can be obviously subjected to operative differences, which can accentuate some aspects.

**Table 4.3.** Properties of different MgO samples, produced with manual printing.

<b>MgO type</b>	<b>Compression Strength [MPa]</b>		<b>Porosity [%]</b>
	Orto layer	Para layer	
<b>OGO 83</b>	1,98 ± 0,3	2,24 ± 0,71	42,96 ± 1,25
<b>MgO95_HR</b>	2,06 ± 0,32	1,73 ± 0,23	41,46 ± 0,75
<b>MgO95_LR</b>	1,45 ± 0,32	2,01 ± 0,29	42,63 ± 1,03
<b>RKM 83</b>	4,47 ± 2,5	5,15 ± 1,6	31,35 ± 1,47

The value obtained with RKM83 MgO is higher, more of 4 MPa, than the other (around 2 MPa) which are all in the same range. The porosity of the RKM83 samples is very lower and, supposing the possibility of a higher pressure given during manual printing (deposition and levelling of the powder), a new series of samples with OGO83 and RKM83 (25% of binder) were printed using DESA1 150.150 printer at the company to make a new comparison. Table 4.4 reports the results obtained.

**Table 4.4.** Properties of OGO83 e RKM83 samples, produced with Desa printer.

<b>MgO type</b>	<b>Compression Strength [MPa]</b>		<b>Porosity [%]</b>
	Orto layer	Para layer	
<b>OGO 83</b>	2,35 ± 0,54	1,82 ± 0,66	38,46 ± 1,29
<b>RKM 83</b>	3,09 ± 0,52	2,49 ± 0,86	35,75 ± 0,95

The properties of RKM83 sample produced with the printer becomes lower and more similar to the other. The printing Microstructural analysis with SEM microscope is performed on these sample to observe difference in binding phase. Figure 4.2 and 4.3 shows OGO83 and RKM83 samples respectively, at different magnifications.

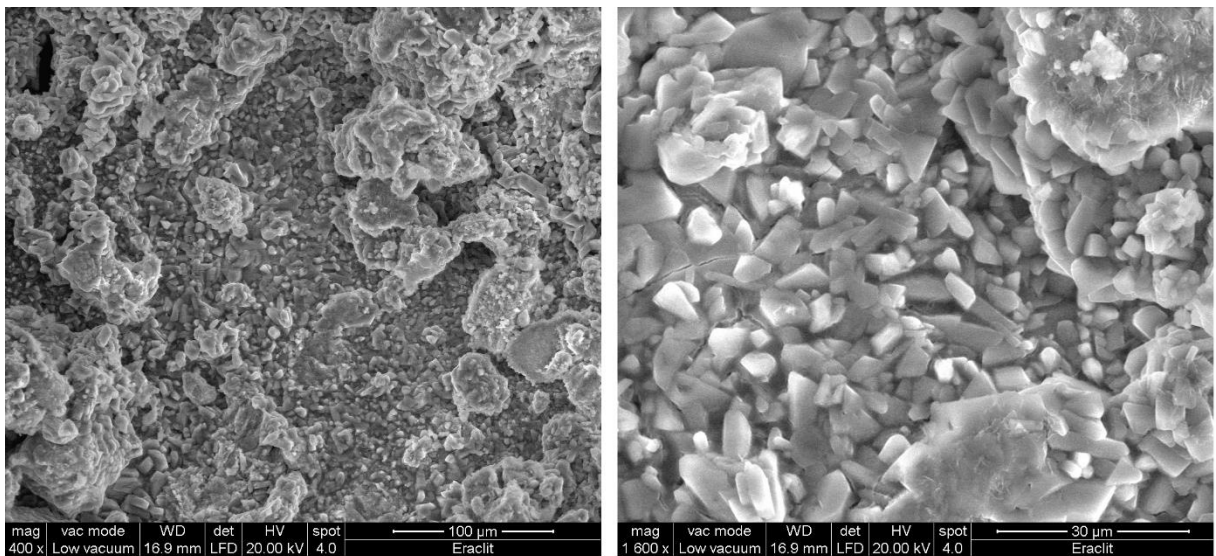


**Figure 4.2.** SEM image of binding phase of OGO83 sample, on the left 400x; on the right 1600x.

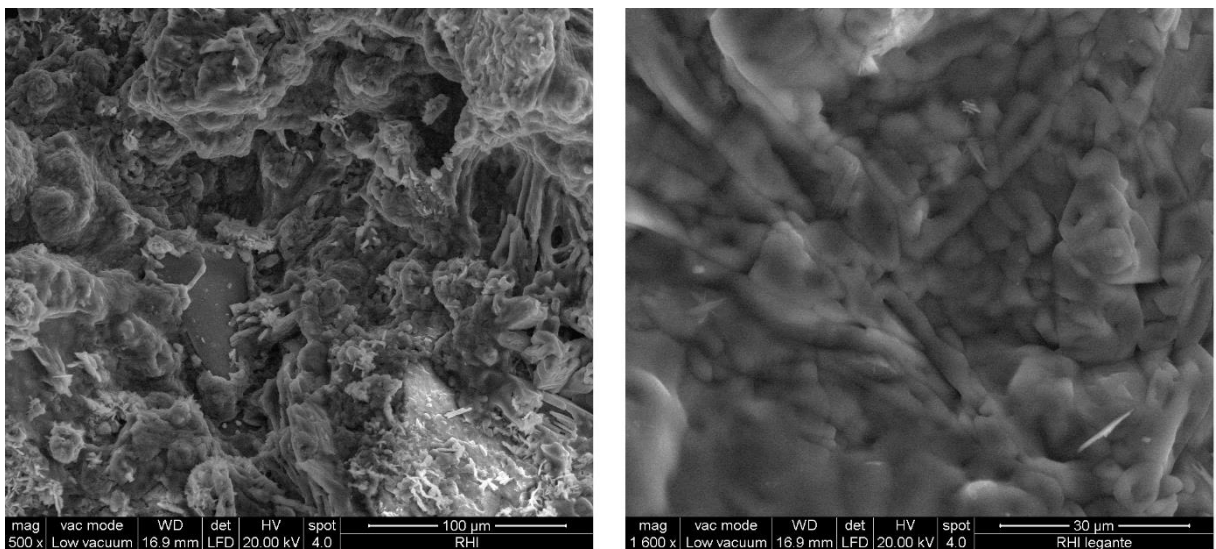


**Figure 4.3.** SEM image of binding phase of RKM83 sample, on the left 500x; on the right 1600x.

The SEM image of RKM83 shows a more homogenous material, with less small crystal, that is consistent with the hypotheses of a better developing of the phase.

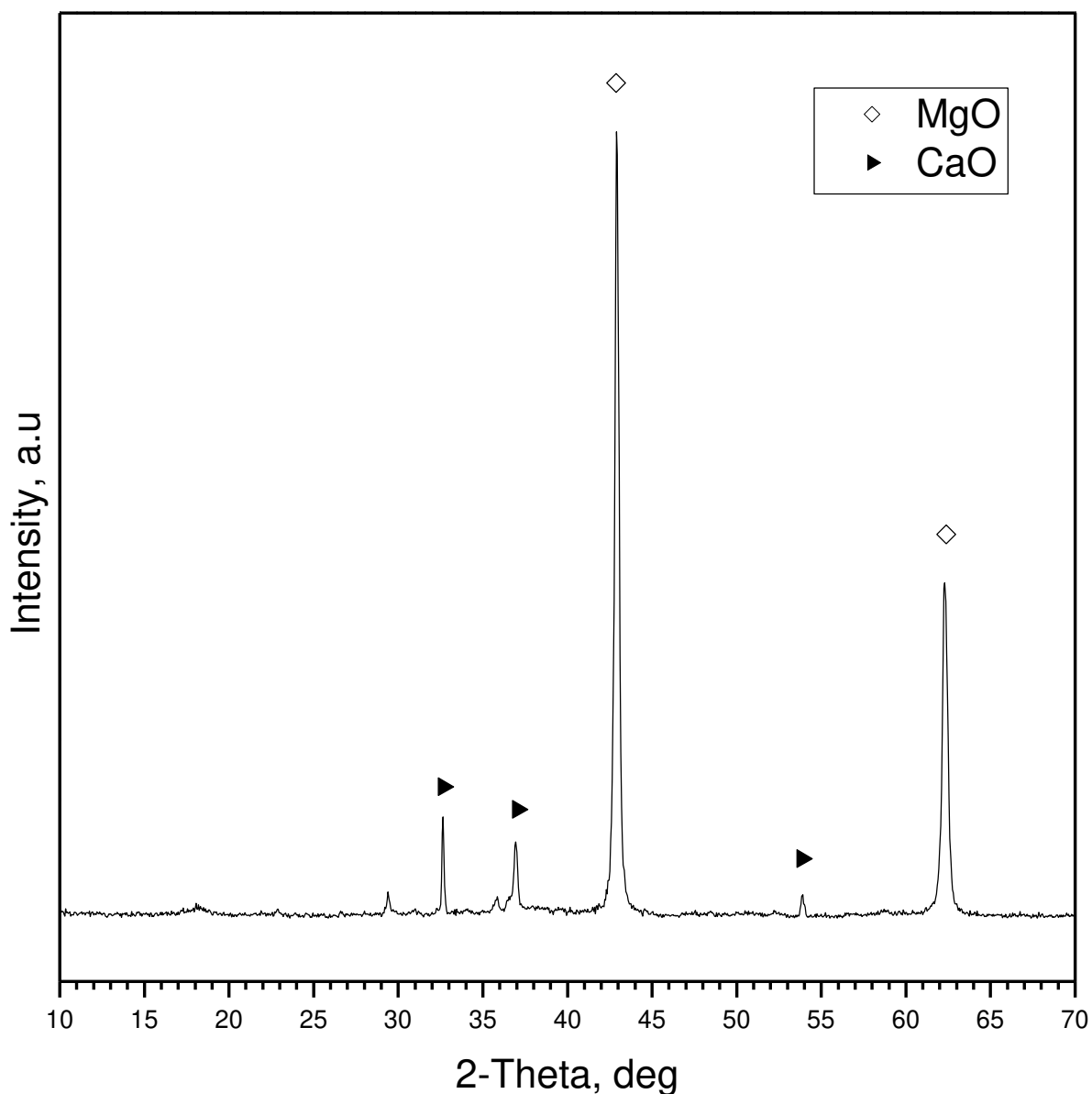


**Figure 4.4.** XRD pattern of MgO from RHI Magnesita.

The XRD pattern (Figure 4.4) confirmed the presence, as main phase of magnesium oxide (MgO, PDF#87-0652) and Calcium oxide as secondary one. The identification of MgO typical pattern will result very useful to the phase analysis of single reagents in complete printed material XRD.

### **4.1.3 Conclusions**

The analyses on magnesium oxide powders have demonstrated that composition and purity are not so important to achieve good mechanical properties while the reactivity is the parameter that must be controlled. To a better developing of the binder phase a not extremely high reactivity is suitable, for giving the time to a homogeneous and complete reaction. Nevertheless

the product has to remain a light burned MgO, with SSA at least around 10 m<sup>2</sup>/g, to perform the bonding reaction fast enough to follow the construction speed. The typical particle size of MgO powders is already fine and suitable to the printing process.

The OGO83 can be substituted with RKM83, lower cost more and stable supply. However, the color of the mix is modified toward the beige. After further request we find that the same supplier can provide also a white MgO, very similar to OGO83.

## **4.2 Acid Phosphates analysis**

Mono potassium phosphate (MKP, KH<sub>2</sub>PO<sub>4</sub>) was selected as second binder component. Also mono sodium phosphate (MSP, NaH<sub>2</sub>PO<sub>4</sub>), although the poor literature on its use for cements and on its binding phase, is been evaluated for the high solubility in water. The most important parameters for phosphate are indeed the solubility, higher the solubility faster and more complete the reaction, and the fine particle size to obtain a homogenous well-dispersed mix. To limit the cost and have a simply, daily, and in low quantity supply a product from ferti-irrigation agricultural filed is used. The particles of this product are crystal up to 2 mm. The large size of MKP crystal complicates dispersion and homogeneity in the mix and the dissolution in water. For this reason, the performance of the milled MKP powder is been evaluated. Other mono potassium phosphates used in alimentary filed (E340) are finer particles but purer and with higher cost, that is very prohibitive in large scale applications.

Part of the results described were obtained with the collaboration of students, F. Zanetti (2017) [119] and A. Zecchini (2018) [120].

### ***4.2.1 Materials and Methods***

Two different mono potassium phosphate were studied during the thesis, both of them came from the agricultural field. The first ICL MKP (ICL Italy srl, Milano, Italy) and the second AgriMKP (Agri2000Italy srl, Alberone di Ro (Fe), Italy).

As already mentioned, the solubility of MKP in water is around 230 g/L at 20°C and the crystals of the MKP agricultural products are quite irregular and bigger (up to 2mm), so the advantages of a sift step or a milling step were evaluated to improve the reaction rate.

The reduction of MKP particle size is especially necessary in the printing with reduced layer thickness. A second printer is been build up by Desamanera for the Industrial Engineering Department (DII) of University of Padova, with an increased resolution to 3 mm instead the 5,7 mm present in company printer. The printer is prevalently used for research and test new

formulations. Due to 3 mm voxel, with this printer the particle size of the MKP have to be surely decreased by milling o sieving to create a more homogeneous and smooth powder bed. Also the use of a mono sodium phosphate was preliminary studied. The MSP has as higher solubility of 1100 g/L and, because of its use as advance additive, the products is a fine white powder. Table 4.5 reports the solubility of different phosphates.

**Table 4.5.** Different acid phosphate solubility and particle characteristics. Data given by the producers.

	<b>ICL MKP</b>	<b>Agri MKP</b>	<b>ICL MSP</b>
<b>Solubility in water</b>	230 g/L at 20°C	230 g/L at 20°C	1100 g/L at 20°C
<b>Particle size</b>	Irregular white crystal	Irregular white crystal	Fine powder

The sieving of the MKP powder was performed at 3 sieves opening of 500 µm, 300 µm and 150 µm. The milling was performed with a jaw crusher Retsch BB50 (Retsch GmbH, Haan, Germany). To prepare the printing mix with finer MKP the fraction between 80 µm to 400 µm was selected.

The improvement of the finer MKP powder was evaluated in term of strength and resolution of bar samples, size of 30 x 30 x 130 mm<sup>3</sup>, printed samples using a mix with 20% of binder and the 3 m layer printer at DII laboratory. The dimensions of the different mixes were collected and compared, after accurate cleaning (no machine post-processing). The mechanical strength was measured after post-processing to have more precise and planar surface.

X-ray diffraction (XRD) pattern of commonly used MgO was collected to have a reference during the analysis of the complete printing mixes, using an X-ray diffractometer (D8 Advance, Bruker Italia Srl, Milano, IT) with Cu K $\alpha$  radiation, step scan 0,02°, 2 s per step. The samples are milled in a very fined powder and every time the same amount is collected to perform the acquisition. The Match! software package (Crystal Impact GbR, Bonn, Germany) was used for a semi-automatic phase identification, supported by data from PDF-2 database (ICDD-International Centre for Diffraction Data, Newtown Square, PA, USA).

The geometrical bulk density was calculated as mass on volume, sample dimensions collected with a digital caliber. The apparent density of sample was measured by means of a helium pycnometer (Micromeritics AccuPyc 1330, Norcross, GA). The total porosity of the sample was therefore calculated as the ratio between their geometrical bulk and apparent density.



The strength of the samples was measured with a Instron 1121 UTM (Instron Danvers, MA) with a cross head speed of 1 mm/min. At least five samples were tested for each type of loading direction.

#### 4.2.2 Results and discussion

First of all is important to note that, due to its solubility in water, the MKP powder must be conserved in closed box and dry place. The humidity tends to pack and agglomerate the powder. The sifting test, reported in Table 4.6, on AgriMKP has demonstrated that most of the crystals remain on the 500  $\mu\text{m}$  sieve, around 80%. The ICL MKP seems to work better, 70% between 150  $\mu\text{m}$  and 500  $\mu\text{m}$ .

Table 4.6. Sieving result of different supplier MKP.

	Agri MKP	ICL MKP
Granulometry (microns)	Passed quantity [%]	Passed quantity [%]
> 500	81,5	12,1
300 < x < 500	16,4	34,8
150 < x < 300	2,0	40,4
< 150	0,1	11,7

But the visual and microscope observation have shown the irregular shape of the crystals, that have acicular shape with a dimension predominant. So, especially for ICL MKP, a lot of bigger crystals pass the sieve favorably orientating on the short side. Agri MKP is more regular than ICL one. Figure 4.5 shows the sieved crystals.

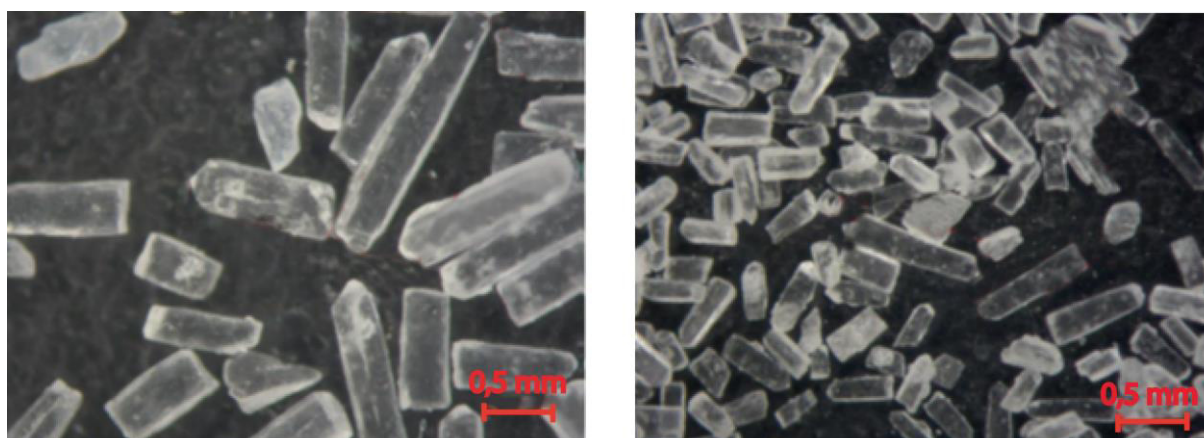


Figure 4.5. Sieving of MKP, on the left the residues at 300  $\mu\text{m}$ ; on the right the residues at 150  $\mu\text{m}$ , x1,6 of magnification.

The milling of the MKP gives a more homogenous powder that can be easily sieved to exclude too fine and too coarse part (below 50  $\mu\text{m}$  and above 500  $\mu\text{m}$ ).

The printing test, performed using the as supplied and the milled and sieved Agri MKP powder, show an increase in quality of the bed, resolution of the part and final strength given by the finer MKP. Table 4.7 shows the resolution results on bar printing.

**Table 4.7.** Resolution results of bars printed with different MKP granulometry.

MKP state	Bar dimensions			Deviation from 3D file		
	L [mm]	B [mm]	H [mm]	L [%]	B [%]	H [%]
<b>3d file</b>	135	30	30	/	/	/
<b>As supplied</b>	152,70	51,98	42,40	13,1	73,2	41,3
<b>Milled and sieved</b>	144,8	40,46	35,69	7,2	34,8	18,9

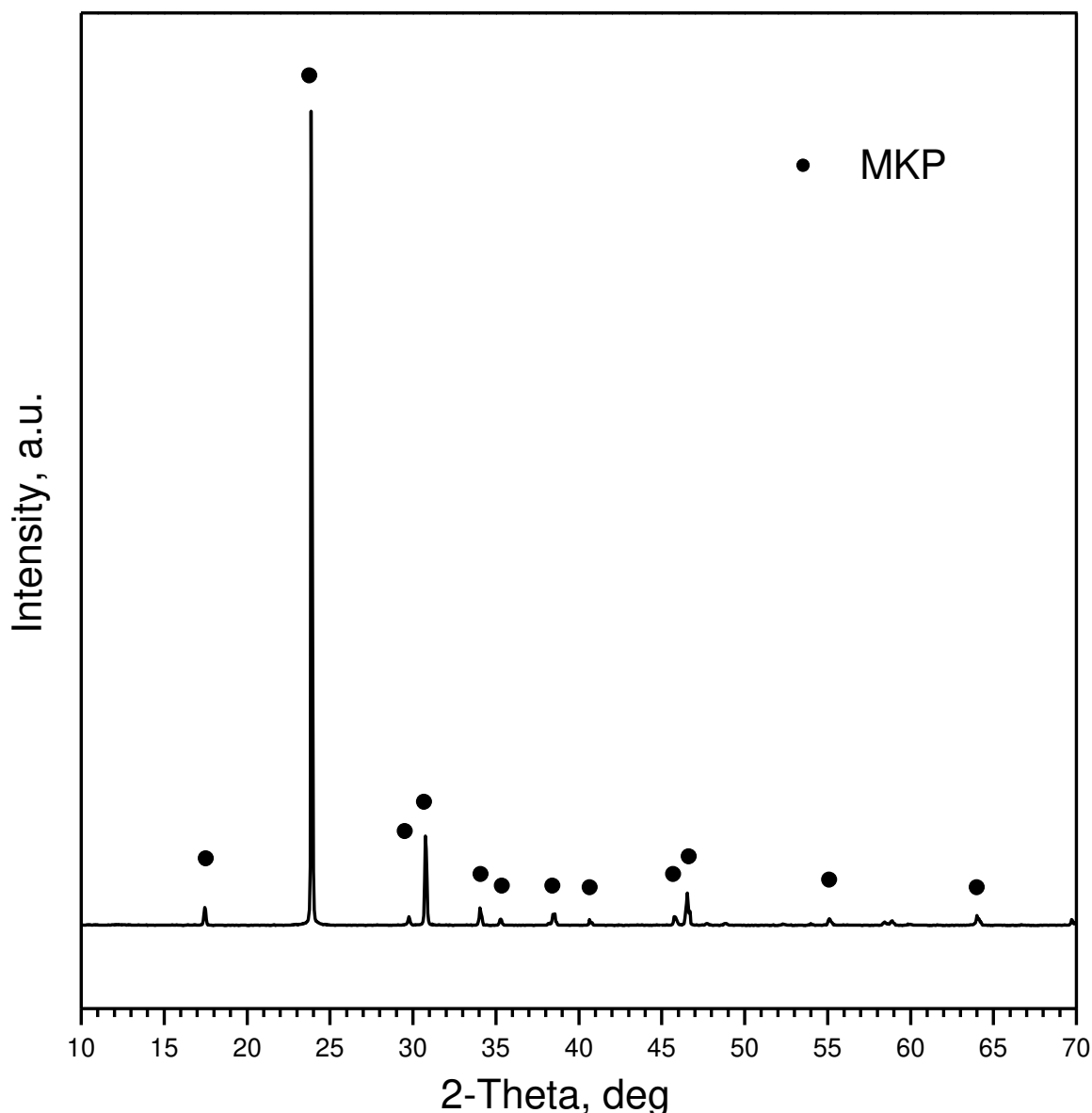
These tests have been performed during the setting up phase for the new printing parameters with the 3 mm voxel printer, for this reason the absolute values, compared to the file dimensions, are not so efficient.

Table 4.8 reports the flexural strength of the bars polished at precise dimension.

**Table 4.8.** Mechanical properties of bars printed with different MKP granulometry.

MKP state	Flexural Strength [MPa]	
	Orto layer	Para layer
<b>As supplied</b>	1,11 $\pm$ 0,16	1,30 $\pm$ 0,13
<b>Milled and sieved</b>	2,01 $\pm$ 0,27	2,38 $\pm$ 0,34

The printing mix with milled MKP is become the standard raw material for mixes used in 3 mm voxel, in which a higher bed surface quality is necessary.



**Figure 4.6.** XRD pattern of MKP crystal from Agri 2000 srl.

In the XRD pattern, Figure 4.6, was identified the MKP ( $\text{KH}_2\text{PO}_4$ , PDF#79-0585). The identification of MKP typical pattern will result very useful to the phase analysis of single reagents in complete printed material XRD.

Passing now at the use of MSP, the first preliminary manual printing tests had shown some issues. The printing with a very fine, highly soluble powder gave a very fast and violent reaction with difficulties to complete water soaking of the layer and fully consolidation. Therefore, printing process with MSP could be complicated, the evaluation of MSP potentialities is also important to validate its binding capacity. The comparison between MKP and MSP products is performed producing a tile of paste mixed materials. The tile is then cut in cubes,  $30 \times 30 \times 30 \text{ mm}^3$  and tested.

**Table 4.9.** Comparison between MKP and MSP paste.

<b>Sample</b>	<b>Compressive Strength [MPa]</b>	<b>Porosity [%]</b>
<b>MKP paste</b>	1,74 ± 0,75	45,7 ± 4,6
<b>MSP paste</b>	5,16 ± 1,03	43,9 ± 1,19

The MSP paste achieves higher value of strength with a similar porosity then MKP paste, as shown in Table 4.9. Although it uses in printing cannot be considered before performing further test, MSP can develop a good binding phase and due to the high value of solubility can be completely dissolve in water and used as impregnation solution for secondary reaction with MgO residues. In chapter 5 the use of this phosphate dissolve in water to impregnate and reinforce printed samples is described.

### **4.2.3 Conclusions**

The analyses have demonstrated that large and irregular crystal of phosphate powder use n agricultural sector is not suitable so suitable for printing process. A milling strategy works better than a sieving one to prepare an optimal powder particle size.

To print at low layer thickness the milling and sieving of MKP crystal have to be carried out, with benefits on resolution and strength. For the 5,7 mm voxel used in the bigger printer located at the company the benefits of optimization process for optimize the MKP powder have to be carefully evaluated. For large dimension hundreds kg of material is easily used, with important working costs and necessity of the appropriate tools. For the moment the milling of MKP is not performed for large scale pieces with 5,7 mm voxel, while is used for 3 mm voxel.

The Agri MKP can substitute the originally ICL MKP, with benefits of cost and supply stability The MSP shows some issues to be used in printing process in the place of MKP, but the good mechanical properties suggest its use in post-printing process.

### **4.3 Evaluation of Printing mixes**

The goal of this section is to evaluate the characteristic of the printing mixes to modify their composition if necessary and create a standard reference for new materials implementation. The packaging and the residual porosity are evaluated measuring the density value with following the normative and comparing with the simpler procedure that can be followed at the company

without dedicated devices. The flowability and the angle of repose are studied to understand the behavior during deposition and formation of the powder bed. [121], [122]

The large of the tests was carried out at Federal Institute for Materials Research and Testing (BAM), Berlin during the secondments of H2020 AMITIE project.

### 4.3.1 Materials and Methods

The printing mixes prepared with standard Bianco di Zandobbio (BdZ) and river Sand aggregate and 20% of binder were tested. Both these aggregates are local low-cost product, with stable availability in large amount. To have a more complete picture of the situation also the single aggregate and the MgO, that is the finest powder, were analyzed. The aggregate was selected, for a 5,7 mm voxel, starting below 2 mm, otherwise the biggest particles generate defects on the bed.

Sand is available in a single product with a particle size starting below 2 mm, but with the around the 80% below 600  $\mu\text{m}$ . Whereas BdZ is available in 4 granulometry: 100 – 200  $\mu\text{m}$ ; 200 – 500  $\mu\text{m}$ ; 500 – 700  $\mu\text{m}$ ; 0,7 – 1,3 mm and it generally used in a mixture with 20% of the finer fraction and the rest divide equally in the other three. Due to possible flowability problems and to the interest in very fine printing mix, the finest fraction was also analyzed all alone and as aggregate in a printing mix with milled MKP.

The standard bulk density measurements were performed following the *normative EN ISO 60* to have a standardized reference for simpler tests that can be also performed with specific device.

The powder was charge in a funnel with the lower orifice closed with a removable cover and 20 to 30 mm above the measuring cylinder, coaxial with it. The cover was quickly removed and the material flow into the measuring cylinder, that had a capacity of 100 ml. When the cylinder was full, we drew a straightedge blade across the top of the holder to remove the excess material and weighed the contents of powder inside. We took three measurement for each sample. The final loose bulk density was determinate by the formula  $\rho_{tap} = m/V$ , where  $m$  is the mean value of mass measured and  $V$  the constant volume of the measuring cylinder.

The real density of the different powder was measured by means of a helium pycnometer (Micromeritics AccuPyc 1330, Norcross, GA). The value for the mixes was obtained as partial sum of the density of the various fraction. With the various density the Packing Factor (PF) of the power cab be calculated as ratio between bulk and real density.

The flowability was evaluated using the Hausner Ratio (HR), one of the most used parameters. HR is obtained from freely settled bulk density (bulk), tapped bulk density (tap) following the formula  $HR = \rho_{tap}/\rho_{bulk}$ . The range of value of HR is reported in table 4.10

**Table 4.10.** HR index and correlated flow behavior.

<b>Flow Character</b>	<b>Hausner Ratio</b>
Excellent/very free flow	1.00 – 1.11
Good/free flow	1.12 – 1.18
Fair	1.19 – 1.25
Passable	1.26 – 1.34
Poor/cohesive	1.35 – 1.45
Very poor/very cohesive	1.46 – 1.59
Very, very poor/approx. non-flow	> 1.60

The density measurement was performed using Jolting volumeter “Stampfvolumeter” (stav 2003, Jel). The analysis was performed, as described in *normative EN ISO 787-11*, filling with the powder ( $200 \pm 10$  ml) a 250 ml graduate glass cylinder, recording weight and volume initial bulk density was measured. After the cylinder was placed in the holder and tamped for 1250 times, and the volume was read off. The powder was tamped again in steps of 1250 revolutions, reading off the volume of the material after each step, until the difference between the volume at the end of two successive steps of 1250 tappings was less than 2 ml. The final value of volume (weight is the same of initial) was recorded and tap density was evaluated.

The measurement must be performed two time. The mean values were reported in the following pages.

The repose angle (AR) measurement was performed the test following *normative DIN ISO 4324*. Figure 4.7 show the set up for the test. The powder was charge in a conic glass funnel with the lower orifice (inner diameter 10mm) closed with a removable cover and 75 mm above a round plat with matt surface (diameter 100mm) was placed coaxial with opening. The cover was removed, and a steady stream of material flowed on the based plate, helping with the rotation of crank inside the funnel. When all the material flowed out, forming a cylinder cone over the plate, the height of the cone was measured and the angle of repose, was calculated using the following formula  $tg\varphi = 2h/100$ , where  $\varphi$  is the repose angle, h the height of material cone and 100 the diameter of the plate. Five measurement were taken for each sample.

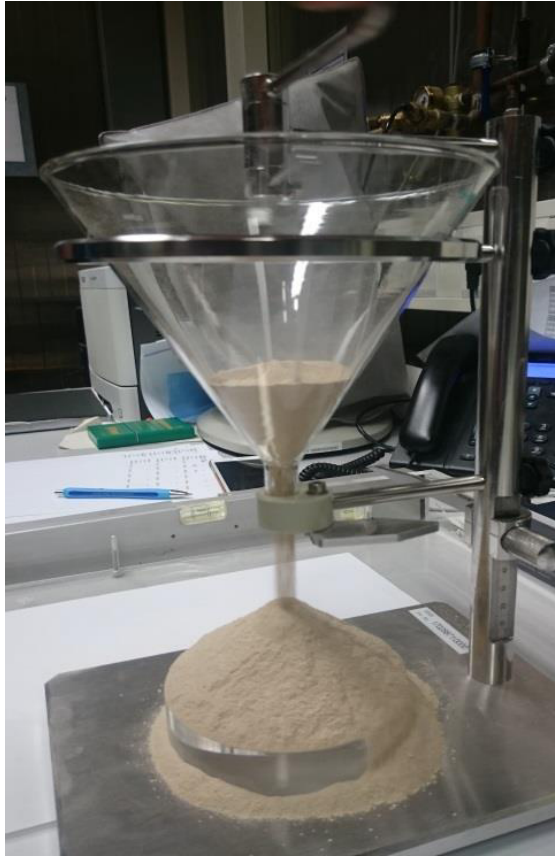


**Figure 4.7.** Setup of angle of repose test.

X-ray diffraction (XRD) pattern of different printing mixes was collected to make a direct comparison with the analysis of the complete printed parts, using an X-ray diffractometer (D8 Advance, Bruker Italia Srl, Milano, IT) with Cu K $\alpha$  radiation, step scan 0,02°, 2 s / step. The Match! software package (Crystal Impact GbR, Bonn, Germany) was used for a semi-automatic phase identification, supported by data from PDF-2 database (ICDD-International Centre for Diffraction Data, Newtown Square, PA, USA).

#### ***4.3.2 Results and discussion***

The printing bed quality with a fine and a coarse printing mix is shown in Figure 4.8, validating the necessity to maintain the particle size around the half of the voxel.



**Figure 4.8.** Quality of different particle size bed; on the left the fine powder; on the right the coarse powder.

The bulk and tap density measurements should be performed on dried material, dry in the oven at  $105 \pm 2$  °C for 2 h and allow it to cool in the desiccator. Since Desamenera powders are not dry and store in a controlled area, for the first aggregate both analysis on dry and Desamanera as stored material are conducted. The values show that the results are not so different, and it was decided to continue the test only on as stored material.

The measurements, performed following *normative EN ISO 60* and reported in Table 4.11, gave the standardize value of bulk density. The BdZ fine shows lower value then BdZ complete mix. A very fine mix could have both problems of packaging and flow. A wide particle size distribution in the range suitable to have a defect-free bed is the best option.

**Table 4.11.** Bulk density measured with normative test.

Sample	Type	Bulk density, normative test [g/cm <sup>3</sup> ]
BdZ, complete mix	Aggregate	1,620 ± 0,032
Sand	Aggregate	1,406 ± 0,006
BdZ, fine	Aggregate	1,378 ± 0,005
MgO RKM83	Binder	0,995 ± 0,036
Printing mix, BdZ standard	Mix	1,597 ± 0,007
Printing mix, Sand standard	Mix	1,502 ± 0,003
Printing mix, BdZ fine	Mix	1,363 ± 0,003



The results are quite similar to the ones done during tapping test, shown below. The results are also quite similar to the one that are used at Desamanera, obtain with simpler and non-standardize method, to make calculation about printing materials for every specific necessity. The density of dolomite standard mix is considered as 1,55 g/cm<sup>3</sup> that is quite similar to 1,592 g/cm<sup>3</sup>, the measured value. Sand standard mix is considered as 1,47 g/cm<sup>3</sup> that is very similar 1,502 g/cm<sup>3</sup>.

Starting from the density values obtained with the measurement described above and with the calculation of the true density, the packing factor was calculated. True density of BdZ was 2,85 g/cm<sup>3</sup>; of Sand was 2,6 g/cm<sup>3</sup>; of MgO was 3,3 g/cm<sup>3</sup>; of MKP was 2,34 g/cm<sup>3</sup>.

Packing factors (PF), reported in Table 4.12, express the quantity of real material and pores there are inside a powder bed.

**Table 4.12.** Packing factor of the different raw materials and mixes.

<b>Sample</b>	<b>Type</b>	<b>Packing factor</b>
BdZ, complete mix	Aggregate	56,25
Sand	Aggregate	56,24
BdZ, fine	Aggregate	47,85
Printing mix, BdZ standard	Mix	55,24
Printing mix, Sand standard	Mix	57,19
Printing mix, BdZ fine	Mix	47,12

Typically, good values of packing are between 0,5 – 0,7. Packing factor depends on the particle shape, the particle size distribution, interaction between particles and external factor of process. The PF of printing mixes is already suitable, but the values can be improved working on the aspects described above.

Higher the PF lower the porosity and the free space in which deposited water can be moved inside the bed. The minimum dimension of the pores and the relative capillary force can change the water absorption behavior. For example, in simply test carried out pressing at 5 kN a tablet of powder, a different diffusion behavior of a water droplet was observed. The depth became shorter while the diameter was increased.

**Table 4.13.** Dimensions of water droplet on different printing mix.

Printing bed	BdZ Fine		BdZ standard		Sand	
	normal	5 kN	normal	5 kN	normal	5 kN
Diameter [mm]	11,545	13,665	13,01	14,465	12,4525	13,72
Depth [mm]	5,525	4,715	5,945	5,335	5,75	5,57

All these aspects could be a great relevance in this type printing process and will be evaluated in detail for future step improvements.

In the evaluation of density for HR index calculation an important thing to consider is the influence of pouring operation on the starting volume level (so bulk density value). The standard pouring operation was achieved by tilting and turning the cylinder about its long axis whilst adding the material, then the powder was homogenized turning the cylinder for few second and put it gently in vertical position.

As already mentioned, the normative measurements shown in previous table, gave result quite similar to the ones done during tapping test, that are for this reason considered acceptable. Table 4.14 reports the complete results of HR.

**Table 4.14.** Bulk density tap density and HR value of the different raw materials and mixes.

Sample	Type	Bulk density [g/cm <sup>3</sup> ]	Tap density [g/cm <sup>3</sup> ]	Hausner Ratio
BdZ, complete mix	Aggregate	1,566 ± 0,042	1,877 ± 0,022	1,19 ± 0,018
Sand	Aggregate	1,423 ± 0,043	1,587 ± 0,015	1,115 ± 0,023
BdZ, fine	Aggregate	1,364 ± 0,027	1,619 ± 0,012	1,19 ± 0,015
MgO RKM83	Binder	0,990	1,470	1,485
Printing mix, BdZ standard	Mix	1,592 ± 0,018	1,927 ± 0,013	1,21 ± 0,005
Print mix, sand	Mix	1,518 ± 0,011	1,716 ± 0,027	1,131 ± 0,010
Printing mix, BdZ fine	Mix	1,372 ± 0,003	1,692 ± 0,016	1,23 ± 0,014

All the aggregates show excellent value of HR and, so, allow good flowability of the particles during the deposition of the printing bed. The complete printing mix show worse HR than the only aggregate, in any case the values still remain satisfying to have a quite good flow of the powders. The MgO powder has shown very poor value and could be responsible for the decrease of HR index of printing mixes. The possible clogging problem, generated by the finest part, must

be considered if the composition of the printing mix is modified increasing the binder quantity or if new cements are tested (cements are generally finer than MgO).

The angle of repose measurements are reported in table 4.15. As already shown from the other flowability test the properties of the aggregates are good, while the MgO powder, because of its fineness, have the worst behavior.

**Table 4.15.** Angle of repose value.

<b>Materials</b>	<b>Type</b>	<b>Angle of repose [°]</b>
Printing mix, BdZ_20%	Mix	40,23 ± 0,38
BdZ, complete mix	Aggregate	36,35 ± 0,20
MgO RKM83	Binder	50,89

The indication of slope angle of material is useful for the deposition of sequence layer one above the other. During the buildup of a piece the powder bed must be contained, otherwise too much materials should be needed to maintain the same powder bed dimension, the powder falling down because of the slope. To contain the powder bed Desamanera has developed a wood formwork system. The AR value was very useful to define the correct position at which set the formworks, according to their height.

Excessive distance constrains to use more powder while with too short distance the power flow over the formwork before the insertion of the next one.

### **4.3.3 Conclusions**

The analyses have demonstrated the suitability of the two main used aggregates (BdZ and River Sand) for the printing process. The presence of particle larger than 1,5 mm should be avoided to obtain a smooth powder bed without defects.

Both the aggregates bring to good flowable printing mix with a satisfying packing factor, around 56%. New mixes modification could be studied to achieve high packing density acting on particle shape, particle size distribution, interaction between particles and external factor of process. In this case also the water absorption behavior has to be controlled and verified.

The angle of repose evaluation gives the possibility to define and prepare a suitable formwork system to contain the powder bed.

## 4.4 Characterization of printed part

In this section the results of the analyses, carried out to verify the formation of binding phase and the presence of unreacted binders, are shown. As already discovered in previous pages the reaction should be not completed and post-printing treatments have to be considered. This part, due to its relevance, will be describe in the dedicated next Chapter 5. Other measurement aimed to analyze the condition in which the reaction phase is developed and the in-temperature behavior of binding phase and aggregates.

After a complete studied of the printed part characteristics is described. Thanks to the ADMIN4D project a wide range of analyses, performed by certificated structures, is been performed. Further analyses are performed with the aim to evaluate interest aspects, useful for validating the use in specific sectors or thinking about new possible applications.

In the conclusion a general review of the actual properties and connected applications is given.

### 4.4.1 Materials and Methods

The completeness of reaction was verified by XRD analysis, monitoring the presence of binding phase (Struvite-k) and unreacted reagents (MgO and MKP). The morphology of the printed parts was investigated by an optical stereoscope (STEMI 2000-C, Carl Zeiss AG, Oberkochen, DE) to visual evaluation of residual MKP crystals.

The X-ray diffraction (XRD) pattern of both printing mix and printed part was collected using an X-ray diffractometer (D8 Advance, Bruker Italia Srl, Milano, IT) with Cu K $\alpha$  radiation, step scan 0,02°, 2 s / step. The Match! software package (Crystal Impact GbR, Bonn, Germany) was used for a semi-automatic phase identification, supported by data from PDF-2 database (ICDD-International Centre for Diffraction Data, Newtown Square, PA, USA).

The printed parts patterns will be also used to evaluate the effectiveness of the post printing treatments. The data about this important topic will be shown in the next chapter 5 entirely dedicated to post-treatments.

Other general tests were carried out on printed parts produced with different aggregate (BdZ and Sand) and binder quantity (20%, 25%, 40%) according to the available materials, printer operative setup and environmental conditions commonly present during company everyday activities.

The environment developed by the binding phase was studied to evaluate the condition in which eventual additives (water retainer, fibers, ecc) or sensors (Admin4d project works on this) could be added. The temperature developed by the reaction was measured inserting a thermocouple inside the printing bed with BdZ as aggregate and 25% of binder. In order to evaluate the

temperature reached at different distance from the printed material, two different size frame shape, with the thermocouple positioned in the middle, were printed. The frame had an internal free space of  $400 \times 400 \text{ mm}^2$  and a height of 100 mm, the wall thickness was 80 mm. the second one has an intern free space of  $150 \times 150 \text{ mm}^2$  and a height of 100 mm, the wall thickness was 20 mm. A final test with the thermocouple inside the printed cube was performed, to evaluate the temperature reached from the material. The piece had a dimensions of  $150 \times 150 \times 150 \text{ mm}^3$ . The pH variation of water, in which a printed piece was immersed, was monitored using litmus paper. This method is surely not so precise, but it was performed yet, because of the idea of having a general indication and not an extremely precise measurement. The same operation, was also performed during printing, putting litmus paper inside the reacting powder.

The in-temperature behavior of printed samples was investigated by DTA/TG (STA409/429, Netzsch Gerätebau GmbH, Selb, DE), operating in static air using a heating rate of  $5^\circ\text{C}/\text{min}$  up to the maximum temperature of  $1000^\circ\text{C}$ . The analysis was conducted on the aggregates and on the binding phase to separate the eventual contribution of the different components. The aim is to evaluate the possibility of this materials to operate at high temperature for possible interesting applications (such as for refractory customized pieces).

The certifications were carried out on two printing mix with Po Sand as aggregate and 20% and 40% of binder respectively to monitoring the outer of binder percentage. These samples were already post-treated with the water addition process, that will be describe in detail in the next Chapter 5. The mechanical strength, compression and bending test, of the printed samples was measured by *Laboratorio di Scienza delle Costruzioni* (Laboratorio ufficiale della repubblica italiana D.P.R. 06/06/201, n. 380, art 59) of IAUV University of Venice.

Samples for compression had an average size of  $100 \times 100 \times 100 \text{ mm}^3$ , while samples for bending an average size of  $40 \times 40 \times 160 \text{ mm}^3$ . The samples were treated with the standard waste post-treatment (describe in detailed in Chapter 5). Tests are performed using a universal material testing machine (Galdabini 200 kN certificate 568/2019 – prot. 03/09/2019), with a cross-head speed of  $1 \text{ mm} / \text{min}$ . In Flexural test the spacing of supporting rollers was set at 100 mm, distance of supporting and loading roller was set at 50 mm. At least five samples were tested for each type of loading direction. During these tests, the certification institute used the final collapse load as reference of strength calculation, in order to normalized and simplify the choice of the maximum reached value.

The geometrical bulk density was calculated as mass on volume, sample dimensions collected with a digital caliber. The apparent density of sample was measured by means of a helium pycnometer (Micromeritics AccuPyc 1330, Norcross, GA). The total porosity of the sample

was therefore calculated as the ratio between their geometric bulk and apparent density. The porosity value is the average between all the tested sample, both bars and cubes.

*Laboratori CERT - t2i – trasferimento tecnologico e innovazione* (Organismo notificato per il CPR N° 1600) evaluated the fire resistance was evaluated, according to UNI EN 13501-1:2009; the final products, according to UE legislation 1907/2006 REACH; and the waste production products, according to UE legislation 1357/2004.

#### 4.4.2 Results and discussion

The XRD patterns, reported in Figure 4.9, show the formation of *struvite-k* in the printed part as binding phase and the presence of residual MgO and MKP. The large presence of aggregate (BdZ) make a little complicated the identification of the binders.

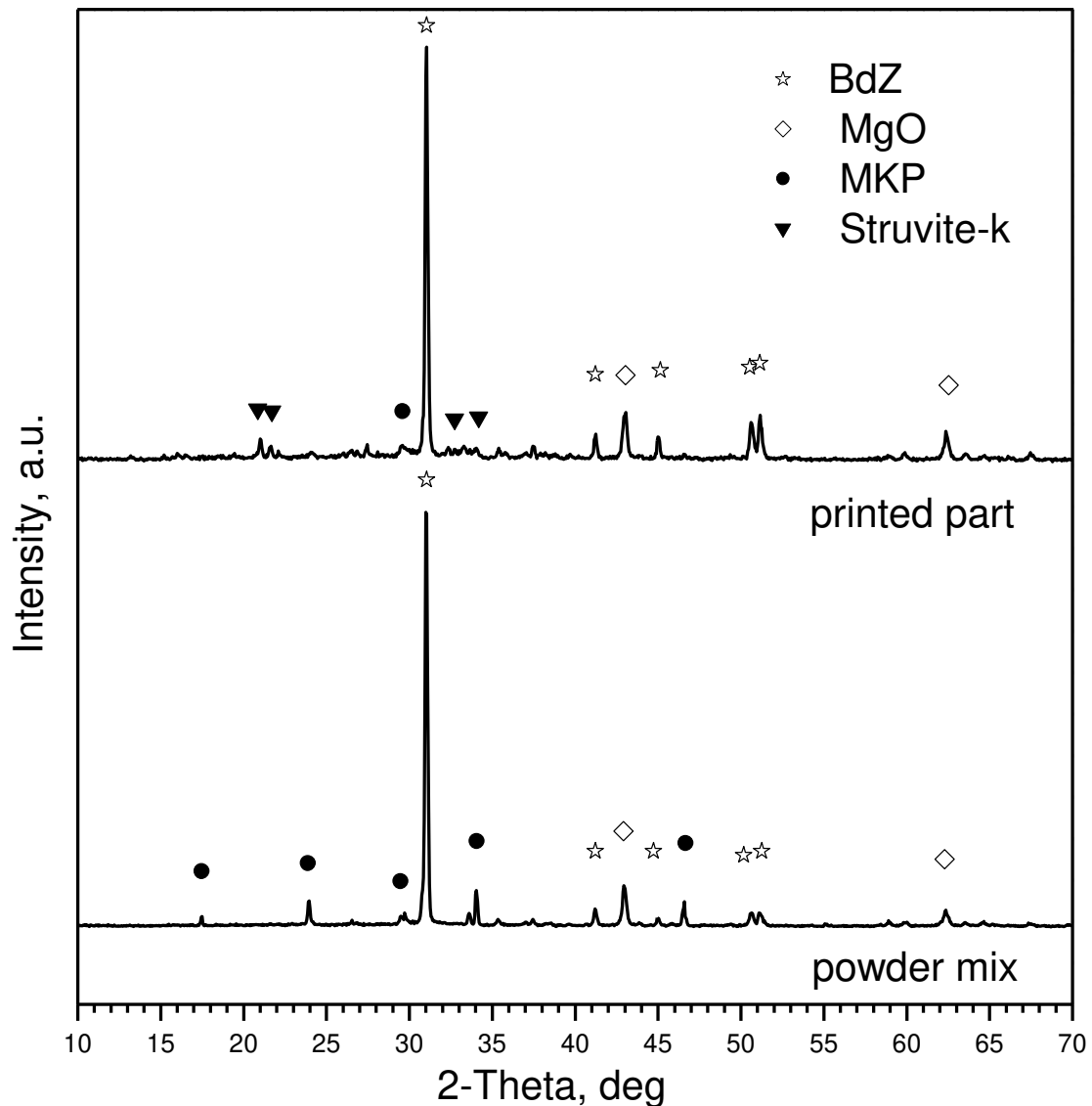


Figure 4.9. XRD patterns of printing powder and corresponding printed part.

According to *Biwan Xu et al. (2018)* the presence to *struvite-k* is sign of reaction completeness (final developed binding product). [123] In this case MgO is more visible due to its excess. But also MKP crystals are still presented, although MKP peaks are less relevant. The microscope observation allows to find the presence of some large unreacted MKP crystals, as shown in Figure 4.10.



**Figure 4.10.** Unreacted MKP crystal.

The reaction temperature measurements confirm that the exothermic reaction can achieve high temperature and the powder bed limits the heat transfers and shades the piece. The position and the quantity of reacting material determine the results.

The thermocouple inside the printed material registered a maximum temperature above 70°C after 30 – 45 minutes, during the same printing a temperature of 53°C is registered from the contact with the external surface. The values are in consistence with the result for MKPC paste described in *Biwan Xu et al. (2018)*, with a maximum of exothermic heat flow before 1 hour. [123] Figure 4.11 shows the complete curve of temperatures.

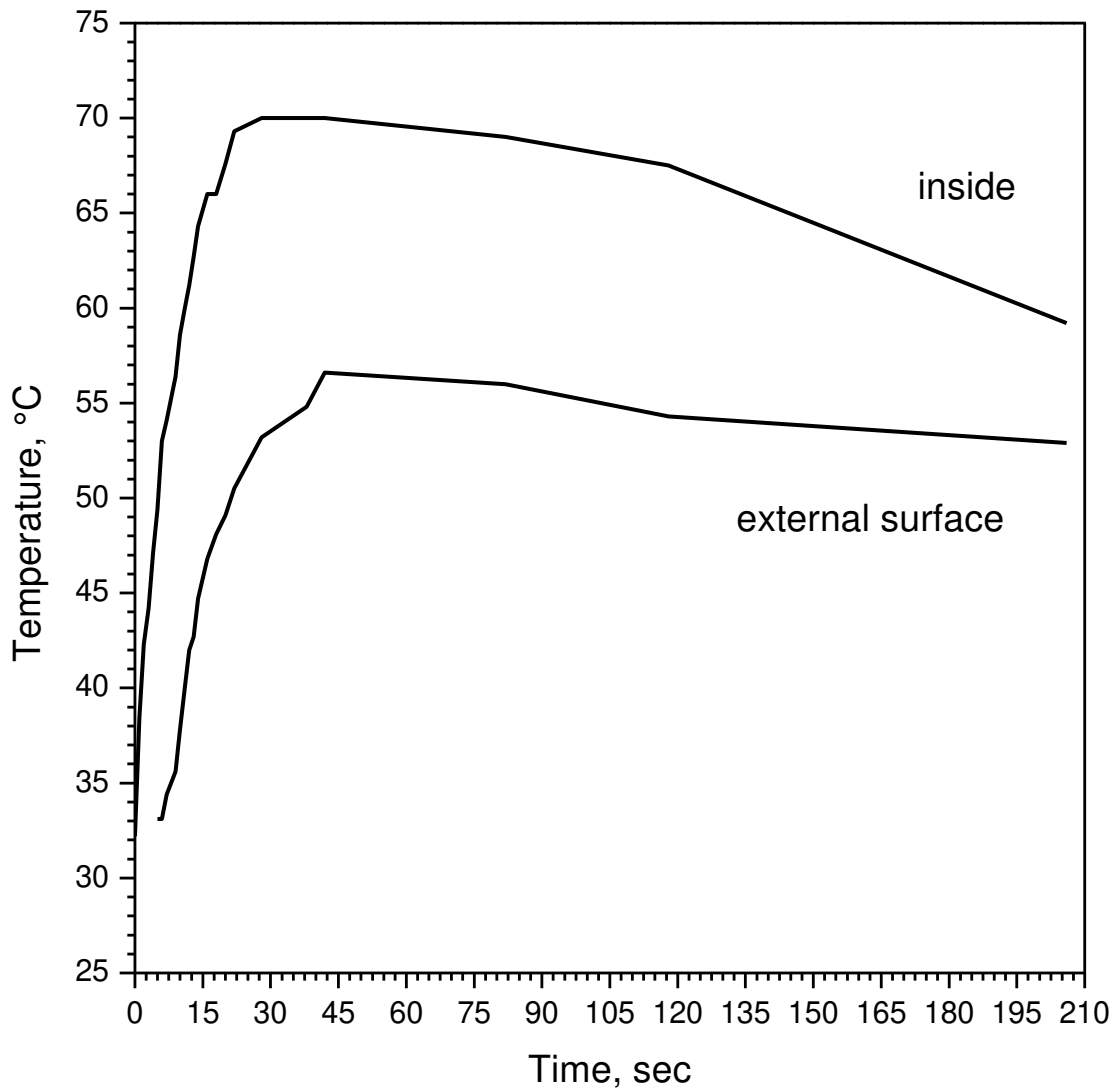


**Figure 4.11.** Curve of temperature during printing inside the material and at the external surface

During the printing of the frames, instead, a lower maximum temperature and in a longer time was detected. The thermocouple in the small box, 70 mm far from the printed frame, revealed a temperature of 40,5°C after 120 minutes; whereas in the big box, detector 190 mm far from the printed frame, a temperature of 34°C was found after 4 hours and 30 minutes. Figure 4.12 shows the complete curve of temperatures of the two boxes.



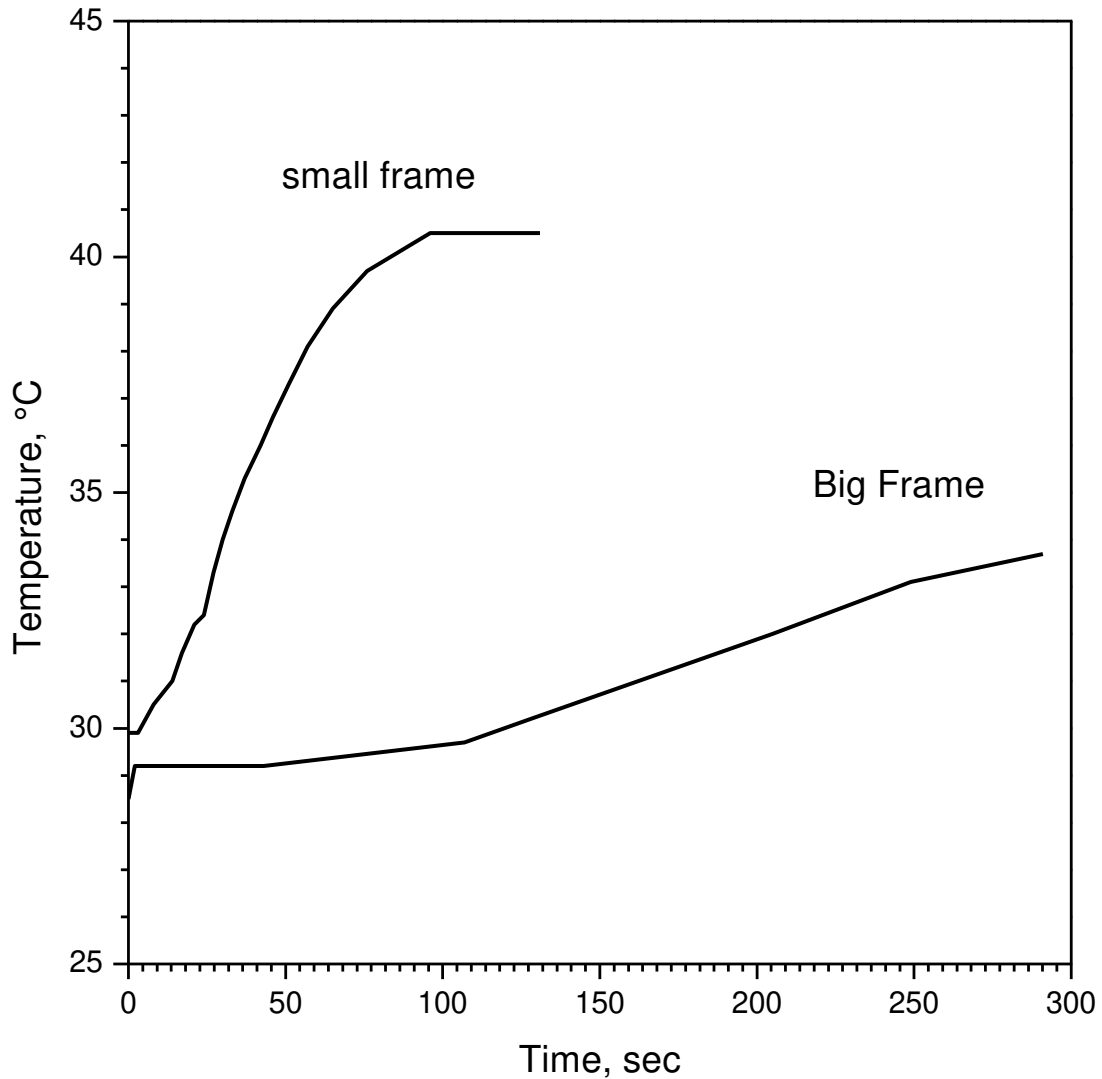


**Figure 4.12.** Curve of temperature during printing, at the center of different dimension frame

The pH of printing reaction measured inside the activated powder achieved a maximum value of 9. While the pH variation of the water, with a piece immersed, changed from 6 to 8 in 40 hours and then to 10 after 160 hours.

The reaction, as expected from literature [90], [124] shows a pH around 8-9, lower value compared with traditional binders. The pH reached from the water in contact with a printed piece are probably correlated to ions release from the materials and the presence of unreacted MgO that increase a little the basicity.

For this reason, MKPCs are not suitable to passivated and protect from corrosion steel reinforces but are very interesting for metals waste treatment.

AS reported by DTA and TGA curves, Figure 4.13 (a) e (b), the struvite-k binding phase shows the loss of bonding crystal water starting around 120°C, BdZ shows the decarbonation starting around 800°C, while Sand shows a stable behaviour rise in temperature.

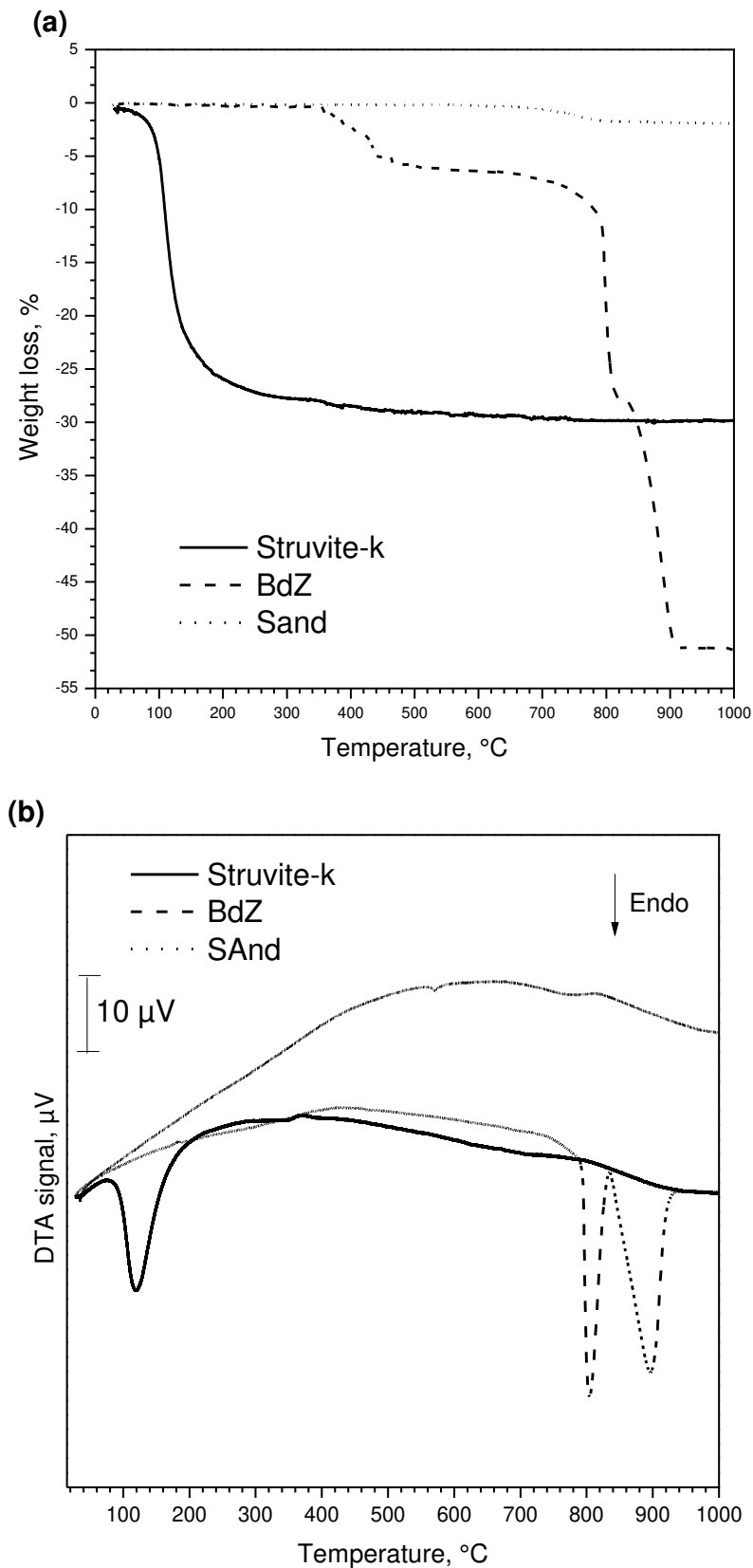


**Figure 4.13.** (a) TGA curve and (b) DTA curve of struvite-k (binding phase) and BdZ and Sand (aggregates).

The loss of crystal water was already discovered in various work and generates an important decrease in mechanical strength after 150°C [123], [125], [126]. These articles report the residual strength at 1000°C as around 30% of the initial one with the most important decrease between 150°C and 400°C. Further investigations have to be carried out in order to better understand the behavior of 3D printed samples, but this first result bring to the necessity of study other binders, such as CAC for high temperature applications.

The mechanical properties evaluated during certification test are in line with the result of every day testing carried out at the University. The selection of the max collapse load (instead of the first significant peak value) makes compression strength averagely higher than that usual. All the data are collected in Table 4.16.

**Table 4.16.** Strength and porosity values given by certificate test, for 20% to 40% binder amount.

Sample type	Flexural Strength [MPa]		Compression Strength [MPa]		Porosity [%]
	Orto layer	Para layer	Orto layer	Para layer	
<b>Sand_20%</b>	1,82 ± 0,08	2,00 ± 0,15	3,36 ± 0,50	4,44 ± 0,62	42,02 ± 0,99
<b>Sand_40%</b>	2,92 ± 0,36	3,42 ± 0,29	5,45 ± 0,68	7,64 ± 0,92	37,27 ± 0,72

The increase of binder percentage (40% from 20%) increase the properties and reduce the porosity. The choice of the optimum binder value could be made time to time following the requests of use condition, the relative cost of the different materials proportion, the presence or absence of other coatings.

The fire reaction certificate, carried out according to UNI EN 13501-1:2009, reports the printed parts as not inflammable (fire reaction: A1, fumes production: s-, on fire particle: d-).

The products certificate, carried out according to UE legislation 1907/2006 REACH, reports the printed parts as compliant without obligation of communications.

The waste certificate, carried out according to UE legislation 1357/2004, reports the product as EWC 16.03.04, inorganic wastes other than those mentioned in 16.03.03.

### 4.4.3 Conclusions

The analysis on the printed part have confirmed the necessity of post-printing treatments in order to push forward the reaction rate. MgO and MKP are present in the printed part yet.

The reaction environment is also studied, resulting in reaction temperature between 70°C, core of the piece, and 40°C, just around the printed part. The geometry and the dimension of the part obviously affects the reached temperatures. The pH of the reaction is around 9.

The printed material is certificate as uninflamable. But for applications or long exposition at high temperature, the TGA and DTA analyses reveal some issues in binding phase degradation. Also the correct aggregate must be selected, because of BdZ decarbonating around 800°C. For this reason, the use of high temperature traditional cement should be tested. Use of various nature cements could be, in any case, a hot topic for technology diffusion and growth. In final chapter first approaches on those uses will be described.

The certification test of samples, produced with Sand and 20% to 40% of binders, show good mechanical properties, 2-3 MPa in flexion and 4-6 MPa in compression, with a porosity varying between 42% and 37%. The materials could become competitive with non-structural concretes [127] and porous stones [128], with the great advantage of AM production.

The positivity of fire resistance test and material classification as compliant without obligation of communications, could validates the application for public sector, such as isolation terminal and sound wall parts, outdoor opera, ecc.



# Post-printing treatments

In this chapter the execution and improvements, given by the post-treatments on printed samples, are evaluated. The strategy is very common with ceramic materials to achieve high density parts without the large shrinkage associated with sintering to full density. Both low and high temperature infiltrations are possible depending on the part material and binding mechanism [15]. In powder-bed 3d printing the reaction occurs without thorough mixing of the reagents, and so infiltration treatments are very useful increase the reaction rate and improve the properties. *Behzad Nematollahi et al.* [36] describe very high increases for their geopolymer-based parts after post-printing curing treatment.

As already described in previous chapters, the printed parts show an incomplete binding reaction for different reasons (absence of mixing, quality and dimension of raw materials, ecc). Various ideas are been evaluated to improve the situation, keeping in great consideration the materials compatibility and availability, the process feasibility for large scale.

The first easier approach consists in the addition of water after printing and shape consolidation to push the reaction forward. The second try to use cement and geopolymer to reduce the porosity coating the surface. The third studies low viscous solutions to impregnate and consolidate the structure.

## 5.1 Water addition treatment

The analyses on printed sample, described in previous chapter 4, have confirm that after printing the bonding phase reaction is not complete. Due to the particular conditions of 3d printing process and raw materials (such as absence of mixing, very fast reaction, limited amount of water available, MKP limited solubility), not all the potassium phosphate crystals are been dissolved and not all the magnesium oxide powder is been activated and reacted. The unreacted reagents are still presented in the piece, as optical microscope images and XRD patterns have confirmed.

So, the easiest way to increase the reaction degree is to add other water that dissolves MKP and activates the MgO. In this way the unreacted powders are further exploited, creating the same binding phase and increasing the properties. The primary structure is already consolidated, and no resolution or distortion problems are generated.

Part of this work was carried out during a student bachelor thesis, G. Rangon (2018). [129]

### 5.1.1 Materials and methods

Standard bar samples were printed with the optimized printing parameters for both configurations, continuous and droplets deposition. The printing mix with Bianco di Zandobbio and 25% of Desamanera binder was used. After, half of the samples were maintained as printed (non-treated), meanwhile the rest of the samples were soaked with water. The large size of the commercialized piece (the ones printed by the company for the customers) required to maintain the procedure as simple as possible. So, the water addition is been performed in a single step until the saturation of the surface is reached; in case of very high thickness the operation is been repeated to soak also the core of the piece.

The samples are been dried in normal condition, avoiding to rapid water evaporation in order to prevent local inhomogeneity or phosphate deposition. After complete drying the sample are cut and polished to prepare the final bars and cubes. The samples are been tested at least 5 days after the water addition to be completely dry.

X-ray diffraction (XRD) pattern of post-treated samples was collected using an X-ray diffractometer (D8 Advance, Bruker Italia Srl, Milano, IT) with Cu K $\alpha$  radiation, step scan 0,02°, 2 s per step. The samples are milled in a very fined powder and every time the same amount is collected to perform the acquisition. The Match! software package (Crystal Impact GbR, Bonn, Germany) was used for a semi-automatic phase identification, supported by data from PDF-2 database (ICDD-International Centre for Diffraction Data, Newtown Square, PA, USA).

The geometrical bulk density was calculated as mass on volume, sample dimensions collected with a digital caliber. The apparent density of sample was measured by means of a helium pycnometer (Micromeritics AccuPyc 1330, Norcross, GA). The total porosity of the sample was therefore calculated as the ratio between their geometric bulk and apparent density. The porosity value is the average between all the tested sample, both bars and cubes.

The compressive and flexural strength of the samples was measured with a Instron 1121 UTM (Instron Danvers, MA) with a cross head speed of 1 mm/min. Both the perpendicular and the parallel direction to the layer were tested. At least five samples were tested for each type of loading direction. Samples for bending had an average size of 30 x 30 x 150 mm<sup>3</sup> while samples for compression had an average size of 30 x 30 x 30 mm<sup>3</sup>.

Due to the manual post processing some samples were not exactly dimensioned, especially in planarity of the plane, and this determined high standard deviation in compression test.

### 5.1.2 Results and discussion

The water addition the final pieces are visibly consolidated and both the mechanical test and XRD analysis confirm this. The procedure permits to complete soaking of the sample in an easy way, very important in large scale.

Table 5.1 reports all the data about the mechanical properties and the porosity of the *as printed* and *water-treated* samples, produced with the old continuous configuration for water deposition. The compressive strength of the water treated samples was  $3,09 \pm 0,52$  MPa and  $2,92 \pm 0,68$  MPa respectively in orthogonal and parallel direction to the layer, with an increase of almost double from the as printed samples.

**Table 5.1.** Mechanical properties of as printed and water treated samples.

	Mechanical Strength [MPa]		Porosity [%]
	Orto layer	Para layer	
<b>As printed</b>			
Flexural strength	$2,32 \pm 0,11$	$2,32 \pm 0,09$	$39,8 \pm 1,4$
Compressive strength	$1,47 \pm 0,54$	$1,42 \pm 0,56$	
<b>Water treated</b>			
Flexural strength	$3,88 \pm 0,27$	$3,70 \pm 0,33$	$35,6 \pm 1,0$
Compressive strength	$3,09 \pm 0,52$	$2,92 \pm 0,68$	

The tests carried out on samples printed with the new droplets configuration show similar results, water treatment increased the properties. For example, the compressive strength of the water treated samples was  $3,04 \pm 0,92$  MPa and  $2,02 \pm 0,72$  MPa respectively in orthogonal and parallel direction to the layer, whereas the initial values were  $1,50 \pm 0,20$  MPa and  $1,68 \pm 0,30$  MPa. Porosity was decreased from  $41,0 \pm 1,0$  to  $37,35 \pm 0,9$ .

From XRD patterns of treated samples an increase in binding phase peaks is notable, together with a decrease in MgO peaks. The secondary water makes the compounds left inside the piece react. Figure 5.1 shows the sample phases before and after the water addition respectively.



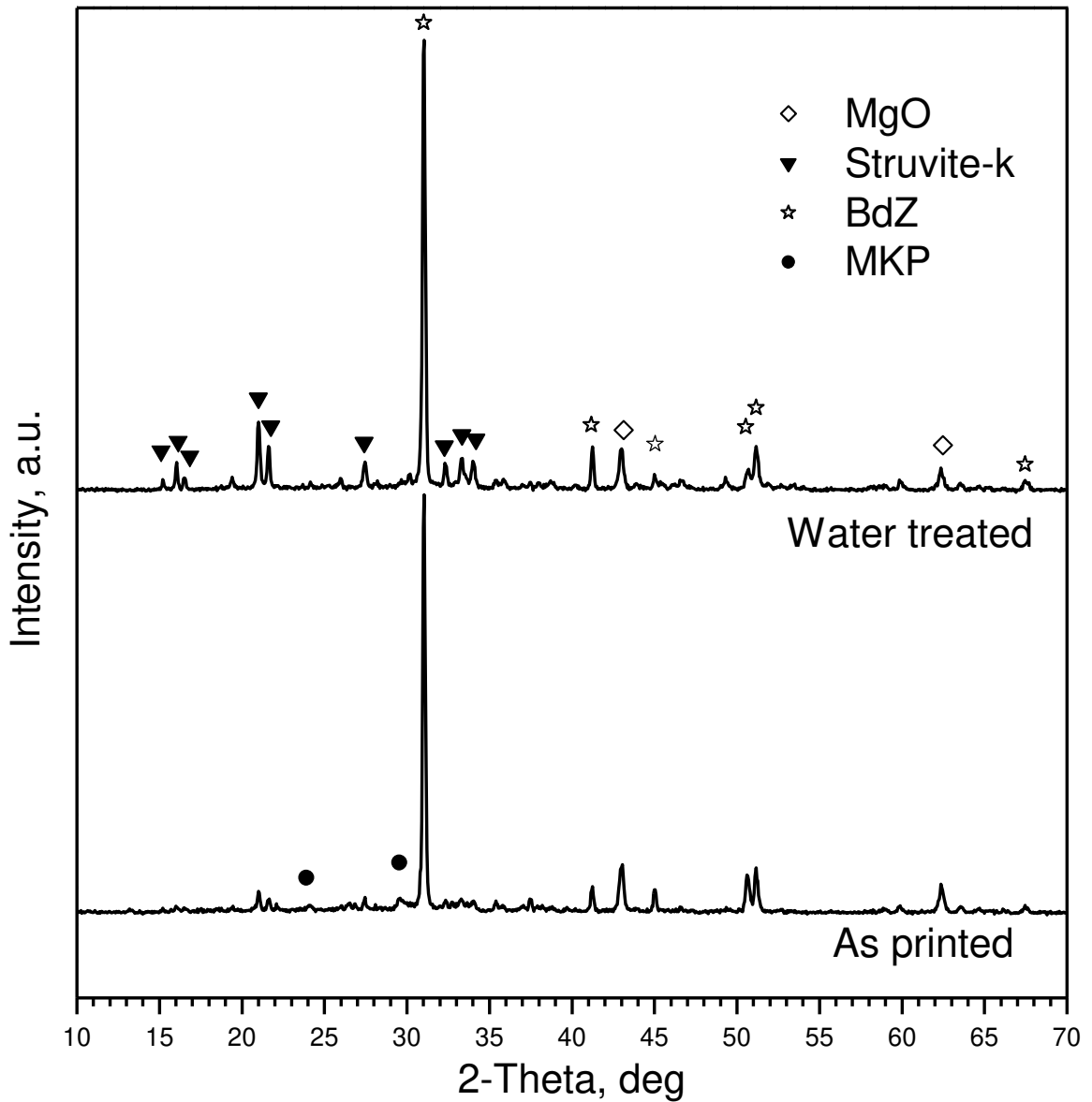


**Figure 5.1.** XRD pattern of as printed sample and water-treated respectively.

Peaks of the binding phase (Struvite-k) is increased after water addition. MgO remains appreciable yet while MKP seems completely disappeared (MgO is present in excess and it is a very fine powder more homogeneously).

Further investigations on water post-treatment are planned, in order to study the best way to generate secondary reaction binding phase. The hypothesis of long curing in high humidity chamber is been considered to increase the reaction rate.

## 5.2 Slurry infiltration

Infiltration is the most commonly used post-processing procedures for cementitious materials. The infiltrating slurry should have enough fluidity and low viscosity to flow through the open pores and a low contact angle with the bulk material to make the infiltration more effective. However, infiltration with fluid materials are very complicate in large scale 3D printed structures. The method allows to enhance the surface properties and to reduce the absorption of liquid, more than increase the consolidation of the whole structure. Geopolymer for example has already studied as coating protection for different application, as concrete protection against chemical attack and corrosion. [130], [131]

Part of this work was carried out during a student master thesis, A. Cervesato (2018). [132]

### 5.2.1 Materials and Methods

Two different materials, according to materials availability, were investigate. A commercially quick drying self-levelling cement (Fassa Bortolo SM 485, Fassa srl., Spresiano (TV), Italy), a completed pre-mixed formulation for floor screed, is used. And a geopolymer mixture contains metakaolin (Argical 1200S, Imerys S.A., Paris, France) as source of alumino-silicate building blocks, soluble potassium silicate solution (205 K, Tillmanns spa, Milano, Italy), potassium hydroxide pellets (KOH, Sigma–Aldrich, Steinheim, Germany) and distilled water, is prepared. The composition of the metakaolin and of the sodium silicate solution are summarized in Table 5.2.

**Table 5.2.** Composition of the metakaolin and of the silicate solution.

<b>Reagent</b>	<b>SiO<sub>2</sub> [wt%]</b>	<b>Al<sub>2</sub>O<sub>3</sub> [wt%]</b>	<b>K<sub>2</sub>O [wt%]</b>	<b>Fe<sub>2</sub>O<sub>3</sub> [wt%]</b>	<b>CaO [wt%]</b>	<b>H<sub>2</sub>O [wt%]</b>
<b>Argical 1200 S</b>	55	39	< 1	1.8	< 0,6	/
<b>205 K</b>	57,5	/	28	/	/	14,5

The two materials were prepared ad used to infiltrate a bar of 30 x 30 x 150 mm<sup>3</sup>, printed with BdZ\_25% in standard condition. A sufficient quantity of solution to impregnate a printed bar can be identified in 50 g. The commercial cement is a read to use product (need to be only mixed with water), instead, for the Geopolymer, the precursor materials had to be prepared, following the optimization of previous works conducted at the university.

First, a solution of potassium silicate, sodium hydroxide and water, was prepared with the following molar ratios:  $K_2O/SiO_2 = 0,621$ ,  $H_2O/K_2O = 17$ . The solution was prepared at least

24 hours in advance, was stored in oven at 40°C until residual particle dissolution and then was stored in the fridge at 4 °C to stable and preserve during time. The composition in summarized in Table 5.3.

**Table 5.3.** Chemical composition of the alkaline solution.

	<b>205 K (g)</b>	<b>KOH (g)</b>	<b>H<sub>2</sub>O(g)</b>
<b>Alkaline solution</b>	13,19	4,45	15,83

The final geopolymer solutions had the following molar ratios:  $K_2O/SiO_2 = 0,250$ ,  $SiO_2/Al_2O_3 = 4$ ;  $K_2O/Al_2O_3 = 1$ . Concerning the content of water, the first paste had a molar ratio  $H_2O/K_2O = 17$ . Nevertheless, a second one was also prepared with a molar ratio of 18.

For Geopolymer final use, the metakaolin powder was added to the alkaline solution under mechanical stirring at 1000 rpm for 5 minutes at room temperature. such time as to homogenize the preparation and obtain the desired rheological properties for a sufficiently long time, to be able to carry out the impregnation. It is important not to exceed this time limit to avoid the early hardening that would prevent infiltration. Table 5.4 summarizes the two final geopolymer formulation.

**Table 5.4.** Formulation of the two geopolymer pastes

	<b>Argical 1200S (g)</b>	<b>Alkaline solution (g)</b>	<b>H<sub>2</sub>O (g)</b>
<b>GP K-17</b>	16,53	33,47	/
<b>GP K-18</b>	16,14	32,18	1,18

The geopolymer mixture has a color very closed to the one of the printed parts. A visual evaluation of phenomena results very complicated. Fassa Bortolo cement has a dark color already different to printed parts.

For this reason, geopolymer formulation was added with 5% weight (2,5 g with 50 g of preparation, as in the case in question) of inorganic pigment in order to visually assess the penetration occurred. A fine powder of iron oxide (Siof spa, Pozzolo Formigaro (AL), Italy) was used with a characteristic reddish color, which gives the geopolymer a red appearance sufficiently intense to be clearly distinguished from the beige of the printed bars.

After preparing, the paste was transferred into a plastic cup, into which the bar is immersed and left under immersion for 20 minutes. The process is a sort of dip-coating which also should

allow penetration into the pores in addition to the formation of a surface film. Figure 5.2 shows sample immersed and after coating.



**Figure 5.2.** Sample geopolymer infiltration methods.

After extraction, the excess of materials is removed and then the sample is left to dry completely, allowing the hardening reaction to progress.

The coated samples were broken with hammer and chisel in order to have a clean fracture surface (cutting the sample surface dirtying problem occurs). Then the coating quality was visually and with an optical stereoscope (STEMI 2000-C, Carl Zeiss AG, Oberkochen, DE) analyzed. A SEM (ESEM, Quanta 200, FEI, Hillsboro, OR) with the EDX chemical microanalysis with element composition, is used to better evaluated the penetration of the coating, monitoring the presence of aluminum (only contained in Geopolymer).

### 5.2.2 Results and discussion

The infiltrated samples are shown in Figure 5.3 and Figure 5.4. During immersion, it is noted that the paste begins to consolidate significantly in the immediate proximity of the bar and a slight rise of water only (a few mm) compared to the level of the paste. This suggest that the porous sample is taking out water out from the paste, which become more viscous and create a skin on the surface. Geopolymer paste works better than Fassa cement, which contains already bigger particles in the mix.



**Figure 5.3.** Geopolymer infiltrated sample.



**Figure 5.4.** Commercial cement infiltrated sample.

As supposed, a deep infiltration inside the part is very complicated following this method and the observation of the sample sections confirms a very limited and irregular penetration. To better evaluate the penetration depth a chemical analysis of the element present was performed at different distance from the surface.

The EDX analysis shows that the solution is entered inside the part for about 1 mm. The results of GP K-18 solution are reported in Figure 5.5, 5.6, 5.7, 5.8. Approximately the same behavior was shown from the formulation with less water, GP K-17.

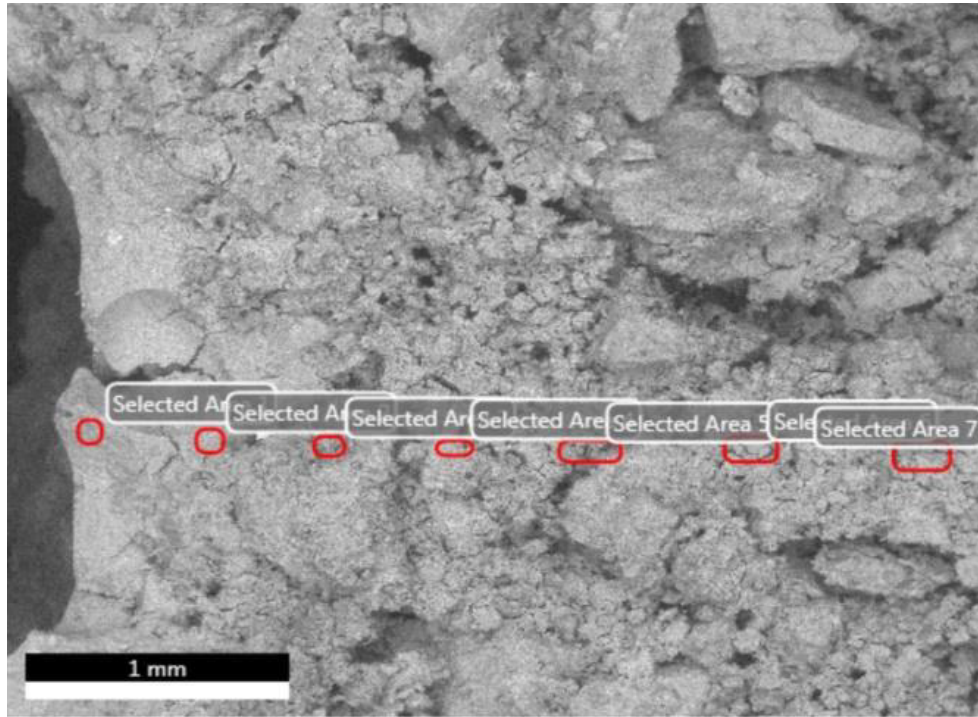


Figure 5.5. SEM image of infiltrated sample section.

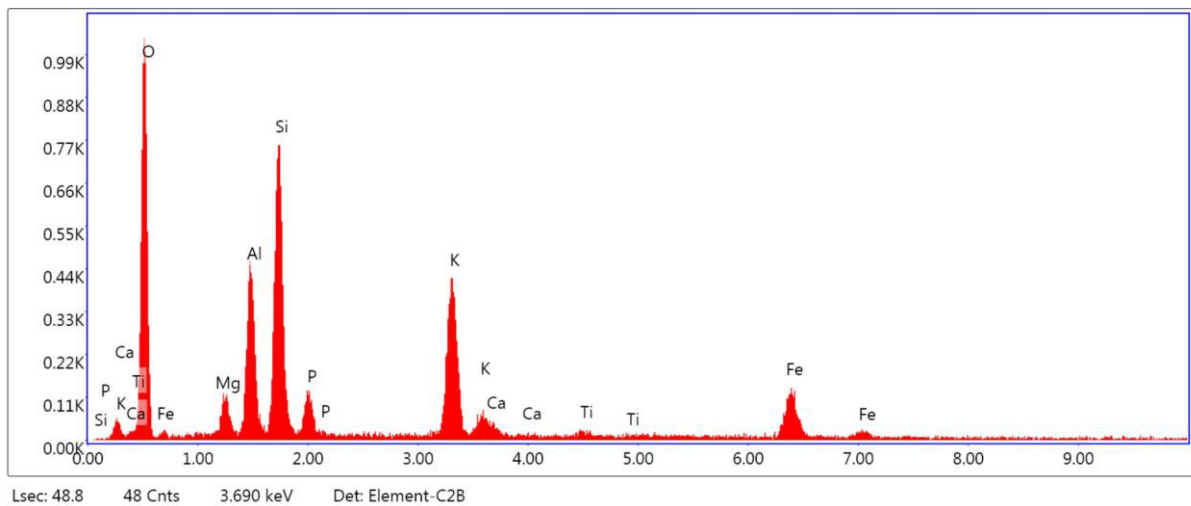
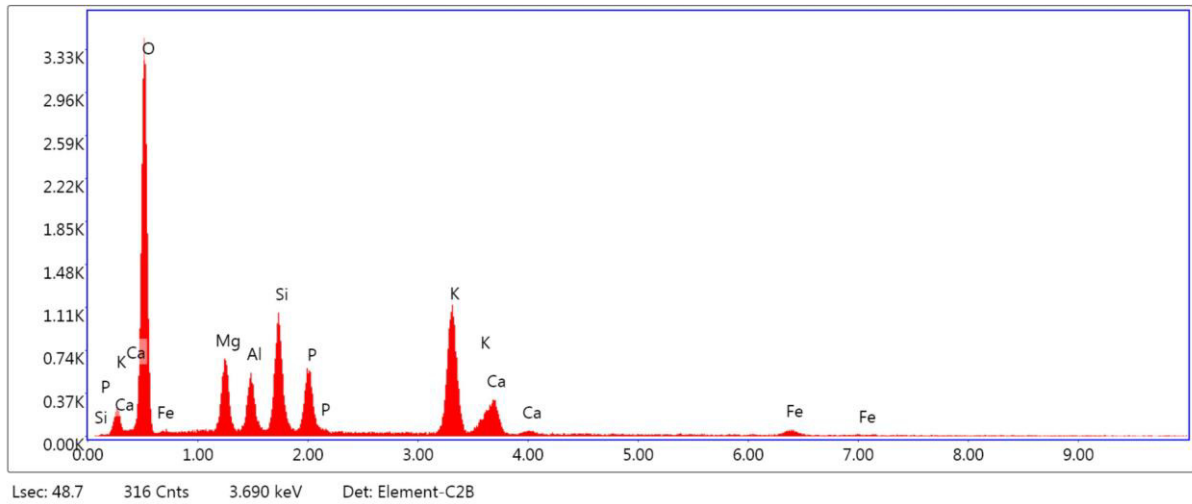
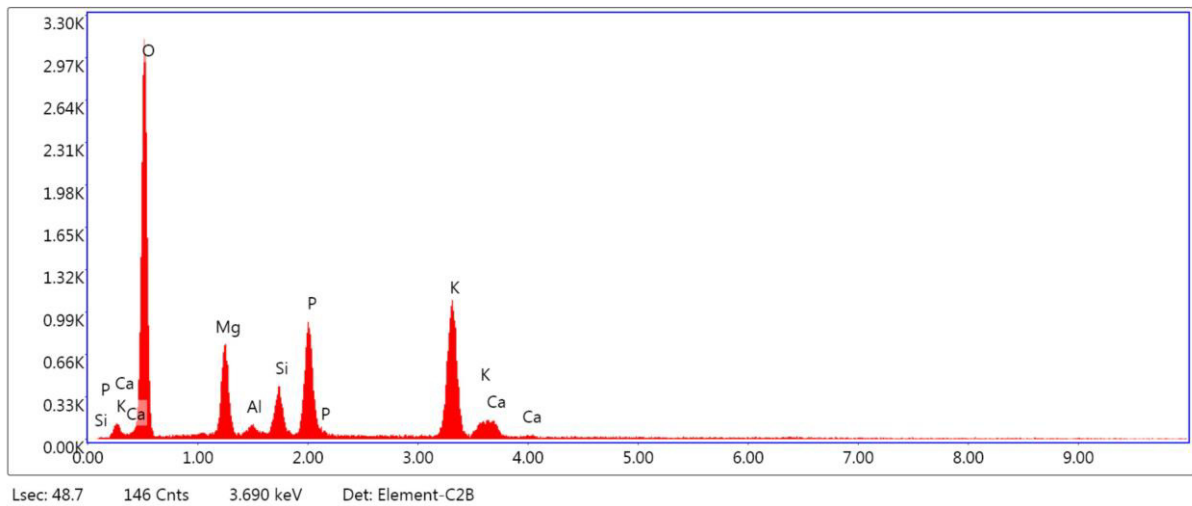


Figure 5.6. EDX compositional analysis on area 1 (surface zone).



**Figure 5.7.** EDX compositional analysis on area 2 (middle zone).



**Figure 5.8.** EDX compositional analysis on area 3 (internal zone).

In the first graph, referred to the external surface point, the peak of Al is high due to the presence of geopolymer, while in the third, 1 mm inside the piece, the value is strongly decreased. The infiltration with cement and geopolymer paste cannot be used as structural reinforcing practice, but only to create a surface coating with new specific characteristics. The large dimensions of the pieces, which could not in any case be infiltrated in depth, do not push towards the study of these solutions until specific surface properties are needed for new applications (e.g. water or waste managing piece).

## 5.3 Liquid impregnation

The goal of this section is to impregnate the printed samples with low viscosity solutions, to achieve an easy and complete penetration. Different approaches were studied.

A colloidal silica solution (nanosilica particles dispersed in water) is tested with the idea of filling the open porosity of the sample. This type of material is already studied as for concrete surface treatment.[133], [134] A solution of mono sodium phosphate dissolved in water was studied to react with the unreacted MgO and create a secondary bonding phase. The sodium phosphate is chosen due to its high solubility in water (more than 3 times higher than potassium). Part of this work was carried out during a student bachelor internship, C. Grigolato.

### 5.3.1 Materials and Methods

Ludox HS-30 (W.R. Grace, United States) was been selected as the colloidal silica solution between the ones available at university. It contains nanosilica 30 wt. % suspension in water. The phosphate solution was prepared dissolving mono sodium phosphate anhydrous,  $\text{NaH}_2\text{PO}_4$ , (technical grade, BK Giulini GmbH, Germany) in distilled water if a ratio of 1:2. The solution was maintained stirred for few minutes in order to permit a complete dissolution of the crystals. Also, simple water impregnation, describe in section 5.1 as the new standard post-treatment procedure, was performed to have a direct comparison with these new solutions.

Bar samples were printed at the company, with Desal 150.150 and a voxel size of 5,7 mm, using the Sand\_25% mix and standard parameters. The samples were after cut and finished in order to obtain cubes as much as regular as possible.

In order to validate and standardize the procedure numerous experiments are carried out to understand the fastest and most effective way to impregnate the sample.

The solutions were simply poured onto the sample until the saturation is reached (wetted surface and no more absorption of the solution). Just treated samples are shown in Figure 5.9.





**Figure 5.9.** (a) impregnated samples; (b) Surface of just impregnated sample.

To understand how maximize the absorption, the treatment was repeated on samples already infiltrated with different time intervals between one infiltration and the other. The solution was absorbed by the samples even the subsequent times but in a lower quantity and always smaller for each subsequent repetition.

The conclusion was that repeating the infiltration was not an effective method because, although bringing a greater total absorption of the solution, the absorbed quantity was not sufficient to motivate the expenditure of time necessary to allow the sample to dry again.

The impregnated samples were left to dry for 24 hours or until the weight of the sample resulted stable in two different weighing.

The morphology of the parts was investigated by an optical stereoscope (STEMI 2000-C, Carl Zeiss AG, Oberkochen, DE). The geometrical bulk density was calculated as mass on volume, sample dimensions collected with a digital caliber. The apparent density of sample was measured by means of a helium pycnometer (Micromeritics AccuPyc 1330, Norcross, GA). The total porosity of the sample was therefore calculated as the ratio between their bulk and true density.

The compressive strength of the samples was measured with a Instron 1121 UTM (Instron Danvers, MA) with a cross head speed of 1 mm/min. Only the direction perpendicular to the layer was tested, to limit the number of samples to be produced (considering also the preliminary test and solution not described here). At least ten samples were tested for each type of solution. Samples had an average size of 30 x 30 x 30 mm<sup>3</sup>.

### 5.3.2 Results and discussion

Both the solutions have water-like behavior and permit an easy impregnation of the porous samples, the saturation is reached in a short time.

The treatment, with both the solutions, increase the mechanical properties, reducing at the same time the residual porosity more than the simple water addition.

The compressive strength of non-treated and water-treated samples were ~ 1,20 MPa and ~ 2,15 MPa respectively. The treatment doubles the value. The colloidal silica treatment increases the strength to ~ 3,50 MPa while the Na-phosphate to ~ 4,40 MPa.

Regarding the porosity, non-treated samples have porosity values around 47%, the value remains more or less the same in water-treated samples. The samples treated with colloidal silica solution present value of porosity decreased to 38% and the one treated with phosphate solution to 36%. The complete results are reported in table 5.5.

**Table 5.5.** Mechanical properties of different impregnation samples, with normal MgO quantity.

<b>Standard samples – Sand_25%</b>				
Type	Compression strength [MPa]	geometric density [g/cm <sup>3</sup> ]	apparent density [g/cm <sup>3</sup> ]	Open porosity [%]
<b>Na-Phosphate solution</b>	4,42 ± 0,87	1,526 ± 0,015	2,415	36,79 ± 0,63
<b>Ludox HS-30</b>	3,55 ± 0,61	1,506 ± 0,054	2,463	38,87 ± 2,18
<b>Simple water</b>	2,17 ± 0,49	1,350 ± 0,025	2,511	46,26 ± 1,01
<b>Not treated</b>	1,23 ± 0,24	1,336 ± 0,019	2,567	47,96 ± 0,75

The morphological images, obtained at the optical microscope and shown in Figure 5.10, 5.11 and 5.12, confirm the presence of impregnating solutions in the porosity of the sample. For Ludox solution the deposit is prevalently concentrated in the interface zone between layer, whereas the phosphate solution creates a more homogeneous reacted zone. This is consistent with the hypothesis that the first solution simply fills and consolidates the structure instead the second reacts with residual MgO creating a secondary bonding phase.

Further analyses (XRD, SEM) are currently on going to study the different consolidation mechanisms.

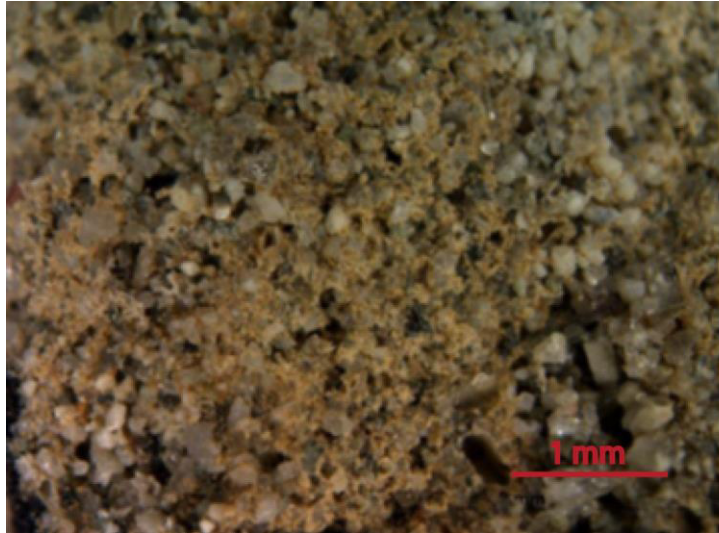


**Figure 5.10.** Microstructure of not treated sample, normal MgO quantity.

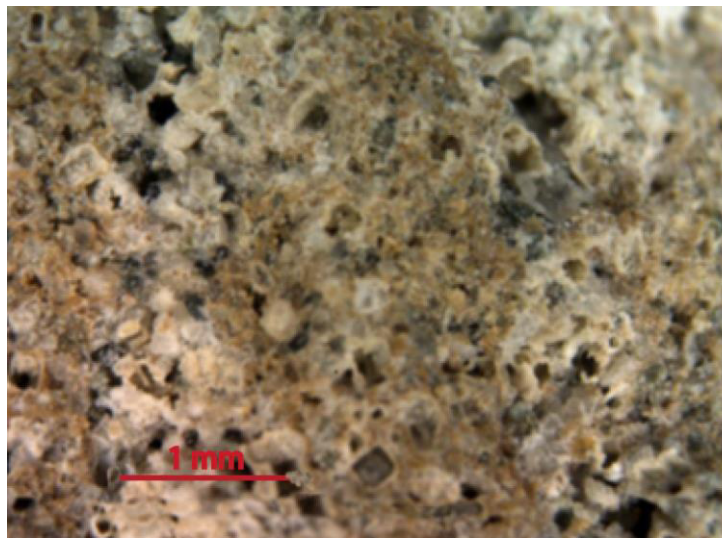


**Figure 5.11.** Microstructure of colloidal silica solution impregnate sample, normal MgO quantity.

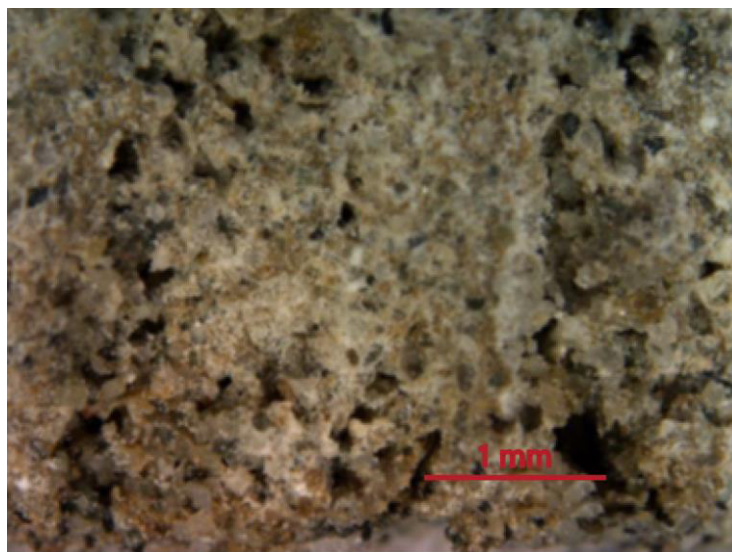


**Figure 5.12.** Microstructure of *Sodium phosphate solution impregnated* sample, normal MgO quantity.

Given the excellent result of the Na-phosphate solution, due to its reaction with residual MgO, it was decided to produce and test samples with a higher quantity of MgO. The mass ratio between MgO and MKP is pushed from 1:1 to 1,5:1.

The samples were prepared and treated following the same procedure of the previous ones. Table 5.6 reports all the data. The value of porosity of the non-treated, colloidal silica-treated and phosphate-treated samples showed a decrease from 46% to 37%, similar to the normal MgO samples. The mechanical strength of phosphate-treated samples reached higher values, according to the larger presence of free MgO. The morphological images showed the same filling behavior of the normal MgO samples for both the two solutions.

**Table 5.6.** Mechanical properties of different impregnation samples, with MgO excess.

<b>MgO Excess samples – Sand_25%</b>				
Type	Compression strength [MPa]	geometric density [g/cm <sup>3</sup> ]	apparent density [g/cm <sup>3</sup> ]	open porosity [%]
<b>Na-Phosphate solution</b>	5,26 ± 0,97	1,525 ± 0,033	2,440	37,51 ± 1,33
<b>Ludox HS-30</b>	3,07 ± 0,65	1,485 ± 0,028	2,497	40,54 ± 1,11
<b>Not treated</b>	1,16 ± 0,29	1,377 ± 0,031	2,586	46,73 ± 1,18

The possibility to increase the quantity of magnesium oxide have to be carefully considered. The increase in the quantity of magnesium oxide makes sense only if afterwards the impregnation is carried out with Na-phosphate solution. In any case the benefits have to be carefully analyzed because the increase of binder modifies the cost and, over a certain percentage, flowability problems can occurs (MgO is the finer powder and MgO excess could lead to a problematic flow behavior).

## 5.4 Conclusion

The addition of water just after printing is a simple operation that nevertheless improves the performance of the product. The printing condition and the raw materials quality doesn't allow a complete reaction and the secondary water helps to push forward the reaction rate without definition problem, because the piece is already shaped.

This procedure is become part of Desamanera standard post-printing processing. Further investigations are planned to study the best curing conditions and duration.

Cement paste infiltration are not effective to reduce sample porosity and increase the strength, the penetration depth is only about 1 mm. These materials could be nevertheless useful to coat the external surface, modifying fox example its absorption and chemical resistance.

To impregnate completely the piece and consolidate the whole structure, water-like solution must be used. A colloidal silica solution, with filling properties, and a Na-phosphate solution, with reactive properties, are bene studied. These solutions allow a complete impregnation and increase the significantly the compressive strength.



# Summary and conclusions

In this chapter, an overview of already started works, a summary of principal conclusions and an outlook on future researches are given. Both process, printer, material and application field are mentioned.

## Ongoing works

### *Voxel variations - 3 mm printer: Desa1 60.60 PaSta*

During the PhD period, Desamanager developed and designed a new printer, Desa1 60.60 – PaSta, with an increased resolution. The printing head is modified to arrive at a distance between the nozzles of 3 mm. The structure and the moving system follow the same idea of the other printer, the dimension is smaller, more compatible with university experimentations, with a printing area around 60 x 60 x 60 cm<sup>3</sup>. In addition to the new printing head, also an automatic opening-closing system is implemented for the recoater.

The printer is operative since May 2018 in the laboratory of DII.

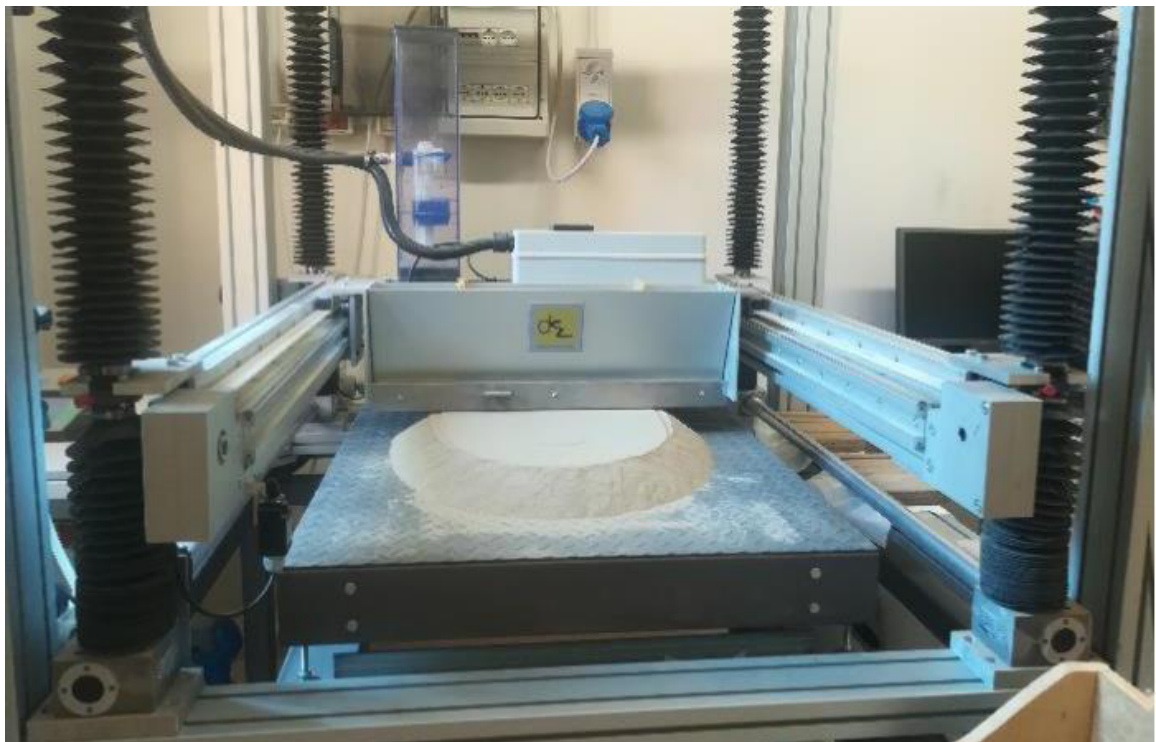


**Figure 6.1.** The new printer installed at DII Laboratory.

The reduced dimension allows to easily test new binders and raw materials in small amount. The 3 mm resolution permits a more detailed printing in small piece but, obviously, with an increasing in printing time. So, in larger scale industrial sector the adoption of a 3 mm printing head has to be evaluated according to the value for money evaluation.

If a detailing post-production is required and certain time must be in any case dedicated to this, a 5 mm resolution could be the best solution, offering an already good printed piece in a lower time.

The parameters setup was mainly focused on the water deposited amount. The voxel, from 5,7 mm to 3 mm, and so the water need is more or less 6,8 time smaller. The pressure (volume of water) and the opening time must be reduced, besides the new printing-head presents lower head-loss. Due to geometrical limits of material and tools united to the water surface tension, the deposition of small size precise droplets is not so simple, and the system have to be brought to operate at stress conditions. The 3 mm resolution should be the lower value with the actual head configuration and electro valves. New type of electro valves is currently under investigation to enhance the resolution until 2 mm and to increase the precision of working close to the critical parameters zone.

After the parameter setup, the printer is been used to print and test the already used and the new mixes. The printing quality and resolution are good. The layer interfaces are less disrupted by water droplet, due to the smaller dimension. The mechanical properties are around 3 MPa with a porosity of 35%. Figure 6.2b shows the 3 mm interface in the section of the sample.

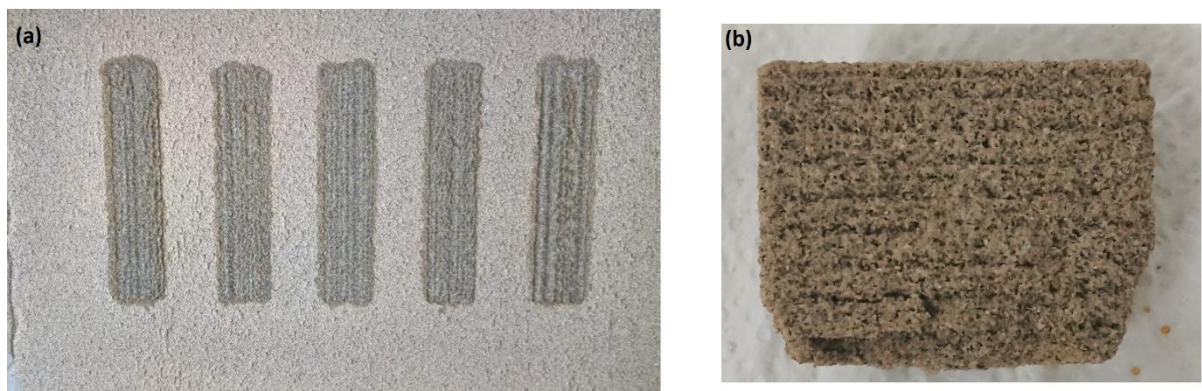


**Figure 6.2.** (a) bar samples during printing and (b) section of 3 mm layer piece.



### *Binders variations*

Desamnera 3d printing technology can be suitable also for other binders, always activated by water. Also, other low viscosity solutions could be used as activator but in this case a preliminary studied about their compatibility with the printing head must be performed.

The choice of different cements, e.g. calcium aluminate cements (CAC) for high temperature, solfo aluminate cements (SAC) for high early strength and rapid setting, Pozzolanic cements for high durability and resistance, is correlated to the achieve of specific performance, e.g. the resistance at high temperature or at aggressive environments. The satisfaction of these specific issues can open the use of printed part in new fields.

The majority of cements is activated by mixing with water, so perfectly suitable to be tested with the Desa printer. Printing test, using the small printer at DII laboratory, with 3d printing cements (proprietary formulation provided by BASF, Trostberg, Germany) are already be performed.

The printing with cements presents however some issues. First of all, as already described in *General introduction*, the setting time is generally much longer than the one required by the printing process. Although the use of fast setting cements, an important diffusion accurses and the samples have a very poor resolution.

**Table 6.1.** Dimensions of sand samples with 30% cement mix.

Sample	Bar dimensions			Deviation from 3D file		
	L [mm]	B [mm]	H [mm]	L [%]	B [%]	H [%]
<b>3d file</b>	135	30	30	/	/	/
<b>Cement 30%</b>	158	53	47	17	76	56

Second, the water post-treatment is absolutely required. The traditional cements need a more intimate and continuous contact between water and clinker. The samples just printed are very breakable, while after the water treatment becomes more solid.

The third issue is correlated to the fineness of the powder and the flowability of the mixes. Cement clinkers are finer than MgO powder (80% below 17  $\mu\text{m}$ ) and above a certain amount the powder mix show flowability problems.

Mixes with Sand and 25-30% of Cement starts to not flow and exit from the recoater or the powder bed deposited quality has deteriorated.

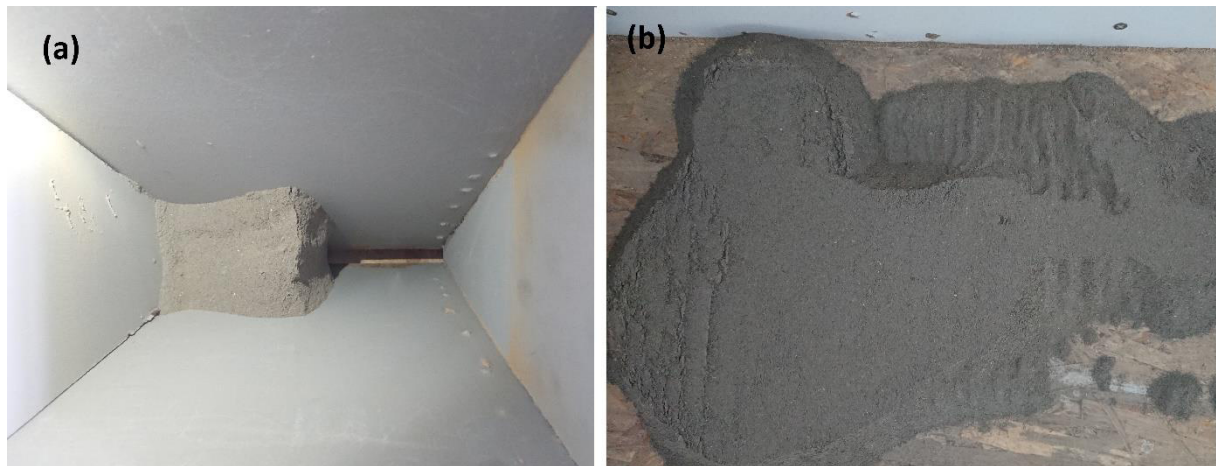


**Figure 6.3.** (a) cement mix clogged into the recoater; (b) laying problems of cement mix.

To solve these problems different strategy can be studied. Additives that increase the flowability of the powder (proprietary formulation provided by BASF, Trostberg, Germany), additives for water retention (proprietary formulation provided by BASF, Trostberg, Germany). Also additives to accelerate the setting reaction, such as silicate, could be added to water.

A printing mix with Sand plus 30% of BASF binder and an additive for powder fluidification and another one for water retention was analyzed. The mix flows out from the recoater without problem and create a good printing bed. The final compressive strength after water addition arrive at value of  $\sim 3,7$  MPa with a porosity around 40%.

To increase the resolution also other additive for water retention are under investigation. A methyl hydroxyethyl cellulose (Culminal MECH, Ashland, United States) and a high-molecular weight synthetic copolymer (Starvis S 5514 F, BASF, Trostberg, Germany) were tested. Both powders are mixed in low percentage (below 1% of total powder amount) and allow, tested in manual simple experiments, to reduce diffusion of water.

As describe in § 4.4 the reaction could reach temperature above  $60^{\circ}\text{C}$  and pH around 8 or 9. The evaluation of environmental conditions could be important to define the product with the optimum behavior for example methyl cellulose generally shows swelling behavior at temperature above  $50^{\circ}\text{C}$ , and also the pH can be modified the polymer operation.

Starting from the good result achieved, in § 5.3, for the samples infiltrated with colloidal silica solution, the possibility of printing with this solution as printing liquid is studied. Since colloidal silica is a water-based solution with a wt% of solid nanosilica, the bonding reaction should be activated (water part of the solution) and the porosity in the bed immediately filled (solid silica). The first studies have demonstrated the possibility to print with the solution and the printed samples achieved strength of  $4,81 \pm 0,51$  MPa with a porosity of  $36 \pm 1$  %. However, some

issues are discovered. The solution has a higher viscosity than water and, so, the values of pressure and opening time have to be recalculated in order to deposit a sufficient amount of solution. The solution remained attached at the end of nozzles or in cavities deposits the solid silica generating partial clogging problems. The printing head has to be cleaned and the liquid completely flushes out. For more aggressive liquid also the compatibility with printing head materials have to be studied.

### *Aggregates variations*

The possibility to substitute a part of standard aggregates with alternative one is started to be investigated. These substitutions can allow to introduce new specific functionalities to printed piece. For example, the production of complex shape isolation panels and walls.

With lightweight aggregate the weight of final piece is reduced (hopefully maintaining good mechanical properties) and specific properties, such as thermal and sound isolating, could be increased. The use of cork and wood fibers (ecological materials) also increase the sound isolating properties. The introduction of reinforcing fibers (polymeric or metal) could increase strength and the toughness.

A first critical point is the mixing of the components in a homogenous material. Natural fibers are generally elongated and bigger than standard particles. Lightweight granules tend to separate during recoater deposition moving down rapidly. Polymeric fibers are difficult to be mixed causing powder agglomeration in little balls and, due to powder layer deposition, the presence of fiber connection reinforce between layer is very limited.

A manual printing test with wood fiber is been carried out, the printed part result consistent, showing a good compatibility between the materials. Further research is under developing.

Poraver® expanded glass granules (Dennert Poraver, Schlüsselfeld, Germany) are selected to partially substitute the BdZ in a lightweight mix. An equal mixture of 0,25 – 0,5 mm and 0,5-1 mm Poraver granules is prepared and calculating the equivalent volume the 75% of BdZ is replaced with Poraver. A final mix with 25% of binder is prepared. Bar samples is been printed using the standard printing parameters. The

Post-printing treatment with water addition is highly necessary because the Poraver adsorbs part of the printing water. The mechanical strength achieved, after water treatment, are around ~2 MPa both for compression and bending test, with an open porosity around ~43% and a closed porosity around ~8%. Even if the mechanical properties are lower than pure BdZ material, the density is decreased from 1,55 g/cm<sup>3</sup> to 1,03 g/cm<sup>3</sup>.

A block of 300 x 200 x 100 mm<sup>3</sup> (Figure 6.4), made with a core of lightweight material (10 cm) and the sides of standard BdZ material (5 cm), is printed as proof of concept.



**Figure 6.4.** Block with core part in lightweight material.

## Conclusions

The possibility to print large piece with good resolution and adequate strength is been demonstrated. The printing process optimization permitted to increase the quality of the printed parts and to make more stable and repeatable the various operations. A drop on demand water deposition was developed. Meanwhile a water vessel, with automatic refilling, was mounted integral with the printing head and a reacting system, that deposits powder immediately after water, was implemented. The printing parameters, for a 5,7 mm voxel, were become a laying speed of 50 m/s, a printing speed of 50 m/s, an electro valves opening time of 18 ms, with a pressure of  $\Delta h = 1000$  mm and powder voxel deposition divided in 30% - 70%.

Even if the process was become more stable and the manual operations were reduced, the interface between layer presented an important macro porosity, due to water-powder bed interaction issue. This topic must be further investigated in the future.

The analyses on the raw materials and the printing mixes have allowed to find the fundamental characteristics of different reagents (reactivity, particle size, proportion between reagents, ecc) and to select the best products and supplier according to a small company necessity. The printed parts characterization has shown a not completed binding reaction, for this reason different post-printing treatments are been studied. The easiest one consists in the secondary addition of water; other possible treatments uses infiltration with geopolymer and cements slurry and impregnation with reactive or filling liquid.

The mechanical properties of samples printed with river Po Sand as aggregate and 40% of binder, after water treatment, have reached ~ 3 MPa in flexion and ~ 6 MPa in compression, with a porosity around 37%. The printed parts have also been certificated as compliant product without obligation of communications, and the waste don't need specific discharge.

To further increase resolution and quality of smaller components a new printing head with a voxel of 3 mm (instead 5,7 mm) is been developed. To extend the fields of application the use of different cements, such as high temperature cements, is started to be studied. Also variation of the aggregate (lightweight, natural fibers, ecc) and use of additives are started to be considered. The first results have shown a good versatility of the technology to implement these new solutions.

## **Future objectives**

For the future, various topics could be followed and further studied. First of all, the investigation in water deposition method and water-powder bed interaction has to be carried out. The macro porosity the interface is one of the critical aspects. Probably also new printing head configuration (manifold, electro valves, nozzles) could be studied, especially for lower voxel dimension (as already done for 3 mm).

The printing process could become even more stable and automated developing an automatic powder re-filler to the recoating system and designing a simpler and stable formworks structure. The optimized composition and particle size distribution of printing mixes have to be reached both for flowability and packaging maximization. And the printing with cements (CAC, SAC, scc) have to be improved in term of fast setting, without resolution loss. The possibility to use various high-performance binders could open the application in new specific fields.

Following the reusing and environmental-friendly approach, new type of aggregate should be tested. Materials such as fly ash, slag and construction wastes are already use in traditional concrete and could be insert also in Desamanera formulations. Another very interesting theme is the possible reuse of the own waste powders produced by company post-production.

Finally, new potential technical markets could be searched and analyzed. For example, the production of road and sewer components (barrier, pipe connection, ecc), of engineered nonstructural construction pieces (wall, panel, ecc), of high temperature blocks, of outdoor and public opera (Admin4d project already aims to produce such components directly containing sensors).



# Bibliography

- [1] ASTM, “Standard Terminology for Additive Manufacturing Technologies,” 2012.
- [2] Y. Huang, M. C. Leu, J. Mazumder, and A. Donmez, “Additive manufacturing: Current state, future potential, gaps and needs, and recommendations,” *J. Manuf. Sci. Eng. Trans. ASME*, vol. 137, no. 1, pp. 1–10, 2015.
- [3] B. P. Conner *et al.*, “Making sense of 3-D printing: Creating a map of additive manufacturing products and services,” *Addit. Manuf.*, vol. 1–4, pp. 64–76, Oct. 2014.
- [4] C.W. Hull, “US4575330A - Apparatus for production of threedimensional objects by stereolithography,” 1986.
- [5] H. Paris, H. Mokhtarian, E. Coatanéa, M. Museau, and I. F. Ituarte, “Comparative environmental impacts of additive and subtractive manufacturing technologies,” *CIRP Ann. - Manuf. Technol.*, vol. 65, no. 1, pp. 29–32, 2016.
- [6] S. A. M. Tofail, E. P. Koumoulos, A. Bandyopadhyay, S. Bose, L. O’Donoghue, and C. Charitidis, “Additive manufacturing: scientific and technological challenges, market uptake and opportunities,” *Mater. Today*, vol. 21, no. 1, pp. 22–37, 2018.
- [7] M. K. Thompson *et al.*, “Design for Additive Manufacturing: Trends, opportunities, considerations, and constraints,” *CIRP Ann.*, vol. 65, no. 2, pp. 737–760, 2016.
- [8] “Wohlers Report,” 2013.
- [9] S. Ford and M. Despeisse, “Additive manufacturing and sustainability: an exploratory study of the advantages and challenges,” *J. Clean. Prod.*, vol. 137, pp. 1573–1587, 2016.
- [10] C. Weller, R. Kleer, and F. T. Piller, “Economic implications of 3D printing: Market structure models in light of additive manufacturing revisited,” *Int. J. Prod. Econ.*, vol. 164, pp. 43–56, 2015.
- [11] A. Zocca, P. Colombo, C. M. Gomes, and J. Günster, “Additive Manufacturing of Ceramics: Issues, Potentialities, and Opportunities,” *J. Am. Ceram. Soc.*, vol. 98, no. 7, pp. 1983–2001, 2015.
- [12] I. Gibson, D. W. Rosen, and B. Stucker, *Additive Manufacturing Technologies*. Boston, MA: Springer US, 2010.
- [13] L. Jyothish Kumar, P. M. Pandey, and D. I. Wimpenny, *3D Printing and Additive Manufacturing Technologies*. Singapore: Springer Singapore, 2019.
- [14] B. Y. Tay, J. R. G. Evans, and M. J. Edirisinghe, “Solid freeform fabrication of

- ceramics,” *Int. Mater. Rev.*, vol. 48, no. 6, pp. 341–370, 2003.
- [15] B. Utela, D. Storti, R. Anderson, and M. Ganter, “A review of process development steps for new material systems in three dimensional printing (3DP),” *J. Manuf. Process.*, vol. 10, no. 2, pp. 96–104, 2008.
- [16] W. Kollenberg, “Ceramic and Multi-Material 3D-Printing,” *Keramische Zeitschrift*, vol. 66, pp. 233–236, 2014.
- [17] J. Deckers, J. Vleugels, and J. P. Kruth, “Additive manufacturing of ceramics: A review,” *J. Ceram. Sci. Technol.*, vol. 5, no. 4, pp. 245–260, 2014.
- [18] Z. Chen *et al.*, “3D printing of ceramics: A review,” *J. Eur. Ceram. Soc.*, vol. 39, no. 4, pp. 661–687, 2019.
- [19] N. Travitzky *et al.*, “Additive manufacturing of ceramic-based materials,” *Adv. Eng. Mater.*, vol. 16, no. 6, pp. 729–754, 2014.
- [20] L. Gorjan, R. Tonello, T. Sebastian, P. Colombo, and F. Clemens, “Fused deposition modeling of mullite structures from a preceramic polymer and  $\gamma$ -alumina,” *J. Eur. Ceram. Soc.*, vol. 39, no. 7, pp. 2463–2471, Jul. 2019.
- [21] R. S. . Cesarano, “Robocasting provides moldless fabrication from slurry deposition,” *Ceram. Ind.*, vol. 148, pp. 94–100, 1998.
- [22] Murilo D.M. Innocentini *et al.*, “Lattice-shaped geopolymers catalyst for biodiesel synthesis fabricated by additive manufacturing,” *Ceram. Int.*, vol. 45, pp. 1443–1446, 2019.
- [23] Z. Chen, D. Li, W. Zhou, and L. Wang, “Curing characteristics of ceramic stereolithography for an aqueous-based silica suspension,” *Proc. Inst. Mech. Eng. Part B J. Eng. Manuf.*, vol. 224, no. 4, pp. 641–651, 2010.
- [24] J. Will, *et al.*, “Porous ceramic bone scaffolds for vascularized bone tissue regeneration,” *J. Mater. Sci. Mater. Med.*, vol. 19, no. 8, pp. 2781–2790, 2008.
- [25] A. Butscher *et al.*, “New depowdering-friendly designs for three-dimensional printing of calcium phosphate bone substitutes,” *Acta Biomater.*, vol. 9, no. 11, pp. 9149–9158, 2013.
- [26] J. J. Beaman, J. W. Barlow, D. L. Bourell, R. H. Crawford, H. L. Marcus, and K. P. McAlea, *Solid Freeform Fabrication: A New Direction in Manufacturing*. Boston, MA: Springer US, 1997.
- [27] C. R. Deckard, “Method and apparatus for producing parts by selective sintering,” 1989.
- [28] T. Friedel *et al.*, “Fabrication of polymer derived ceramic parts by selective laser curing,” *J. Eur. Ceram. Soc.*, vol. 25, no. 2–3, pp. 193–197, 2005.



- [29] B. Cappi et al, “Direct inkjet printing of Si<sub>3</sub>N<sub>4</sub>: Characterization of ink, green bodies and microstructure,” *J. Eur. Ceram. Soc.*, vol. 28, no. 13, pp. 2625–2628, 2008.
- [30] M. Krinitcyn et al., “Laminated Object Manufacturing of in-situ synthesized MAX-phase composites,” *Ceram. Int.*, vol. 43, no. 12, pp. 9241–9245, 2017.
- [31] G. Franchin and P. Colombo, “Porous geopolymer components through inverse replica of 3D printed sacrificial templates,” *J. Ceram. Sci. Technol.*, vol. 6, no. 2, pp. 105–112, 2015.
- [32] R. A. Buswell, R. C. Soar, A. G. F. Gibb, and A. Thorpe, “Freeform Construction: Mega-scale Rapid Manufacturing for construction,” *Autom. Constr.*, vol. 16, no. 2, pp. 224–231, 2007.
- [33] G. De Schutter, K. Lesage, V. Mechtcherine, V. N. Nerella, G. Habert, and I. Agusti-Juan, “Vision of 3D printing with concrete — Technical, economic and environmental potentials,” *Cem. Concr. Res.*, vol. 112, no. August, pp. 25–36, Oct. 2018.
- [34] D. Delgado Camacho *et al.*, “Applications of additive manufacturing in the construction industry – A forward-looking review,” *Autom. Constr.*, vol. 89, no. February, pp. 110–119, May 2018.
- [35] F. Craveiro, J. P. Duarte, H. Bartolo, and P. J. Bartolo, “Additive manufacturing as an enabling technology for digital construction: A perspective on Construction 4.0,” *Autom. Constr.*, vol. 103, no. October 2018, pp. 251–267, 2019.
- [36] B. Nematollahi, M. Xia, and J. Sanjayan, “Current Progress of 3D Concrete Printing Technologies,” in *ISARC 2017 - Proceedings of the 34th International Symposium on Automation and Robotics in Construction*, 2017, no. Isarc, pp. 260–267.
- [37] B. Nematollahi, J. Sanjayan, and F. U. A. Shaikh, “Synthesis of heat and ambient cured one-part geopolymer mixes with different grades of sodium silicate,” *Ceram. Int.*, vol. 41, no. 4, pp. 5696–5704, May 2015.
- [38] R. A. Buswell, W. R. Leal de Silva, S. Z. Jones, and J. Dirrenberger, “3D printing using concrete extrusion: A roadmap for research,” *Cem. Concr. Res.*, vol. 112, no. June, pp. 37–49, 2018.
- [39] N. Labonnote, A. Rønquist, B. Manum, and P. Rüther, “Additive construction: State-of-the-art, challenges and opportunities,” *Autom. Constr.*, vol. 72, pp. 347–366, 2016.
- [40] P. Wu, J. Wang, and X. Wang, “A critical review of the use of 3-D printing in the construction industry,” *Autom. Constr.*, vol. 68, pp. 21–31, 2016.
- [41] S. Lim, R. A. Buswell, T. T. Le, S. A. Austin, A. G. F. Gibb, and T. Thorpe, “Developments in construction-scale additive manufacturing processes,” *Autom.*

- Constr.*, vol. 21, no. 1, pp. 262–268, 2012.
- [42] F. Bos, R. Wolfs, Z. Ahmed, and T. Salet, “Additive manufacturing of concrete in construction: potentials and challenges of 3D concrete printing,” *Virtual Phys. Prototyp.*, vol. 11, no. 3, pp. 209–225, 2016.
- [43] B. Khoshnevis, “Automated construction by contour crafting - Related robotics and information technologies,” *Autom. Constr.*, vol. 13, no. 1, pp. 5–19, 2004.
- [44] B. Khoshnevis, S. Bukkapatnam, H. Kwon, and J. Saito, “Experimental investigation of contour crafting using ceramics materials,” *Rapid Prototyp. J.*, vol. 7, no. 1, pp. 32–41, 2001.
- [45] B. Khoshnevis, D. Hwang, K. T. Yao, and Z. Yeh, “Mega-scale fabrication by Contour Crafting,” *Int. J. Ind. Syst. Eng.*, vol. 1, no. 3, p. 301, 2006.
- [46] C. Gosselin, R. Duballet, P. Roux, N. Gaudillère, J. Dirrenberger, and P. Morel, “Large-scale 3D printing of ultra-high performance concrete - a new processing route for architects and builders,” *Mater. Des.*, vol. 100, pp. 102–109, 2016.
- [47] S. Lim *et al.*, “Development of a Viable Concrete Printing Process,” in *Proceedings of the 28th International Symposium on Automation and Robotics in Construction, ISARC 2011*, 2011, pp. 665–670.
- [48] R. R. Wolfs and T. T. Salet, “An optimization strategy for 3d concrete printing,” in *22nd EG-ICE workshop, Eindhoven*, 2015.
- [49] “<https://www.tue.nl/en/our-university/departments/built-environment/research-meets-practice/structures-laboratory-eindhoven/#top>.” [Accessed October 30, 2019]
- [50] M. Krause, J. Otto, A. Bulgakov, and D. Sayfeddine, “Strategic Optimization of 3D-Concrete-Printing Using the Method of CONPrint3D®,” in *ISARC 2018 - 35th International Symposium on Automation and Robotics in Construction and International AEC/FM Hackathon: The Future of Building Things*, 2018, no. Isarc.
- [51] V. N. Nerella and V. Mechtcherine, “Studying the Printability of Fresh Concrete for Formwork-Free Concrete Onsite 3D Printing Technology (CONPrint3D),” in *3D Concrete Printing Technology*, no. March, Elsevier, 2019, pp. 333–347.
- [52] B. Panda, S. C. Paul, L. J. Hui, Y. W. D. Tay, and M. J. Tan, “Additive manufacturing of geopolymer for sustainable built environment,” *J. Clean. Prod.*, vol. 167, pp. 281–288, Nov. 2017.
- [53] “<http://robots.iaac.net>.” [Accessed October 30, 2019]
- [54] “<http://www.winsun3d.com/En/Product/prolist/id/1>.” [Accessed October 30, 2019]
- [55] “<https://3dprint.com/38144/3d-printed-apartment-building/>.” [Accessed October 30,

- 2019]
- [56] “<https://www.apis-cor.com/perspectives-and-challenges>.” [Accessed October 30, 2019]
- [57] “<https://www.3dnatives.com/en/apis-cor-3d-printed-house-060320184/>.” [Accessed October 30, 2019]
- [58] “<https://www.3dwasp.com/en/3d-printed-house-gaia/>.” [Accessed October 30, 2019]
- [59] “<https://www.dezeen.com/2019/02/27/gaia-wasp-3d-printed-house-biodegradable-video/>.” [Accessed October 30, 2019]
- [60] “<https://www.arup.com/news-and-events/new-3d-printed-house-points-the-way-to-a-more-sustainable-construction-industry>.” [Accessed October 30, 2019]
- [61] D. Lowke, E. Dini, A. Perrot, D. Weger, C. Gehlen, and B. Dillenburger, “Particle-bed 3D printing in concrete construction – Possibilities and challenges,” *Cem. Concr. Res.*, vol. 112, no. July, pp. 50–65, 2018.
- [62] “<https://d-shape.com/>.” [Accessed October 30, 2019]
- [63] G. Cesaretti, E. Dini, X. De Kestelier, V. Colla, and L. Pambaguian, “Building components for an outpost on the Lunar soil by means of a novel 3D printing technology,” *Acta Astronaut.*, vol. 93, pp. 430–450, Jan. 2014.
- [64] G. J. Gibbons, R. Williams, P. Purnell, and E. Farahi, “3D Printing of cement composites,” *Adv. Appl. Ceram.*, vol. 109, no. 5, pp. 287–290, 2010.
- [65] E. Vorndran *et al.*, “Hydraulic setting Mg 3 (PO 4 ) 2 powders for 3D printing technology,” *Adv. Appl. Ceram.*, vol. 110, no. 8, pp. 476–481, Nov. 2011.
- [66] P. Shakor, J. Sanjayan, A. Nazari, and S. Nejadi, “Modified 3D printed powder to cement-based material and mechanical properties of cement scaffold used in 3D printing,” *Constr. Build. Mater.*, vol. 138, pp. 398–409, 2017.
- [67] M. Xia and J. Sanjayan, “Method of formulating geopolymer for 3D printing for construction applications,” *Mater. Des.*, vol. 110, pp. 382–390, Nov. 2016.
- [68] M. Xia, B. Nematollahi, and J. Sanjayan, “Printability, accuracy and strength of geopolymer made using powder-based 3D printing for construction applications,” *Autom. Constr.*, vol. 101, no. January, pp. 179–189, 2019.
- [69] A. Pierre, D. Weger, A. Perrot, and D. Lowke, “Penetration of cement pastes into sand packings during 3D printing: analytical and experimental study,” *Mater. Struct. Constr.*, vol. 51, no. 1, pp. 1–12, 2018.
- [70] D. Weger *et al.*, “3D printing of concrete structures using the selective binding method – Effect of concrete technology on contour precision and compressive strength,” in *11th fib International PhD Symposium in Civil Engineering, At Tokyo*, 2016.

- [71] D. Weger, D. Lowke, C. Gehlen, D. Talke, and K. Henke, “Additive manufacturing of concrete elements using selective cement paste intrusion—effect of layer orientation on strength and durability,” *Proc. RILEM 1st Int. Conf. Concr. Digit. Fabr.*, no. September, pp. 2016–2017, 2018.
- [72] “<https://www.voxeljet.com/applications/>.” [Accessed October 30, 2019]
- [73] “<http://www.michael-hansmeyer.com/digital-grotesque-II>.” [Accessed October 30, 2019]
- [74] “<https://concr3de.com/>.” [Online]. Available: <https://concr3de.com/>. [Accessed October 30, 2019]
- [75] E. Gartner, “Industrially interesting approaches to ‘low-CO<sub>2</sub>’ cements,” *Cem. Concr. Res.*, vol. 34, no. 9, pp. 1489–1498, 2004.
- [76] M. S. Imbabi, C. Carrigan, and S. McKenna, “Trends and developments in green cement and concrete technology,” *International Journal of Sustainable Built Environment*, vol. 1, no. 2. The Gulf Organisation for Research and Development, pp. 194–216, 2012.
- [77] S. A. Miller, V. M. John, S. A. Pacca, and A. Horvath, “Carbon dioxide reduction potential in the global cement industry by 2050,” *Cem. Concr. Res.*, vol. 114, no. August 2017, pp. 115–124, Dec. 2018.
- [78] A. Naqi and J. Jang, “Recent Progress in Green Cement Technology Utilizing Low-Carbon Emission Fuels and Raw Materials: A Review,” *Sustainability*, vol. 11, no. 2, p. 537, Jan. 2019.
- [79] U. N. Environment, K. L. Scrivener, V. M. John, E. M. Gartner, É. Polytechnique, and F. De Lausanne, “Eco-efficient cements : Potential economically viable solutions for a low-CO<sub>2</sub> cement-based materials industry ☆,” *Cem. Concr. Res.*, vol. 114, no. February, pp. 2–26, 2018.
- [80] J. L. Provis, “Alkali-activated materials,” *Cem. Concr. Res.*, vol. 114, pp. 40–48, 2018.
- [81] J. Davidovits, *Geopolymer Chemistry & Applications*. .
- [82] S. A. Walling and J. L. Provis, “Magnesia-Based Cements: A Journey of 150 Years, and Cements for the Future?,” *Chemical Reviews*, vol. 116, no. 7. pp. 4170–4204, 2016.
- [83] S. Sorel, “Improved composition to be used as a cement and as a plastic material for molding various articles,” U.S. Patent 53,092, 1866., 1866.
- [84] A. S. Wagh and S. Y. Jeong, “Chemically Bonded Phosphate Ceramics: I, A Dissolution Model of Formation,” *J. Am. Ceram. Soc.*, vol. 86, no. 11, pp. 1838–1844, 2003.
- [85] E. Soudée and J. Péra, “Mechanism of setting reaction in magnesia-phosphate cements,” *Cem. Concr. Res.*, vol. 30, no. 2, pp. 315–321, 2000.

- [86] Y. Li, J. Sun, J. Li, and T. Shi, “Effects of fly ash, retarder and calcination of magnesia on properties of magnesia-phosphate cement,” *Adv. Cem. Res.*, vol. 27, no. 7, pp. 373–380, 2015.
- [87] N. Yang, C. Shi, J. Yang, and Y. Chang, “Research Progresses in Magnesium Phosphate Cement–Based Materials,” *J. Mater. Civ. Eng.*, vol. 26, no. 10, p. 04014071, Oct. 2014.
- [88] E. Soudée and J. Péra, “Influence of magnesia surface on the setting time of magnesia–phosphate cement,” *Cem. Concr. Res.*, vol. 32, no. 1, pp. 153–157, Jan. 2002.
- [89] G. Mestres *et al.*, “Magnesium phosphate cements for endodontic applications with improved long-term sealing ability,” *Int. Endod. J.*, vol. 47, no. 2, pp. 127–139, 2014.
- [90] A. J. Wang, X. J. Fan, J. M. Li, and D. Chen, “Curing behavior and structure of magnesium phosphate chemically bonded ceramics with different MgO to KH<sub>2</sub>PO<sub>4</sub> ratios,” *Int. J. Appl. Ceram. Technol.*, vol. 12, no. 6, pp. 1124–1130, 2015.
- [91] J. Davidovits, “J. Davidovits, *J. Therm. Anal.* 37 (8) (1991) 1633.,” *J. Therm. Anal.*, vol. 37, no. 8, p. 1633, 1991.
- [92] V.D. Glukhovskiy, “Ancient, modern and future concretes,” in *First International Conference on Alkaline Cements and Concretes*, VIPOL Stock Company, Kiev, 1994, pp. 1–9.
- [93] P. Duxson, S. W. Mallicoat, G. C. Lukey, W. M. Kriven, and J. S. J. van Deventer, “The effect of alkali and Si/Al ratio on the development of mechanical properties of metakaolin-based geopolymers,” *Colloids Surfaces A Physicochem. Eng. Asp.*, vol. 292, no. 1, pp. 8–20, Jan. 2007.
- [94] P. Duxson, A. Fernández-Jiménez, J. L. Provis, G. C. Lukey, A. Palomo, and J. S. J. van Deventer, “Geopolymer technology: the current state of the art,” *J. Mater. Sci.*, vol. 42, no. 9, pp. 2917–2933, May 2007.
- [95] “<https://www.desamanera.com/en/desamanera/>.” [Accessed October 30, 2019]
- [96] “<http://www.starsup.it/project/desamanera-s-r-l>.” [Accessed October 30, 2019]
- [97] “<http://www.rise-amitie.eu/>.” [Accessed October 30, 2019]
- [98] “<http://www.improvenet.it/>.” [Accessed October 30, 2019]
- [99] “UIBM, Brevetto N.102015000071593.”
- [100] “UIBM, Brevetto N. 102016000020325.”
- [101] J. Clayton, D. Millington-Smith, and B. Armstrong, “The Application of Powder Rheology in Additive Manufacturing,” *JOM*, vol. 67, no. 3, pp. 544–548, Mar. 2015.
- [102] E. Sachs *et al.*, “Three-Dimensional Printing: The Physics and Implications of Additive Manufacturing,” *CIRP Ann. - Manuf. Technol.*, vol. 42, no. 1, pp. 257–260, Jan. 1993.

- [103] S. Spath and H. Seitz, “Influence of grain size and grain-size distribution on workability of granules with 3D printing,” *Int. J. Adv. Manuf. Technol.*, vol. 70, no. 1–4, pp. 135–144, Jan. 2014.
- [104] J. W. Park, K. H. Kim, and K. Y. Ann, “Fundamental Properties of Magnesium Phosphate Cement Mortar for Rapid Repair of Concrete,” *Adv. Mater. Sci. Eng.*, vol. 2016, pp. 1–7, 2016.
- [105] J. Yang, “Binding properties of magnesium potassium phosphate cement,” pp. 3–5, 2004.
- [106] H. Ma and B. Xu, “Potential to design magnesium potassium phosphate cement paste based on an optimal magnesia-to-phosphate ratio,” *Mater. Des.*, vol. 118, pp. 81–88, 2017.
- [107] M. Arlete Carvalho and A. M. Segadães, “The Hydration of Magnesium Phosphate Cements: Effect of Powder Characteristics on the Reaction Kinetics,” *Mater. Sci. Forum*, vol. 591–593, pp. 833–838, Aug. 2008.
- [108] L. Grossi, “Caratterizzazione di campioni ottenuti da stampa 3D indiretta su polvere minerale. Tesi di laurea triennale, DICEA, Università degli studi di Padova.” 2015.
- [109] A. De Marzi, “Stampa 3D indiretta di polveri ceramiche con diversi tipi di leganti. Tesi di laurea triennale, DII, Università degli studi di Padova.” 2015.
- [110] F. gobbin, “Leganti inorganici per la stampa 3D indiretta su polveri ceramiche. Tesi di laurea magistrale, DII, Università degli studi di Padova.” 2016.
- [111] RHI, “RHI - CCM per l’alimentazione animale.”
- [112] “[https://icl-sf.com/it-it/products/specialty\\_agriculture/2851-select-mkp/.](https://icl-sf.com/it-it/products/specialty_agriculture/2851-select-mkp/)” [Accessed October 30, 2019]
- [113] C. Tarabotti, “Sviluppo della testa di una stampante 3d per polveri minerali, Tesi di laurea magistrale, DII, Università degli studi di Padova.” 2019.
- [114] T. T. Le *et al.*, “Hardened properties of high-performance printing concrete,” *Cem. Concr. Res.*, vol. 42, no. 3, pp. 558–566, Mar. 2012.
- [115] &NA;, “Guide for the Use of the International System of Units (SI),” *Med. Sci. Sport. Exerc.*, vol. 31, no. 1, pp. 198–205, Jan. 1999.
- [116] V. R. Salvini, V. C. Pandolfelli, and D. Spinelli, “Mechanical Properties of Porous Ceramics,” in *Recent Advances in Porous Ceramics*, InTech, 2018.
- [117] S. Meille, M. Lombardi, J. Chevalier, and L. Montanaro, “Mechanical properties of porous ceramics in compression: On the transition between elastic, brittle, and cellular behavior,” *J. Eur. Ceram. Soc.*, vol. 32, no. 15, pp. 3959–3967, Nov. 2012.

- [118] M. F. Ashby and R. F. M. Medalist, “The mechanical properties of cellular solids,” *Metall. Trans. A*, vol. 14, no. 9, pp. 1755–1769, Sep. 1983.
- [119] F. Zanetti, “Nuovo legante inorganico per la stampa 3d di pietra artificiale. Tesi di laurea triennale, DICEA, Università degli studi di Padova,.” 2017.
- [120] A. Zecchini, “Stampa 3D di oggetti ceramici di grandi dimensioni tramite la tecnologia indiretta del letto di polvere. Tesi di laurea magistrale, DII, Università degli studi di Padova,.” 2018.
- [121] A. B. Spierings, M. Voegtlin, T. Bauer, and K. Wegener, “Powder flowability characterisation methodology for powder-bed-based metal additive manufacturing,” *Prog. Addit. Manuf.*, vol. 1, no. 1–2, pp. 9–20, Jun. 2016.
- [122] A. Santomaso, P. Lazzaro, and P. Canu, “Powder flowability and density ratios: the impact of granules packing,” *Chem. Eng. Sci.*, vol. 58, no. 13, pp. 2857–2874, Jul. 2003.
- [123] B. Xu, B. Lothenbach, A. Leemann, and F. Winnefeld, “Reaction mechanism of magnesium potassium phosphate cement with high magnesium-to-phosphate ratio,” *Cem. Concr. Res.*, vol. 108, no. September 2017, pp. 140–151, Jun. 2018.
- [124] M. Le Rouzic, T. Chaussadent, G. Platret, and L. Stefan, “Mechanisms of k-struvite formation in magnesium phosphate cements,” *Cem. Concr. Res.*, vol. 91, pp. 117–122, 2017.
- [125] X. Zhang, G. Li, M. Niu, and Z. Song, “Effect of calcium aluminate cement on water resistance and high-temperature resistance of magnesium-potassium phosphate cement,” *Constr. Build. Mater.*, vol. 175, pp. 768–776, Jun. 2018.
- [126] Y. Li, T. Shi, B. Chen, and Y. Li, “Performance of magnesium phosphate cement at elevated temperatures,” *Constr. Build. Mater.*, vol. 91, pp. 126–132, Aug. 2015.
- [127] A. López-Uceda, J. Ayuso, M. López, J. Jimenez, F. Agrela, and M. Sierra, “Properties of Non-Structural Concrete Made with Mixed Recycled Aggregates and Low Cement Content,” *Materials (Basel)*, vol. 9, no. 2, p. 74, Jan. 2016.
- [128] Y. Koubaa, M. Jamei, and H. Guiras, “Hydro-mechanical Properties of Highly porous Limestone Rock used for Historic Monuments in North-East Tunisia,” *J. Civ. Environ. Eng.*, vol. 08, no. 03, 2018.
- [129] G. Rangon, “Stampa 3D di grandi dimensioni di pietra artificiale e di componenti ceramici. Tesi di laurea triennale, DICEA, Università degli studi di Padova,.” 2017.
- [130] S. Sufian, S. Mat Yakob, N. E. Rabat, and R. Md Zin, “A REVIEW ON GEOPOLYMER AS A NEW GREEN COATING MATERIAL,” *J. Ind. Technol.*, vol. 26, no. 1, pp. 59–73, 2018.

- [131] S. Sikora, E. Gapys, B. Michalowski, T. Horbanowicz, and M. Hynowski, "Geopolymer coating as a protection of concrete against chemical attack and corrosion," *E3S Web Conf.*, vol. 49, p. 00101, Aug. 2018.
- [132] A. Cervesato, "Ottimizzazione di componenti in pietra artificiale ottenuti per stampa 3D. Tesi di laurea magistrale, DII, Università degli studi di Padova,," 2018.
- [133] Pascal COLLET et al., "Concrete porosity reduction by Colloidal silica nano technology," in *8th International Conference on Concrete Under Severe Conditions-Environment & Loading, CONSEC 2016, Lecco, Italy*, 2016.
- [134] P. Hou, X. Cheng, and Z. Zhou, "Influence of the Surface Treatment of Hardened Cement Mortar with Colloidal Nano-Silica and TEOS," in *5th International Conference on Durability of Concrete Structures, Shenzhen University, Shenzhen, Guangdong Province, P.R.China*, 2016, pp. 4–7.



# Curriculum vitae

## **Personal data**

Name: Filippo Gobbin

Date of birth: 10 September 1991

Place of birth: Abano Terme (PD), Italy

Gender: Male

Nationality: Italian

## **Education and research**

- 10/2010 - 09/2014 BSc in Materials and Chemical Engineering, University of Padova (Italy).
- 10/2014 - 09/2016 MSc in Materials Engineering, University of Padova (Italy).
- 11/2016 - present: PhD in Industrial Engineering, University of Padova (Italy).
- 11/2016 - present: apprenticeship at Desamanera srl, Rovigo (Italy)

## **Oral and poster Presentations**

- Poster of Desamanera srl at 3DP session of yCAM 2018– young Ceramists Additive Manufacturing Forum in Padova, Italia; 04/05/2018
- Oral “Large scale additive manufacturing of artificial stone” of Unipd-Desamanera srl at S15: 3<sup>rd</sup> international symposium on additive manufacturing and 3d printing technologies of ICACC '19 - 43rd International Conference & Exposition on Advanced Ceramics and Composites in Daytona Beach, Florida, USA; 29/01/2019
- Poster of Unipd-Desamanera srl at poster session A of ICACC '19 - 43rd International Conference & Exposition on Advanced Ceramics and Composites in Daytona Beach, Florida, USA; 29/01/2019

## **Students thesis co-advised**

- Nicolò Bissoli, BSc, Stampa 3D di pietra artificiale: effetto di diversi parametri di processo, 2016/2017
- Francesca Zanetti, BSc, Nuovo legante inorganico per la stampa 3D di pietra artificiale, 2016/2017
- Giorgia Rangon, BSc, Stampa 3 di grandi dimensioni di pietra artificiale e di componenti ceramici, 2017/2018

- Evita De Marchi, BSc, Caratterizzazione di campioni di pietra artificiale ottenuti con manifattura additiva, 2017/2018
- Alberto Zecchini, MSc, Stampa 3d di oggetti ceramici di grandi dimensioni tramite la tecnologia indiretta del letto di polvere, 2017/2018
- Angela Cervesato, MSc, Ottimizzazione di componenti in pietra artificiale ottenuti per stampa 3d, 2017/2018
- Beatrice Cesaro, BSc, Stampa additiva di miscele cementizie, 2018/2019